Preparation and Properties of polybenzodioxane PIM-1 and its copolymers with poly(ethylene glycol)

A thesis submitted to the University of Manchester for the degree of Doctor of Philosophy in the faculty of Engineering and Physical Sciences

2011

Gul Mohammad Laghari

The School of Chemistry

Table of Contents

Word count: 44,451

List of Figures

List of Tables

Abbreviations

ACF	Active Carbon Fibres
BCA	5,5',6,6'-tetrahydroxy-3,3,3',3'-tetramethyl-1,1'-spirobisindane
BET	Brunauer-Emmett-Teller
Br	Broad
COFs	Covalent-Organic-Frameworks
CBCF	Carbon-Bonded Carbon Fibres
C_n	Cyclic PIM-1 chain in MALDI
^{13}CNMR	Carbon Nuclear Magnetic Resonance Spectroscopy
D	Doublet
DCM	Dichloromethane
DCTB	2-[(2E)-3-(4-tert-Butylphenyl)-2-methylprop-2-enylidene]malononitrile
DMA	Dynamic Mechanical Analysis
DMAc	Dimethylacetaldehyde
DMF	Dimethylformamide
DMSO	Dimethyl sulfoxide
EI/CI	Electronic Ionization/Chemical Ionization
FCS	Fluorescence correlation spectroscopy
F-PIM	Fluoro endcapped PIM-1
FT-IR	Fourier-transform Infrared
FTRF	Fast Transient Fluorescence Technique
GPC	Gel Permeation Chromatography
HATN	Hexaazatrinaphthylene
^{1}HNMR	Proton Nuclear Magnetic Resonance Spectroscopy
HPA	Heteropolyacids
HPAN	Heteropolyanion
IRMOF	Isoreticular Metal-Organic-Framework
IUPAC	International Union of Pure and Applied Chemistry
LALS	Low Angle Light Scattering
L_B	THSB Endcapped chain in MALDI
LDPE/PS	Low-density polyethylene/polystyrene
LE/SE	long emission (LE) and short emission (SE)

L_F	Fluoro endcapped PIM-1 chain in MALDI
L_N	Linear PIM-1 chain in MALDI
MALDI-TOF	Matrix-Assisted Laser Desorption/Ionisation Time of Flight
MEOPEG	Poly(ethylene glycol) monomethyl ether
M_n	Number Average Molar Mass
MOFs	Metal-Organic-Frameworks
M_{peak}	Peak Average Molar Mass
M_w	Mass Average Molar Mass
NMR	Nuclear Magnetic Resonance
PEG	Poly(ethylene glycol)
PIM	Polymers of Intrinsic Microporosity
PLA	Poly(lactic acid)
PMMA	Poly(methyl methacrylate)
ppm	Parts per Million
PPO	poly(propylene oxide)
PPSPI-PPS	poly(4-vinylphenyl-dimethyl-2-propoxysilane)-*b*-polyisoprene-*b*-poly (4-vinylphenyl-dimethyl-2-propoxysilane)
PSD	Pore Size Distribution
PS	Poly(Styrene)
PtBAPCEMA	Poly(*t*-butylacrylate)-*b*-poly(2-cinnamoylethyl methacrylate)
PTFE	Poly(tetrafluoroethylene)
PTMSP	Poly(1-trimethylsilyl-1-propyne)
PVP	P(Styrene)-*b*-poly-4-vinylpyridine
RALS	Right Angle Light Scattering
RI	Refractive Index
RIE	Reactive Ion Etching
S	Singlet
SB	Styrene-Butadiene
SA	Surface Area
SDA	Structure Directing Agent
TFTPN	Tetrafluoroterephthalonitrile
T_g	Glass Transition Temperature
TGA	Thermogravimetric Analysis

THF	Tetrahydrofuran
THSB	5,5’,6,6’-tetrahydroxy-3,3,3’,3’-tetramethyl-1,1’-spirobisindane
UV	Ultraviolet
UV/Vis	Ultraviolet / Visible

Abstract

This thesis describes the synthesis of soluble Polymer of Intrinsic Microporosity (PIM-1), fluoro-endcapped PIM-1 (F-PIM-1) and copolymers of F-PIM-1 with poly(ethylene glycol) monomethyl ether (MeOPEG). The main aim of the project was to alter the porosity of microporous PIM-1 in three ways: (a) synthesis of copolymers of F-PIM-1 with MeOPEG (b) blending of PIM-1 with MeOPEG in various proportions; and (c) adsorption of MeOPEG from aqueous solution byPIM-1.

PIM-1 and F-PIM-1 were synthesized by step growth polymerization of tetrafluoroterephthalonitrile (TFTPN) with 5,5',6,6'-tetrahydroxy-3,3,3',3'-tetramethyl-1,1'-spirobisindane (THSB), using the conventional method and a newly reported high shear mixing method. F-PIM-1 oligomers were then coupled to poly(ethylene glycol) monomethyl ether (MeOPEG). The products were analyzed by NMR, IR, MALDI ToF MSS, TGA and polystyrene based GPC as well as multidetector GPC techniques. The high shear technique generally produced high molar mass products and yields. This method was also more successful for copolymerization.

Blending of PIM-1 and MeOPEG in different proportions resulted in macrophase separation. Copolymer products were used to facilitate mixing of blends (as compatibilizers), however only 5% of MeOPEG could be solubilised into a PIM-1 phase. The effect of compatibilizer was found to be affected by interaction between PIM-1 and copolymer. However, N_2 adsorption studies showed that after thermal removal of MeOPEG, PIM-1 regained stable porosity with significant BET surface area.

Fluorescence studies were aimed at applications of PIM-1 and copolymers in sensors. PIM-1 and copolymers, spin-coated on the polyester-based substrate Melinex, were studied with and without methanol treatment in an environment of different solvent vapours. The effect of time and volume on wavelength shift and change in intensity was studied. Polar solvents tended to cause a red shift with decrease in intensity while less polar solvents behaved otherwise. Based on fluorescence experiments, solvent profiles for PIM-1 and copolymers were established.

Declaration

I declare that no portion of the work referred to in this thesis has been submitted in support of an application for another degree or qualification of this or any other university or institute of learning.

Copyright and ownership of intellectual property rights

1. The author of this thesis (including any appendices and/or schedules to this thesis) owns any copyright in it (the 'Copyright') and he has given The University of Manchester the right to use such Copyright for any administrative, promotional, educational and/or teaching purposes.

2. Copies of this thesis, either in full or in extracts, may be made **only** in accordance with the regulations of the John Rylands University Library of Manchester. Details of these regulations may be obtained from the Librarian. This page must form part of any such copies made.

3. The ownership of any patents, designs, trademarks and any and all other intellectual property rights except for the Copyright (the 'Intellectual Property Rights') and any reproductions of copyright works, for example graphs and tables ('Reproductions'), which may be described in this thesis, may not be owned by the author and may be owned by third parties. Such Intellectual Property Rights and Reproductions cannot and must not be made available for use without the prior written permission of the owner(s) of the relevant Intellectual Property Rights and/or Reproductions.

4. Further information on the conditions under which disclosure, publication and exploitation of this thesis, the Copyright and any Intellectual Property Rights and/or Reproductions described in it may take place is available from the Head of the School of Chemistry.

“Live so that when your children think of fairness and integrity, they think of you”

Brown Jr., H. Jackson

(Dedicated to my parents and family)

Acknowledgements

I am thankful to my supervisor Dr Peter Budd for providing me opportunity to work in his research group. His support, guidance and valuable feedback made the research work interesting and boosting confidence. I am also thankful to Higher Education Commission, Pakistan for sponsorship of my PhD work.

I am also indebted to Professor Neil McKeown of Cardiff University for his guidance and suggestions in synthesis work.

I would like to thank past members of Peter Budd group including Carin, Kevin, James, Amdromachi and Siren for their help and discussions. Thanks are also due to present members of Peter Budd group (Chris, Nasser, Nhamo, Alexandra, Hosna and Louise) for support and friendly working environment.

I am particularly grateful to Keith Nixon for his assistance with GPC, Martin for help with TGA and generally to other technical staff at school of chemistry. It would be unjust not to acknowledge help provided by Nasser for GPC, Nhamo for N_2 adsorption analysis, Andromachi for surface tension and Chris for synthesis.

In last I would like to mention the support and love of my family and friends in Pakistan without which it would have been a difficult task to accomplish.

CHAPTER-1

GENERAL INTRODUCTION

1.1. Aim of the project

Polymers of Intrinsic Microporosity (PIMs) are composed of rigid ladder-like components with units that force the backbone to twist or turn. This helps in prevention of efficient packing to fill space in the solid state and results in a microporous structure. PIM-1 (Fig. 1.1) is one of the widely known polymers among PIMs and has been investigated for various potential applications. [1]

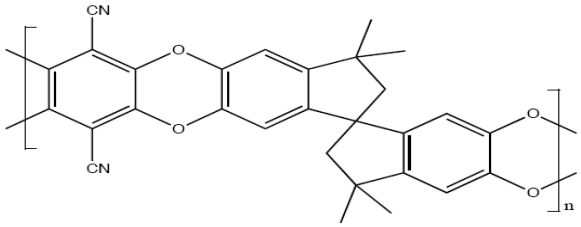

Fig. 1.1 Structure of PIM-1

The overall aim of this PhD project is to modify the pore structure and properties of PIM-1 through copolymerization, blending and adsorption. Fluoro-endcapped oligomers of PIM-1 were prepared for subsequent coupling to polyethylene glycol monomethyl ether (MeOPEG). Fluorescence studies were undertaken for their relevance to sensor applications.

1.2. Porous Materials

Porous materials are defined as solids with cavities or channels that are deeper than they are wide. The pore size is pore width (diameter or distance between opposite walls). Porous solids are usually classified by IUPAC on the basis of their pore size into three broad classes. ***Microporous materials*** have pores less than 2 nm in size. ***Mesoporous materials*** have pores between 2 and 50 nm and the term ***Macroporous materials*** apply to materials with pores bigger than 50 nm. The term ***Porosity*** refers to the ratio of pore volume to overall volume occupied by solid.[2] It is necessary not to mix up nanoporous materials with the IUPAC definition of porous materials. In the field of chemical functional porous materials, the term "nanoporous" is consistently used for porous materials having pore diameters between 1 and 100

nm, hence nanoporous materials consists of microporous as well as mesoporous structures.[3]

Mankind has been using porous materials in one way or other for various applications since ages. The use of charcoal and gypsum can be traced back to Egyptian, Greeks and Romans times. The interest for tailoring synthetic porous materials for specific applications has been an important aspect of modern day chemistry and material science. Porous materials like oxide molecular sieves, porous coordination solids, porous carbons, sol-gel derived oxides and porous heteropolyanion salts are the major classes that have been developed and found various applications in the last century. The development of conventional materials like zeolites, porous carbons and novel materials like Metal Organic Frameworks (MOF) has been drawing more and more attention of chemists and material scientists, as they can be tailored for different commercial applications like heterogeneous catalysis, chemical separations and sensor technologies by incorporation of different organic and inorganic functional groups.[2,4]

Porous solids are capable of interacting with atoms, ions or molecules at their surface as well as in bulk. Due to this ability and ordered structure, they have been used for ion exchange, adsorption (for separation) and catalysis. The applications of porous materials are related to their porous structure; hence, the distribution of sizes, shapes and volumes of the void spaces in porous materials has always been an interesting research aspect. [5]

The major challenge to the researchers has been to create uniformity within the pore size, shape and volume for better applications. Depending on applications, a material may have microporous, mesoporous or macroporous structure. Traditional Microporous materials like zeolites can for example be used to separate molecules on the basis of their size by selectively adsorption. This implies that the presence of pores of various sizes within a porous material would limit its ability for separation of molecules. However, on the other hand, a material with predominant pore structure of one type (for example microporous) with some regions of another pore size (like mesoporosity) may provide a balance between selectivity and permeability. [5, 6]

Apart from pore sizes, the chemical nature of a porous material also plays an important role for its applications. Hydrophobic materials like molecular sieves comprising pure silica are capable of adsorbing organic components from water, while hydrophilic aluminosilicate molecular sieves can be useful to separate water from organic solvents. Ordered mesoporous solids have been of interest to the researchers due to their intermediate pore size (2 to 50 nm). They can be used to prepare hierarchical structures in the form of films, fibres and spheres having quite consistent mesoporosity.[7] Porous materials possessing pores on the micro-, and meso- and even macro scale can lead to opportunities for new application. [8, 9]

In addition to traditional applications of porous materials like catalysis, separation and ion exchange, new novel and prospective applications, such as materials possessing low dielectric constant for use in electronic devices[10], one dimensional super conducing carbon nanotubes[11], nanocomposites with interior space for sensing applications, and metal organic framework (MOF) for catalysis, separation and hydrogen storage[12] are the focus of current global research in this field.

1.3. Types of porous materials

This section represents an overview of some conventional as well as relatively new (novel) classes of modern day porous materials. Depending upon type, these materials possess macro, meso and microporous regions. However, discussion will be more focussed on microporous materials due to obvious relevance to present project. The discussion will be followed by a brief overview of PIMs, new trends in PIM research and their applications. In the conclusion, relevance of present project to the recent PIM research would be established.

1.3.1. Zeolites

Zeolites and zeolite-like materials are porous crystalline solids based essentially on tetrahedral networks which contain channels and cavities. Sorbate molecules of various sizes and shapes can be accommodated in these intracrystalline voids and

undergo chemical reactions. Zeolites are based on open and fully crosslinked framework structures of corner-sharing SiO_4, and AlO_4, tetrahedra with general formula $M_{m/z}[m\ AlO_2\ .\ n\ SiO_2].\ q\ H_2O$. In this formula, M represents exchangeable cations, $[m\ AlO_2\ .\ n\ SiO_2]$ is anionic framework and H_2O is the sorbate phase. Although being highly in demand, only 6 out of 63 natural zeolites occur in large beds, giving rise to a need for their synthesis in the laboratory as per particular applications.[13]

The interest in synthesizing zeolites increased when the first synthetic zeolite (mordenite) was synthesized by Barrer in 1948; however, the commercially significant zeolites A, X, and Y were discovered by Milton and Breck through 1950's at Union Carbide. Since then numerous zeolites have been produced in laboratory. Zeolites can also occur as aluminophosphates ($AlPO_4$ structures); Silicoaluminophosphates (SAPO); metal-substituted aluminophosphates (MeAPO); and as crystalline silicotitanates. The variants in general structure involve Ge substitution for Si and Fe, Co, Mn, Zn, Ti, or Mg for Al. The synthetic zeolites are prepared under hydrothermal conditions from synthetic gels containing a source of the T atoms (for example, when T is Si, colloidal silica, fumed silica or silicon alkoxide), a mineralizing agent (OH^- or F^-), and a template like alkali metal ions such as Na^+ and soluble organic species such as quaternary amines, uncharged amines and alcohols. The template acts as Structure Directing Agent (SDA).[14] Fig. 1.2 shows the structure of LTA Zeolite – A.

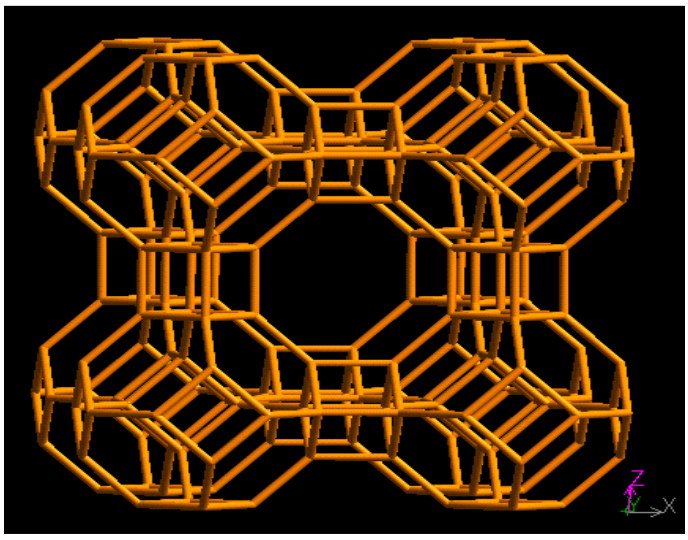

Fig. 1.2 Structure of LTA Zeolite A [15]

Zeolites have channels or cavities of molecular dimensions (0.3–1.5 nm). These channels and cavities are produced by the tetrahedral primary building blocks linked through oxygen atoms. Zeolites have been widely used for applications such as molecular sieves (because their pore sizes are comparable to molecular dimensions), adsorbents, catalysts, as well as in environmental protection and fine chemical production.[16]

1.3.2. Porous Carbons

Porous carbons have generated a great interest in the last few decades due to their high surface area, wide range of porosity and easy processing technique. They are usually produced by a process known as carbonization in which heat-treatment is carried out in an inert atmosphere. Porous carbons occur in a variety of macroscopic forms, however, the complexity of the structure prevents their preparation with strictly controlled pore structure, although voluminous research has been done and great effort has been made toward the control of pore size and its distribution.[4,17]

Porous carbons can be classified into ***graphitizing carbons & non-graphitizing carbons***. These names are given as graphitizing carbons possess some sort of order in their structure, resembling graphite, while non-graphitizing carbons do not have that type of order. During carbonization of graphitizing carbons, a liquid crystalline material is formed called the carbonaceous mesophase. The carbonization of non-graphitizing carbons is characterized by occurrence of cross-linking reactions.[18]

Graphitizing carbons are macroporous and possess high pore volumes but low specific surface areas. On the other hand, Nongraphitizing carbons generally are microporous and their micropores are usually closed. The most significant class of porous, nongraphitizing carbons is ***active carbons*** with high open porosity and high specific surface area, up to 1200 m^2 g^{-1} in commercial active carbons. The active carbons are obtained from coals, peat, wood, organic by-products of industry and agriculture. The adsorptive capacity in carbonized materials is enhanced by the

process of activation, which involves modification of porosity with oxidizing gases such as H_2O, CO_2 or H_3PO_4. The major use of activated carbons is for liquid-phase applications such as water treatment, decolourization, foods and pharmaceuticals, chemicals, and mining. Some of its gas-phase applications include solvent recovery, air purification, gasoline recovery, catalysis, gas separation, cigarette filters, and military and nuclear applications.[14, 19, 20] Fig. 1.3 shows a schematic representation of the activated carbon.

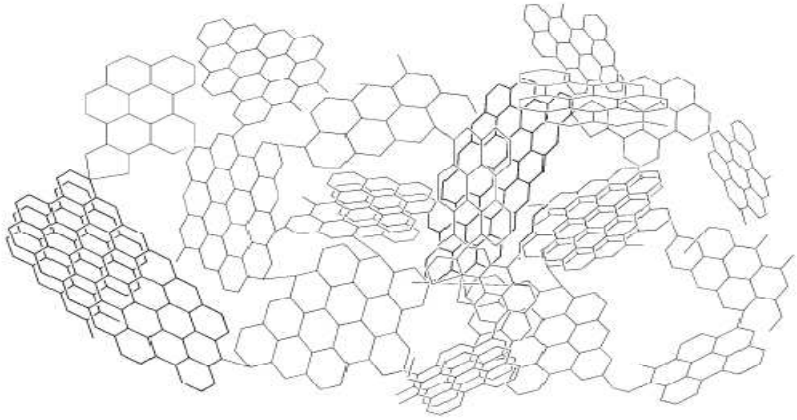

Fig. 1.3 A Schematic representation of nanoporous activated carbon[21]

The modern research in chemistry and engineering has resulted in production of some novel type of carbons or their hybrids for various commercial applications. Some significant types include ***Carbon molecular sieves, CMS*** prepared by deposition of carbon from the vapour phase and widely used for separation of N_2 from air by pressure swing adsorption. Their membranes also show high selectivity between hydrogen and C_1-C_4 hydrocarbons.[22, 23] ***Active carbon fibers, ACF*** can be microporous or mesoporous and exhibit rapid diffusion of adsorbates in to and out of the fibers. They are prepared by carbonization and activation of phenolics, acrylics, vinyl polymer and isotropic pitch fibers.[24] A specific type of ACF, called ***Carbon-Bonded Carbon Fibers, CBCF*** exhibits molecular sieve character, showing selectivity between CO_2 and CH_4. Recently there has been increasing interest in the development of porous carbon anodes for Li ion batteries.[25-27]

1.3.3. Sol-Gel Derived Oxides

Sol-gel derived material was synthesized and reported by M. Ebelmen in 1845 in France.[28] Sol-gel research saw an overwhelming response from material scientist in 1990s when more than 50,000 papers were published worldwide on the process. Sol-gel processing using colloidal dispersions of hydrous oxides was developed in early 1960's in Europe and USA, however, over the years this technique has been used to produce a range of materials for various applications.[29]

A typical Sol-Gel process consists of (i) preparation of a homogenous solution of precursor(s) in an organic solvent miscible with water or the reagent; (ii) treating this solution with a reagent and converting it to the 'sol' form; (iii) polycondensation of resultant 'sol' into 'gel' by ageing; (iv) converting the 'gel' into desired shapes like thin film, fiber, sphere or grains and (v) sintering of this shaped 'gel' at low temperatures (normally 25 - 100 °C or above). The resultant porous solid matrices are called XEROGELs. There are many metallic oxides used in this process, however, silica, zirconia, titania, alumina and thoria are important resources.[4, 28, 29]

The most important of xerogels is amorphous silica. The fundamental property of the sol-gel process is that it is possible to generate ceramic material at a temperature close to room temperature. Incorporation of soft dopants, such as fluorescent dye molecules and organic chromophores into xerogels like amorphous silica have found widespread application as high surface area catalysts, catalyst supports, chromatographic stationary phases, and gas sorbents.[30, 31]

1.3.4. Porous Heteropolyanion Salts

Large anionic metal oxide clusters are known as heteropolyanions and their salts are often porous materials. Due to their considerable thermal stability and chemical reactivity, these salts have generated increasing commercial interest for their use as heterogeneous catalysts.[32, 33] Heteropolyanions contain metal-oxygen octahedra MO_6 and serve as the basic structural unit for Heteropolyacids (HPA) and their salts (polyoxo-compounds). The MO_6 octahedra are linked together and form an

extremely stable and compact skeleton of the heteropolyanion (HPAN). The cations in this case are usually hydrogen, alkali metal, and other metal ions. HPA and their salts are thermally stable, chemically reactive and often porous.[34]

The crystalline structure of heteropolyanions can be primary, secondary, or tertiary. The primary structure is that of heteropolyanion that is the metal oxide cluster molecule. The secondary structure is the regular three-dimensional arrangement consisting of polyanions, counter cations and additional molecules. The secondary structure is responsible for the bulk-type catalysis of solid HPA catalysts. The tertiary structure represents the assembly of the secondary structure assembles into solid particles and relates to properties such as particle size, surface area and pore structure.[35]

The salts of heteropolyanions are divided as **A-class** (water soluble) and **B-class** (water insoluble) salts on the basis of adsorption of these salts. Class A salts are nonporous with low surface area; however, they show unique "pseudo-liquid" absorption behaviour toward polar molecules that plays an important role in catalysis. Class B salts have high porosity in terms of surface areas.[4, 36]

1.3.5. Metal Organic Frameworks (MOF)

Metal Organic Frameworks (MOFs) chemistry was established in early 1990s and these porous materials were apparently an extension of the earlier work on three dimensional cyanide frameworks. In $K_2Zn_3[Fe(CN)_6]_2.xH_2O$, octahedral Fe^{2+} and tetrahedral Zn^{3+} cations are joined together by CN^- groups to form a three dimensional network with cavities occupied by K^+ cations and water molecules. In MOFs, these CN^- ligands were replaced by larger ligands like carboxylates to create larger cavities. The term "metal-organic framework" first appeared in the literature in 1997; however, another term "Coordination Polymers" has also been used in literature over the last few years.[4, 37]

The synthesis of MOFs is based on predesigned structures and termed as isoreticular chemistry. It uses well-defined and rigid molecular building blocks that

maintain their structural integrity throughout the construction process. However, another approach used is that of well-defined conditions like pH, type of solvent and temperature, which results in the in situ formation of building blocks. The resultant materials were termed as IRMOFs (Isoreticular Metal-Organic Frameworks) by Yaghi and co-workers. The forces of attraction for MOF can be strong metal-ligand bonding or by weaker bonding forces such as hydrogen-bonding and π- π interactions.[38]

IRMOF materials are prepared in a self-assembly process in which each oxide-centered Zn_4O tetrahedron is linked by six carboxylate molecules forming a three-dimensional cubic porous network. Hundreds of MOFs have been reported so far with different central metal atoms and organic ligands. Fig. 1.4 shows the schematic representation of the self-assembly process from corner and bridging units, building blocks and the resulting three-dimensional frameworks of different IRMOF materials.

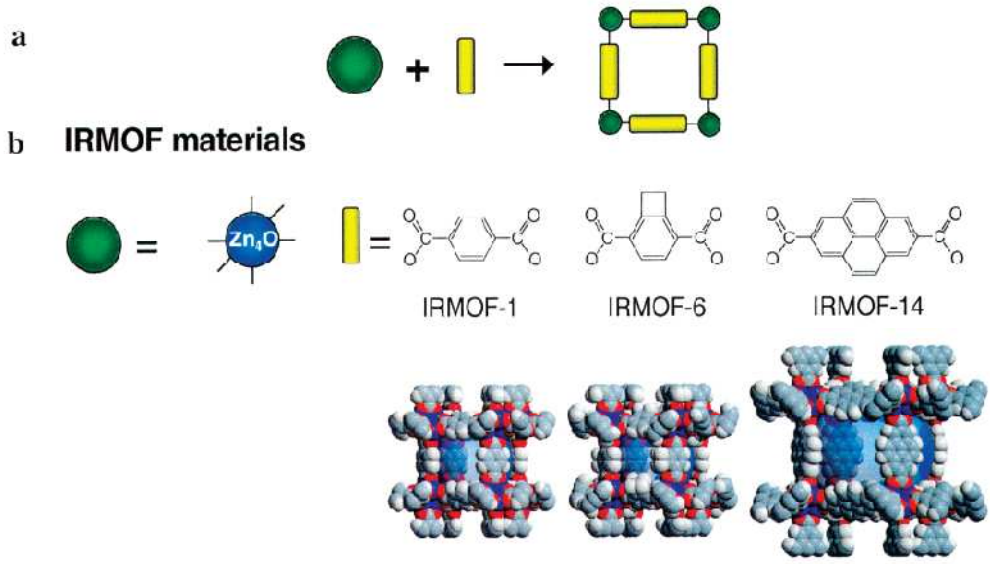

Fig. 1.4 Structures for IRMOF-1, IRMOF-6 & IRMOF-14[39]

IRMOFs exhibit high surface areas (IRMOF-177 is claimed to have surface area up to 4500 m^2 g^{-1}), defined structure and easy processing. They have generated increasing interest due to their potential applications in gas storage, catalysis and gas separation.[40, 41]

1.4 Polymers of Intrinsic Microporosity (PIMs)

Recently there has been an effort to develop microporous polymers by connecting rigid ladder-like components with units that force the backbone to twist or turn. This results in inefficient packing of the polymers chains in the solid state leading to microporous structure. These materials synthesized first at the University of Manchester were named as “polymers of intrinsic microporosity” (PIMs). The PIM materials can be conveniently subdivided into two types: 3-D network polymers that are insoluble ***(Network PIMs)*** and others that are soluble into organic solvents and can be processed into useful forms like casting into membranes ***(Non-Network PIMs).*** [42, 43]

1.4.1. Network PIMs

Metalloporphyrins and Metallophthalocyanines are known for their biological and catalytic activity. If these compounds are linked to rigid non-planar units, the resultant structure will be the one in which these macrocycles will point to different directions and generate free volume. Based on this approach, initially phthalocyanine and porphyrin macrocycles were linked to a spiro-center containing linker and amorphous, glassy network polymers were obtained. These materials show high apparent surface areas (500–1000 m^2 g^{-1}) by nitrogen adsorption at 77 K. These polymers are not soluble in routine organic solvents and are termed Network PIMs. This type of structure helps preventing self-association of the planar macrocycles, creating a microporous network structure due to inefficient packing. Later on, similar materials with hexaazatrinaphthylene (Hatn) were also obtained.[21, 44]

The structures of network PIMs obtained by linking phthalocyanines or porphyrins with rigid spirocyclic spacers are shown in Fig. 1.5. These network polymers are potential candidates for use as heterogeneous catalysts and for selective chemical adsorption due to high accessible surface area. The hexaazatrinaphthylene (Hatn) Network polymer with similar properties is shown in Fig. 1.6.

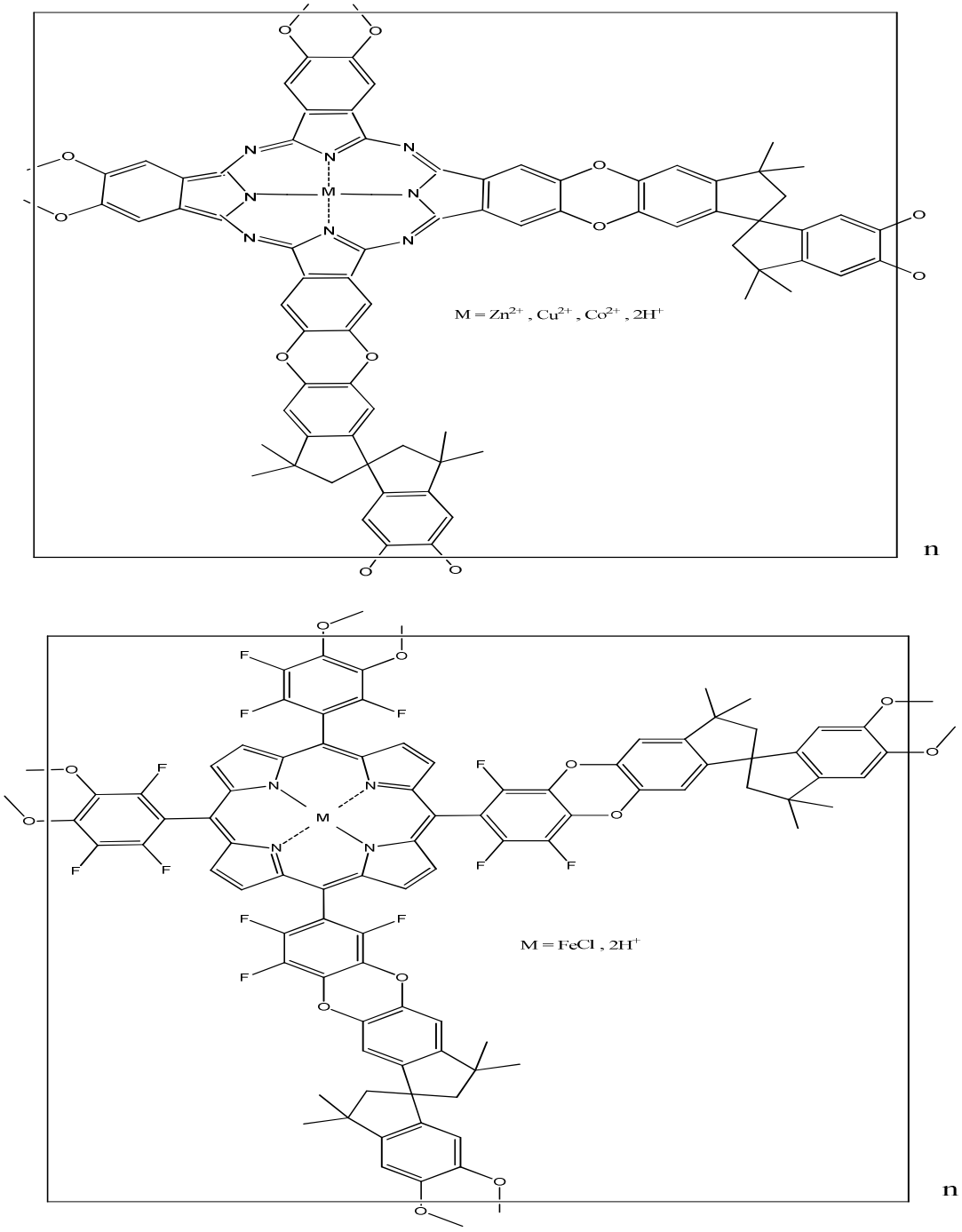

Fig. 1.5 Nanoporous network polymers based on phthalocyanine (above) and porphyrin (below) Macrocycles[45]

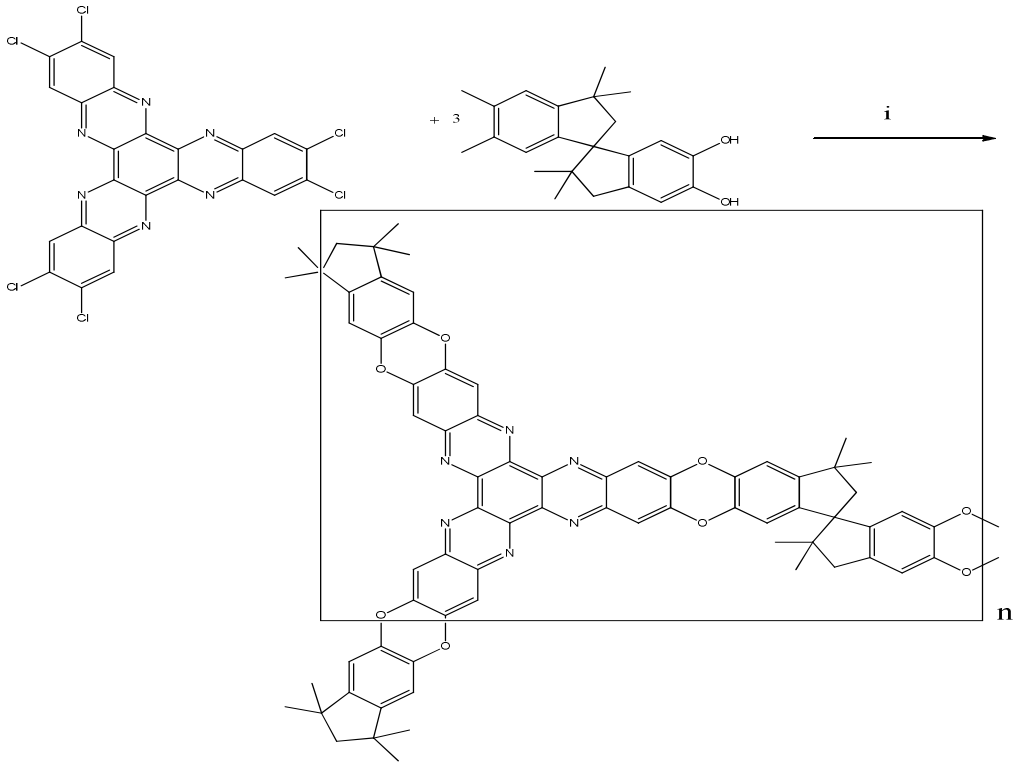

Fig. 1.6 Preparation of the Hatn derived network PIM[46]

.

1.4.2. Non-Network PIMs

Non-network PIM polymers are synthesized by using monomers with highly rigid and contorted structures. These structures do not allow efficient packing in the final microporous product. An important aspect of the non-network PIMs is their easy processing using solvent-based techniques and solubility in solvents like Chloroform and Tetrahydrofuran (THF). The basic reaction involves a tetrol type of monomer reacting with a tetrahalo- unit, resulting in formation of dibenxodioxane linkages through condensation. The reaction is aromatic nucleophilic substitution in nature. Fig. 1.7 represents a model reaction for non network PIM formation.[43]

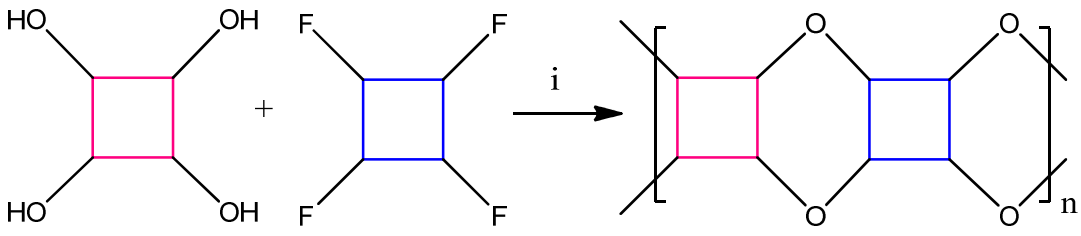

Fig. 1.7 Non-Network PIM formation[43]

Various non-network PIMs can be synthesized depending on starting monomers, however, PIM-1 and PIM-7 are two of the most important materials synthesized and investigated so far. PIM-1 is prepared by reaction of bis-catechol (5,5',6,6' tetrahydroxy 3,3,3'3;' tetramethyl 1,1' spirobisindane) with tetrafluoroterephthalonitrile (TFTPN), K_2CO_3 using solvent DMF at 65 °C under N_2 atmosphere.[43] The polymerization of PIM-1 takes place in 72 to 96 hours, however, recently a Canadian research group has demonstrated an easier synthetic route (reaction time just 6-8 minutes) which involves high shear mixing of monomers and salt in presence of DMAc and heating to 150 °C in N_2 environment.[47] The scheme for synthesis of PIM-1 is shown at Fig. 1.8

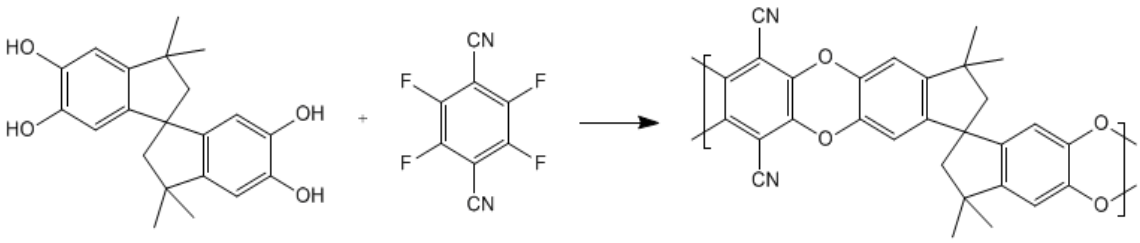

Fig. 1.8 Preparation of PIM-1[43]

Unlike conventional linear polymers that are non-porous materials, as their structural units are efficiently packed, PIMs are formed by monomers possessing a site of contortion due to a spiro centre and result in the formation of microporous structure. Fig. 1.9 portrays a molecular model of PIM-1 showing its randomly contorted macro-molecular shape and the fused ring ladder chain which prevents the efficient filling of the space.[6]

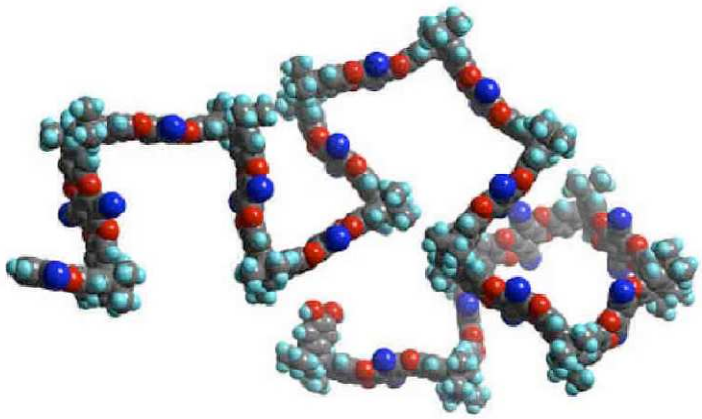

Fig. 1.9 Molecular Model of PIM-1[6]

The PIM materials are ultramicroporous, showing micropore dimensions in the range of 0.4-0.8 nm based on micropore analysis (Horvath–Kawazoe method). They show high thermal stability well above 300 °C without any detectable glass transition or melting point. The Nitrogen adsorption analysis of these materials shows that they possess high surface areas in the range of 700–900 m^2 g^{-1}. They also form stable, transparent and homogenous films on solvent casting onto glass or poly(tetrafluoroethylene) (PTFE) substrates.[43]

1.4.3. Recent developments in PIM research and their potential applications

Synthesis of microporous materials has always been a challenge for researchers, in the sense of minimizing the tendency of open network materials to collapse or deform. The porous structure of these materials tends to collapse when guest or solvent molecules are removed from their pores. In this context the focus has been to devise synthetic strategies capable of producing materials that can sustain porosity. The notable design strategies to produce microporous organic networks include hyper-crosslinked polymer, covalent organic framework and polymers of intrinsic microporosity. One of the main advantages of some PIM polymers, over other microporous materials, is their ability to dissolve in organic solvents and subsequently be processed into thin films by casting from solution. Although some of the covalent organic frameworks have performed better with respect to hydrogen uptake, PIM polymers are promising for applications like catalysis, separation membranes and adsorption due to ease of processing and solubility. [48]

Network polymers of intrinsic microporosity have been derived from triptycene monomers having alkyl groups attached to their bridgehead positions. The length of alkyl chains has been shown to control the adsorption of gas and BET surface area. The microporosity for these network polymers having shorter or branched alkyl chains appeared to be higher than bulky alkyl chains. The triptycene based network PIMS having methyl or isopropyl chains showed high hydrogen uptake due to high concentration of subnanopores. [49]

Synthesis of a microporous cobalt phthalocyanine network PIM has been reported which contains subnanometer pores (0.6-0.7 nm) and has shown efficiency for catalysis of sulphide ions for desulphurization of salt water. [50] PIM-polyimides have shown high surface area and thermal stability. These materials prepared by reaction of diamines of a bis(carboxylic anhydride) produced significantly permeable as well as selective membranes for many gas pairs. [51]

New starting materials for PIM synthesis have been derived from 1,1-spiro-bis(1,2,3,4-tetrahydronaphthalene) where the fused five-membered spirocyclic rings were replaced with six-membered rings. The main objective of this research was to increase the flexibility of the polymer framework in order to increase solubility in a wider range of organic solvents and subsequent improvement for film formation of resultant PIMs. The PIM materials prepared using these monomers have shown good solubility in organic solvents and respectable surface areas. [52]

Another interesting work reported is synthesis of microporous fluoro polymers with intrinsic microporosity (MP1 and MP2) exhibiting high surface area (1050 m^2/g for MP2) and promising hydrogen storage capacity. [53] Gas transport behaviour of PIM-1/silica nanocomposite membranes has been studied. The investigation involved use of density, thermal stability, and nano-structural morphology for changes in free volume and estimation of volume of the void cavities. [54]

FTIR and quantum chemical calculations were carried out to study permeability and permselectivity of polyetherimides and PIMs. It was shown that these properties were sensitive to the presence of low molecular mass compounds (chloroform, lower alcohols and water) capable of hydrogen bonding. [55]

In a very recent development, the structure of PIM-1 has been characterized with X-ray scattering and molecular dynamic simulations. The research presents the first broad scattering vector (q) range X-ray scattering data for PIM-1 and comparison of wide angle X-ray scattering (WAXS) patterns with structure factors calculated from molecular dynamics (MD) simulations. [56]

PIM-1 and PIM-1 copolymers incorporating ethanoanthracene units have been investigated for free volume by N_2 adsorption, positron annihilation lifetime spectroscopy (PALS), Xe sorption and ^{129}Xe NMR spectroscopy. [57] The copolymers were shown to possess microporosity like PIM-1.

PIM-1 has been studied for sensor application by spin coating on Ni-coated metalized polyethylene terephthalate (PET) substrate to a dry thickness of approximately 600 nm and a silver nanoparticle stack layer spin coated onto the PIM layer. The sensor appeared to be broadly responsive for organic vapours that provide vivid shifts in colour at relevant concentrations. [58]

1.5 Synthesis of porous materials by block copolymerization

In order to prepare porous materials from block copolymers, the etchable or labile block should be physically accessible to the solvent, reagent or process utilized for degradation; and the hard block or matrix material should be able to hold the resultant porous structure. Various approaches like nanolithography, nanoporous membranes and monoliths have been used to prepare porous materials based on block copolymerization.[59] The choice of a particular synthesis technique (or combination of these) depends on the polymerization mechanism, the structure of copolymer (di-block, tri-block, multi-block etc), the desired molecular weight range, and the required monodispersity of each block and the purity of end product.[60]

The first porous membrane from a block copolymer was developed in 1988 by Lee et al. A tri-block copolymer of poly(4-vinylphenyl-dimethyl-2-propoxysilane)-*b*-polyisoprene-*b*-poly(4-vinylphenyl-dimethyl-2-propoxysilane) [PPSPI-PPS] with a lamellar morphology was cast into a thin film.[61] In 1989, the same authors prepared membranes for a series of PPS-PI-PPS tri-block copolymers.[62] In 1993, Hedrick et al. synthesized a polyimide based nanofoam containing thermally labile blocks such as poly(methyl methacrylate) (PMMA) or poly(propylene oxide) (PPO) by condensation polymerization. The thermolysis of the labile block above T_g resulted in a porous structure which was ordered yet thermally stable and having low dielectric constants.[63] Mansky et al. reported an important work in 1996 regarding the

preparation of oriented thin films of PS-PBD block copolymers that were degraded by ozonolysis for use as nanolithography masks.[64]

In 1997, Liu et al. reported the synthesis, self-assembly, and hydrolysis of poly(*t*-butylacrylate)-*b*-poly(2-cinnamoylethyl methacrylate) [PtBAPCEMA] diblock copolymers by anionic polymerization. It was shown that a microstructure was formed containing PtBA cylinders hexagonally packed in a PCEMA matrix. Thin films of this material when exposed to UV irradiation resulted in cross-linking of the PCEMA phase.[65] Ozonolysis/degradation process was used by Hashimoto et al. in 1997 for a PS-PI block copolymer / PS homopolymer blend to generate nanoporous films. The morphology of the block copolymer precursor was unique and the film adopted bicontinuous morphology with the so-called gyroid phase. The films were cast by evaporation from toluene and the film thickness of the blend was also significant (100-300 μm).[66]

Park et al. used Block Copolymer Lithographic approach when this group used a PS-PI or PS-PB block copolymer spin coated on a SiN substrate which was subsequently annealed. Using the established O_3 degradation technique, the authors showed that the polydiene phase was etched out leaving behind a mask that had periodic material density contrast as a result of the porous structure. Subsequent reactive ion etching (RIE) resulted in anisotropic etching of the substrate. SEM analysis of the etched film proved that the holes were approximately 20 nm in diameter with a period of about 40 nm. [67]

An extensive amount of literature was published in the late nineties and post 2000 period about nanoporous membranes. Some important examples include preparation of porous membranes based on PI-PCEMA-PtBA triblock copolymer,[68] PS-*b*-poly-4-vinylpyridine (PVP) block copolymer and pentadecyl phenol (PDP),[69] supramolecular complex containing PSPVP and an alkylsulfonate Zn(II) complex zinc dodecylbenzenesulfonate [$Zn(DBS)_2$] [70] and PS-PVP block copolymer with 2-(4-hydroxybenzene-azo)benzoic acid (HABA) spin cast as a thin film onto a silicon wafer (and a gold coated silicon wafer).[67]

1.6 Polyethylene Glycol (PEG) and its copolymers

Polyethylene glycol (PEG) is a neutral polyether and can be linear or branched and exists in various molecular weights. It appears to be a simple molecule yet it has generated a great deal of interest due to its non toxic nature and ability to react with other molecules or polymers.[71] The structure of a monofunctional PEG molecule is $HO\text{-}(CH_2CH_2O)_n\text{-}CH_2CH_2\text{-}R$ (where R = OH, alkyl or aryl group).

At molecular weights less than 1000, PEG usually occurs as a viscous, colourless liquid. However, higher molecular weight PEG can be a waxy, white solid. Oligomers / polymers are known both as poly(ethylene glycol) as well as poly(ethylene oxide), where the former normally refers to a molecular weight of less than 50000 and the later refers to more than this molecular weight.[72] PEG can be prepared with a methoxy group at one end, however PEGs with various functionalities and purities have been prepared and are available.[73]

In addition to well known PEG-poly(propylene oxide) (PPO) copolymers, PEGs have been widely used for preparation of copolymers like polyethylene glycol–polylactic acid (PEG–PLA) block copolymer, [74] Polyurethane- PEG copolymers,[75] PEG-poly(acrylamide) copolymers,[76] and PEG-poly(methylmethacrylate) (PMMA).[77]

1.7 Adsorption

The properties of a liquid in the bulk and near an interface are always different. There is always a change in composition near an interface for a binary polymer solution. *An increase in concentration of the solute in the interfacial region is known as adsorption.* Adsorption that involves formation of a chemical bond is known as *chemisorption* and the one involving only physical forces of attraction is known as *physisorption*. In some cases there is a decrease in concentration of solute near interface, which is referred as *negative adsorption or depletion*. Occurrence of both (adsorption or depletion) depend on net adsorption energy of polymer segments.[78]

1.8 Adsorption isotherms

It is necessary for the adsorption process that the adsorbent and adsorbate are in contact for a sufficient time period. During that contact, equilibrium will be established between the amount of adsorbate adsorbed and the amount of adsorbate in solution. An adsorption isotherm is the graph between the amounts of adsorbate (x) adsorbed on the surface of adsorbent (m) and pressure (if gas) or concentration at constant temperature. There are various types of adsorption isotherms based on Freundlich, Langmuir and BET theories.[79]

The dynamic equilibrium between adsorption and desorption of adsorbate, *X*, (e.g., gas or solute) onto an adsorbent, *M*, can be shown as follows:

$$X + M_{surface} \Leftrightarrow XM_{surface} \tag{1}$$

If we define the ratio of number of adsorption sites occupied to the number of available sites (or surface coverage) as (θ) and rate constants of adsorption and desorption as k_a and k_d respectively, then the rate of change of surface coverage for a adsorption step will be

$$\left[\frac{d\theta}{dt}\right]_{ads} = k_a f_a(C,\theta) \tag{2}$$

Where f_a is an adsorption function depending on the concentration of adsorbate *(C)* and the surface coverage. Similarly, for desorption step

$$\left[\frac{d\theta}{dt}\right]_{des} = k_d f_d(C,\theta) \tag{3}$$

Where f_d is desorption function. At dynamic equilibrium, it can be inferred from above equations:

$$\frac{k_d}{k_a} = \frac{(d\theta/dt)_{des}}{(d\theta/dt)_{ads}} \tag{4}$$

The above equation was further simplified and rearranged in the light of Langmuir postulates.

$$\theta = \frac{KC}{(1+KC)} \qquad (5)$$

Where *C* is concentration of gas molecules (or pressure) and *K* is defined as k_a/k_d. It is important to mention that Langmuir isotherm is based on monolayer coverage, sites equivalence and sites independence.[80] A plot of θ vs. *C* gives the shape of the Langmuir isotherm. A typical Langmuir isotherm is shown in Fig. 1.10.

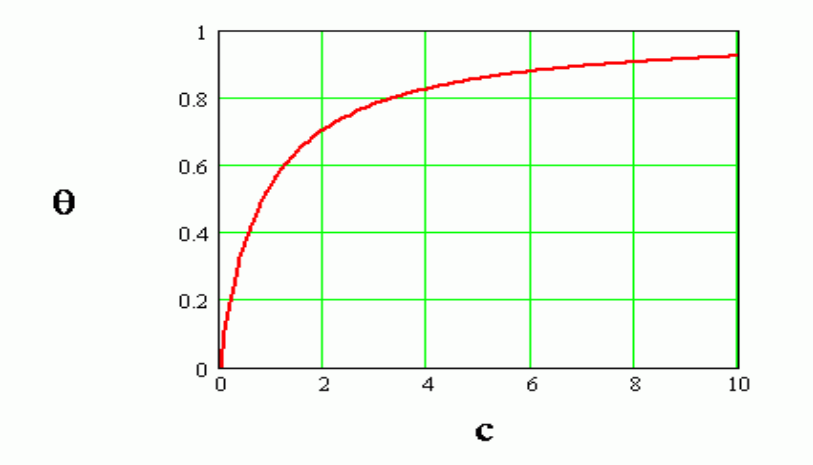

Fig. 1.10 Typical Langmuir Isotherm plot[81]

Freundlich's equation (or isotherm) is based on an empirical expression which represents the isothermal variation of adsorption of a quantity of gas adsorbed by unit mass of solid adsorbent with pressure. The equation is as under

$$kp^{1/n} = \frac{x}{m} \qquad (6)$$

In this equation x is the mass of the gas adsorbed on mass m of the adsorbent at pressure p, while k and n are constants whose values depend upon adsorbent and gas at particular temperature. Taking log on both sides of equation, we get

$$\log k + \frac{1}{n}\log p = \log\left(\frac{x}{m}\right) \tag{7}$$

This is a straight line equation and a plot of log(x/m) and *p* should result a straight line.[59] A typical Freundlich's isotherm is given in Fig. 1.11.

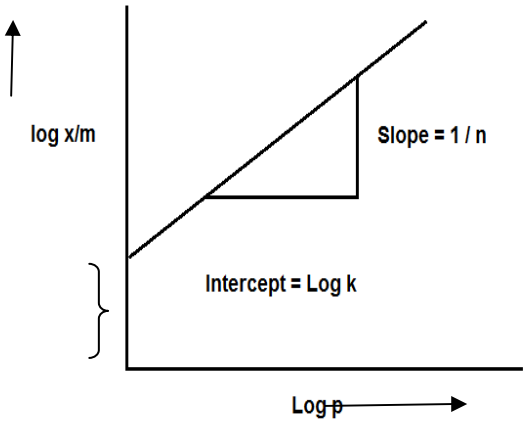

Fig. 1.11 Typical Freundlich Isotherm plot[82]

Stephen Brunauer, Paul Hugh Emmett, and Edward Teller extended Langmuir model to develop a new model for multilayer systems, which in now known as BET adsorption desorption model (or isotherm). Their equation is given below:

$$\frac{1}{v[(p_0/p)-1]} = \frac{c-1}{v_m c}\left(\frac{p}{p_0}\right) + \frac{1}{v_m c} \tag{8}$$

Where *p* is equilibrium and p_0 is the saturation pressure of adsorbates at a particular temperature. While *v* is the amount of gas adsorbed, v_m is the monolayer adsorbed gas quantity and *c* is the BET constant and is related to heat of adsorption for the first layer (E_l) and enthalpy of liquefaction (E_L) of the gas.

$$C = \exp\left(\frac{E_I - E_L}{RT}\right) \tag{9}$$

A plot of $1/v[(p_0/p)-1]$ vs p/p_0 should ideally give a straight line with slope c-$1/v_m c$ and $1/v_m c$ as intercept. From slope and intercept v_m can be calculated.[83]

$$v_m = \left(\frac{1}{slope + \text{int}\, ercept} \right) \qquad (10)$$

Fig. 1.12 gives various types of shapes possible for BET isotherm based on different values of E_l and E_L.

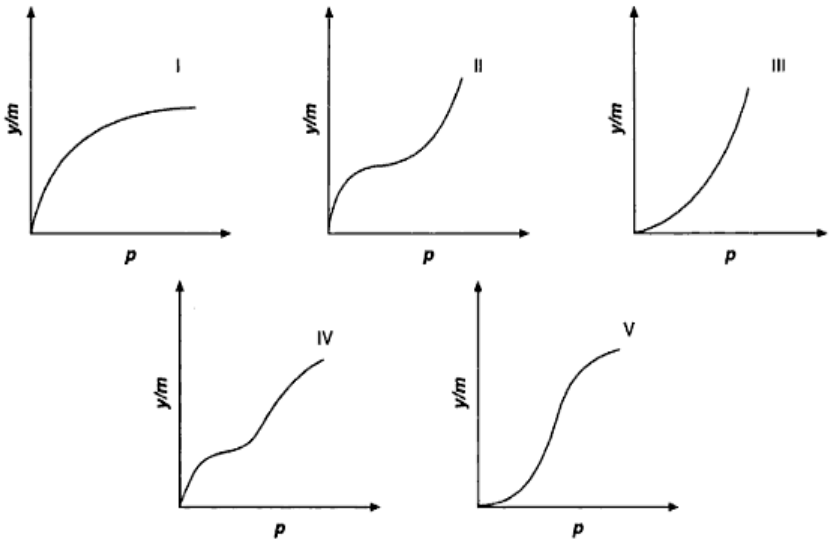

Fig. 1.12 Various shapes of adsorption isotherms[53]

Type I isotherms show adsorption of a monolayer and can be explained by the Langmuir Adsorption Isotherm. Langmuir model assumptions include: all adsorption sites are equal; adsorbed molecules do not interact; adsorption follows same mechanism; and at maximum adsorption only monolayer is formed. These conditions are rarely met in reality; however, this problem is addressed by BET model, which accounts for multilayer formation. There is a sharp uprise in adsorption at low p/p^0 value due to micropore filling and then plateau indicating small amount of multilayer adsorption. This adsorption phenomenon is related to microporous materials. This can be further subdivided into adsorption exhibited by ultramicroporous materials (pores of molecular dimensions) and supermicroporous materials (wider micropores). Ultramicroporous materials experience micropore filling at very low p/p^0 while

supermicroporous materials do the same at relatively wider range of p/p^0 values. If p/p^0 value is very low in BET equation and BET constant c has high values, it leads to monolayer formation. Adsorption of N_2 on charcoal at low temperatures is a typical example for this type of isotherms.

Type II isotherms deviate significantly from Langmuir isotherms. This type of adsorption behaviour is exhibited by nanoporous and macroporous materials. However, sometimes mircoporous materials also show this phenomenon. The value of BET constant *c* is much higher in this case, due to higher enthalpy of adsorption for monolayer. The intermediate region of the curve reflects adsorption of monolayer. Typical examples for Type II isotherms include N_2 adsorbed on iron catalyst or silica gel at low temperatures. Type III isotherms also deviate from the Langmuir model, with a very low value of BET constant *c*. This type of isotherm shows multilayer formation. This type of adsorption is characteristic of nanoporous and macroporous materials, however, with weak interaction energy between adsorbate and adsorbent compared to Type II isotherms. Adsorptions of Br_2 or I_2 on silica gel are good examples of type III isotherms.

Type IV isotherms involve formation of monolayer followed by multilayer. This is typical of mesoporous materials with gradual adsorption at low p/p^0 and uprising in intermediate region. There is also a visible adsorption hysteresis due to capillary condensation. Benzene adsorbed on iron oxide or silica gel refers to this type of isotherm. Type V isotherms are shown by nanoporous materials with weak adsorbate – adsorbent interaction. It is similar to type IV and also shows capillary condensation of gas. A good example of this type of isotherms is adsorption of water vapours on charcoal. [84]

1.9 Fluorescence

Emission of light from any substance (occurring in its excited electronic state) is called ***luminescence***. Depending upon the nature of excited states, the phenomenon of luminescence can be further divided into two types: fluorescence and phosphorescence. ***Fluorescence*** corresponds to the relaxation of the molecule

from the singlet excited state to the singlet ground state with emission of light. ***Phosphorescence*** is the relaxation of the molecule from the triplet excited state to the singlet ground state with emission of light. The average lifetime for fluorescence ranges from $<10^{-10}$ to 10^{-7} s from singlet states, while for Phosphorescence the average lifetime is 10^{-5} to 10^{+3} s from triplet excited states. Hence fluorescence is quite faster than phosphorescence.[85]

The quantum efficiency of a fluorescence process can be expressed in terms of quantum yield. It is defined as:

$$\text{Quantum Yield} = \phi = \frac{\text{No. of quanta emitted}}{\text{No. of quanta absorbed}}$$

The higher value of Φ will represents higher fluorescence. While a non fluorescent molecule will have zero or very close to zero value of Φ, making it impossible to measure the fluorescence. A schematic diagram representing a diatomic molecule is shown in Fig. 1.13 below.

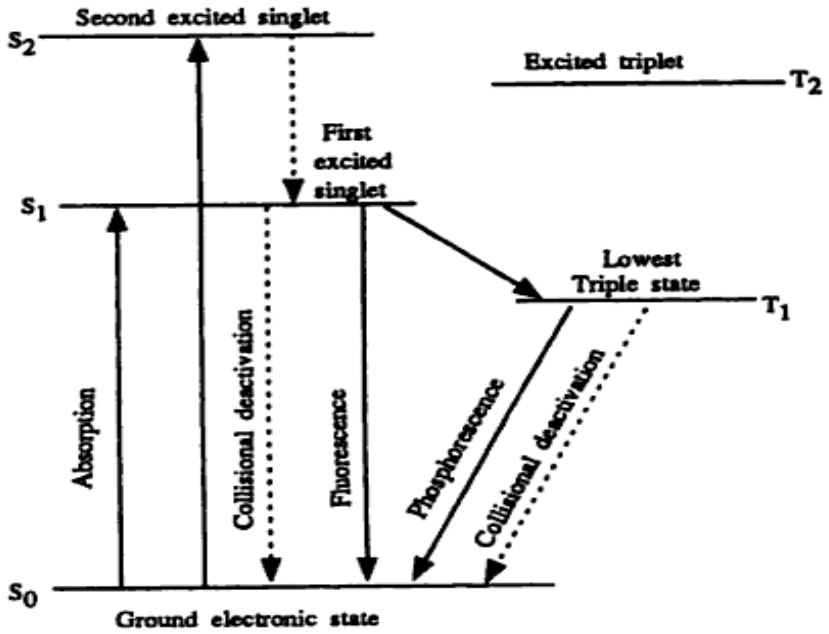

Fig. 1.13 Schematic Energy Level (Jablonski) Diagram for a diatomic molecule[55]

Fluorescence efficiency of a molecule is reduced due to a process known as quenching. Quenching is defined as reduction of fluorescence by a competitive deactivating process resulting from a particular interaction of fluorophore and other substances present in the system. There are many reasons of quenching but more important are temperature, concentration, oxygen and impurities.[86]

1.10 Conclusion and objectives of project

Porous materials have always fascinated the material scientists as they pose synthesis and processing challenges and find many commercial applications due to their pore structure. These materials can contain macro, meso or micro size pores, for applications like catalysis, hydrogen storage, separation of liquids/gases or sensor devices. Research work on traditional porous materials like oxide molecular sieves, porous carbons and sol-gel derived oxides is known for many decades, with appropriate synthetic routes and relevant applications. More recently, chemists and material scientists have focussed on new novel porous materials like metal organic frameworks (MOFs), heteropolyanion salts and organic microporous polymers.

Polymers of Intrinsic Microporosity (PIMs) are a relatively new class of organic polymers, with rigid and contorted backbone and composed of fused ring components, resulting in microporosity. PIMs are available both as insoluble network and soluble non-network polymers and exhibit high internal surface area (BET = 500-1100 m^2/g). PIMs are easy to process and transformed to membranes by casting through solvent. They have been investigated for applications for heterogeneous catalysis, hydrogen storage, separation membranes and chemical sensors.

The way forward in latest PIM research is synthesis of PIM-polyimides and copolymers of PIMs for alteration of porosity, blending of PIMs with appropriate polymers and spectroscopic studies for sensor application. The present PhD project envisages synthesis of fluoro terminated PIM-1 oligomers for copolymerization with poly(ethylene) glycol monomethyl ether (MeOPEG), blending of PIM-1 with MeOPEG and impact of copolymer compatibilizer and fluorescence studies in presence of various solvent vapours for sensor application.

In order to achieve the overall aim, the objectives were set as: (1) To prepare PIM-1 and its flouro-ended (F-PIM-1) oligomers of various molar masses and their characterization for subsequent blending studies and copolymerization respectively (Chapter-2). (2) Coupling of F-PIMs with MeOPEG and characterization, for modifying PIM pore structure to improve permeability and selectivity for liquids/gases (Chapter-3). (3) Investigating Surface Activity of products for insight to adsorption

(Chapter-4). (4) Preparing Polymer Blends of PIM-1 and check effectiveness of copolymers as compatibilizers for change in pore structure (Chapter-4). (5) N_2 adsorption studies for PIM-1, FPIMs and copolymers to check changes in surface area and pore structure (Chapter-4). (6) Adsorption of PIM-1 by MeOPEG in aqueous solution for subsequent thermal removal of MeOPEG and change in porosity (Chapter-4). (7) Fluorescence studies on PIM-1 and copolymers in presence of various solvent vapours for sensing applications and developing solvent profile based on wavelength / intensity changes (Chapter-5).

References

(1) Budd, P. M. *Science,* **2007**, *316*, 210-211.

(2) Sing, K. S. W.; Weitkamp, J. *Handbook of Porous Solids;* Wiley-VCH: Vol. 1, 2002; pp 1-10.

(3) Lu G. Q.; Zhao X. S. *Nanoporous Materials – Science and Engineering,* Imperial College Press: Vol. 4, 2004.

(4) Barton, T. J.; Bull, L. M.; Klemperer, W. G.; Loy, D. A.; McEnaney, B.; Misono, M.; Monson, P. A.; Pez, G.; Scherer, G. W.; Vartuli, J. C.; Yaghi, O. M. *Chem. Mater.* **1999,** *11*, 2633-2656.

(5) Davis, M. E. *Nature,* **2002,** *417,* 813-821.

(6) Budd, P. M.; McKeown, N. B.; Fritsch, D. *J. Mater. Chem.,* **2005,** *15,* 1977–1986.

(7) Bruinsma, P. J.; Kim, A. Y.; Liu, J.; Baskaran, S. *Chem. Mater.,* **1997,** *9,* 2507–2512.

(8) Velev, O. D.; Jede, T. A.; Lobo, R. F.; Lenhoff, A. M. *Nature* **1997,** *389,* 447–448.

(9) Stein, A. *Microporous Mesoporous Mater.,* **2001,** *44–45,* 227–239.

(10) Miller, R. D. *Science*, **1999,** *286,* 421–423.

(11) Tang, Z. K. et al. *Science*, **2001,** *292,* 2462–2465.

(12) Zhao, X. S. *J. Mater. Chem.,* **2006,** *16,* 623–625.

(13) Meier, W. M. *Pure & App. Chem.* **1986,** *58(10)* 1323-1328.

(14) Sherman, J. D. *Proc. Natl. Acad. Sci. USA* **1999,** *96,* 3471–3478.

(15) http://izasc.ethz.ch/fmi/xsl/IZA-SC/ftc_main_image.xsl?-db=Atlas_main&-lay=fw&STC=LTA&-find (last visited 19-05-2011).

(16) Zhao, X. S.; Su F.; Yan Q.; Guo W.; Bao, X. Y.; Lv, L.; Zhou Z. *J. Mater. Chem.* **2006,** *16,* 637–648.

(17) Wang, Y. X.; Tan, S. H.; Jiang, D. L. *J. of Mater. Sc. Letters* **2003,** *22,* 1343 – 1345.

(18) McEnaney, B.; Rand, B. *Brit. Ceram. Trans*. **1985,** *84,* 157.

(19) Patrick J. W. *Porosity in carbons. Characterisation and applications;* Edward Arnold London: 1995.

(20) Rodriguez, R.; Thrower, P A; *Chemistry and physics of carbon,* Marcel Dekker: vol. 21, 1995.

(21) Budd, P. M.; Ghanem, B.; Msayib, K.; McKeown, N. B.; Tattershall, C. *J. Mater. Chem*., **2003,** *13,* 2721–2726.

(22) Juntgen, H.; Knoblauch, K.; Harder, K. *Fuel* **1981,** *60*, 817.

(23) Sircar, S.; Golden, T. C.; Rao, M. D. *Carbon* **1996,** *34*(1), 1-12.

(24) Suzuki, M. *Carbon* **1994,** *32*, 57.

(25) Dahn, J. R.; Zheng, T.; Liu, Y. H.; Xue, J. S. *Science* **1995,** *270*, 590.

(26) Zheng, T.; Xue, J. S.; Dahn, J. R. *Chem. Mater*. **1996,** *8*(2), 389-393.

(27) Liu, Y. H.; Xue, J. S.; Zheng, T.; Dahn, J. R. *Carbon* **1996,** *34*, 193.

(28) Attia, S. M.; Wang, Jue; Wu, Guangming; Shen, Jun; Ma, Jianhua; J. *Mater. Sc. Technol*. **2002**, *18,* 211-218.

(29) Segal, D.L. *Journal of Non-Crystalline Solids* **1984,** *63,* 183-191.

(30) Iler, R. K. *The Chemistry of Silica*; Wiley: New York, 1979.

(31) Reisfeld, R. *Opt. Mat.* **2001,** *16 (1-2),* 1-7.

(32) Gregg, S. J.; Sing, K. S. W. *Adsorption, Surface Area and Porosity*, *2nd ed.* Academic Press: London, 1982.

(33) Okuhara, T.; Mizuno, N.; Misono, *M. Adv. Catal.* **1996,** *41*, 113-252.

(34) Kozhevnikov, I.V. *Russian Chemical Reviews (Translated from Uspekhi Khimii)* **1987,** *56,* 1417-1443.

(35) Misono, M. *Chem. Commun.* **2001,** 1141–1152.

(36) Ito, T.; Song, I. K.; Inumaru, K.; Misono, M. *Chemistry letters* **1997,** *26 (8)* 727-728.

(37) James, S. L. *Chem. Soc. Rev.* **2003,** *32,* 276–288.

(38) Yaghi, O. M.; O'Keeffe, M.; Ockwig, N. W.; Chae, H. K.; Eddaoudi, M.; Kim, J. *Nature*, **2003,** *423,* 705-714.

(39) Duren, T.; Sarkisov, L.; Yaghi, O. M.; Snurr, R. Q. *Langmuir* **2004,** *20,* 2683-2689.

(40) Chae, H. K.; Siberio-P., Diana Y.; Kim, J.; Go, Y.; Eddaoudi, M. Matzger, A. J.; O'Keeffe, M.; Yaghi, O. M. *Nature* **2004,** *427,* 523-527.

(41) Ferey, G.; Mellot-Draznieks, C.; Serre, C.; Millange, F. *Acc. Chem. Res.* **2005,** *38,* 217-225.

(42) McKeown, N. B.; Budd, P. M.; Msayib, K. J.; Ghanem, B. S.; Kingston, H. J.; Tattershall, E. C.; Makhseed, S.; Reynolds, K. J.; Fritsch, D. *Chem. Eur. J.* **2005,** *11,* 2610 – 2620.

(43) Budd, P. M.; Ghanem, B. S.; Makhseed, S.; McKeown, N. B.; Msayib, K. J.; Tattershall, E. C. *C h e m . C o m m u n.* **2004,** 2 3 0 – 2 3 1.

(44) Mackintosh, H. J.; Budd, P. M.; McKeown, N. B *J. Mater. Chem.* **2008,** *18,* 573–578.

(45) McKeown, N. B.; Makhseed, S.; Budd, P. M. *Chem. Commun.* **2002,** 2780-81.

(46) McKeown, N. B.; Hanif, S.; Msayib, K.; Tattershall, C. E.; Budd, P. M. *Chem. Commun.* **2002,** 2782-83.

(47) Song, J.; Du, N.; Dai, Y.; Robertson, G. P.; Guiver, M. D.; Thomas, S.; Pinnau, I. *Macromolecules* **2008**, *41(20),* 7411-7417.

(48) Maly, K. E. *J. Mater. Chem.,* **2009,** *19,* 1781–1787.

(49) Ghanem, B. S.; Hashem, M.; Harris, K. D. M.; Msayib, K. J.; Xu, M.; Budd, P. M.; Chaukura, N.; Book, D.; Tedds, S.; Walton, A.; McKeown, N. B. *Macromolecules*, **2010,** *43* (12), 5287–5294.

(50) Makhseed, S.; Al-Kharafi, F.; Samuel, J.; Badr, A. *Catalysis Communications*, **2009,** *10(9),* 1284-1287.

(51) Ghanem, B. S.; McKeown, N. B.; Budd, P. M.; Al-Harbi, N. M.; Fritsch, D.; Heinrich, K.; Starannikova, L.; Tokarev, A.; Yampolskii, Y. *Macromolecules*, **2009**, *42* (20), 7881–7888.

(52) Carta, M.; Msayib, K. J.; McKeown, N. B. *Tetrahedron Letters*, **2009,** *50,*5954–5957.

(53) Makhseed, S.; Samuel, J.; Bumajdad, A.; Hassan, M. *J. Appl. Pol. Sc.,* **2008,** *109,* 2591–2597.

(54) Ahn, J.; Chung, W.; Pinnau, I.; Song, J.; Du, N.; Robertson, G. P.; Guiver, M. D. *J. Membr. Sci.,* **2010,** *346,* 280–287.

(55) Yampolskii, Y.; Alentiev, A.; Bondarenko, G.; Kostina, Y.; Heuchel, M. *Ind. Eng. Chem. Res.*, **2010,** *49* (23), 12031–12037.

(56) McDermott, A. G.; Larsen, G. S.; Budd, P. M.; Colina, C. M.; Runt, J. *Macromolecules*, **2011,** *44,* 14–16.

(57) Emmler, T.; Heinrich, K.; Fritsch, D.; Budd, P. M.; Chaukura, N.; Ehlers, D.; Ratzke, K.; Faupel, F. *Macromolecules*, **2010,** *43* (14), 6075–6084.

(58) Rakow, N. A.; Wendland, M. S.; Trend, J. E.; Poirier, R. J.; Paolucci, D. M.; Maki, S. P.; Lyons, C. S.; Swierczek, M. J. *Langmuir,* **2010,** *26*(6), 3767–3770.

(59) Hillmyer, M. A. *Adv. Polym. Sci.* **2005,** *190,* 137–181.

(60) Riess, G. *Prog. Polym. Sci.* **2003,** *28,* 1107–1170.

(61) Lee, J.; Hirao, A.; Nakahama, S. *Macromolecules* **1988,** *21,* 274-276.

(62) Lee, J.; Hirao, A.; Nakahama, S. *Macromolecules* **1989,** *22,* 2602-2606.

(63) Hedrick, J.; Labadie, J.; Russell, T.; Hofer, D.; Wakharker, V., *Polymer* **1993,** *34(22),* 4717-26.

(64) Mansky, P.; Harrison, C. K.; Chaikin, P. M. *Appl. Phys. Lett.* **1996,** *68(18),* 2586-2588.

(65) Liu, G.; Ding, J.; Guo, A.; Herfort, M.; Bazett-Jones, D. *Macromolecules* **1997,** *30,* 1851-1853.

(66) Hashimoto, T.; Tsutsumi, K.; Funaki, Y. *Langmuir* **1997,** *13,* 6869-6872.

(67) Park, M.; Harrison, C.; Chaikin, P. M.; Register, R. A.; Adamson, D. H. *Science* **1997,** *276,* 1401-1404.

(68) Liu, G.; Ding, J.; Stewart, S. *Angew. Chem. Int. Ed.* **1999,** *38,* 835-838.

(69) Brinke, G. T.; Ikkala, O. *The Chemical Record*, **2004,** *4,* 219–230.

(70) Valkama, S.; Ruotsalainen, T.; Kosonen, H.; Ruokolainen, J.; Torkkeli, M.; Serimaa, R.; Brinke, G. T.; Ikkala, O. *Macromolecules,* **2003,** *36,* 3986-3991.

(71) Harris, M. J. *Poly(ethylene Glycol) Chemistry – Biotechnical and Biomedical Applications*; Plenum Press: New York, 1992; pp. 1-3.

(72) Atala, A.; Lanza, R.; Thomson, J.; Nerem, R. *Principles of Regenerative Medicine;* Academic Press: Burlington, USA , 2008, pp. 609.

(73) French, A. C.; Thompson, A. L.; Davis, B. G. *Angew. Chem. Intl Ed.* **2009,** *48,* 1248-1252.

(74) Xiao, R. Z.; Zhao Z. W.; Zhou, G. L.; Wang, J. J.; Li, F. Z.; Wang, A. M. Int. *J. Of Nanomedicine* **2010,** *5*, 1057 – 1065.

(75) Taite, L. J.; Yang, P.; Jun. H.; West, J. L. *Journal of Biomedical Materials Research Part B: Applied Biomaterials* **2007**, 1-9.

(76) Auzanneau, F. I.; Christensen, M. K.; Harris, S. L.; Meldal, M.; and Pinto, B. M. *Can. J. Chem.* **1998,** 76(8), 1109–1118.

(77) Wei, Y.; Wang, X.; Gao, J.; Chen, Y. *J. of App. Pol. Sc.* **2010,** *118(2),* 943-949.

(78) Fleer; G.J.; Cohen S. M. A.; Scheutjens J.M.H.M.; Cosgorve T.; Vincent B. *Polymers at Interface,* Chapman & Hall, 1993.

(79) Finenegg, G.H.; *Fundamentals of Adsorption* Engineering Foundation, New York: 1984; pp. 207-218.

(80) Sohn, S.; Kim, D. *Chemosphere* **2005,** *58,* 115-123.

(81) http://www2.stetson.edu/~wgrubbs/datadriven/langmuir/isotherm.gif (last visited 19-05-2011)

(82) http://www.xamplified.com/freundlich-adsorption-isotherm/ (last visited 19-05-2011)

(83) Ghosh, P. *Colloid and Interface Science;* PHI Learning Pvt. Ltd.: 2009; pp. 224-225.

(84) Settler, K. D. *Handbook of Nanophysics – Functional Nanomaterials*; CRC press New York: 2011; pp. 9-5 – 9-7.

(85) Lakowicz, R. J. *Principles of Fluorescence Spectroscopy;* Springer Science Business Media LLC.: 2006.

(86) Guilbault, G. G. *Practical Fluorescence;* Marcel Dekker Inc.: 1990; pp. 6-32.

CHAPTER 2

SYNTHESIS OF PIM-1 AND FLUORO-ENDED PIM-1 OLIGOMERS

2.1. Introduction

It has already been described in section 1.3 that activated carbons and zeolites are conventional porous materials and are being used for numerous commercial applications. Metal organic frameworks (MOFs) have also generated great interest due to ease of processing, large surface areas and potential application for gas storage, separation and catalysis. However, recently new novel materials known as Polymers of Intrinsic Microporosity (PIMs) have got global attention due to their organic nature and microporous structure suitable for various applications. PIM-1 is the most widely known member of this series.

The first objective of the project, as outlined at the start of chapter 1, was to produce high molecular weight PIM-1 and its fluoro endcapped oligomers (F-PIM-1). F-PIM-1 oligomers would be utilized in the next step for coupling to polyethylene glycol monomethyl ether (MeOPEG), while high molecular PIM-1 was required to investigate the interfacial activity, adsorption and fluorescence. For this purpose, it was necessary to understand the polymerization of PIM-1 and F-PIM-1. The PIM-1 synthesis procedure is already established;[1,2] Studies were carried out to repeat and optimize the PIM-1 synthesis. The products formed were analyzed by appropriate techniques. The synthesis of PIM-1 containing excess amount of fluoro monomer (F-PIM-1) was also repeated, following Grant's[3] method, and the product subsequently characterized.

PIM-1 was also prepared by a new method recently reported by a Canadian group[4, 5] that involved application of high shear mixing and high temperature of 155 °C. This method was also successfully applied for synthesis of F-PIM-1 oligomers and both types of products were characterized by appropriate techniques. The effect of changing salts on PIM-1 polymerization was also studied. These studies provided insight into PIM-1 and F-PIM-1 synthesis. PIM-1 synthesis is based on dibenzodioxane ring formation through polycondensation; hence it is important to have a brief introduction about these concepts.

2.1.1. Polycondensation and ladder polymers

Polycondensation is step growth polymerization involving removal of a small molecule like HX, methanol, water or ammonia. One of the most common examples of a polycondensation reaction is the formation of linear polyesters from difunctional terephthalic acid and ethylene glycol. The presence of trifunctional monomers usually leads to formation of branched or network products.[6, 7] The gain in molecular weight is gradual as initially only dimers and oligomers are formed with reactive end groups. These oligomers are converted to large polymer chains with passage of time. Polycondensation reactions require long reaction times and high degree of reaction and result in high molecular weight polymers with high polydispersity.[8. 9]

Normally two routes are used for polycondensation reactions. One involves a monomer having two unlike functional groups on its structure (AB type) and in the second case two different monomers containing identical functional groups in their structure are used (AABB type). An example of the former type is reaction of hydrocarboxylic acids and an example of the latter type is the reaction of diols with dicarboxylic acids.[7] Fig 2.1 shows these two reactions.

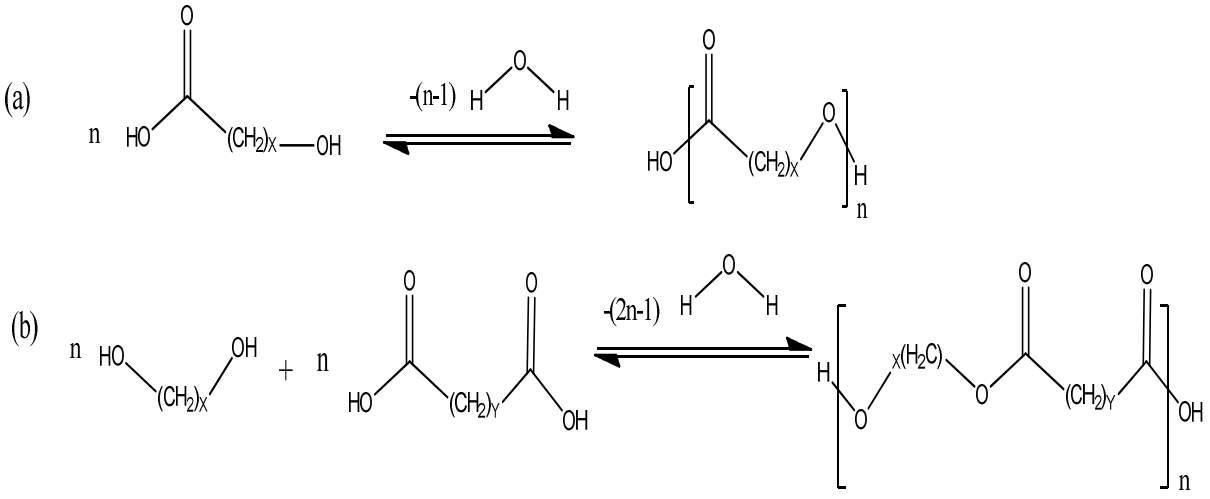

Fig. 2.1 (a) AB type polycondensation (b) AABB type polycondensation

A ***ladder polymer*** is a double strand macromolecule that comprises of constitutional units connected in such a way that adjacent constitutional units are joined to each

other through three or four atoms, two on one side and either one or two on the other side of each constitutional unit. A ***spiro polymer*** is a double-strand macromolecule consisting of an uninterrupted sequence of rings, with adjacent rings having only one atom in common. Alternatively, a spiro macromolecule is a double-strand macromolecule with adjacent constitutional units joined to each other through three atoms, two on one side and one on the other side of each constitutional unit. [10]

Due to the restricted rotation of bonds, the ladder and spiro polymers have high thermal stability and are resistant to chemical degradation. However the rigidity of their structures comes with insolubility or partial solubility in common organic solvents, due to which they can precipitate out before completion of polymerization. Polymers like polybenzoxazole and polyquinoxalines are typical examples of ladder polymers. Fig. 2.2 shows two different types of ladder polymers.

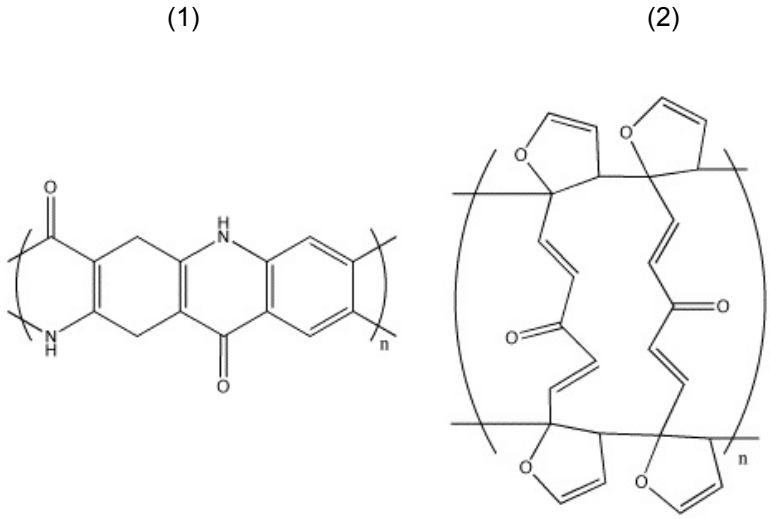

Fig. 2.2 A representation of ladder polymers: (1) Ladder polymer with periodic covalent bonds (2) Ladder polymer with double stranded chain

The Diels Alder reaction has widely been used for synthesis of ladder and semi ladder polymers. The Diels Alder reaction is a reaction between a diene and a dienophile molecule resulting in an adduct with a ring structure. When diene and dienophile are part of a ring system, their reaction results in a polycylic product. This is apparent from the reaction of 2-vinyl butadiene and benzoquinone.[11] (Fig. 2.3).

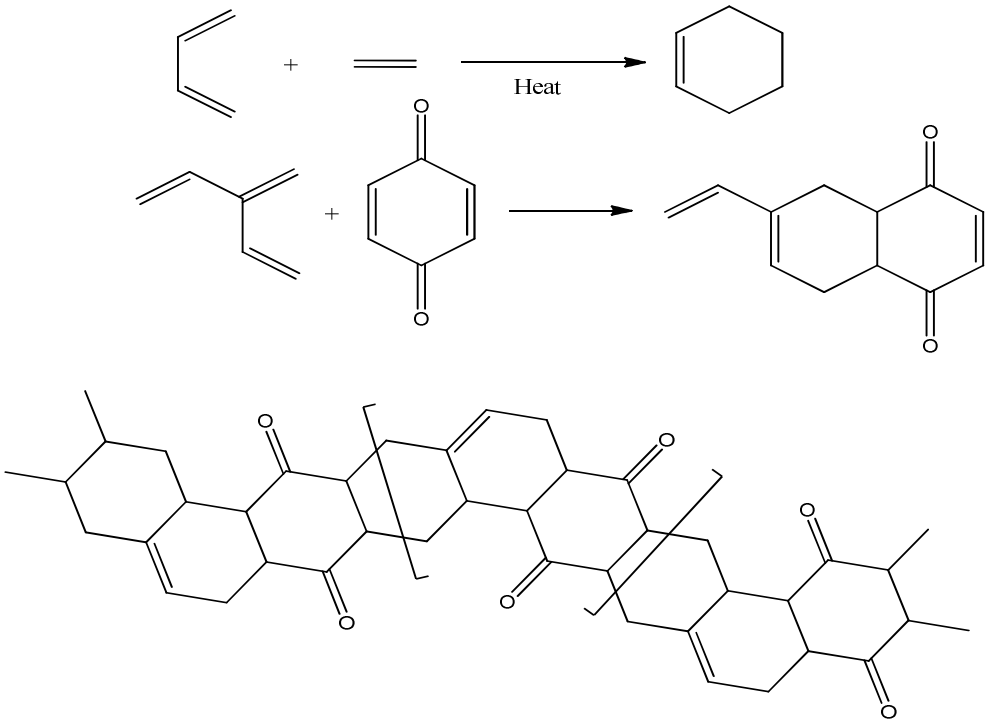

Fig. 2.3 (a) Diels Alder Reaction (b) Reaction of 2-vinyl butadiene and Benzoquinone

Apart from the Diels Alder reaction, other routes for synthesis of ladder polymer include reactions of aromatic tetraamines with aromatic tetraketones, dihalobanzoquinone reactions with aromatic tetraamines and condensation of catechols with tetrahaloaromatic compounds. The last method has found more success than the other two methods,[12] the reason being that dipotassium or disodium salt of catechol in a suitable solvent like DMSO react much better with polyhalogenated benzenes (or heterocycles), giving good yields of the corresponding dibenzo-p-dioxins. [13, 14, 15]

2.1.2. Carothers equation for degree of polymerization

An important equation that relates the number-average degree of polymerization to the extent of reaction and average functionality of a step-growth polymer is known as the Carothers equation.[16] According to this equation the number-average degree of polymerization, X_n, is related to the extent of reaction, p, and average functionality, f_{avg}, of the polymer system as follows:

$$X_n = \frac{2}{2 - pf_{avg}} \qquad (1)$$

The molecular weight of a polymer will be directly proportional to the extent of conversion or the average functionality. Another quantity, the stoichiometric imbalance (*r*) is also related to number average degree of polymerization (X_n) as per following relation:

$$X_n = \frac{1+r}{1-r} \qquad (2)$$

When two dissimilar and reactive difunctional monomers react with molar imbalance, the number-average molecular weight of a polymer can be theoretically determined. In case a monomer is in excess of the other, the end groups in the final product will be the same as that of excess monomer. The stoichiometric imbalance (*r)* for reaction of a difunctional monomer AA with A functional groups and an excess of difunctional monomer BB with B functional groups is defined as:

$$r = \frac{N_A}{N_B} \qquad (3)$$

In this equation N_A represents the moles of A functional groups and N_B is the moles of B functional groups.[16, 17]

2.1.3. Reactions involving dibenzodioxane ring formation

2.1.3.1 Reaction of cyanodifluorobenzenes with catechols

There are three main routes for dibenzodioxane ring formation including acid/base catalyzed condensation of halogenophenols, acid catalyzed coupling of diols and condensation of catechol with halogeno aromatic compounds.[18] Due to direct relevance to PIM synthesis we will focus only on last type. The reaction between a catechol or its dihydroxynaphthlene derivatives with difluorobenzonitriles follows double displacement of fluorine atoms and result in a dibenzodioxane ring by aromatic nucelophilic substitution (S_NAr) reaction. The substitution can either be for

one or both fluorine atoms depending on conditions of the reaction.[19] The reaction scheme is shown in Fig. 2.4.

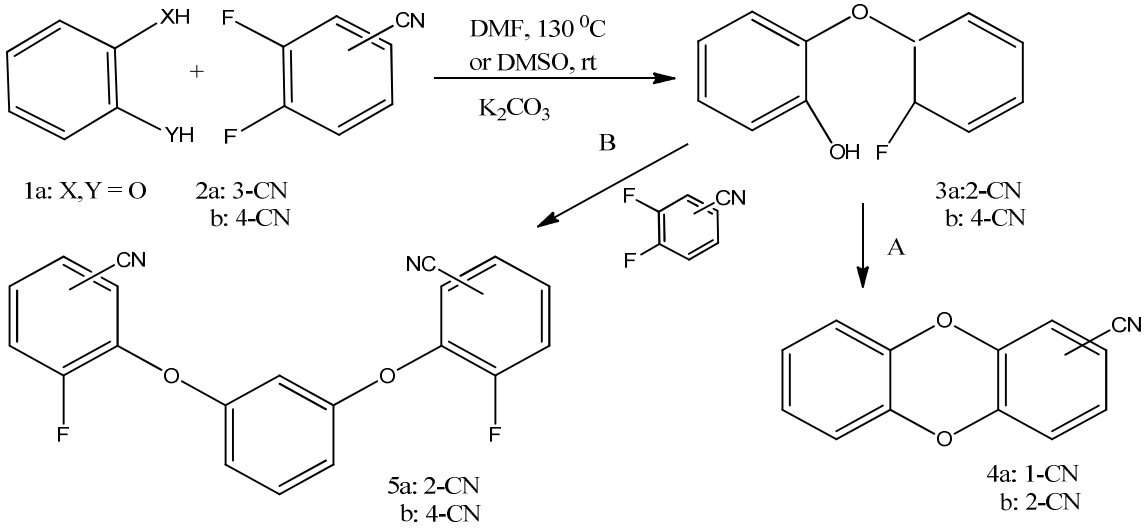

Fig. 2.4 Formation of dibenzodioxanes by reaction of catechols with cyanodifluoronitriles[19]

2.1.3.2 PIM-1 and its oligomers

PIM-1 is one of the most known members of PIM series. It was first prepared at Manchester University by step polymerization reaction of tetrafluoroterephthalonitrile (TFTPN) with 5,5',6,6'-tetrahydroxy-3,3,3',3'-tetramethyl-1,1'-spirobisindane monomer in the presence of a base (potassium carbonate). PIM-1 formation is the result of a double nucleophilic aromatic substitution reaction between these two monomers in presence of the base.[20]

It has a spiro-centre which serves as the site of contortion. Due to this unique structure, it is a thermally stable, amorphous, and glassy polymer. It is soluble in solvents like chloroform, tetrahydrofuran (THF), dioxane and shows a high apparent BET surface area by nitrogen analysis. PIM-1 forms stable membranes when dissolved in chloroform or THF after subsequent slow evaporation of solvent. The

membranes of PIM-1 have been investigated for use in pervaporation and gas separation.[21]

PIM-1 reaction is highly sensitive to stoichiometry and high molecular weight product can only be synthesized by care about molar balance, inert atmosphere and purity of starting materials. Molar imbalance can result in formation of fluoro end capped or hydroxyl end capped products. However, end capped products are also useful for coupling of PIM-1 to other polymers. In the present work, both PIM-1 and fluoro end capped PIM-1 were synthesized and used for coupling and further analysis.[2,3] Fig. 2.5 shows structures for PIM-1 and its fluoro end capped PIM-1 oligomer.

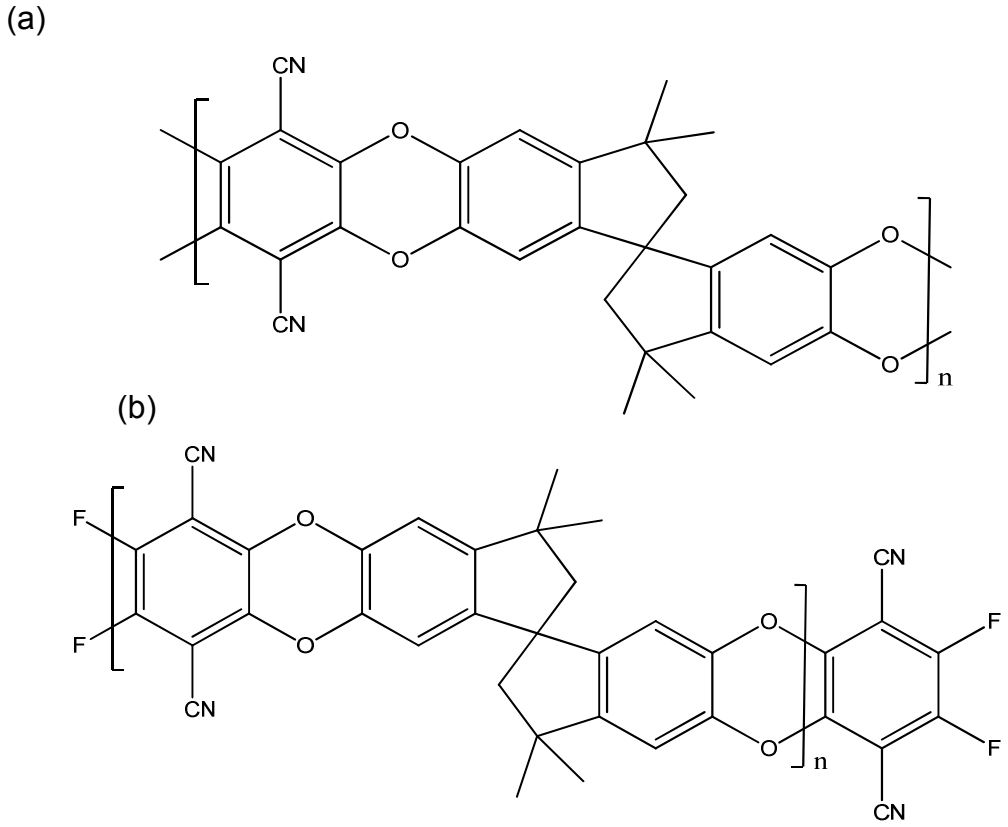

Fig. 2.5 (a) Structure of PIM-1 (b) Structure of Fluoro endcapped PIM-1

2.1.4. Analysis of PIM-1 and Fluoro endcaped PIM-1

PIM-1 and fluoro PIM-1 were synthesized and subsequently analyzed by appropriate techniques. For verification of product formation, techniques like FTIR and NMR

were used with help from other techniques like GPC and MALDI. For BET surface area measurement, nitrogen adsorption was undertaken and degradation behavior was monitored by TGA, Fluorescence work on PIM-1 and oligomers was also undertaken. However, GPC and MALDI analysis was very helpful to have an insight of molecular weight distribution and type of polymers chains present in polymers.

2.1.4.1 Gel Permeation Chromatography (GPC)

It is necessary to have a look at the basics of GPC before discussing the GPC results and comparing them with each other. There are two types of GPC technique in common use nowadays, known as “Conventional or Polystyrene based GPC” and “Multi-detector GPC”.

In conventional GPC, the molecules are separated on the basis of their hydrodynamic volume and then characterized by a detector or series of detectors as they elute from the GPC column. The detector usually employed is a Refractive Index (RI) Detector and/or UV/Vis. The molecular weights and molecular weight distribution are determined from the measured retention volume by means of a calibration curve (log M_W vs. RV), which is set up with a number of polystyrene standards of known molecular weight. It is normally assumed that flow rate is constant during measurement. It is important to select standards that cover the entire Molecular Weight range of the sample to be analyzed. This method gives us a molecular weight distribution, from which weight average (M_w), number average (M_n) and z-average (M_z) molecular weights can be calculated. The limitation of the conventional method is that the molecular weight is dependent on calibration standards like polystyrene. The unknown sample to be analyzed may not have the same hydrodynamic volume as the standard. Hence the results from Conventional Calibration should be referred to as Relative Molecular Weight or 'Polystyrene Equivalent' Molecular Weight.[22] However, the conventional method is still very useful for comparing samples.

The multidetector technique, based on a triple detector system, is considered far better than the conventional technique as it not only gives absolute molecular

weights of the compound but can help to analyze molecular weight distribution, branching, structure and molecular size. Low Angle Light Scattering (LALS) and Right Angle Light Scattering (RALS) help determine absolute molecular weight, while the viscometer detector is important for getting information regarding branching in structure.

2.1.4.2. Matrix Assisted Laser Desorption Ionization Time of Flight (MALDI ToF) Mass Spectrometry (MALDI Analysis)

Matrix Assisted Laser Desorption Ionization Time of Flight (MALDI ToF) Mass Spectrometry is a powerful tool which not only provides the molecular weight distribution in a polymer but also can identify the chain end groups in a polymer sample. MALDI uses short pulses of laser light to form intact gaseous ions of sample analyte molecules that are embedded in a matrix. This energy is absorbed by the matrix and subsequently transferred to sample molecules, hence causing ionization in vapour form. The mixture of ionized matrix and analyte molecule next goes to vacuum of ion source. After a particular time delay, external voltage gets ions out of ion source and packets of ions are accelerated by an electronic potential. As these packets of ions have different charge to mass ratio m/z, so when they enter into a field free drift tube, they do so with different velocities before striking an ion detector. The signal produced by the detector depends on number of ions striking it. This signal is processed and converted to MALDI Spectrum by a special computer programme.[23] Fig. 2.6 illustrates the working of a MALDI equipment.

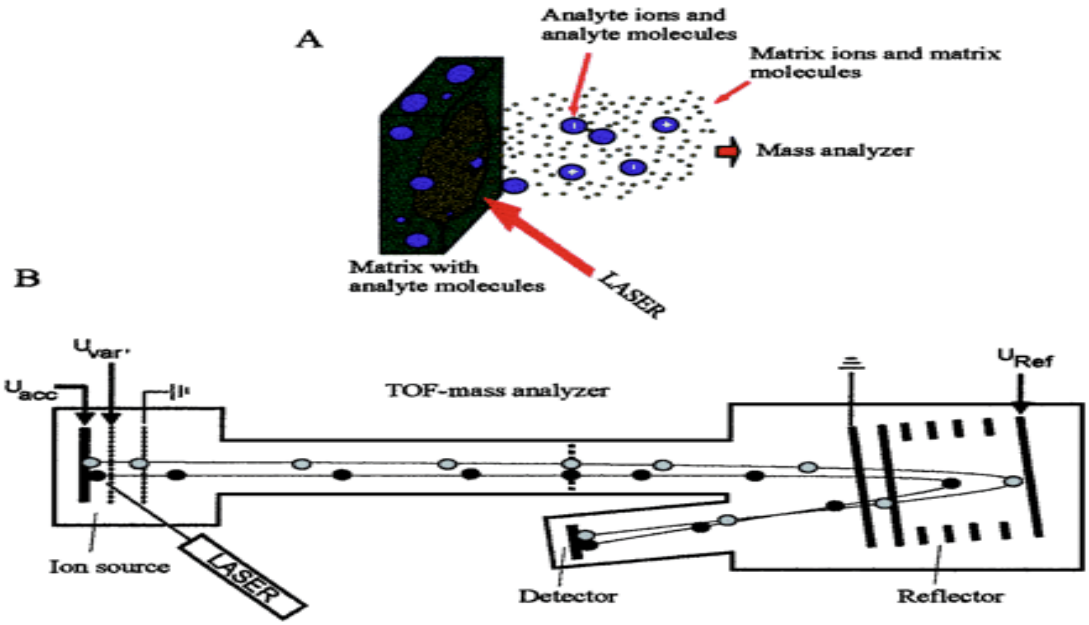

Fig. 2.6 Schematic diagram for a MALDI-ToF Mass Spectrometer[24]

2.2 Experimental

2.2.1 Materials

All starting materials and solvents were purchased from Sigma-Aldrich. In some synthesis of PIM-1 and F-PIM-1 (GP-24, GP-33, GP-39), tetrafluoroterephthalonitrile (TFTPN) was provided by Lanxess Deutschland GmbH. The chemical and solvents were used as received unless otherwise stated.

Analytical grade water was provided from a Millipore Elix 3 water purification system. All glassware and syringes / needles were oven dried at 100 °C overnight and cooled to room temperature under nitrogen before use.

2.2.2 Experimental Techniques

2.2.2.1 Mass measurements

Masses of all the samples were measured using an Oertling NA114 0.1 mg analytical balance.

2.2.2.2 Gel Permeation Chromatography (GPC)

For single detector GPC experiments, 0.2% w/v solutions of polymer samples were prepared in tetrahydrofuran (THF). 3 ml of a material solution in solvent (2 mg/ml) were stirred overnight and filtered through a 0.45 µm syringe micro-filter (Gelman Science). Then 1 drop of the marker was added and sample injected in the column.

Dodecane was used as flow rate marker and the flow rate was kept at 1 mL per minute. The detector and column temperatures were 35 °C and 30 °C, respectively, while the injection volume was 100 µL. The GPC experiments were performed on a Single detector GPC using a Viscotek GPCmax VE2001 instrument, with three 30 cm Polymer Labs PLgel columns (2 x 10 µm MIXED-B and 1 x 10 µm 500 Å) along with a Viscotek 3580 refractive index detector. Calibration was against a series of polystyrene standards (600-1,800,000 Daltons).

Some samples were analyzed by a Multidetector GPC system. The analysis was carried out on Viscotek triple-detector GPC system fitted with two ViscoGEL HHRM columns in series. The mobile phase was Chloroform at a flow rate of 1 ml/min, and 100 µl injected. The calibration of GPC system was done with narrow dispersed polystyrene standard (96K Dalton). The samples were dried in vacuum oven before preparation of the solution. For sample preparation, 9 mg of material was dissolved in 5 mL of chloroform by stirring overnight. The solution once prepared was filtered using a 0.45 µ filter.

2.2.2.3 Fourier Transform Infrared (FTIR) Spectroscopy

The samples were prepared by dissolving 2mg/mL of compound in tetrahydrofuran (THF) and evaporated as thin film on sodium chloride plates. FT-IR spectra were recorded on a Perkin Elmer RX1 FT-IR spectrometer in the range 600 - 4000 cm^{-1}.

2.2.2.4 Nuclear Magnetic Resonance (NMR) Spectroscopy

Samples for Proton Nuclear Magnetic Resonance (^{1}H NMR) were prepared by dissolving 10 mg of polymer per mL of $CDCl_3$. The samples were run on a Varian INOVA 300 MHz spectrometer for obtaining ^{1}H NMR spectra. The chemical shifts were reported as parts per million (δ) using tetramethylsilane (TMS) as internal standard. Some of these samples were also used for ^{19}FNMR spectroscopic analysis.

Samples for ^{13}C NMR were prepared by dissolving 50 - 100 mg of polymer in 2 cm^3 of $CDCl_3$. The 'fast pulse' spectra were recorded on a Bruker 400 and Bruker 500 MHz spectrometers. The chemical shifts were reported in part per million (δ) scale.

2.2.2.5 Matrix Assisted Laser Desorption / Ionization Time of Flight (MALDI ToF) Mass Spectrometry

Samples for MALDI ToF MS spectra were supplied as dry powder. The spectra were recorded on a Micromass TOF Spec 2e spectrometer with a nitrogen laser at 337 nm. The matrix used was either Dithranol or 2-[(2E)-3-(4-tert-Butylphenyl)-2-methylprop-2-enylidene]malononitrile (DCTB), doped with. The analyte was mixed with matrix in volatile solvent tetrahydrofuran (THF) before analysis. MALDI technique can't provide structural information for whole molar mass range of polymer as it has the limitation to detect fractions of polymer with molar mass up to 10000 g/mol.

2.2.2.6 Thermogravimetric Analysis (TGA)

Thermal analysis was carried out using TA Q5000 V3.1 build 246 equipment. About 10-15 mg of sample were loaded in aluminum or platinum pans and weight loss as a function of temperature was measured with heating rates of 10 °C, 5 °C or 3 °C per minute. The analysis was carried out for different samples of PIM-1, TFTPN

endcapped PIM-1 and MeOPEG. The flow rate of N_2 and air was 10 mL/min and 25 mL/min for balance and sample respectively.

2.2.2.7 Nitrogen Sorption Measurement

The sorption experiments were carried out on a Coulter SA 3100 Surface Area and Pore Size Analyzer. The samples were initially degassed for 960 minutes at 110 °C under high vacuum. Nitrogen adsorption / desorption isotherms were recorded at 77 K and the BET Surface Areas were accordingly calculated.

2.2.2.8 Electron Ionization and Chemical Ionization (EI/CI) mass spectroscopic analysis

Samples for EI/CI mass analysis were provided as solid powder. The Mass spectra were recorded on a Micromass Trio 2000 (EI/CI) instrument.

2.2.3 Purification of 5,5',6,6'-tetrahydroxy-3,3,3',3'-tetramethyl-1,1'-spirobisindane (THSB)

5,5',6,6'-tetrahydroxy-3,3,3',3'-tetramethyl-1,1'-spirobisindane (BCA) (20.42 g, 60 mmol) was dissolved in 300 mL methanol and heated to boiling on a hot plate. After an hour of stirring and boiling, the volume of the solution was reduced to about half and solid particles started appearing. The solution was then removed from the hot plate and put on stirring at room temperature. 300 mL of dichloromethane (DCM) was added in solution with constant stirring. The solution was then left in fumehood for overnight recrystalization. After 24 hours, white solid THSB was crystallized in the bottom of flask. The solid was collected by vacuum filtration and dried for 72 hours in the oven. The net weight of BCA after recrystalization was 12.1 g (59.4%).

2.2.4 Purification of Tetrafluoroterephthalonitrile (TFTPN)

Tetrafluoroterephthalonitrile (TFTPN) (11.75 g, 58.75 mmol) was placed in a conical flask and 75 mL dichloromethane (DCM) was added to it. The solution was stirred and refluxed for about an hour until its volume was reduced to 40% of the original volume. At that point the solid TFTPN particles started to appear in solution. The solution was removed from the hot plate and allowed to cool and recrystalize overnight in fumehood. The white solid was then filtered and dried for 72 hours in vacuum oven. The weight of recrystalized TFTPN was 10.37 g (88.3%). It still appeared light brownish, whereas the pure product should be white. The recrystalization process was repeated and this time the product was white solid with net weight of 8.8 g (74.7%).

2.2.5 Synthesis of Model Compound (3,13-dicyanobenzo-1,2,4',5'-bis-1,4-benzodioxane)

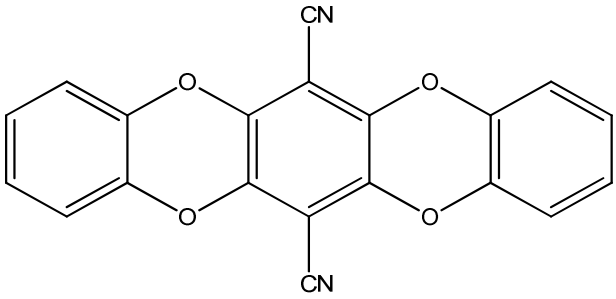

Figure 2.7 Structure of Model Compound

1.00 g (5 mmol) of tetrafluoroterephthalonitrile (TFTPN) was mixed with 1.10 g (10 mmol) of pyrocatechol (1,2-dihydroxybenzene) and 4.14 g (29.96 mmol) of K_2CO_3 (2.07 g, 14.98 mmol) in a 2-neck round bottom flask. To this mixture was added DMF (40 mL) and stirred at 65 °C under nitrogen atmosphere. A yellow precipitate appeared immediately. The reaction was allowed to proceed for 24 hours. The reaction mixture was allowed to cool to room temperature. The precipitate was collected by vacuum filtration and washed with 200 mL of acetone and filtered again. The precipitate was filtered again and put in a vacuum oven for drying overnight. The weight of crude product was 1.512 g (72%). The crude product was added to 500 mL of water and heated to 100 °C to remove the base. The solution mixture was filtered

through vacuum filtration and dissolved in 500 mL of chloroform and heated up to 55 °C to obtain a supersaturated solution. The final product after recrystallization and subsequent vacuum filtration was a bright yellow powder that was dried in a vacuum oven. The weight of product was 1.3 g (62%).

2.2.6 PIM-1 Synthesis

2.2.6.1 PIM-1 Synthesis by Conventional Method

As per standard procedure for synthesis of PIM-1, 10 mmol (2.00 g) of tetrafluoroterephthalonitrile (TFTPN) were mixed with 10 mmol (3.40 g) of 5,5',6,6'-tetrahydroxy-3,3,3',3'-tetramethyl-1,1'-spirobisindane (BCA) in a 250 mL RB flask (2-neck) and 65 mL DMF was added to it. The reaction mixture was heated to 65 °C and stirred under nitrogen atmosphere. The base K_2CO_3 (11.05 g, 80 mmol) was added to the flask and reaction was allowed to proceed for 96 hours. The reaction mixture was then cooled to room temperature, added to an excess of distilled water (~ 650 mL) and stirred for an hour. The crude product was collected by vacuum filtration and washed with distilled water (325 mL) and acetone (650 mL). The crude product was dried in a vacuum oven to obtain a bright yellow powder. The weight of crude product was 4.3 g (79.4%).

The crude product was dissolved in 184 mL of THF (40 mL solvent per gram of crude product) and filtered through glass wool to remove any impurities or particulates. The filtered solution was added to a vigorously stirred non-solvent mixture (acetone 368 mL + THF 184 mL). The resultant mixture was stirred for an hour before vacuum filtration. The final product was washed with acetone and the purification step was repeated twice to remove any oligomeric / low molecular weight material or impurities. The product weight was 2.7 g (63.5%).

2.2.6.2 PIM-1 Synthesis by High Shear Mixing (Canadian) Method

15 mmol (3.003 g) of tetrafluoroterephthalonitrile (TFTPN) were mixed with 15 mmol (5.106 g) of 5,5',6,6'-tetrahydroxy-3,3,3',3'-tetramethyl-1,1'-spirobisindane (BCA) in a 250 mL RB flask (3-neck) along with 6.2 g (45 mmol) K_2CO_3, and 25 ml of Dimethylacetamide (DMA). An IKA T50 homogenizer was attached for creating high shear. The setup was then connected to a condenser and placed in an oil bath preheated to 150 °C. Under inert (Nitrogen) atmosphere, the reaction mixture was vigorously stirred (approximately 5000-10000 rpm) for 2 minutes. At that point 20 ml toluene was added into the reaction mixture to increase the solubility of polymer and to remove water. Another 20 mL of toluene were added after 2 more minutes. The reaction was allowed to happen for further 4 minutes before stopping the homogenizer.

The purification of the product was carried out by addition of 250 mL of methanol, which resulted in precipitation of polymer and subsequent vacuum filtration. The crude product was then reprecipitated in a chloroform (500 ml / methanol 250 mL) mixture and filtered through vacuum filtration. The polymer was then mixed with distilled water and heated up to 100 °C for 3 hours to remove any contents of base. The final product obtained by vacuum filtration was a bright yellow in colour and was dried overnight in vacuum oven. The final product was yellow in colour with 71% yield (5.8 g).

2.2.7 Synthesis of Fluoro terminated PIM-1 (F-PIM-1)

2.2.7.1 Synthesis of Fluoro terminated PIM-1 (F-PIM-1) by Conventional Method

PIM-1 was prepared in various molar excesses of TFTPN (5% to 25% molar excess). In a typical experimental process PIM-1 with 15% molar excess of TFTPN was prepared by mixing 5,5',6,6'-tetrahydroxy-3,3,3',3'-tetramethyl-1,1'-spirobisindane (BCA) (1.69 g, 4.98 mmol) and tetrafluoroterephthalonitrile (TFTPN) (1.15 g, 5.73 mmol) and Potassium carbonate (3.45 g, 34.9 mmol) in a 2-neck RB flask under nitrogen. In the next step, DMF (50 mL) was added and the reaction

mixture was heated to 65 °C with continuous stirring. The reaction was allowed to happen for 72 hours under nitrogen. The reaction mixture was allowed to cool to room temperature, added to excess of distilled water (500 mL) and stirred for an hour. The brownish yellow product was collected by vacuum filtration and dried in the vacuum oven. The product weight for F-PIM-1 with 15% molar excess of TFTPN was 2.6 g (92%).

2.2.7.2 Synthesis of Fluoro Terminated PIM-1 by High Shear Mixing (Canadian) Method

5,5',6,6'-tetrahydroxy-3,3,3',3'-tetramethyl-1,1'-spirobisindane (BCA) (5.106 g, 15 mmol) and tetrafluoroterephthalonitrile (TFTPN) (3.451 g, 17.25 mmol) were mixed with potassium carbonate (6.22 g, 45 mmol) in a 3-neck round bottom flask. After addition of 25 mL of DMAc, the setup was connected to a condenser and homogenizer and placed in an oil bath preheated to 150 °C. The reaction was carried out under nitrogen for 2 minutes and then 20 mL of toluene was added. After another 2 minutes, 20 mL of toluene was again added. The reaction was then allowed to continue for a further 4 minutes. The homogenizer was stopped after total 8 minute reaction and the reaction mixture was dissolved in 500 mL of distilled water. The reaction mixture was then heated for 2 hours at 100 °C to remove the base. The precipitate was then filtered using vacuum filtration and the product was dried overnight in vacuum oven. The weight of final product was 6.5 g (75.5%).

2.2.7.3 Synthesis of Fluoro Terminated PIM-1 using Caesium Carbonate

The reaction was carried out as per procedure described in 3.3.1 except that the salt used was changed from potassium carbonate to caesium carbonate and BCA to salt ratio was kept at 1:4 instead of 1:3 in previous experiments. The bright yellow final product had a 75% yield (3.2 g).

2.3 Results and Discussion

2.3.1. Synthesis of PIM-1 by Conventional Step Polymerization and High Shear Mixing methods and characterization

2.3.1.1 Synthesis of model compound

PIM-1 polymerization involves dibenzodioxane ring formation through an aromatic nucleophilic substitution mechanism. It was appropriate to understand the reaction mechanism at a molecular level before proceeding to PIM-1 synthesis. A model compound (GP-15) was prepared as per procedure in experimental section. Tetrafluoroterephthalonitrile (TFTPN) was reacted with 1,2-dihydroxy benzene in molar ratio 1:2 and in presence of K_2CO_3 as base to produce a bright yellow product (3,13-dicyanobenzo-1,2,4',5'-bis-1,4-benzodioxide), which was later recrystallized from chloroform to get the final product. The reaction occurs as below (Fig 2.8).

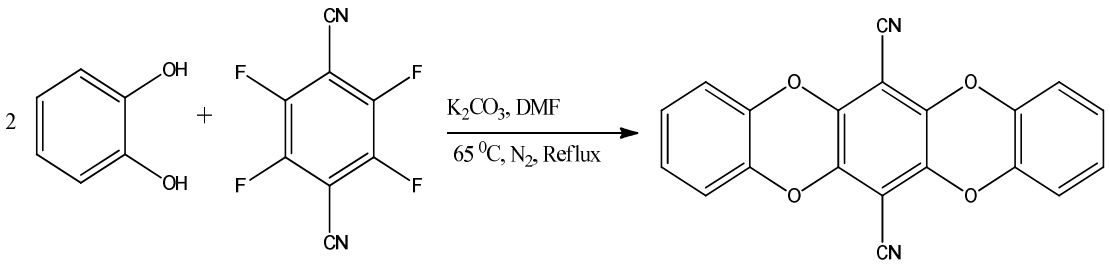

Fig. 2.8 Scheme for reaction of 1,2-dihydroxy benzene with tetrafluoroterephthalonitrile (TFTPN) to form model compound (3,13-dicyanobenzo-1,2,4',5'-bis-1,4-benzodioxide)

The molecular weight of the compound is 340 and the success of the reaction can easily be monitored by carrying out the Electron Ionization and Chemical Ionization (EI/CI) mass spectroscopic analysis. It is quite possible that only one unit of 1,2-dihydroxy benzoic acid is coupled to TFTPN to form a mono-substituted product. The molecular weight for mono-substituted product should be 270. The EI/CI mass spectrum for the model compound is shown in Fig. 2.9.

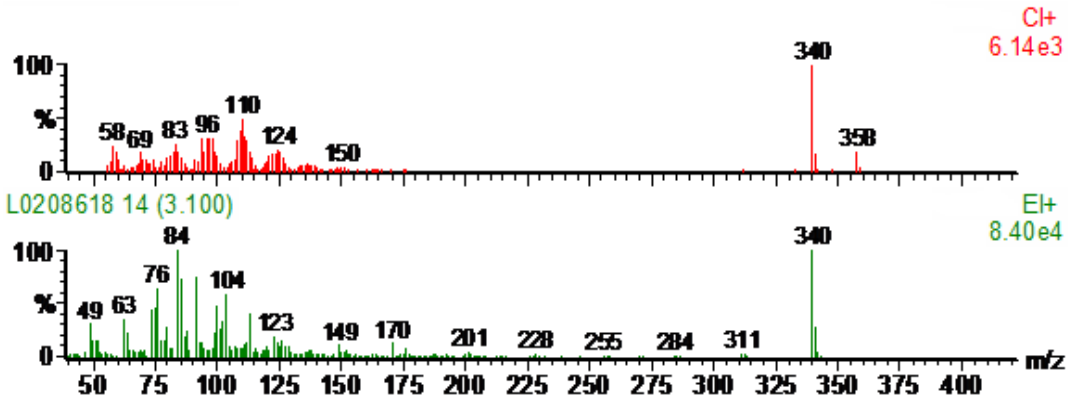

Figure 2.9 Electron Ionization and Chemical Ionization (EI/CI) mass spectrogram for model compound (3,13-dicyanobenzo-1,2,4',5'-bis-1,4-benzodioxide)

It can be seen from mass spectroscopic result that both type of ionizations show a sharp peak at 340 indicating successful synthesis of di-substituted product. There is no peak at 270 indicating that either no mono-substituted product was formed or was washed out during recrystallization. The synthesis of compound was also monitored by FTIR and NMR. Peak of ^{1}HNMR at 7.03 (4H, m, aromatic) and 7.06 (4H, m, aromatic) supported the evidence of successful synthesis. The formation of dibenzodioxane linkage was indicated by absorption band at 1254 cm^{-1} in FTIR analysis corresponding to C-O-C ether linkage. The reaction between a dihalo monomer with catechol follows nucleophilic aromatic substitution mechanism via a Meisenheimer adduct[2, 25], which will be discussed in detail for PIM-1 synthesis. The product was yellow fluorescent solid in good yield.

2.3.1.2 Synthesis and characterization of PIM-1

The model compound study showed that at the molecular level the reaction of dihalo monomers with dihydroxy monomers would result in formation of a dibenzodioxane linkage under suitable reaction conditions. On this basis, the PIM-1 synthesis reaction was performed many times with two different methods. In the conventional step polymerization reaction of PIM-1, tetrafluoroterephthalonitrile (TFTPN) was reacted with 5,5',6,6'-tetrahydroxy-3,3,3',3'-tetramethyl-1,1'-spirobisindane monomer in the presence of a base (potassium carbonate). The solvent used was DMF and reaction was completed in 96 hours at 65 °C under inert atmosphere. The same reaction was also undertaken with a new high shear mixing method, in which DMF

was replaced with DMAc and toluene. The reaction was done at 155 °C and completed in just 6 minutes. Initial attempts by both methods resulted in formation of oligomeric products (GP-2 and GP-33), however, with more care in reaction conditions, purity of solvent and monomers, the polymer was formed with high molar mass (GP-3 and GP-39). In both cases the product was a bright yellow solid and purified as per procedure stated in section 2.2.6. The products formed were characterized by GPC (both polystyrene equivalent and multidetector techniques), ^{1}HNMR, ^{13}CNMR, FTIR and MALDI ToF MS analysis. The GPC results for different samples of PIM-1 are given in Table 2.1.

Table 2.1 Average molar masses of PIM-1 by polystyrene standard and multidetector GPC

Sample	Synthesis method	Product type	Conventional GPC (Polystyrene standards) (Daltons)		Multidetector GPC (Daltons)	
			M_n	M_w	M_n	M_w
PIM-1 (GP-2)	Conventional Step polymerization	oligomer	8820	19400	11700	20600
PIM-1 (GP-3)	Conventional Step polymerization	polymer	18800	98500	18200	76700
PIM-1 (GP-33)	High Shear mixing method	oligomer	18900	44200	15200	46000
PIM-1 (GP-39)	High Shear mixing method	polymer	-	-	33500	81100

Table 2.1 compares molar masses by both conventional step polymerization and high shear mixing method. Both methods resulted in formation of oligomeric as well as high molar mass polymer. Molar masses were initially determined by the conventional GPC method in which polystyrene standards were used, however, multidetector GPC was used to get absolute molar masses of products. It can be seen in Table 2.1 that for oligomer GP-2, M_n and M_w by both polystyrene based GPC and multidetector GPC are in good agreement for products except for GP-3, where M_w by multiple detector GPC appears to be lower than the polystyrene based GPC.

The experiments for these two results were repeated with almost same results again. It can be assumed that the M_w predicted by multidetector GPC in this case is more reliable as it uses three different detectors and is more sensitive while polystyrene based GPC relies on hydrodynamic volume. Fig. 2.10 shows a comparison of multidetector GPC peaks for oligomer GP-33 and polymer GP-39.

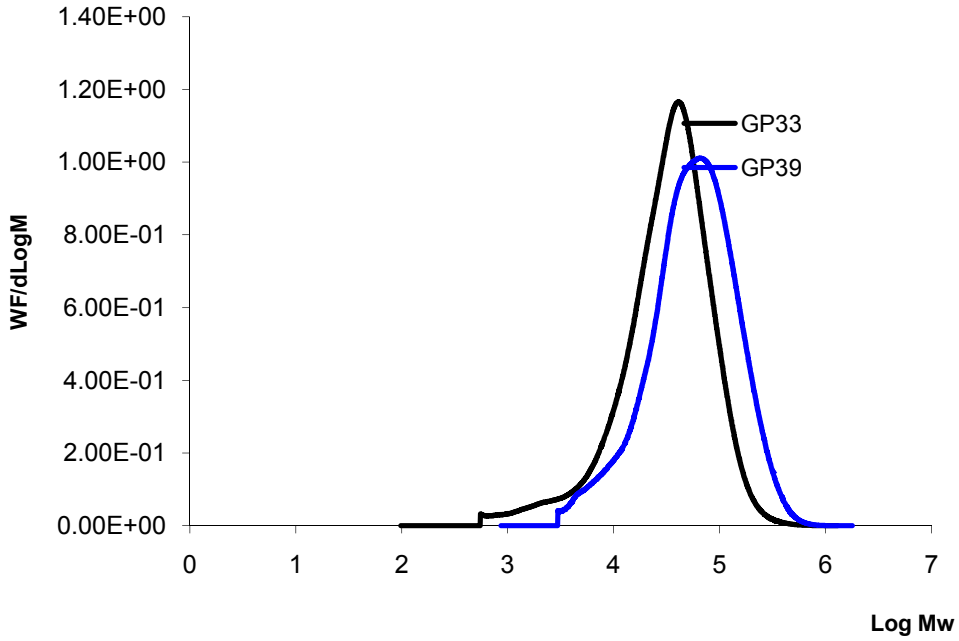

Fig. 2.10 Multidetector GPC plot for PIM-1 (GP33, M_w = 46075 Daltons) and PIM-1 (GP39, M_w = 81108 Daltons)

It can be seen in Fig. 2.10 that PIM-1 (GP-39) exists on high molecular weight area of plot and with molecular weight almost double of the other oligomer PIM1 batch (GP-33). As it would be seen later in chapter on interfacial activity, both polymers PIM1 (GP-3) and PIM-1 (GP-39) were film forming polymers, while both oligomers (GP-2 and GP-33) would not form a self-supported film. This is consistent with normal trend in which polymers of high molar mass are supposed to form films.

PIM-1 polymerization reaction is effectively a two step polycondensation taking place by formation of dibenzodioxane linkage. The reaction is thought to follow a Double Aromatic Nucleophilic Substitution (S_NA_r) mechanism.[2, 26] Catechol monomer (BCA) is deprotonated by the base and attacks the fluoro atom present on the TFTPN monomer. The electron withdrawing nitrile group on TFTPN stabilizes the negative

charge on the intermediate and reaction is completed in two steps for substitution of two fluoro atoms with dioxo linkage. The reaction mechanism is supposed to be S_NAr instead of normal nucleophilic substitution due to the presence of other fluorine atom causing steric hindrance. The model mechanism is given below (Fig. 2.11)

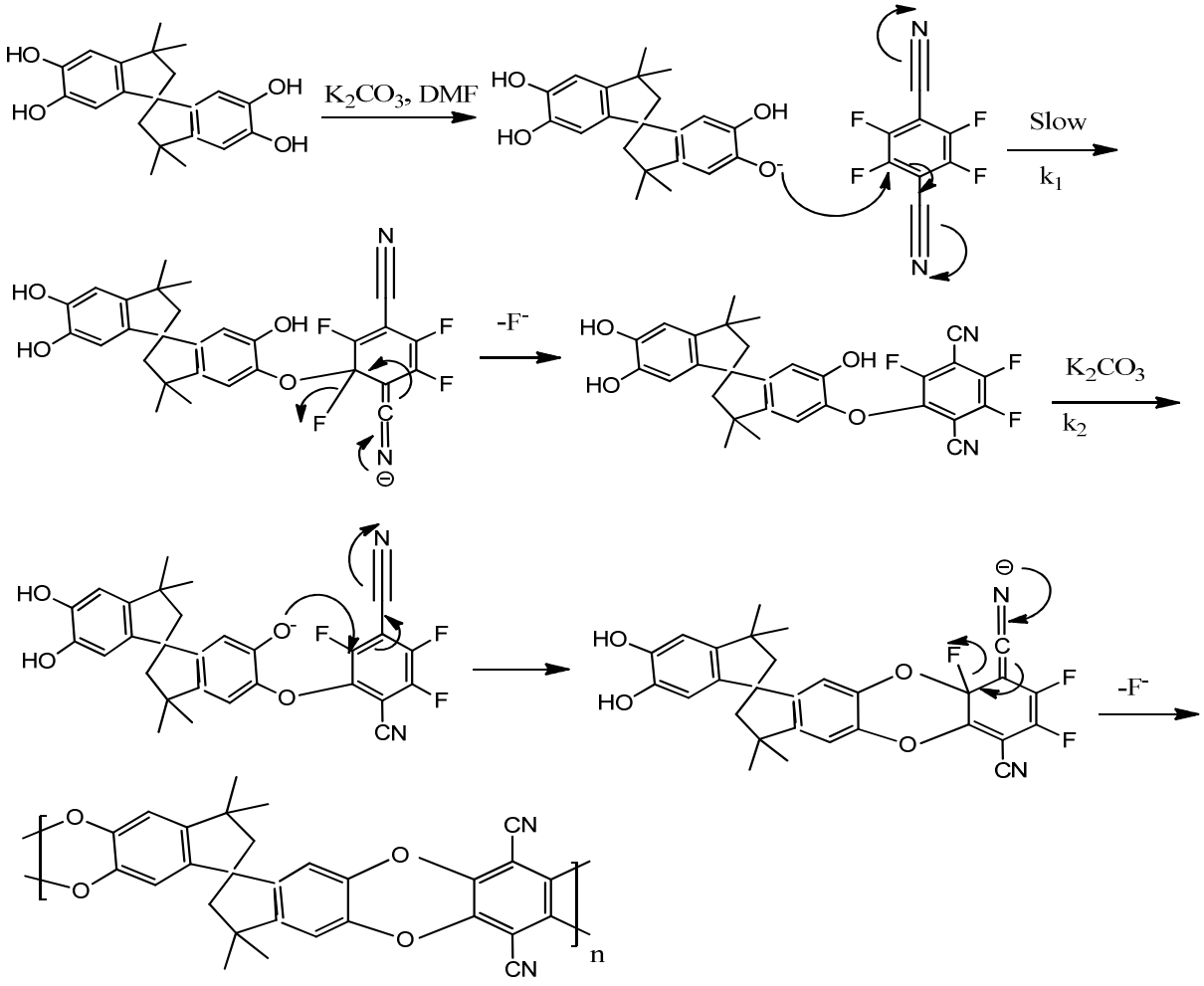

Fig. 2.11 Proposed Reaction Mechanism for Synthesis of PIM-1

The reaction for synthesis of PIM-1 is particularly air/moisture sensitive and the yield is very much affected by the stoichiometry of monomers and purity of solvent. Carothers equation (2) in section 2.1.2 implies that molar mass of a polymer is dependent on molar imbalance and average functionality of the reactants. Using the number average molecular masses for PIM-1 (GP-2) and PIM-1 GP3 (M_n = 18282 Daltons and 11725 Daltons respectively) in Table 2.1 and molecular weight for repeat unit of polymer, *r* values were calculated. Stoichiometric imbalance (*r)* for GP-2 comes out to be 0.962 and that for GP-3 is 0.975. This implies that for the synthesis of GP-2, more weight loss of a monomer resulted in stoichiometric

imbalance and subsequent low molecular mass product. This was personally experienced as the initial two attempts by conventional step polymerization method to synthesize high molecular weight PIM-1 resulted only in oligomeric products. In the third attempt, well dried (72 hours in vacuum oven) monomers along with a new bottle of solvent were used, with particular care to the stoichiometry and inert atmosphere. The final product (GP-3) was a bright yellow powder with high molecular weight. More care was taken later on in synthesis to achieve better products.

The MALDI spectrum can theoretically have following sequences for PIM-1 depending on the product(s) formed. Fig. 2.12 shows the structures of PIM-1 corresponding to various types of MALDI peaks explained below.

(a) $C_n = n(460) + 23$ (cyclic PIM-1 product). Here 460 is repeat unit for PIM, while 23 is mass of Na^+ ion during MALDI analysis.

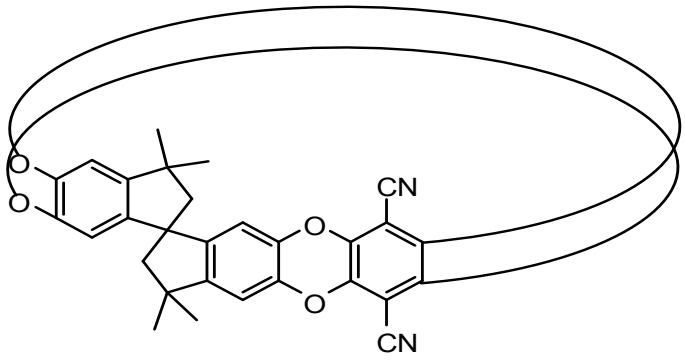

(b) $L_n = n(460) + 23 + 40$ (Linear non cyclic PIM-1). Here 460 and 23 are same as defined above, while 40 is the mass of two each fluorine and hydrogen atoms.

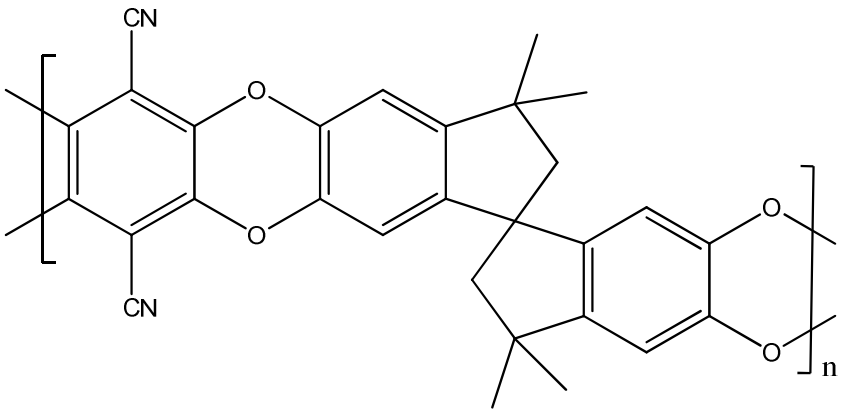

(c) L_F = n(460) + 23 + 200 (TFTPN Endcapped or F-PIM-1). In addition to PIM repeat unit and Na^+ ion, 200 is the mass for TFTPN monomer causing the endcapping.

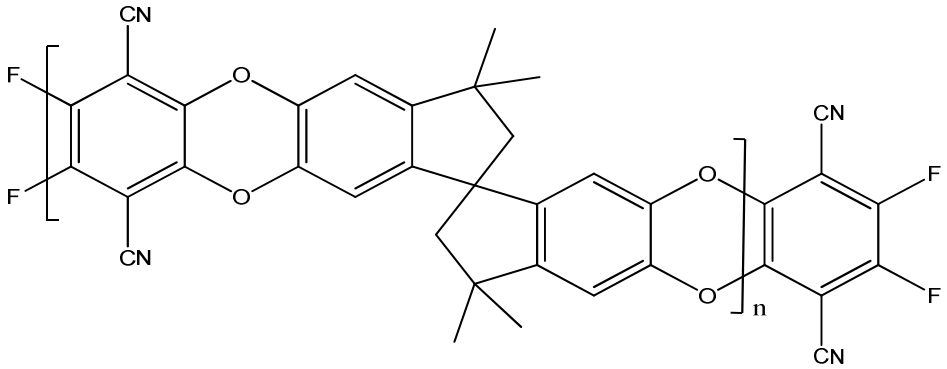

(d) L_B = n(460) + 23 + 340 (THSB Endcapped PIM-1). Here 340 reflect mass of THSB.

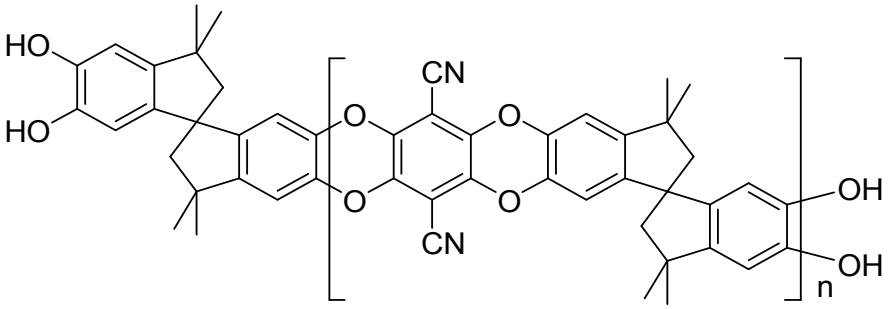

Fig. 2.12 Possible structures for PIM-1 (a) Cyclic, (b) Linear non cyclic, (c) TFTPN Endcapped and (d) THSB Endcapped

The MALDI ToF MS spectrum representing PIM-1 (GP-3) is given in Fig. 2.13. It reveals that almost all of the peaks refer to a cyclic structure. However 2 small peaks could be detected, one (L_8) referring to linear non cyclic PIM1 structure with 8 repeat units and the other (L_{B11}) indicates BCA endcapped PIM-1 structure with 11 repeat units. This suggested that the material was predominantly cyclic in low molar mass region detectable by MALDI technique. The production of cyclic chains in low molar mass region can be explained on the basis of “backbiting degradation”. Although the classical polycondensation theory does not include cyclization reactions, however, the recent research has shown that polycondensation can be thermodynamically or kinetically controlled. Especially when the ring-chain equilibrium is on the side of cycles, there is more probability of cyclic products. Polycondensations of salicylic acid derivatives and polycondensations of dibutyltin derivatives with long *α*-, *ω*-diols or dicarboxylic acids can be referred as important examples in this regard. [27. 28. 29]

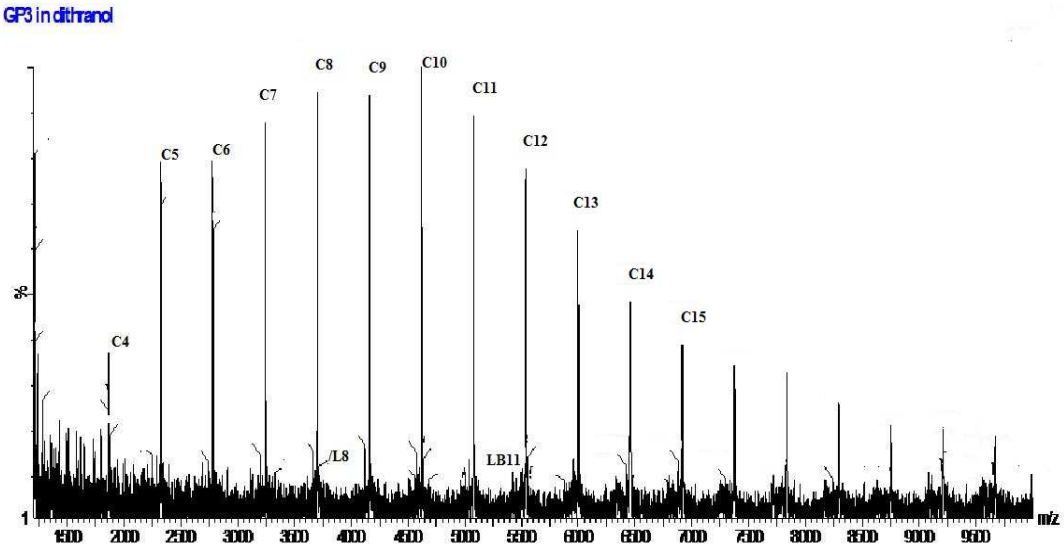

Fig. 2.13 MALDI ToF MS spectrum for PIM1 (GP3). C_n peaks referring to cyclic PIM-1, L_n peaks for linear non cyclic PIM-1, while LB for BCA endcapped PIM-1

In order to verify the synthesis outcome, the obvious step was to do the NMR spectroscopic analysis. Both ^{1}HNMR and ^{13}CNMR analysis were performed for this purpose. NMR showed that the products were successfully synthesized. Table 2.2 summarizes peaks seen in ^{13}CNMR spectrum for PIM-1 (GP3).

Table 2.2 ^{13}C NMR (500 MHz, $CDCl_3$) peaks for PIM-1 (GP-3)

Chemical Shift (ppm) observed	Predicted Carbon Environment
28.89 30.35 30.57	Methyl and Methylene Carbons
42.58	-
56.12	Spiro centre carbon
108.40	C-CN
111.29	Aromatic para carbons
138.19	Aromatic carbon shared with cyclopentyl ring
148.67	C-F

A careful look at the chemical shift values in Table 2.2 reveals relevant peaks for the PIM-1 structure. The peak at 148.67 ppm represents carbon attached to fluorine atoms. The carbon peak at 138.19 ppm represents aromatic ring carbons being

shared with cyclopentane ring. While the peaks at 108.40 ppm and 111.29 ppm are the aromatic carbons attached to CN and para carbons on other aromatic rings. The carbon at 56.12 ppm is the spiro center carbon. The peaks at 28.89 ppm, 30.35 ppm and 30.57 ppm are the methyl and methylene carbon. Hence, the spectrum is overall consistent with PIM-1 structure. The product formation result was also verified with proton NMR spectra and FT-IR results. The same analysis was done for PIM-1 (GP-33) and PIM-1 (GP-39) and found consistent with standard PIM-1 analysis.

The TGA plot for degradation of PIM-1 (GP-3) is given in Fig. 2.14. The TGA analysis was performed with temperature increment of 5 °C per minute in platinum pans.

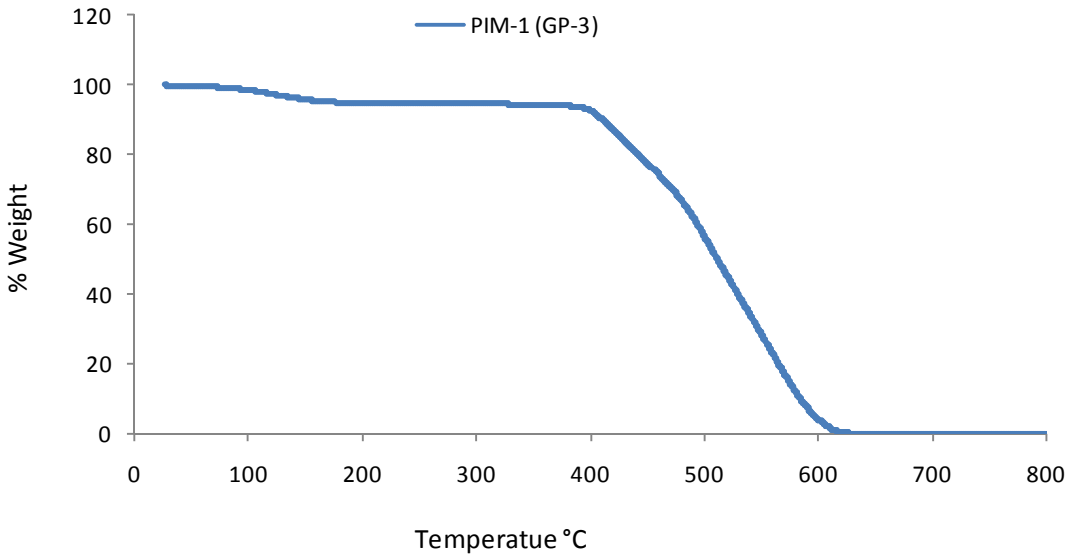

Fig. 2.14 TGA thermogram for degradation of PIM-1 (GP-3)

There was about 4.7% weight loss due to residual solvent / moisture in the sample. After that the PIM-1 starts to degrade gradually starting from 200 °C and continues well above 600 °C and completely degrades at about 640 °C. This shows good stability of PIM-1 due to its rigidity and contorted structure.

Although both the synthetic routes (conventional and high shear) provided good PIM-1 products, however, in general the high shear method appeared to give higher yield

and molar masses compared to conventional PIM-1 synthesis. It appears that the high shear method provides higher surface area for reactivity of monomers, which consequently results in formation high molar mass product. It can be said that the high shear method has a slight edge in the sense that it just requires a few minutes for completion of reaction.

2.3.2 Synthesis of Fluoro Terminated PIM-1 (F-PIM-1) by Conventional Step polymerization and High Shear methods

Synthesis of PIM-1 oligomers having fluorine atoms on either side was necessary to achieve the second objective of the project. The appropriate approach to achieve this goal would be to take TFTPN monomer in excess to the other reactant, which should result in formation of fluoro terminated PIM-1 (F-PIM-1). [3] The approach adopted in this thesis was to synthesize the desired fluoro terminated PIM-1 matrix and also to assess the effect of molar imbalance on product formation. The reaction scheme is given in Fig. 2.15.

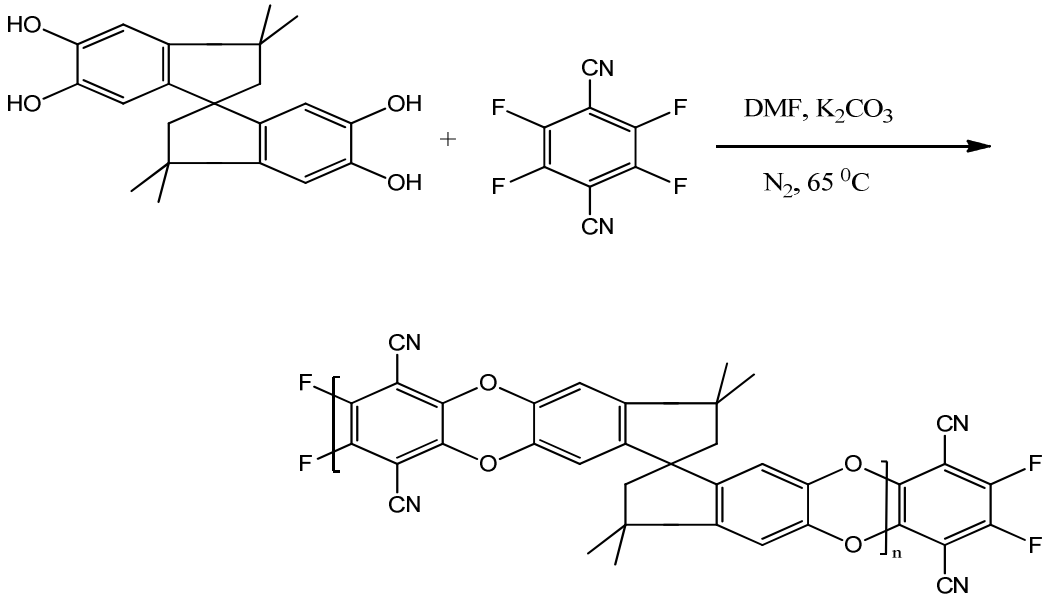

Fig. 2.15 Scheme for Synthesis of F-PIM-1

The reaction was carried out using 5, 10, 15 or 20 % molar excess of TFTPN to BCA monomer. It was later on realized that oligomers formed with 15% molar excess of TFTPN were more appropriate to use for copolymerization.

The above reaction was first carried out by the conventional method, which involved mixing both reactants in solvent (DMF) using K_2CO_3 as salt at 65 °C in a N_2 environment. Initial attempt resulted in formation of a greenish yellow product instead of expected bright yellow product. This indicated formation of a mixture of linear TFTPN endcapped product and conventional PIM-1 (1:1 monomer ratio) along with some side product. Later on in the repeat of this synthesis, the expected bright yellow product was obtained. The same reaction was repeated for successful synthesis of TFTPN endcapped product with either 5% or 10% molar excess of TFTPN monomer. The same reaction was repeated successfully with high shear Canadian method (please refer sections 2.7.4 and 2.7.5 for description of both methods).

The mechanism for formation of TFTPN endcapped product is basically the same as described in case of PIM-1 with the difference that on one side additional TFTPN unit is attached for endcapping of PIM unit.

2.3.3 Characterization of Fluoro Terminated PIM-1 (F-PIM-1) oligomers

It was necessary to carry out GPC, MALDI, FTIR and NMR tests to verify the outcome. In order to analyze the products, Gel Permeation Chromatography (GPC) was performed using polystyrene standards (conventional) analysis. The molar masses obtained by polystyrene based GPC are relative, however, it was envisaged that it will provide a good idea about the molar mass distribution and would be useful for comparison with multidetector GPC data. The molar masses of TFTPN endcapped PIM-1 (F-PIM-1) are given in Table-2.3.

Table 2.3 Molecular weights of PIM-1 by polystyrene standard (conventional) GPC analysis

Compound	Sample Reference	Mol. Mass (Daltons)		M_w / M_n
		M_n	M_w	
F-PIM-1 (05% molar excess)	GP-11 (Conventional)	46,000	50,000	1.1
F-PIM-1 (10% molar excess)	GP-10 (Conventional)	20,000	31,000	1.6
F-PIM-1 (15% molar excess)	GP-6 (Conventional)	4,100	8,100	2.0
F-PIM-1 (15% molar excess)	GP-20 (Canadian)	4,500	8,800	2.0
F-PIM-1 (15% molar excess)	GP-24 (Canadian)	6,400	11,500	2.0

A quick look at the Table 2.3 shows that M_n for F-PIM-1 oligomers decreases as we move from 5% to 15% molar excess of TFTPN monomer. This is in agreement to the fact that PIM-1 condensation polymerization depends strictly on the stoichiometry of the monomers. Fig. 2.16 shows comparison of predicted M_n, M_n obtained, and M_z for stoichiometric imbalances of TFPN (5, 10 and 15% molar excess compared to BCA).

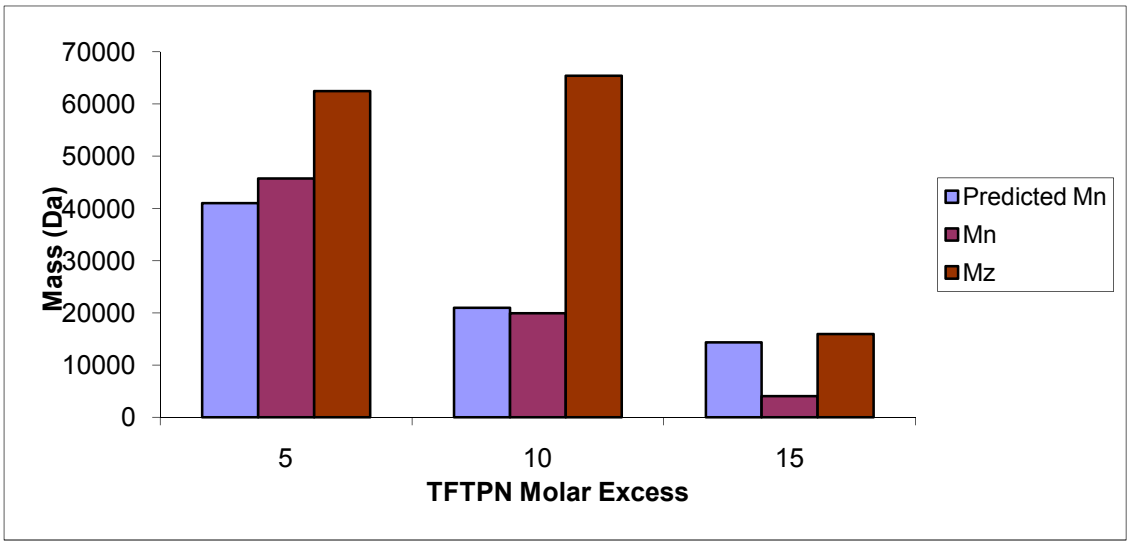

Fig. 2.16 Comparison of predicted M_n, M_n and M_z for molar imbalances of TFTPN

It can be seen that in the cases of 5 and 10% molar excess of TFTPN, the predicted M_n values by Carother's equation are in good agreement with the experimental M_n values. However, in the case of 15% molar excess of TFTPN, the predicted value is more than double that of the experimentally obtained value. It indicates that the limiting reactant might have been used in more amount than required in the experiment giving rise to lower number average molar mass. It is necessary to have a look at GPC peaks of these oligomeric F-PIM-1 products (Fig. 2.17) to evaluate shapes of various mass distributions.

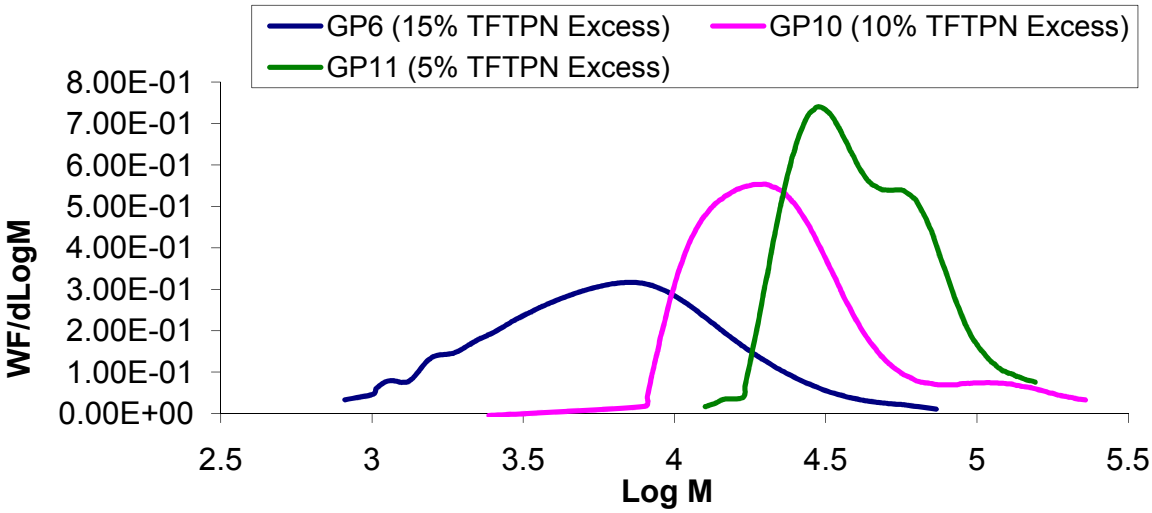

Fig. 2.17 Polystyrene standard (Conventional) GPC plots for F-PIM-1 oligomers prepared by the conventional method

It can be observed in the plot that for larger molar imbalances of monomers (15 and 10% TFTPN molar excess) the plots appear on left side with no shoulders and low molar mass distribution is obtained. However, in case of 5% molar excess of TFTPN, there is a visible and intense shoulder on right side of plot indicating a possible bimodality.

Some selected samples were analyzed by using multidetector GPC in order to compare results obtained by conventional GPC. The results obtained are shown in Table 2.4. All the molecular weights are in Daltons.

Table 2.4 Comparison of Molar masses of F-PIM-1 obtained by polystyrene standard (conventional) and Multidetector GPC

Compound	Sample Reference	Mol. Mass by polystyrene standard (Conventional) GPC (Daltons)		Mol. Mass by Multidetector GPC (Daltons)	
		M_n	M_w	M_n	M_w
F-PIM-1 (Conventional method)	GP-6	4060	8150	4520	6070
F-PIM-1 (Canadian method)	GP-24	6420	11500	6310	8060
F-PIM-1 (Canadian method)	GP-27	6100	9990	3190	9400
F-PIM-1 (Canadian method using Cs_2CO_3)	GP-29	-	-	9360	18800

Polystyrene based GPC is based on concept of hydrodynamic volume. The main assumption is that the sample has same density as the standards, which may not always be the case and could lead to errors. However, in case of multidetector, additional viscometer detector and utilization of the technique of Universal Calibration results in more reliable molecular weights. If we compare the M_n values for GP-6 and GP-24 by both techniques, they follow this trend. In case of GP-27, the molecular weight by conventional method appears to be almost double to that by multidetector technique. The reason for difference in M_n values could be the poor response of light scattering detector in case of multidetector GPC. This may happen at the low molar mass end where due to small response of light scattering detector, data may run into solvent impurities. However, it can be seen that M_w values are more consistent with each other.

Another interesting comparison in Table 2.5 is for molar masses obtained by multidetector GPC analysis for F-PIM-1 prepared by using two different salts K_2CO_3 and Cs_2CO_3. All the products were prepared using 15% molar excess of TFTPN. A quick look at the table indicates that Cs_2CO_3 results in larger PIM-1 blocks compared

to K_2CO_3. This may be due to more efficiency of Cs_2CO_3 in deprotonation of BCA monomer hence facilitating reaction in formation of larger blocks. Caesium carbonate is known as good base for production of high molecular weight polymers.[30, 31, 32] However, after this comparative study, K_2CO_3 was used as salt for preparation of F-PIM-1 blocks as it was good enough to give appropriate sized F-PIM-1 for copolymerization, While, Cs_2CO_3 needed to be used in higher amounts, more costly and larger F-PIM-1 blocks were not required. Polystyrene based GPC data for the polymer GP-29 could not be incorporated in table as experimental work of the project was concluded by that time.

The MALDI ToF mass spectrum of F-PIM-1 (GP-6) prepared by conventional polycondensation method is given in Fig. 2.18. The analysis of the observed MALDI peaks revealed that the compound was a mixture of TFTPN endcapped (L_F) as well as cyclic PIM-1 (C_n) peaks. The spectrum was not very well resolved; however, 6 peaks for TFTPN endcapping confirmed that the desired product has been formed. As the cyclic PIM-1 has no end groups with fluorine attached, it was thought appropriate to use this material for copolymerization. There was no peak in the spectrum corresponding to BCA endcapped PIM-1.

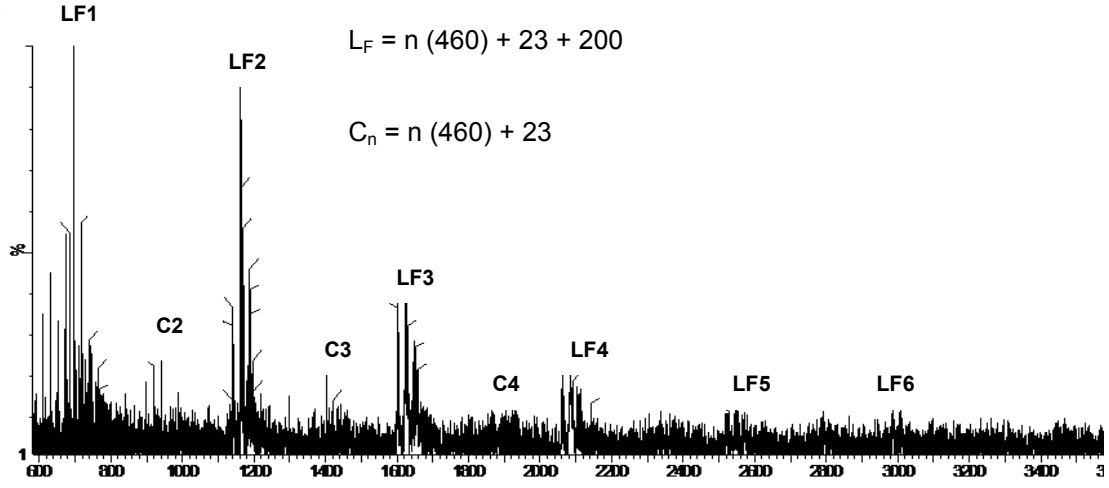

Figure 2.18 MALDI ToF MS Spectrum of F- PIM-1 (GP-6)

Table 2.5 represents comparison of MALDI peaks for F-PIM-1 in 15% molar excess of TFTPN (GP-6) to PIM-1 prepared in just 5% molar excess of TFTPN (GP11). In both cases fluoro endcapped as well as cyclic MALDI peaks can be observed. However, the table indicates that for 15% molar excess of TFTPN (GP-6), fluoro

endcapping of chains start at LF1, LF2 and LF3, which in case of 5% excess (GP-11) appear to by cyclic.

Table 2.5 MALDI ToF MS comparison for F-PIM-1 in 15% and 5% molar excess of TFTPN

F-PIM-1	Cyclic peaks (C_n)	F-PIM-1 Peaks (L_F)
GP6 (15% molar excess of TFTPN)		L_{F1}
	C_{n2}	L_{F2}
	C_{n3}	L_{F3}
	C_{n4}	L_{F4}
		L_{F5}
		L_{F6}
GP11 (5% molar excess of TFTPN)		
	C_{n2}	
	C_{n3}	
	C_{n4}	
	C_{n5}	L_{F5}
	C_{n6}	L_{F6}
	C_{n7}	L_{F7}
	C_{n8}	L_{F8}
	C_{n9}	
	C_{n10}	
	C_{n11}	
	C_{n12}	
	C_{n13}	L_{F13}

It is already established in the case of PIM-1 synthesis that in order to form high molecular weight PIM-1, it is necessary to take the monomers in equimolar ratios.[2, 33, 34]. If a molar imbalance exits for monomer, the product formed is a mixture of cyclic, linear and endcapped with monomer taken in excess.[2, 3] The same is observed for synthesis of F-PIM-1.

A representative IR spectra for F-PIM-1 (GP-6), was recorded as a thin film from chloroform. The resultant spectrum is shown in Fig. 2.19, which is consistent with the normal IR spectrum of PIM-1.

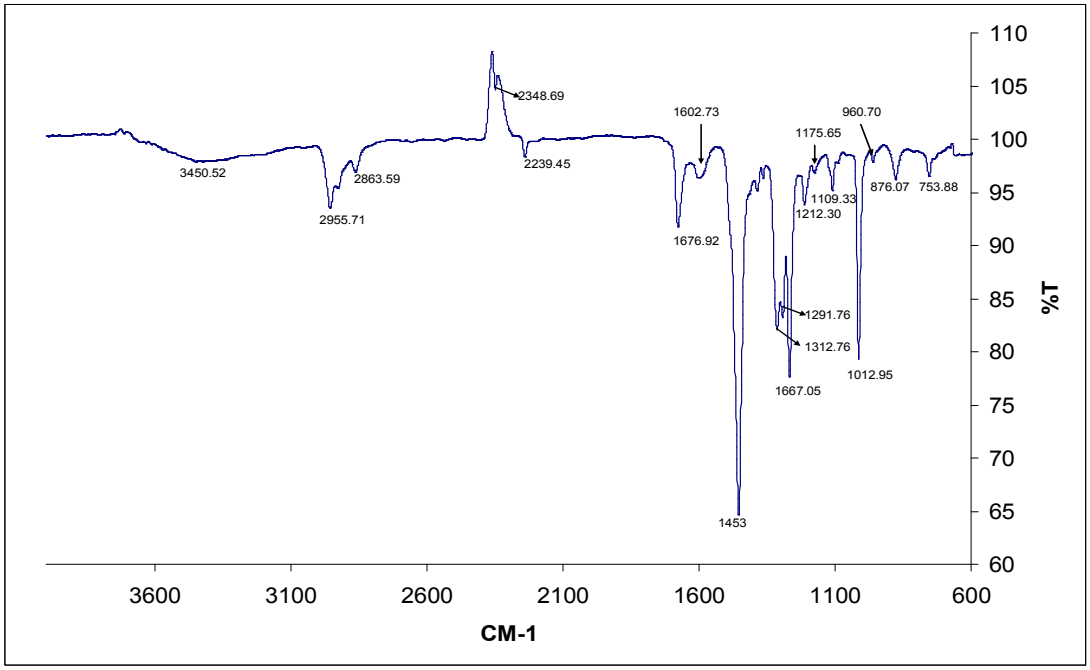

Figure 2.19 FT-IR Spectrum for F-PIM-1 (GP-6)

The fingerprint region shows characteristic absorption peaks for stretching vibrations due to ether linkage in the dioxane backbone in the ranges 1050-1150 cm^{-1} and 1250-1350 cm^{-1}. A moderate peak for CN group can be seen at 2239 cm^{-1}, while the stretching absorption due to the aromatic C=C are placed between 1600-1680 cm^{-1}. The weaker aromatic and aliphatic C-H stretching vibrations can also be noticed in the range 2850-3000 cm^{-1}. The strong peak at 1453 cm^{-1} might be due to C=C linkage.

Nitrogen adsorption/desorption analysis of F-PIM-1 samples was carried out and was analyzed using the Brunauer-Emmett-Teller (BET) equation. In order to obtain surface area, the data are used for a plot of $(p/p_o)/(V_{ads}(1-p/p_o))$ versus p/p_o between 0.02 and 0.20 (where p and p_0 are the equilibrium and the saturation pressure of adsorbates at the temperature of adsorption and *Vads* is the adsorbed gas quantity). This gives us the monolayer volume, which can be used to determine the surface area with the help of following equation.

$$\text{Surface Area } A = \frac{V_m}{22414}\, a_m N_A$$

Where

V_m = Volume of gas in monolayer (reduced to stp) on 1 g solid; units $cm^3\ g^{-1}$

a_m = Surface area per molecule = 16.2 x 10^{-20} m^2 for N_2 at 77 K

N_A = Avogadro number = 6.022 x 10^{23} mol^{-1}

1 mol of an ideal gas occupies 22414 cm^3 at stp

The nitrogen adsorption/desorption isotherm of powder samples of two different F-PIM-1 batches (GP-20) and (GP-32) is given in Fig. 2.20. The BET surface area for GP-20 is 740 m^2/g, which is quite high keeping in view that it is an oligomer of PIM-1. The BET Surface area for GP-32 is 470 m^2/g. The adsorption isotherm for GP-32 is somewhat similar to a normal PIM-1 isotherm, as it shows high uptake of nitrogen at low relative pressure (below 0.05) signifying presence of microporosity in the structure. At higher relative pressures (from 0.05 to unity) the adsorption increases steadily till a maximum and then desorption comes into effect. In comparison, GP-20 shows somewhat different than normal behaviour. The isotherm rises rather gently at low pressure. This could be due to slow adsorption kinetics.

Another important aspect of the plot is hysteresis shown by both batches in desorption. This could be due to swelling of the polymer matrix. Ideally one would expect to desorb all or most of the adsorbed N_2. This would produce a desorption loop superimposed upon the adsorption loop. However, because the N_2 causes swelling of the polymer, not all of it is desorbed.

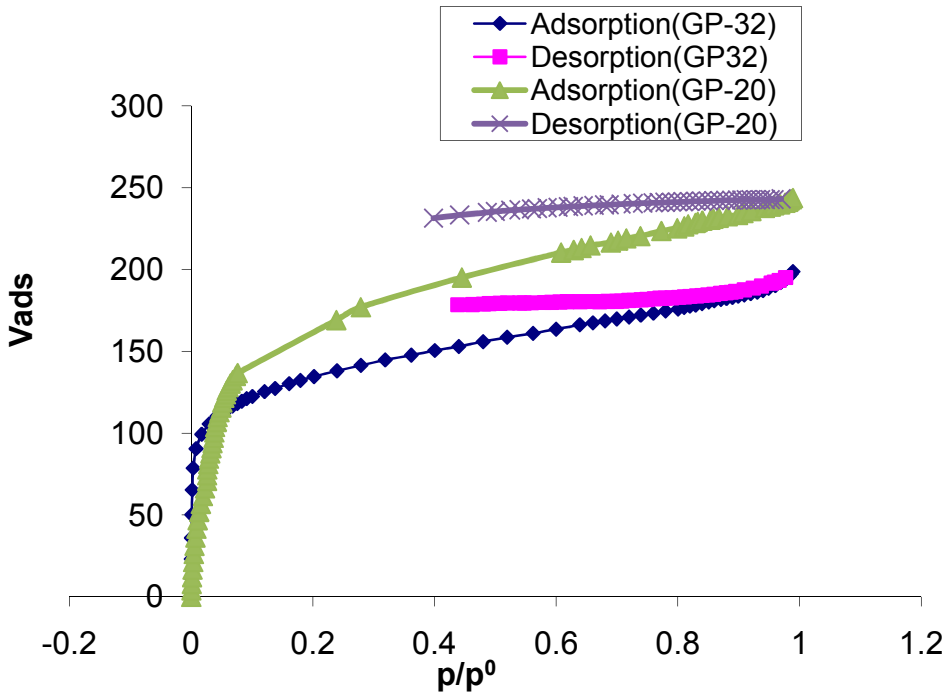

Fig. 2.20 N_2 adsorption desorption isotherm of F-PIM-1 batches (GP-20) and GP-32 at 77 K

F-PIM-1 was dried in desiccator (blue silica beads were used as desiccant) for 72 hours before using it for Thermogravimetric Analysis (TGA).TGA was carried out at a heating rate of 5 °C in air atmosphere for the temperature range 20-800 °C. The TGA plot for degradation of F-PIM-1 (GP20) is given in Fig. 2.21.

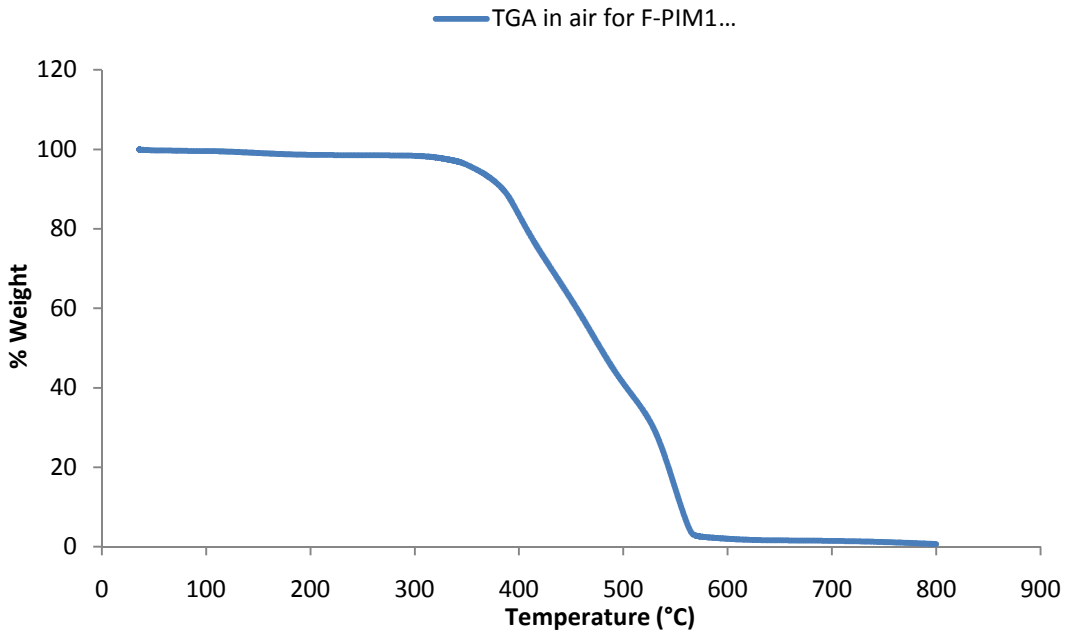

Fig. 2.21 TGA (Air) plot for F-PIM-1 (GP-20)

The sample appears to contain small amount of moisture hence there is small weight loss for water at start of isotherm. The actual degradation of F-PIM-1 starts at round 380 °C and continues smoothly. The sample reaches complete degradation around about 570 °C, signifying good thermal stability of F-PIM-1.

The ^{13}CNMR analysis of products was done as described earlier. It is important to mention here that the solubility of PIM type material is very limited, while for ^{13}CNMR analysis, there is need to prepare very concentrated solution for better results. Hence the peaks may appear weaker, yet all expected peaks were present in the spectrum. A representative ^{13}CNMR spectrum for F- PIM1 (GP-6) is given in Fig. 2.22:

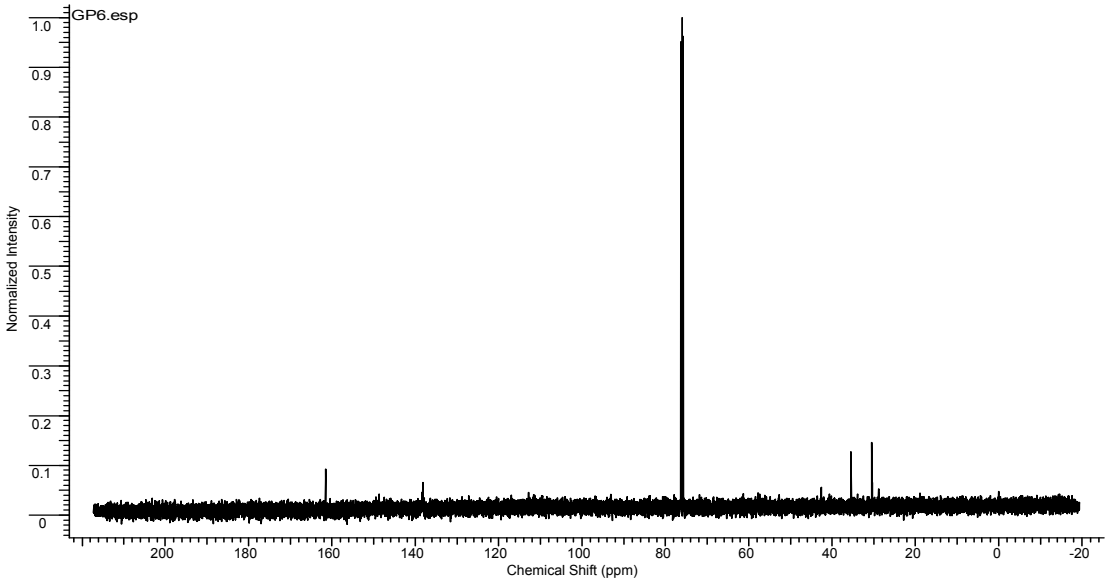

Fig. 2.22 ^{13}CNMR spectrum of TFTPN endcapped PIM-1 – Conventional Method GP-6

Although the spectrum is not very well resolved, the peak at 148.68 ppm represents carbon attached to fluorine atoms. The carbon at 138.18 ppm and 138.42 ppm represent aromatic ring carbons being shared with cyclopentane ring. While the peaks at 108 ppm, 109 ppm and 111 ppm are the aromatic carbons attached to CN and para carbons on other aromatic rings. The peaks at 28.87 ppm, 30.34 ppm and 30.43 ppm are the methyl and methylene carbons. The carbon at 57.78 ppm is the spiro center carbon.

The peaks present in PIM-1 structure are almost same as that for its TFTPN or THSB endcapped oligomers. Hence, the overall the NMR spectrum is consistent with the PIM-1 structure.

2.4 Conclusions

The work done in this chapter refers to the main objective of synthesizing PIM-1 for use for blending, fluorescence and solution adsorption as well as N_2 adsorption studies. The other objective was to synthesize TFTPN endcapped PIM-1 for coupling with MeOPEG and use it also for fluorescence studies.

PIM-1 and TFTPN endcapped oligomers of F-PIM-1 were synthesised using two different synthetic procedures. In the first procedure, the oligomers were prepared by conventional condensation polymerization method with a reaction time of 24 hours. A new high shear method with reaction time of 6-8 minutes was also used for the same synthesis. TFTPN monomer was used in 5-15% molar excess in comparison to BCA monomer to form various oligomers. The synthetic part also involved comparison or products formed by using two different salts, K_2CO_3 and Cs_2CO_3. Products with significant molar masses for PIM-1 and F-PIM-1 oligomers were prepared by both techniques. PIM-1 synthesis by high shear method appeared to be more effective than conventional method. The reason may be greater surface area provided for reaction of monomers by high shear. Both methods produced significant yields when used for synthesis of TFTPN endcapped oligomers. It was noted for TFTPN endcapped PIM-1 synthesis that using Cs_2CO_3 in place of K_2CO_3 resulted in formation of larger oligomers. However, as only moderate sized F-PIM-1 oligomers were required for coupling to poly(ethylene glycol) monomethyl ether, K_2CO_3 was thought appropriate for further synthesis of desired oligomers.

The GPC analysis of products was carried out by both polystyrene based and multidetector techniques. Remarkably, for both PIM-1 and F-PIM-1, both techniques worked in good agreement. The presence of fluoro-ended product was also verified by MALDI ToF MS analysis. MALDI analysis showed presence of cyclic and fluoro ended peaks in samples. Further verification of oligomer synthesis was confirmed by IR and NMR analysis. Both these techniques indicated presence of peaks relevant to PIM-1 structure. TGA analysis resulted in complete decomposition of polymer around 570 °C, indicating its thermal stability. An interesting comparison was for BET plot for two different F-PIM-1 batches. One of the samples, GP-20,

showed steady adsorption in the low pressure region. Both samples showed hysteresis in desorption. The unusual adsorption of GP-20 was explained on the basis of slow kinetics and desorption hysteresis may be related to swelling of polymer.

Further work on synthesis may be required to synthesize BCA endcapped oligomers. It would also be interesting to synthesize and use chloro-endcapped oligomers instead of fluoro-endcapped oligomers for copolymerization. The synthesis was done on a small scale of 5-7 grams; hence any scale up studies would also be of interest in future research.

References

(1) Budd, P. M.; Ghanem, B. S.; Makhseed, S.; McKeown, N. B.; Msayib, K. J.; Tattershall, E. C. *Chem. Commun.* **2004,** 230-231.

(2) Reynolds, K. J. PhD Thesis, University of Manchester*,* 2007.

(3) Grant, L. E. PhD Thesis, University of Manchester*,* 2006.

(4) Naiying D.; Song, J.; Robertson, G. P.; Pinnau, I.; Guiver, M. D. *Macromol. Rapid Commun.* **2008,** *29,* 783-788.

(5) Song, J.; Naiying D.; Dai, Y.; Robertson, G. P.; Guiver, M. D.; Thomas, S.; Pinnau, I.; *Macromolecules* **2008,** *41,* 7411-7417.

(6) Young, R. J.; Lovell, P. A. *Introduction to Polymers;* Chapman & Hall, London: 1991; pp. 294.

(7) Braun, D.; Cherdron, H.; Rehahn, M.; Ritter, H.; Voit, B. *Polymer Synthesis: Theory and Practice;* Springer Verlag, Berlin: 2005; pp. 263-265.

(8) Ebewele, R. O. *Polymer Science & Technology;* CRC Press, Florida, USA: 2000.

(9) Fink, J. K. *High Performance Polymers;* William Andrew Inc. Newyork: 2008; pp. 242-244.

(10) Jones, R. G.; Kahovec, J.; Stepto, R.; Wilks, E. S.; Hess, M.; Kirayama, T.; *Compendium of Chemical Terminology and Nomenclature*, *IUPAC Recommendations;* RSC Publications, Cambridge, UK: 2009; pp. 318-331.

(11) Fringuelli, F.; Taticchi, A. *Diels-Alder Reaction: Selected Practical Methods;* John Wiley & Sons, West Sussex, England: 2002; pp. 3-5.

(12) Lee, H. H.; Denny, W. A. *J. Chem. Soc. Perkin Trans. 1* **1990,** 1071-74.

(13) Gulbenk, A. H.; Horne, D. J.; Johnston, H. U.S. 3,746,707 (C1. 260-243AN; CO 7D) (July 17, 1973)

(14) Gray, A. P.; Cepa, S. P.; Solomon, I. J.' Aniline, O. J. Org. Chem. 41, 2435-2439 (1976)

(15) 7047 Kende, A. S.; Wade, J. J.; Ridge, D.; Poland, A. J. Org. Chem. 39, 931-937 (1974)

(16) Rogers, M. E.; Long, T. E. *Synthetic Methods in Step-Growth Polymers*; John Wiley & Sons, Inc.: 2003; pp. 11-14.

(17) Nomura, N.; Tsurugi, K.; RajanBabu, T. V.; Kondo. T. *J. Am. Chem. Soc.* **2004**, *126*, 5354-5355.

(18) Preedasuriyachai, P., Charoonniyomporn, P., Karoonnirun, O., Thongpanchang, T., Thebtaranonth, Y., *Tetrahedron Lett.,* **2004,** *45*(7), 1343-1346.

(19) Eastmond, G. C.; Gilchrist, T. L.; Paprotny, J.; Steiner, A. *New J. Chem.* **2001,** *25,* 385-390.

(20) McKeown, N. B.; Gahnem, B.; Msayib, K. J.; Budd, P. M.; Tattershall, C. E.; Mahmood, K.; Tan, S.; Book, D.; Langmi, H. W.; Walton, A. *Angew. Chem. Int. Ed.* **2006,** *45,* 1804 –1807.

(21) Budd, P. M.; McKeown, N. B.; Fritsch, D. *Macromol. Symp.* **2006**, *245–246,* 403–405.

(22) Yau, W.W.; Kirkland, J.J.; Bly, D. *Modern Size Exclusion Liquid Chromatography;* Wiley and Sons, New York: 1979.

(23) Montaudo, G.; Samperi, F.; Montaudo, M. S. *Prog. Polym. Sci.* **2006,** *31,* 277–357.

(24) www.biochem.arizona.edu/classes/bioc471/pages/Lecture23/Lecture23.html

(25) Chudek, J. A.; Foster, R. *J. of the Chem. Soc. Perkin Trans. 2: Physical Organic Chemistry (1972-1999)***1982**, 511-12.

(26) Odian, G. *Principles of Polymerization;* Wiley and Sons, New York: 1991.

(27) Kricheldorf, H. R.; Rabenstein, M.; Langanke, D.; Schwarz, G.; Schmidt, M.; Maskos, M.; Kruger, R. P. *High Performance Polymers;* **2001**, *13*, S123-S136.

(28) Hani, M. A.; Chatti, S.; Kricheldorf, H. R.; Zarrouk, H. *Recent Res. Devel. Organic Chem.,* **2007,** *11,* 1-11.

(29) Kricheldorf, H. R.; Stober, O. *Macromol. Rapid Commun.* **1994,** *15,* 87-93.

(30) Kawasaki, S.; Yamada, M.; Kobori, K.; Jin, F.; Kondo, Y.; Hayashi, H.; Suzuki, Y.; Takata, T. *Macromolecules*, **2007**, *40* (15), 5284–5289.

(31) Chan, K. P.; Wang, Y-F.; Hay, A. S. *Macromolecules* **1995**, *28,* 653.

(32) Chan, K. P.; Wang, Y-F; Hay, A. S.; Hronowski, X. L.; Cotter, R. J. *Macromolecules* **1995**, *28,* 6705.

(33) Ghanem, B. S. PhD Thesis, University of Manchester*,* 2005.

(34) Selbie, J. D. PhD Thesis, University of Manchester, 2009.

CHAPTER 3

COUPLING OF F-PIM-1 TO POLYETHYLENE GLYCOL MONOMETHYL ETHER (MeOPEG)

3.1 Introduction

3.1.1 Block Copolymers and their synthesis

A block copolymer is a macromolecule which is composed of blocks in linear sequence.[1] A general example is thermoplastic elastomers which contain a rubbery matrix like polybutadiene or polyisoprene and glassy hard domains like polystyrene. Block copolymers are composed of two or more polymer chains attached at their ends. Linear block copolymers have these chains in sequence, while starlike copolymers may have them attached at common branching point. Copolymers are termed as di-block, tri-block or multi-block based on type of monomers or polymers used in synthesis. A standard notation of representing block copolymers is using letter “b” for block. For example, a di-block copolymers of X and Y is referred as X-b-Y copolymer[2]. Some shapes of block copolymers based on blocks used to prepare are given at Fig. 3.1.

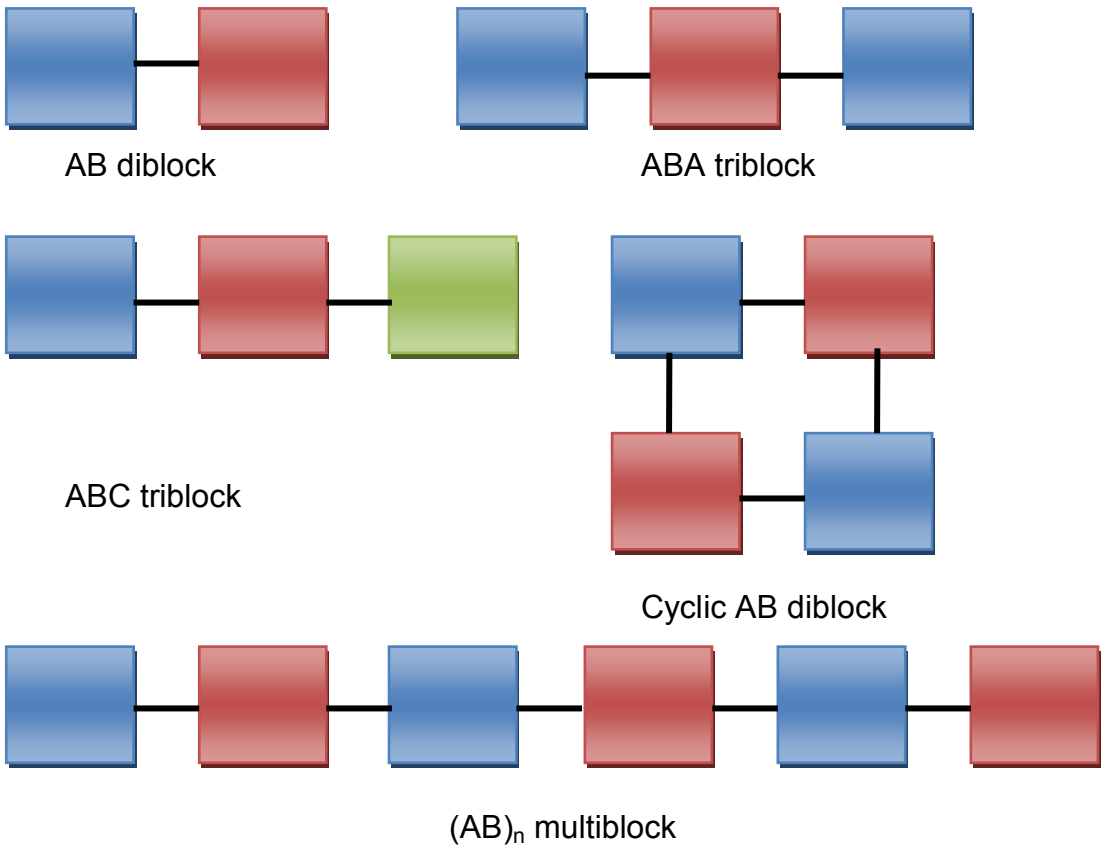

Fig. 3.1 Different block Copolymer Architectures

Block copolymers can be synthesized in many ways like anionic polymerization[3], cationic polymerization[2,4], controlled radical polymerization, including Atom Transfer Radical Polymerization (ATRP)[5] and Reversible Addition-Fragmentation Chain Transfer Polymerization (RAFT)[6], group transfer polymerization[7], step growth polymerization[8], ring opening metathesis polymerization[9], chemical modification or combination of any of these synthetic techniques.[2, 4] However, we can classify block copolymer synthesis in two broad classes, including step and chain polymerization. In step growth polymerization, different blocks with functional end groups react to form the product, while chain growth is sequential polymerization in which initiation of other monomers on the active site of a macromolecular chain of one monomer is considered (Fig. 3.2). Block copolymers (containing hydrophilic and hydrophobic segments in their chains) can possess surfactant like properties and can adsorb on interfaces and also can assemble to form micelles.[10]

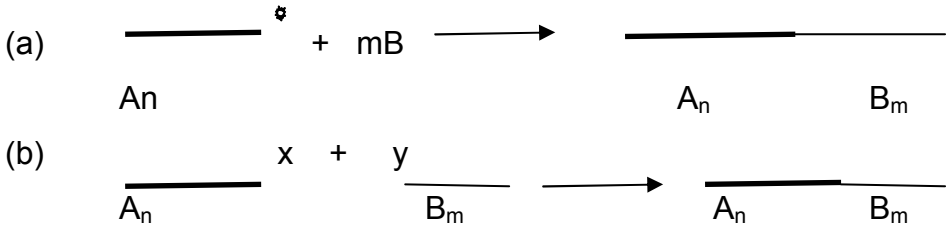

Fig. 3.2 Synthetic routes for block copolymers (a) Chain growth (b) Step growth

3.1.2 Copolymerization of PIM-1 Oligomers

Attempts have been made to synthesize bock copolymers of fluoro-endcapped PIM-1 (F-PIM-1) with polyethylene glycol (PEG) and polypropylene glycol (PPG). In this context two approaches were used.

i) In the first methodology, MEOPEG or polypropylene glycol (PPG) was deprotonated to form an alkoxide which was then reacted with a preformed TFPN terminated PIM-1. This was termed as oligomer-oligomer approach.

ii) The second synthesis involved endcapping of PPG labile oligomer to introduce catechol functionality, which then served as the chain terminator in the step growth polymerization of PIM-1. This was called labile block first or oligomer-monomer approach.

It was concluded by the researcher that PIM-1 polymers prepared under conditions of excess BCA were cyclic and hence unable to react as preformed blocks. No cyclization was however observed when PIM-1 was prepared using any molar excess of the electrophilic TFPN monomer.[11] Keeping in view this conclusion, it was decided to use TFTPN terminated PIM-1 as hard block for coupling to MeOPEG labile blocks.

3.1.3 MALDI ToF MS Analysis of Copolymers

MALDI ToF MS interpretation for polymers composed of 2 or 3 monomers is relatively a simple job, however the possibilities of different structures of product copolymer are enhanced when more than one sites for substitution are available on the reacting polymers. However, it can also be helpful in the sense that correct analysis and calculation of peaks can tell whether the copolymer is a pure material (with only one type of substitution taking place) or a mixture of different mono, di, tri or poly substituted products. In the present work, the hard matrix (F-PIM1) has a total of four fluorine atoms attached (two on either side), which can be substituted/replaced by monohydroxy MeOPEG molecule during the course of reaction. Hence, theoretically there is possibility of mono, di, tri or tetra MeOPEG units coupled copolymer can be formed. The structures of the products formed should be as under (Fig. 3.3):

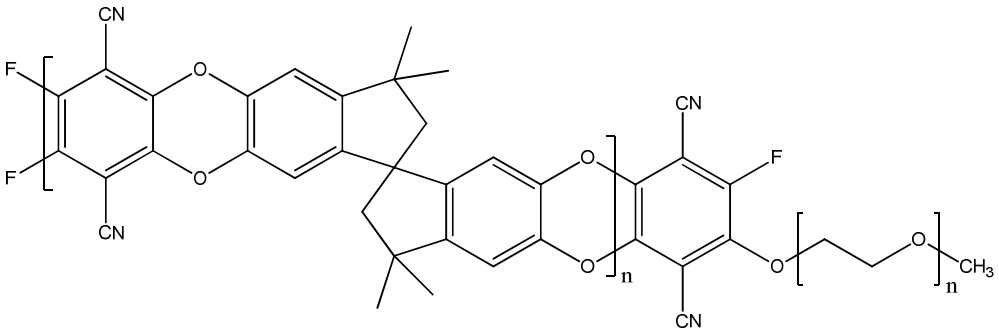

Copolymer with one Fluorine atom replaced by MeOPEG unit

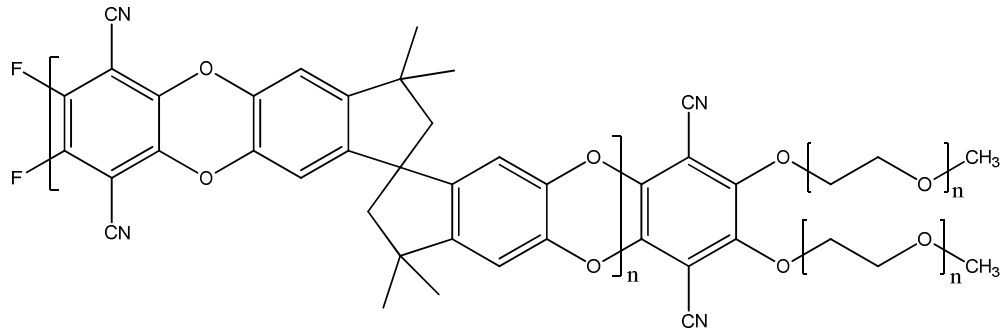

Copolymer with two Fluorine atoms replaced by MeOPEG units (same side of F-PIM1)

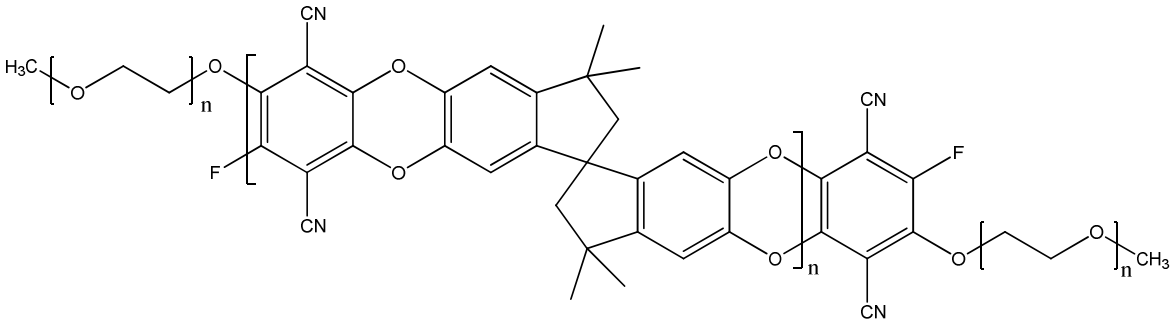

Copolymer with two Fluorine atoms replaced by MeOPEG units (alternate sides of F-PIM1)

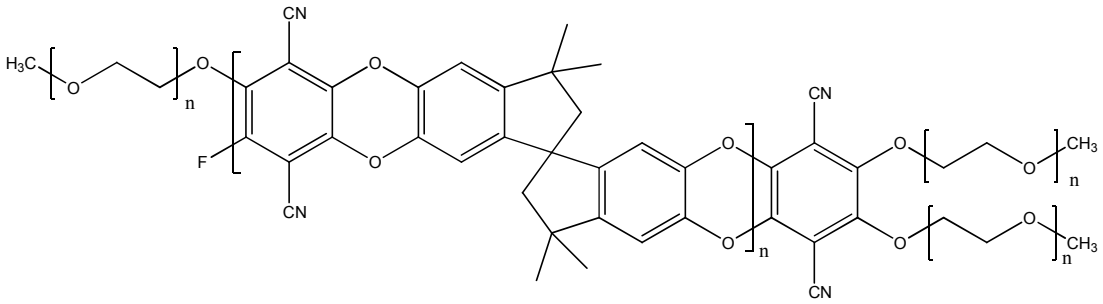

Copolymer with three Fluorine atoms replaced by MeOPEG units

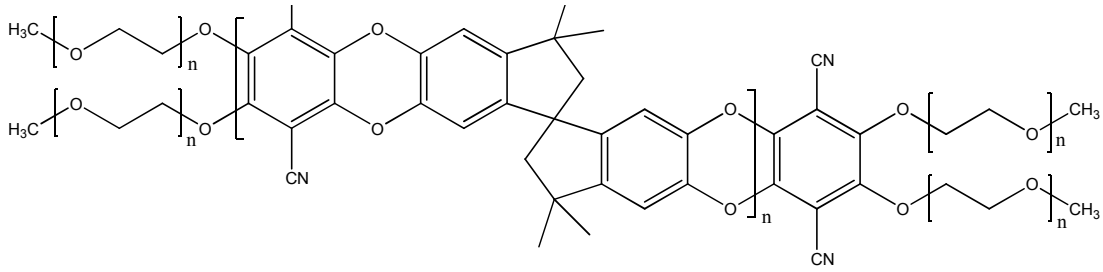

Copolymer with all four Fluorine atoms replaced by MeOPEG units

Fig. 3.3 Possible copolymer structures after replacement of one, two, three or four fluorine atoms with MeOPEG units

MALDI is considered a useful tool capable to predict the distribution of different sized chains in lower molecular weight region. It can be seen in Fig. 3.5 that MeOPEG chains differ in mass by an increment of 44. Similar chain distribution exists for the hard matrix F-PIM-1 oligomer. When the reaction occurs, theoretically all the chains of both reactants have a possibility to couple and form a product. In this copolymerization reaction, when two, three or all four fluorine atoms are replaced with MeOPEG units, the MeOPEG chains attaching to hard matrix can be equal or different length. This gives rise to a large number of possibilities for coupling. It was not possible to evaluate all possibilities; however, an effort has been made to accommodate maximum possibilities in the MALDI interpretation of copolymers.

We have already seen in previous chapter that MALDI peaks for F-PIM-1 are referred to as L_{Fn} and can be calculated by using the formula L_{Fn} = n460+23+200 where 23 represents mass of Na^+ in MALDI, 460 represents the repeat unit in PIM1

structure and 200 is molecular mass of additional TFTPN unit attached in F-PIM1. Similarly for MeOPEG the repeat unit (-OCH_2CH_2-) has mass increment of 44 with a methyl group on one end and hydroxyl unit on the other end. Hence the MALDI formula to calculate MeOPEG chains CH_3-$(OCH_2CH_2)_mOH$ would be P_m = 15+m44+17 (23 would be added for Na^+ if analysis of MeOPEG is being carried out). Hence from this we can predict following formulae for mono, di, tri or tetra MeOPEG units substituted copolymer products:

Mono-substituted copolymer = n460+23+200-20*+15+m44+17

= n460+223-20+m44+32

* -20 represent mass of one proton removed from OH of MeOPEG and fluorine atom from F-PIM1

Di-substituted copolymer = n460+223-40+2x(15+m44+17)

Tri-substituted copolymer = n460+223-60+3x(15+m44+17)

Tetra-substituted copolymer = n460+223-80+4x(15+m44+17)

3.2 Experimental Work

3.2.1 Coupling of Model Compound (3,13-dicyanobenzo-1,2,4',5'-bis-1,4-benzodioxane) (GP-15) with MeOPEG (Product = GP-17) using BuLi as base

Poly(ethylene glycol) mono-methyl ether (M_n 1100, 1.10 g, 1.00 mmol) was dissolved in THF (15 mL). Phenanthroline indicator (1.2 mg) was dissolved in THF (20 mL). The solution of model compound (M_w *340*, 0.34 g, 1 mmol) was prepared by dissolving in THF (60 mL). After preparation of all solutions, 1.6 M Butyl lithium in hexane (7.5 mL) was added to the solution of phenanthroline indicator. The solution of poly(ethylene glycol) mono-methyl ether was then added to the reaction mixture. The solution of model compound was then added to the mixture and stirred at RT for

30 minutes. The reaction mixture was heated in oil bath to 65 °C and reaction allowed to take place at reflux for 24 hours. The resulting solution was then concentrated *in vacuo* to yield the product. Product was then heated in 500 mL of distilled water to remove residual MeOPEG and base. The product was then dried in vacuum oven. The yield of the final product was 50% (0.73 g).

3.2.2 Coupling of F-PIM-1 (GP-6) with Poly Ethylene Glycol monomethyl ether (MeOPEG) (Product = GP-7) using BuLi as base

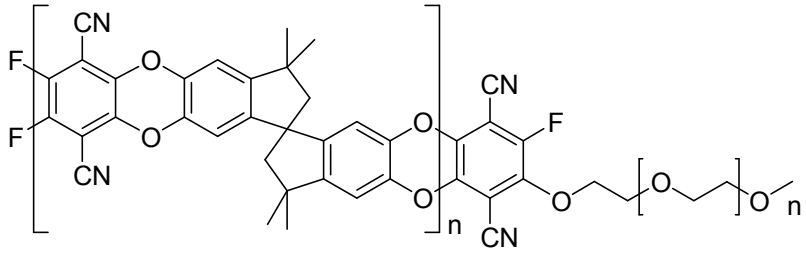

Fig. 3.4 Structure of Block Copolymer of PIM-1 with Poly Ethylene Glycol

Fig. 3.4 shows the structure of copolymer formed when a single MeOPEG chain has attached to F-PIM-1 unit. For synthesis of copolymer, Poly(ethylene glycol) mono-methyl ether (M_n 1100, 0.188 g, 0.171 mmol) was dissolved in THF (2.5 mL). Phenanthroline indicator (0.6 mg) was dissolved in THF (10 mL). The solution of TFTPN terminated PIM-1 (M_n *4059*, 1.500 g, 0.171 mmol) was prepared by dissolving in THF (20 mL).

After preparation of all solutions, 1.6 M Butyl lithium in hexane (1.25 mL, 0.171 mmol) was added to the solution of phenanthroline indicator to form a bright orange solution. The solution of poly(ethylene glycol) mono-methyl ether was then added to the reaction mixture until the yellow endpoint was reached. At that point, the solution of TFPN terminated PIM-1 was added to the mixture and stirred at RT for 30 minutes. The reaction mixture was heated in oil bath to 65 °C and reaction allowed to take place at reflux for 24 hours. The resulting brown solution was then concentrated *in vacuo* to yield the product as an opaque brown glassy mass. Product was then heated in 500 mL of distilled water to remove residual MeOPEG and base. The product was then dried in vacuum oven. The yield of final product was 58% (0.98 g).

3.2.3 Coupling of F-PIM-1 (GP-20) with Triethylene Glycol monomethyl ether (TEGME) by conventional method (Product = GP-22) using K_2CO_3 as base

Triethylene glycol mono-methyl ether (M_w 164.2, 1.10 mL, 7.00 mmol) was added to 2.09 g (0.7 mmol) of TFTPN terminated PIM-1 and 0.77 g (5.6 mmol) K_2CO_3 and 40 mL DMF in a 2-neck round bottom flask. The reaction was carried out for 24 hours at 65 °C under N_2 atmosphere and reflux and constant stirring. The reaction was stopped the next day and the reaction mixture allowed cooling to room temperature. The reaction mixture was then added to 550 mL of distilled water to remove the base and residual TEGME. The precipitate was filtered by vacuum filtration and dried overnight in vacuum oven. The final product was a dark brown solid weighing 2.04 g (65%).

3.2.4 Coupling of F-PIM-1 (GP-20) with MeOPEG by High Shear method using K_2CO_3 as base by High Shear Method (Product = GP-23)

Poly(ethylene glycol) mono-methyl ether (M_n 1100, 3.52 g, 3.2 mmol) and PIM-1 (15% excess of TFTPN) (M_n 3470, 1.388 g, 0.4 mmol) were mixed with Potassium carbonate (0.442 g, 3.2 mmol) in a 3-neck RB flask. After addition of 25 mL of DMA, the setup was connected to a condenser and homogenizer and placed in an oil bath preheated to 155 °C. The reaction was carried out under nitrogen for 2 minutes and then 20 mL of toluene was added. After another 2 minutes, 20 mL of toluene was again added. The reaction was then let to happen for further 4 minutes. The homogenizer was stopped after total 8 minute reaction and the reaction mixture was dissolved in 500 mL of distilled water for removal of base and residual MeOPEG. The reaction mixture was then heated for 2 hours at 100 °C to remove the salt. The final product was obtained through vacuum filtration and dried overnight in vacuum oven with 40% yield (1.26 g).

3.2.5 Coupling of F-PIM-1 (GP-20) with Triethylene Glycol monomethyl ether by High Shear method (Product = GP-21)

Triethylene glycol mono-methyl ether (M_w 164.2, 0.8 mL, 5 mmol) and PIM-1 (15% excess of TFTPN) (M_n 3470, 1.735 g, 0.5 mmol) were mixed with Potassium carbonate (0.552 g, 4.0 mmol) in a 3-neck RB flask. After addition of 25 mL of DMA, setup was connected to condenser and homogenizer and placed in an oil bath preheated to 155 °C. The reaction was carried out under nitrogen for 2 minutes and then 20 mL of toluene was added. The reaction was then let to happen for further 3 minutes. The homogenizer was stopped after total 5 minute reaction and the reaction mixture was dissolved in 500 mL of distilled water for removal of base and residual TEGME. The reaction mixture was then heated for 2 hours at 100 °C to remove the base. The final product was obtained through vacuum filtration and dried overnight in vacuum oven. The bright yellow product was 72% (1.48 g) in yield.

3.2.6 Coupling of F-PIM-1 with larger MeOPEG Block by High Shear method (GP-30)

The reaction of TFTPN terminated PIM-1 (GP-27, M_n = 3190 Daltons) was performed using a larger MeOPEG block having M_n = 2000, as per procedure described in Section 3.2.5. Amount or F-PIM-1 was 0.96 g (0.3 mmol) with MeOPEG weighing 4.80 g (2.4 mmol). The coupling product (GP-30) appeared yellow with 52% yield (1.75 g).

3.2.7Synthesis of Endcapped F-PIM-1 (GP-37)

F-PIM-1 (GP-32) (M_n = 2708 Daltons) was mixed with 1,2-dihydroxy benzene in equilmolar amount (0.5 mmols each) with 1.5 mmols of base K_2CO_3 and dissolved in 25 mL of solvent DMF. The reaction was carried out in presence of nitrogen at 65 °C with stirring for 6 hours. The reaction mixture was cooled to room temperature and filtered under vacuum. The crude product was washed with 100 mL of acetone and

dissolved in 200 mL of chloroform and heated to dissolve it. It was then put in fumehood for recrystalization. The recrystalized was then filtered by vacuum and dissolved in 500 mL of water to remove the base. The mixture was then heated for one hour and filtered by vacuum to get the final product. The product was put in vacuum oven for 72 hours before using for coupling. The final product was a yellow solid with low yield of about (0.44 g) 40%.

3.2.8 Coupling of Endcapped F-PIM-1 (GP-37) with MeOPEG750 (GP-38)

The coupling of endcapped F-PIM-1 (GP-37) with MeOPEG750 was undertaken by high shear mixing method as per same procedure described in section 3.2.4. The yield of coupling product was 55% (0.17 g).

3.3 Results and Discussion

3.3.1 Coupling of Model Compound (3,13-dicyanobenzo-1,2,4',5'-bis-1,4-benzodioxane) (GP-15) and (MeOPEG) to check if nitrile group on F-PIM-1 is competing with Fluorine atoms

Coupling of PIM-1 oligomers bearing either catechol or fluoro endcapping with polyethylene glycol monomethyl ether (MeOPEG) has been tried earlier. [11] It was observed that using catechol endcapped PIM-1 for coupling with polyethylene glycol monomethyl ether (MeOPEG) was not successful; however, fluoro-endcapped PIM-1 (F-PIM-1) showed some promise.[11]

In this context, it was thought appropriate to start coupling reactions with model compound (GP-15) bearing no fluorine atoms on either end (structure of GP-15 at Fig. 3.5). If successful, this would clarify that the nitrile group present on F-PIM-1 structure may also react in the same way to yield grafting copolymers. In case of no success, it would be assumed that nitrile group do not interfere in the reaction and coupling can only occur through condensation involving fluorine atoms.

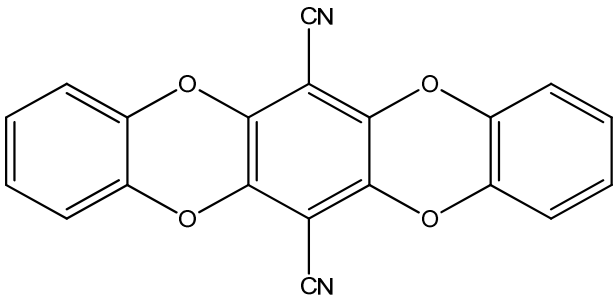

Fig. 3.5 Structure of Model Compound (GP-15)

The coupling reaction between model compound and MeOPEG was performed as described in section 3.2.1. The MALDI spectrum of the product (GP-17) is shown in Fig. 3.6. The resultant product (GP-17) was a greenish yellow solid.

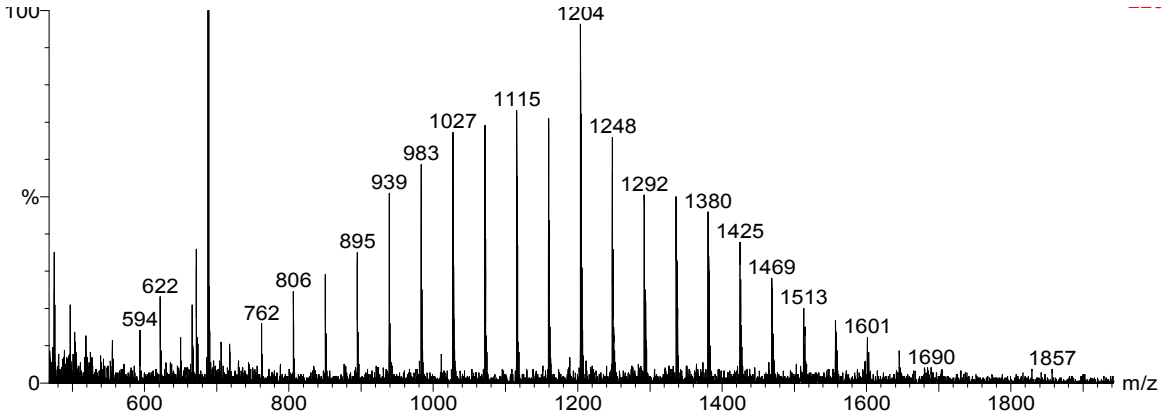

Fig. 3.6 MALDI ToF MS Spectrum of Product (GP17) formed by reaction between model compound (3,13-dicyanobenzo-1,2,4',5'-bis-1,4-benzodioxide) and MeOPEG.

MALDI spectrum of the product (GP-17) at Fig. 3.6 shows two distinct regions. On the left there is a smooth distribution of masses, while between 600 and 800 there is a sharp peak at about 688. A close look reveals that the successive units in smooth mass distribution differ by a mass of 44, which indicates that these represent MeOPEG1100 units. The sharp peak at 688 appears to be the dimer of the model compound. In this context, it can be inferred that nitrile atoms are not taking part for coupling to MeOPEG. The greenish yellow colour of the product may also be a result of dimerization of the model compound.

The IR spectrum of model compound, MeOPEG1100 and product is shown in Fig. 3.7. The model compound and product have almost identical peaks. The characteristic absorption peaks for stretching vibrations due to ether linkage in dioxane backbone are appearing in the finger print region between 1050-1150 cm^{-1} and 1250-1350 cm^{-1}. Both model compound and product are showing weak peaks for nitrile in the range of 2235-2245 cm^{-1}. The spectrum for model compound was noisy and not very well resolved, hence the C-H peak cannot be detected, however, there appears some incorporation of MeOPEG1100 in the same range of 2770-2850. This may be representing residual MeOPEG1100 in the product.

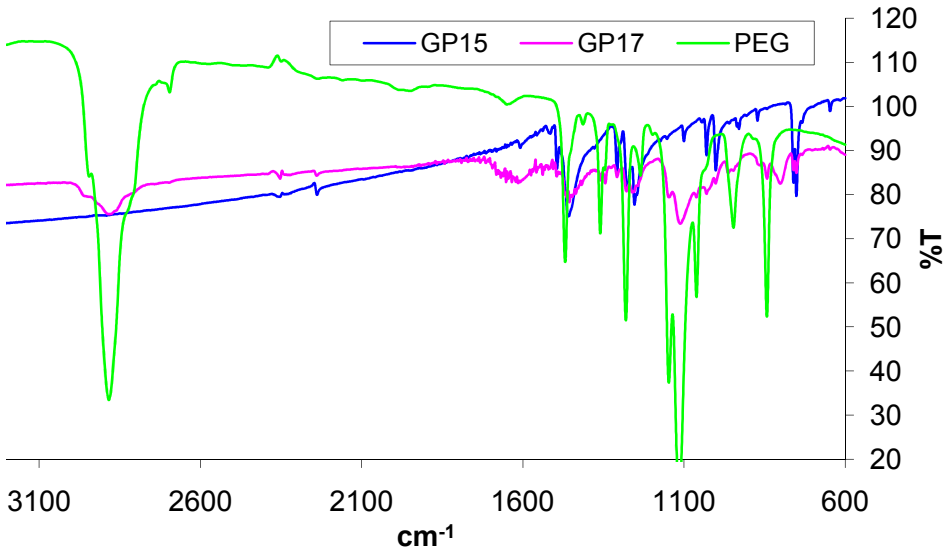

Figure 3.7 IR Spectrum of Model Compound (GP15), MEOPEG and Product (GP17)

All the 3 compounds were also analyzed by ^{13}CNMR. Peaks of NMR are shown in Table 3.1. It can be inferred from the Table 3.1 that the peaks in the region 68-72 ppm refer to MeOPEG block. It indicates that only MEOPEG peaks appeared in ^{13}CNMR spectrum. Peaks for model compound (GP-15) may not have appeared as it was observed earlier that it had very low solubility. In this context, the NMR spectrum was not conclusive. The NMR result supplements the IR and MALDI results and it appears that coupling of the model compound with MeOPEG could not take place.

Table 3.1 ^{13}CNMR peaks for MeOPEG and product (GP-17)

^{13}CNMR Peaks for MeOPEG (ppm)	**^{13}CNMR Peaks for product GP-17 (ppm)**
57.15	59.02
59.80	61.59
67.55	69.44
68.39	70.32
68.67	70.57
70.04	70.61
70.67	71.94
	72.56

3.3.2 Coupling of F-PIM-1 with Polyethylene Glycol Monomethyl Ether (MeOPEG) using Butyl Lithium as Base

In Section 3.3.1 it has been described that coupling of model compound (GP-15) to MeOPEG was unsuccessful. The next step for coupling was replicating synthesis of copolymer of F-PIM-1 with MeOPEG as per procedure adopted in earlier research. [11]

It has already been described in the previous chapter that the initial attempts to synthesize F-PIM-1 (GP-6) appeared to be containing mostly TFTPN endcapped and some cyclic units of PIM-1. However, as the cyclic product has got no fluorine atoms attached to it, theoretically MeOPEG should only couple to TFTPN endcapped oligomer. The F-PIM-1 GP-6 with M_n 4059 Daltons was hence used for coupling with Polyethylene glycol monomethyl ether (MeOPEG1100) in the presence of base n-Butyl lithium and phenanthroline indicator. Both the starting materials were dried in vacuum oven or desiccators (desiccant silica beads) under N_2 for 72 hours before reaction. Both the reactants and indicator were soluble in THF.

It is envisaged that n-Butyl lithium being a strong base would easily deprotonate MeOPEG1100 to the corresponding alkoxide in the presence of phenanthroline

indicator. In order to avoid degradation of the polymer, it was necessary to use appropriate amount of base which otherwise may case reduction of fluorine ends by lithiation on addition of preformed F-PIM-1. THF was an appropriate solvent as it could solubilize all materials involved in coupling reaction. Phenanthroline was considered as an appropriate indicator as its colour should change from orange to yellow during the course of reaction indicating the reaction endpoint. The subsequent addition of F-PIM-1 (GP6) solution and reflux for 24 hour should result in the formation of product, which can be recovered by rotary evaporation of the solvent. The coupled product might contain traces of lithium fluoride and the indicator.

The reaction was done as described and the final product was a brown opaque glassy mass instead of expected yellowish one like F-PIM-1. Apparently, there should not be much difference in the chromophore of PIM-1 and copolymeric product after coupling of MeOPEG units. The subsequent analysis discussed later in this chapter would prove that some of the MeOPEG units were coupled to the PIM-1 in this reaction; however, it is suspected that the base might have caused some side reactions leading to formation of opaque brown product. It is suspected that it might be a mixture of copolymer and some side products. The scheme of the reaction is given below (Fig. 3.8).

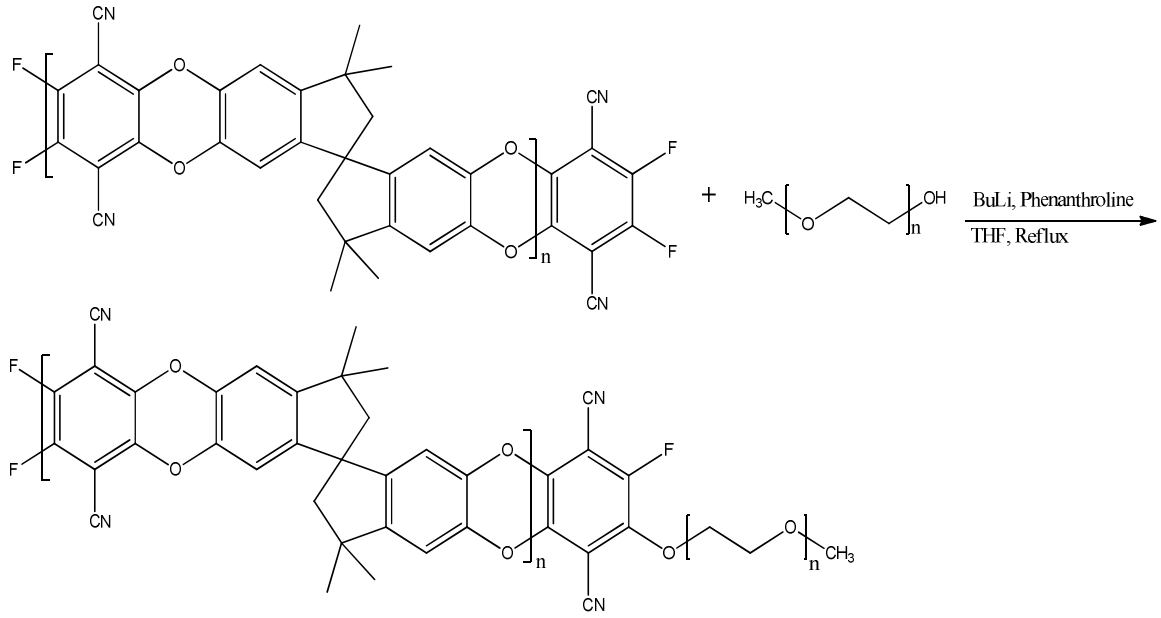

Fig. 3.8 Scheme for reaction of F-PIM-1 (GP-6) with MeOPEG

The appearance of F-PIM-1 (GP-6) (before grinding) and block copolymer (GP-7) can be seen in Fig. 3.9.

Fig. 3.9 Appearance of F-PIM-1 (GP-6) (before grinding) and Copolymer (GP-7)

Table 3.2 shows ^{13}C NMR peaks for F-PIM-1 (GP-6), MeOPEG and product GP-7.

Table 3.2 ^{13}CNMR peaks for F-PIM-1 (GP-6), MeOPEG and copolymer product (GP-7)

Chemical Shift observed (ppm)		
F-PIM-1 (GP-6)	MeOPEG	Copolymer (GP-7)
28	56	28
30	58	30
43	68	43
58	69	58
108		69
109		109
111		111
138		147
148		162
163		

The ^{13}CNMR was not very well resolved, but it showed the relevant peaks. Although a close look at spectrum inTable 3.2 shows the peak at 148 ppm represents carbon attached to fluorine atoms. The carbon at 138 ppm indicates aromatic ring carbons being shared with cyclopentane ring. While the peaks at 108 ppm, 109 ppm and 111

ppm may be the aromatic carbons attached to CN and para carbons on other aromatic rings. The peaks at 28 ppm, 30 ppm are the methyl and methylene carbons. The carbon at 58 ppm is the spiro center carbon.

MeOPEG1100 shows a characteristic spectrum of MeOPEG as it shows strong peaks between 69 - 72 ppm for carbon attached to ether linkage and other 2 peaks between 56 – 59 signifying alkyl group attached to ether linkage.

In above context, it is bit easier to explain the peaks of product (GP-7). It can be seen from the spectrum that there is strong peak at 69 ppm as a peak in the region 68-72 ppm which may be due to either coupling or residual MeOPEG1100 in the product. It was also noted that the length of peak has been reduced considerably, which may be an indication of MeOPEG being used in the reaction. Hence it can be inferred that coupling of MeOPEG to a certain extent has occurred. Rest of the spectrum showed that major F-PIM-1 peaks were also retained.

FT-IR spectra for F-PIM-1 (GP-6), MeOPEG1100 and block copolymer product (GP-7) were recorded as thin film from chloroform. FT-IR spectra of F-PIM-1, MeOPEG and copolymer are shown in Fig. 3.10. It can be observed that F-PIM-1 (GP-6) and product (GP-7) both contain the characteristic peaks to be expected.

It is important to mention that for coupling of MeOPEG with F-PIM-1 by the method described in earlier research[11], equimolar amounts of both starting materials were used. Product was later washed with water to remove any traces of MeOPEG or base. Hence it was tried best to get a copolymer instead of a mixture of reactants.

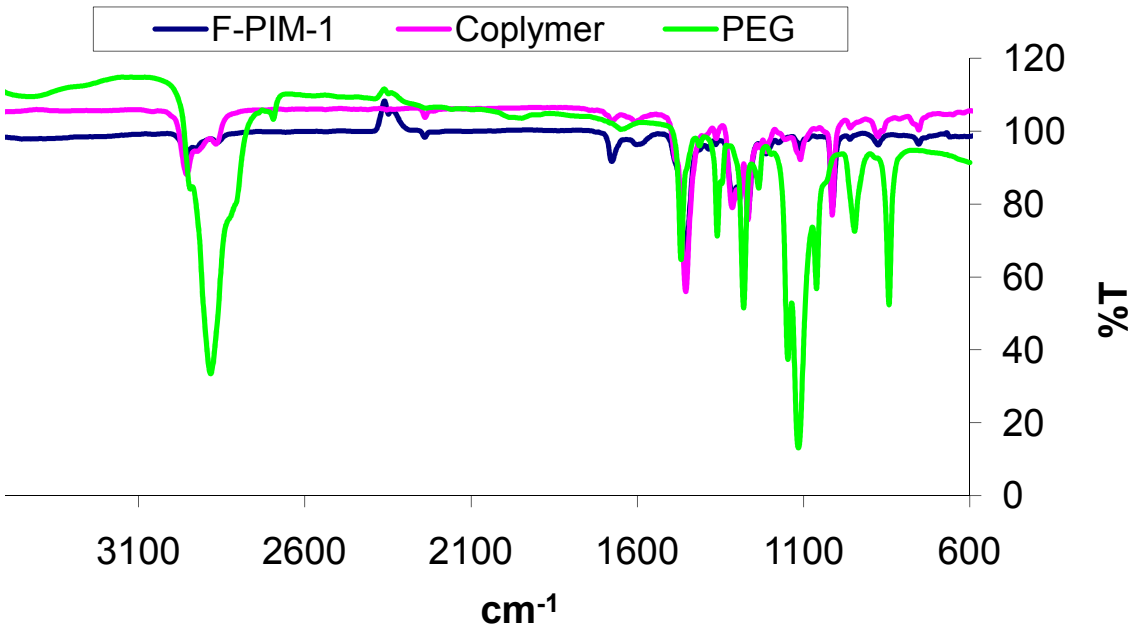

Fig. 3.10 FT-IR Spectrum for F-PIM-1 (GP-6), MEOPEG and product (GP-7)

F-PIM-1 spectrum in the fingerprint region shows characteristic absorption peaks for stretching vibrations due to ether linkage in dioxane backbone in the ranges 1050-1150 cm^{-1} and 1250-1350 cm^{-1}. A small peak for CN group can be seen in the range of 2235-2245 cm^{-1} in both spectrums of F-PIM-1 (GP-6) and product (GP-7). The stretching absorption due to the aromatic C=C are appearing between 1600-1680 cm^{-1}. The weaker aromatic and aliphatic C-H stretching vibrations can also be noticed in the range 2850-3000 cm^{-1}. The strong peak in the range of 1450-1460 cm^{-1} may be due to C=C linkages.

The spectrum for MeOPEG1100 shows 3 peaks in the range of 1050-1150 cm^{-1} referring to the ether linkage and strong absorption at 2883 cm^{-1} represents C-H of CH_2 in the MeOPEG1100. It can be noted that the peak for ether linkage in product has increased to a small extent after coupling reaction. This may be indication of some MeOPEG1100 units coupled to F-PIM-1 matrix. However, IR spectra alone can't be used as solid evidence for the coupling of MeOPEG to F-PIM-1. The results need to be complimented by other analytical techniques.

The conventional GPC analysis can be based on different standards like polystyrene. Hence polystyrene based GPC analysis was undertaken for both the reactants and the product formed. The result of the analysis is shown at Table 3.3.

Table 3.3 Molar masses of F-PIM-1 (GP-6), MeOPEG1100 and product (GP-7) by Polystyrene GPC

Sample	Molar Mass by Polystyrene standard based GPC (Daltons)		
	M_n	M_w	M_w / M_n
F-PIM-1 (GP-6)	4000	8100	2.0
MeOPEG	1400	1500	1.1
Product (GP-7)	5500	15800	2.8

It can be seen in the table that both M_n and M_w increase after coupling of F-PIM-1 to MeOPEG1100. Increase in the molar mass may indicate some coupling reaction occurring, however it is necessary to have a look at the GPC plot of all these reactants and product to see whether there is any real shift to high molar mass side. GPC plot for FPIM-1 (GP-6), MeOPEG and product (GP-7) is given below (Fig. 3.11).

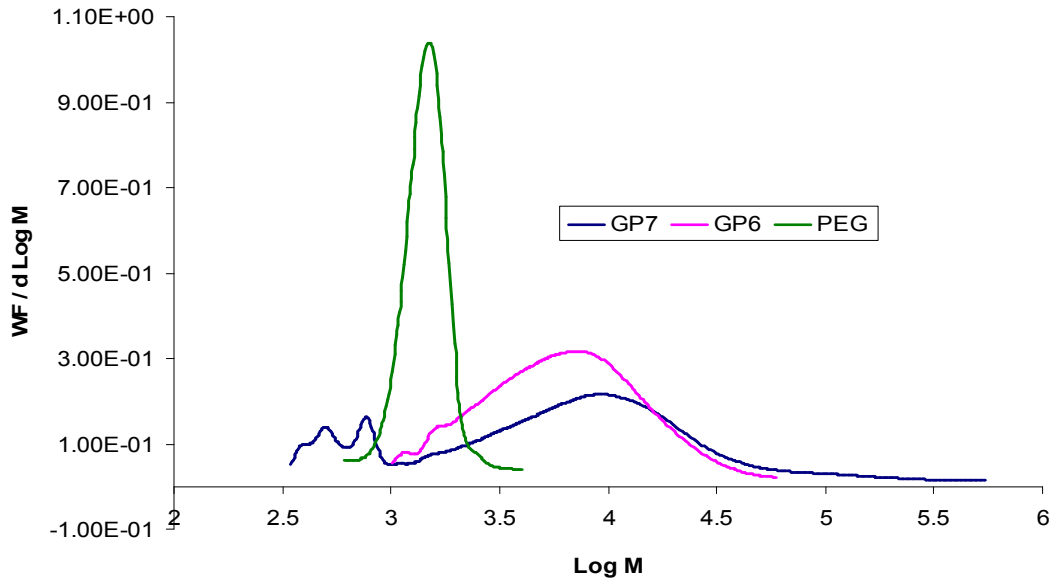

Fig. 3.11 Molecular weight distribution of F-PIM-1 (GP-6), MeOPEG1100 and Copolymer (GP-7)

It can be seen in the plot that the peak shifts to right hand side for product as compared to F-PIM-1. The small shoulder on left side of plot for product GP-7 may be due to residual MEOPEG in the product or some side products. Although gain in molar mass of product may indicate some sort of coupling but the GPC result is not conclusive of clean product formation.

MALDI ToF MS analysis of F-PIM-1 (GP-6) has already been discussed in section 2.3.3 of previous chapter. It was deemed necessary to undertake MALDI analysis of both MeOPEG1100 and copolymer (GP-7) to identify the coupling. The MALDI spectrum for MeOPEG1100 is shown in Fig. 3.12:

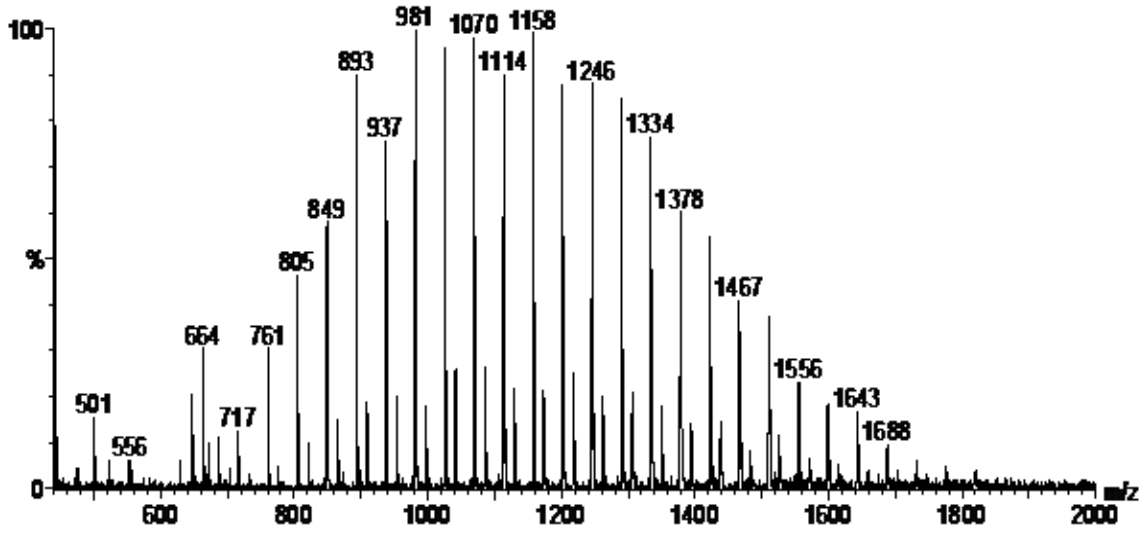

Figure 3.12 MALDI ToF MS Spectrum of Polyethylene Glycol monomethyl ether (MeOPEG)

Polyethylene glycol monomethyl ether (MeOPEG) used in this experiment had an average molar molecular mass of 1100. The molecular formula for MeOPEG is $CH_3(OCH_2CH_2)_nOH$. Hence, the MeOPEG repeat unit ($-OCH_2CH_2-$) varies by mass of 44 and theoretically successive peaks in MALDI spectrum should demonstrate this difference. A close look at spectrum in Figure 3.13 shows that the peaks have a mass difference of 44 and spectrum is consistent with the standard MeOPEG spectrum.

The MALDI spectrum for product (GP-7) is given at Fig. 3.13.

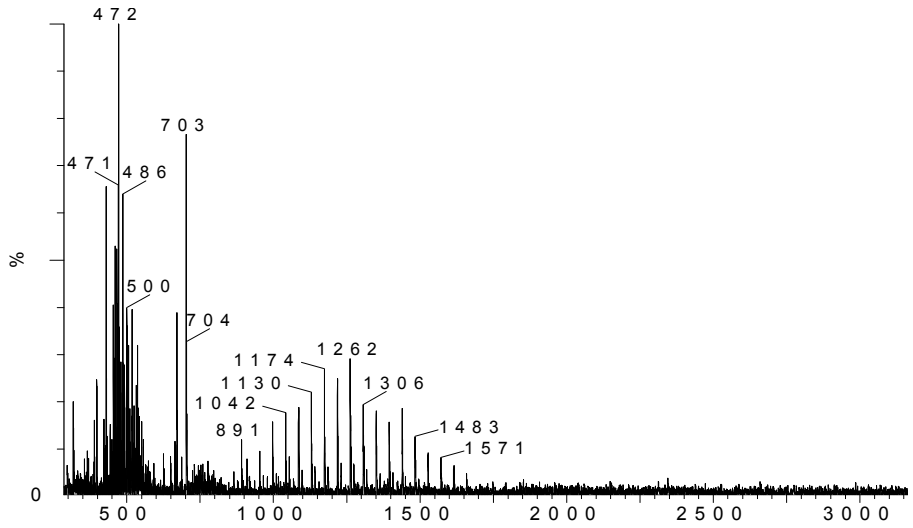

Fig. 3.13: MALDI ToF MS Spectrum of Copolymer (GP-7)

Unfortunately the MALDI spectrum of coupling product GP-7 (Fig. 3.13) was not very well resolved despite many attempts. It has already been described that the product was a glassy brown mass with very low solubility. This might have caused a problem in MALDI analysis and it appears that the material didn't fly well in MALDI to give a good result. There spectrum appears inconclusive for coupling. It can be divided in two regions, one on left side of plot, showing small peaks for F-PIM-1 units and other in the middle of spectrum showing some successive peaks starting form 891 and extending till 1571. This appears to be showing residual MeOPEG1100 as the mass difference between these successive peaks is 44 which should be for MeOPEG1100. However no coupling peaks could be located in MALDI spectrum.

Overall, the analysis of F-PIM-1 (GP-6), MeOPEG and product (GP-7) indicated coupling might have occurred to a limited extent in this reaction, however, there might be some interference from base, other functional groups in F-PIM-1 or impurities and some side reaction might have occurred. It was necessary to investigate the coupling reaction and possible side reactions due to base or other factors.

3.3.3 Coupling of F-PIM-1 with change of base from n-Butyl Lithium to Potassium Carbonate (K_2CO_3)

At this point, the coupling reaction was thoroughly analyzed and it was inferred that the coupling reaction is being competed with by some side reactions, like interference from strong base n-Butyl Lithium (BuLi). It is important to mention that the coupling reaction of F-PIM-1 with MeOPEG in presence of strong base (n-BuLi) was only undertaken to check the success of coupling (or otherwise) reported by earlier research. [11] At this point of research it appeared that n-BuLi was too strong for coupling and it was time to go for a milder base.

It has been observed in section 3.3.1 that no conclusive signs of coupling were observed for model compound to MeOPEG1100. Hence in order to check the possibility of any interference from strong base (BuLi), it was decided to change the base to K_2CO_3. However, it was appropriate to undertake coupling reaction initially for a smaller glycol molecule and based on observations, extend it to a larger MeOPEG block. In this context, Triethylene glycol monomethyl ether (TEGME) appeared to be the obvious choice. It was further suggested to replace n-butyl lithium with potassium carbonate as base to avoid any side reaction or interference that BuLi might have been causing.

It has already been mentioned in section 2.4 of previous chapter that the newly reported high shear method was successfully used to synthesize fluorine ended PIM-1 oligomers. Various F-PIM-1 hard blocks with M_n ranging from 1400-7000 were available to be used for coupling reactions. It was decided to use small sized F-PIM-1 oligomer (GP20, M_n = 1441 by multidetector GPC) for coupling with TEGME.

The coupling reaction was initially carried out by the high shear method which was earlier used for synthesis of F-PIM-1. For the first time, the coupling product (GP-21) appeared bright yellow like PIM-1 or F-PIM-1 instead of a brown or black mass. Encouraged by the result of high shear method for coupling of TEGME with F-PIM-1, the same experiment was repeated using the conventional step polymerization method. The product obtained (GP-22) was also a bright yellow. In both cases F-

PIM-1 used was GP-20 with molar mass M_n = 1441 Daltons. The reaction scheme along with set of conditions for both types of coupling procedures is given at Fig. 3.14.

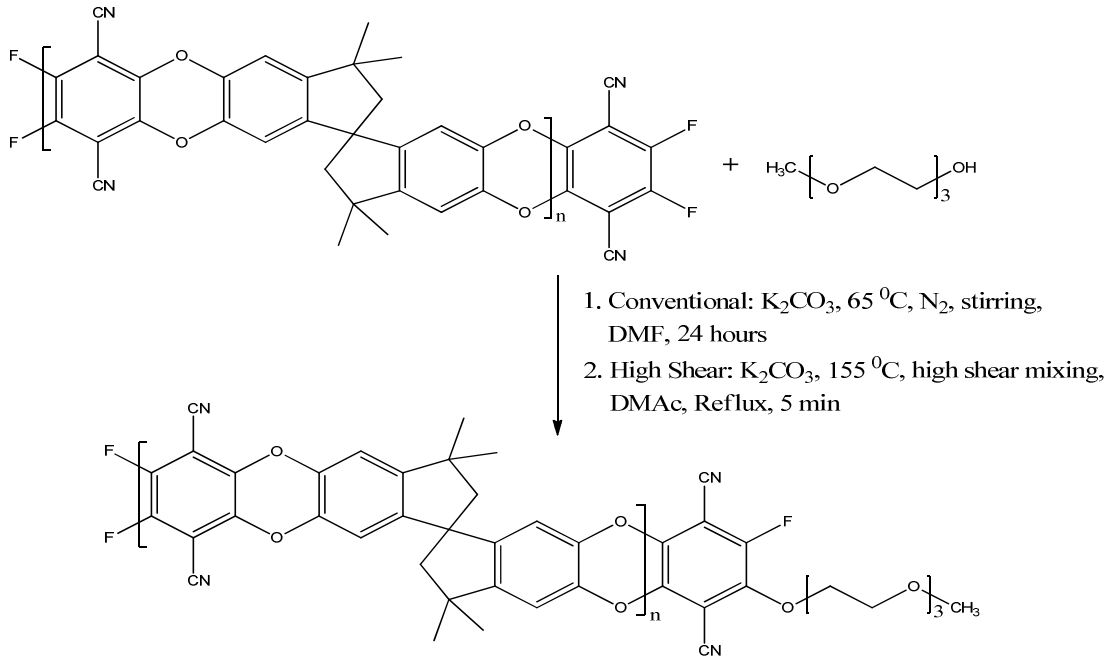

Figure 3.14 Scheme for coupling reaction of F-PIM1 (GP-20) with triethylene glycol monomethyl ether (TEGME) by conventional and high shear methods.

These results were step forward and it was high time to try this high shear method for coupling of MeOPEG1100 to F-PIM-1. The experiment was repeated at same conditions for high shear method again using small F-PIM-1 hard block (GP-20). The resultant product (GP-23) was a yellow fluorescent copolymer. The sample picture in Fig. 3.15 shows the starting F-PIM-1 (GP-20) and three copolymer products.

Fig. 3.15: Sample pictures for FPIM-1 (GP-20), copolymer with TEGME by high shear coupling (GP-21), copolymer with TEGME with conventional coupling (GP-22) and copolymer with MeOPEG by high shear coupling (GP-23)

The results of conventional GPC of TFTPN terminated PIM-1 (GP-20), MEOPEG and their copolymers were compared and showed shift of peaks to high molar mass region indicating formation of copolymers. Fig. 3.16 shows the conventional GPC plot for F-PIM1 (GP-20) and block copolymers synthesized.

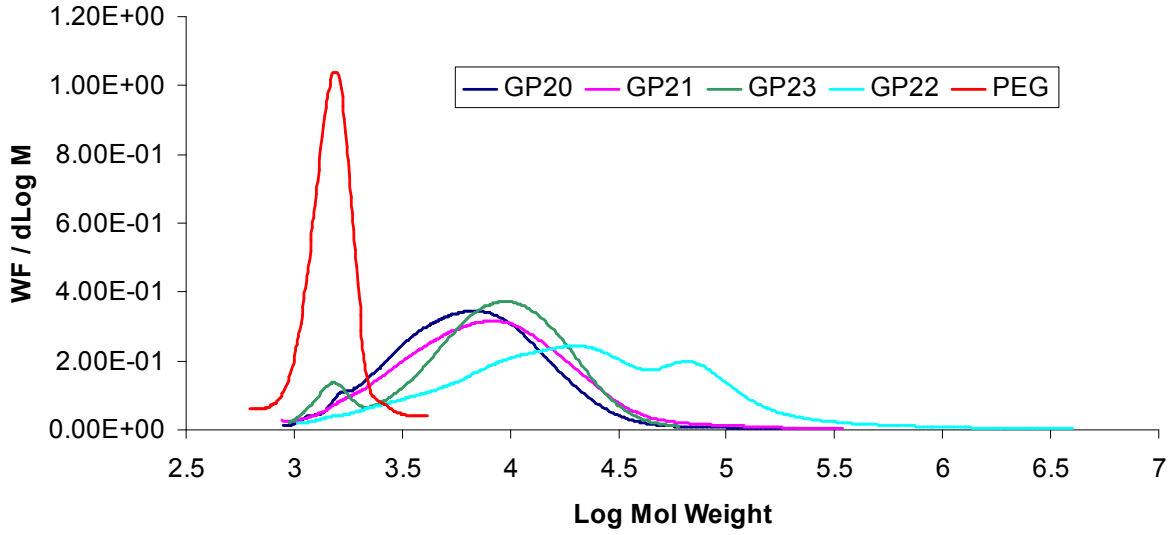

Fig. 3.16 Conventional GPC Plot for F-PIM1 (GP20), Copolymer with TEGME by High Shear method (GP21) Copolymer with TEGME by conventional method (GP22) and Copolymer with MeOPEG using High shear method (GP23)

It can be noted in Fig 3.16 that in all cases the peak for F-PIM-1 (GP-20) shifts to the high molar mass side after formation of copolymers, however, the copolymer with TEGME prepared by conventional method (GP-22) appears to be bimodal. The F-PIM-1 – MeOPEG1100 copolymer (GP-23) shows a small hump in peak on left hand side, referring to the residual MeOPEG in the sample. This a normal phenomenon when coupling a larger labile unit to hard matrix compared to a small ethylene glycol unit like TEGME.

Another important tool can be using ^{19}F NMR as it spans a wide range of chemical shift and not much effected by solvents like $CDCl_3$, DMSO-d or acetone-d. Hence, ^{19}F NMR peaks indicate fluorine atoms in the compound.[12] A change in length of fluorine peaks or their absence in copolymer can signify the replacement of fluorine atoms with MeOPEG units. ^{19}F NMR spectra for F-PIM-1 (GP-20) and copolymer (GP-23) are given at Fig. 17.

(a)

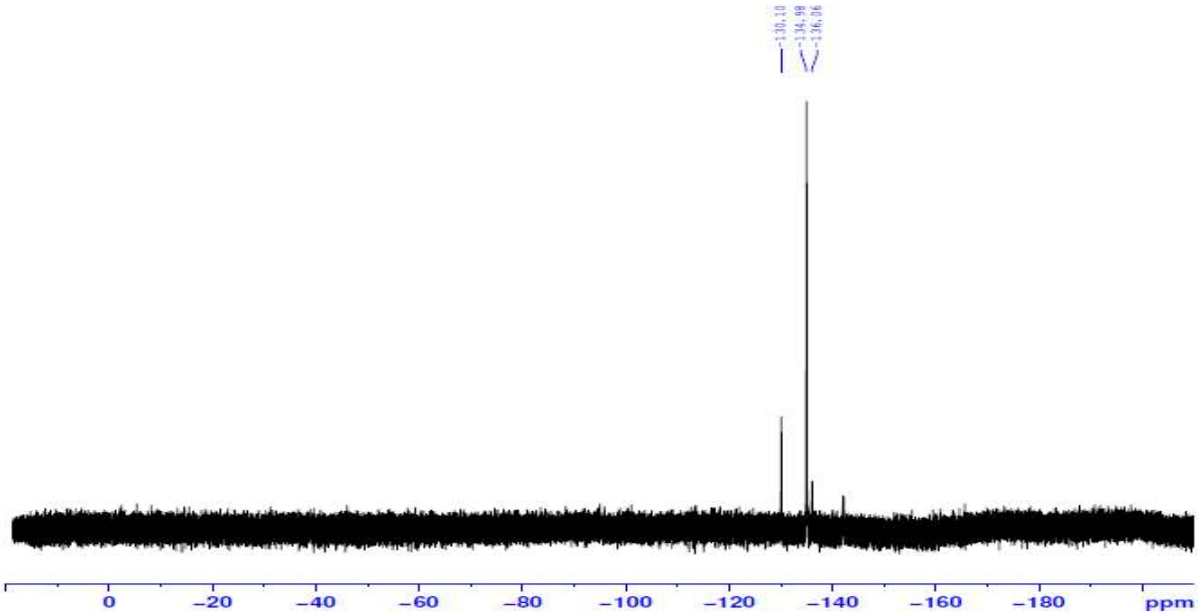

(b)

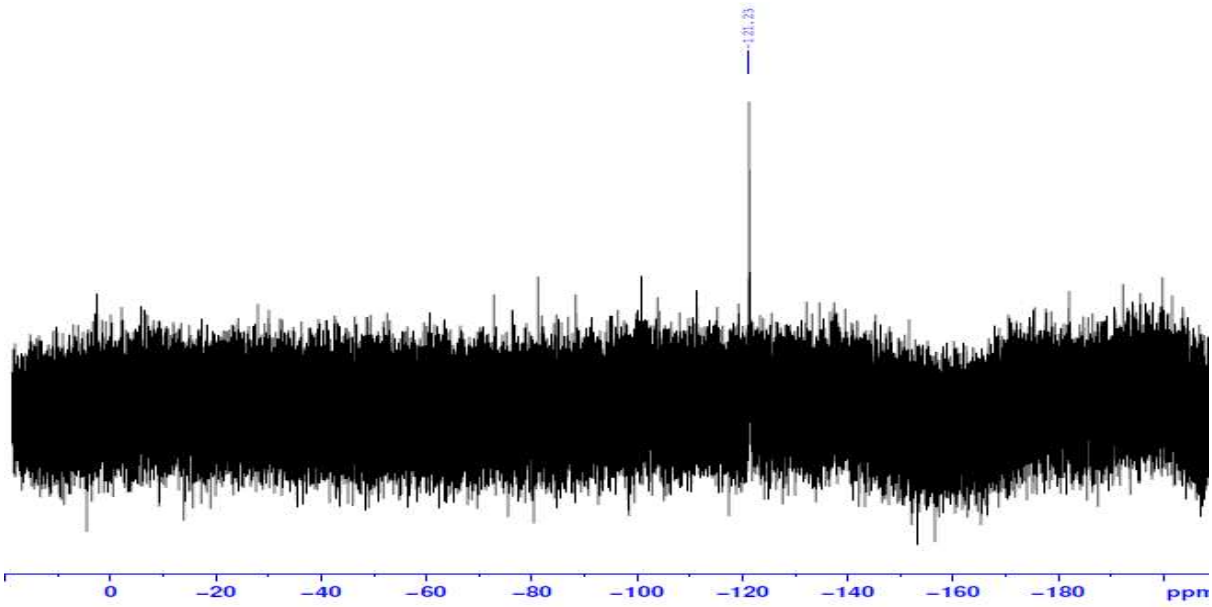

Fig. 3.17 ^{19}F NMR spectra for (a) F-PIM-1 (GP-20) and (b) Copolymer (GP-23)

It can be seen in Fig. 17 (a) that there are three sharp fluorine peaks at 130, 134 and 136 ppm. They represent fluorine atoms endcapping the F-PIM-1. Although there is lot of noise in ^{19}F NMR spectra for product (GP-23), however, it clearly gives only one peak for fluorine at 121 ppm with decreased length. Fluorine peaks for aromatic compounds occur between 50-230 ppm.[12] Hence, this signifies that fluorine atoms in original F-PIM-1 have probably been replaced with MeOPEG units with formation of copolymer.

MALDI ToF MS spectra for two products of F-PIM-1with TEGME (GP-21 and GP-22) and with MEOPEG (GP-23) indicated successful coupling in all cases. MALDI results are helpful to predict whether just one or more of fluorine atoms in F-PIM1 are substituted with labile blocks. Based on MALDI results of these copolymers, it was tried to find out peaks corresponding to mono, di, tri or tetra substitution of labile blocks (TEGME or MeOPEG1100) with fluorine atoms. Fig. 3.18 shows MALDI spectra for copolymers with TEGME (GP-21 and GP-22) and copolymer with MeOPEG (GP-23).

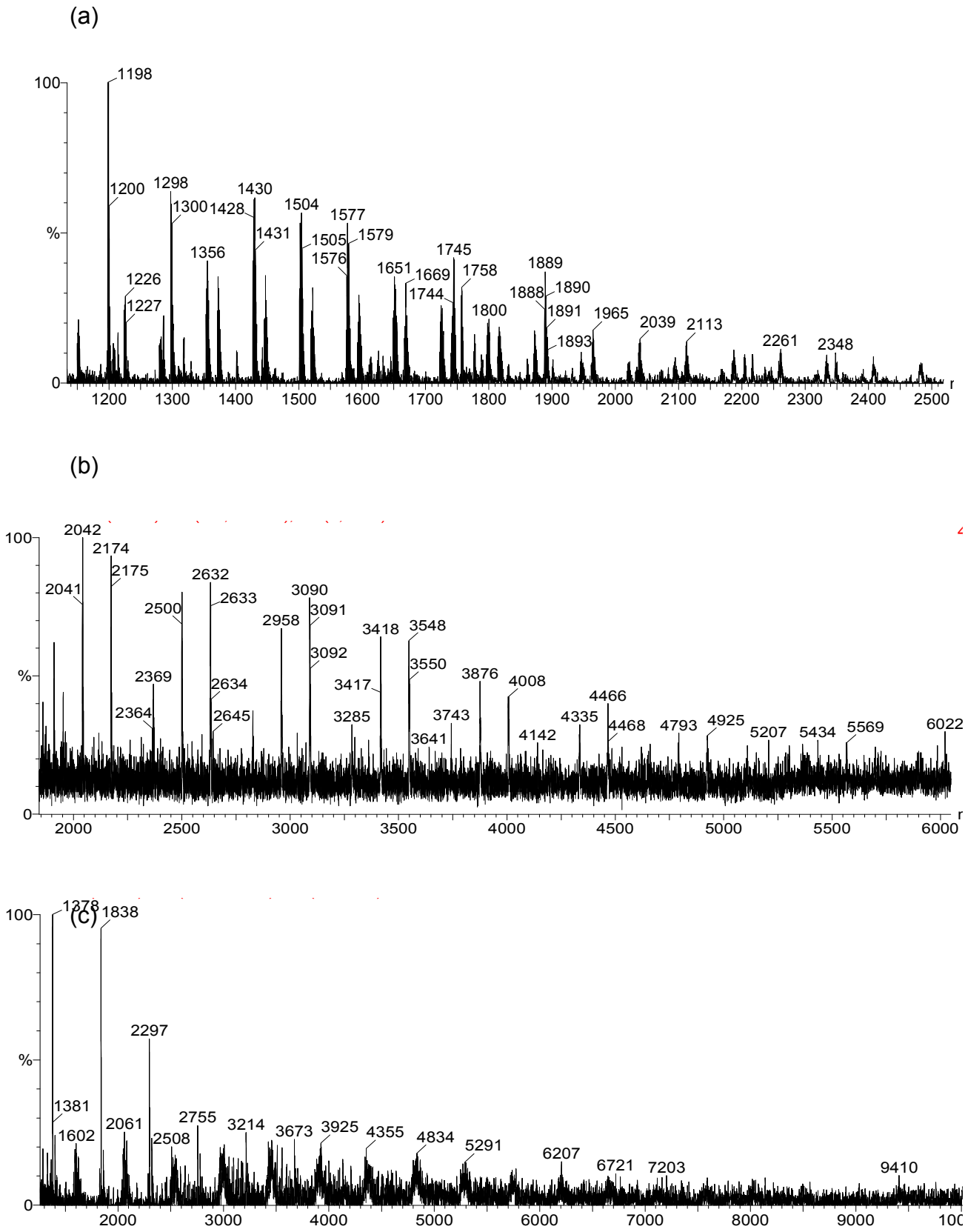

Fig. 3.18 MALDI ToF MS spectra for (a) Copolymer of F-PIM-1 and TEGME by high shear method (GP-21), (b) Copolymer of F-POM-1 with TEGME by conventional method (GP-22) and (c) Copolymer of F-PIM-1 with MeOPEG (GP-23).

MALDI calculations revealed that copolymer of F-PIM-1 with TEGME prepared by high shear method (GP-21) shows 3 peaks for di-substitution, 2 for tri-substitution and one for mono-substitution, however no peak could be found in spectrum representing complete substitution. Same type of copolymer prepared by conventional method (GP-22) was predominantly di-substituted (6 peaks). However, most interesting result was that for desired copolymer of F-PIM-1 coupled with MeOPEG (GP-23). It appears that the product was a mixture of mono, di, tri and tetra substituted polymer chains, with mono substituted and tetra substituted MALDI peaks (7 and 6 respectively) significantly higher than counterpart di or tri substituted chains.

Using the MALDI peak calculations given in introduction part of this chapter (Section 3.1.4), the possible structures for copolymer chains were assigned. A difficulty in assigning structures based on MALDI results is that one peak can refer to multiple structures. An example will illustrate it in detail. One of the MALDI peak for F-PIM1 – MeOPEG1100 copolymer (GP-23) appears at 2755 in MALDI spectrum. It was found that the same peak can refer to a mono substituted chain having 5 F-PIM-1 repeat unit connected to a MEOPEG1100 block having 5 repeat units or it can refer to a tetra substituted chain with single F-PIM-1 repeat unit connected to 4 MeOPEG1100 chains having 18 repeat units. Hence following two structures are possible (Fig. 3.19).

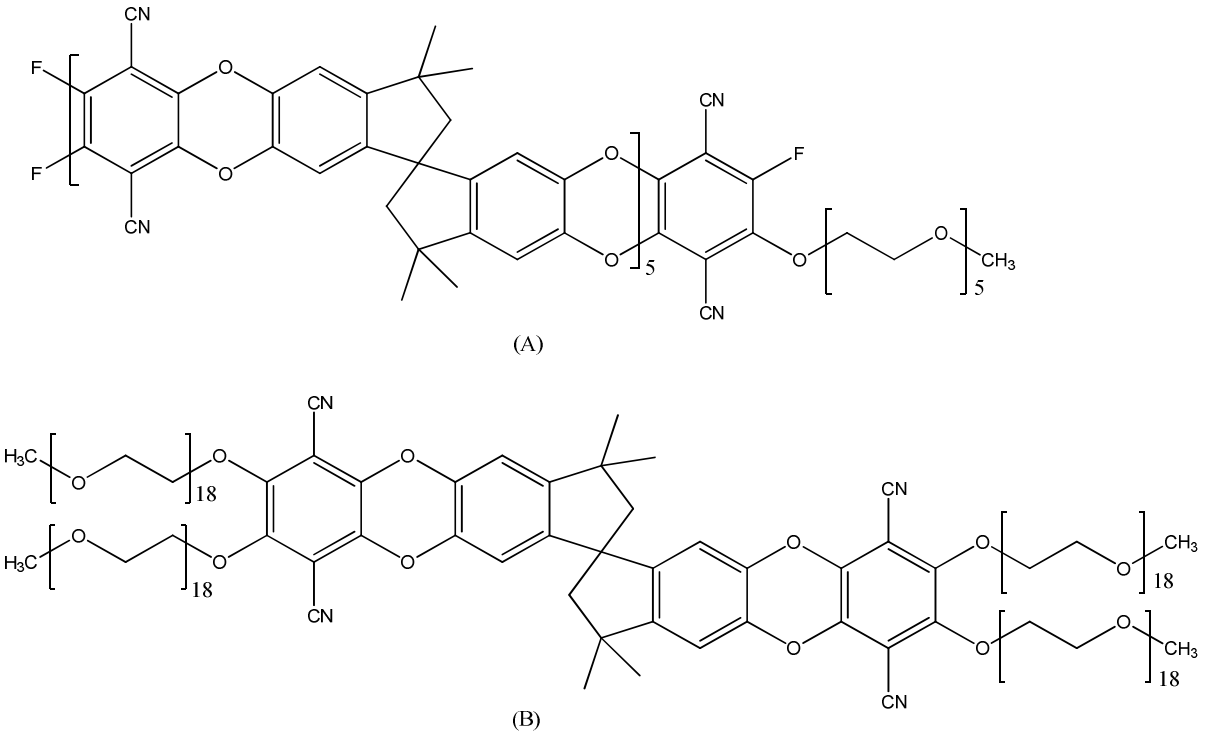

Fig. 3.19 Possible chain structures for MALDI peak appearing at 2755. (A) F-PIM1 block When Mono substituted with MeOPEG1100 block. (B) F-PIM1 block when tetra substituted with MeOPEG block.

Here it is important to note that this calculation was done only taking into account same sized MeOPEG chains substituting fluorine atoms in F-PIM-1 hard block. However, in reality, there is more chance that different sized MeOPEG chains would be attaching to same F-PIM-1 unit. This would certainly increase the number of possible chain structures for single MALDI peak.

It was appropriate to perform the thermogravimetric (TGA) analysis to check whether the thermal treatment of F-PIM1 – MeOPEG copolymer (GP-23) shows 2 stages of F-PIM-1 and MeOPEG degradation or otherwise. The TGA would also indicate how much of MeOPEG content by mass has been incorporated in the copolymer. The TGA analysis was done in air environment with slow heating at a rate of 5 °C per minute to give enough chance to copolymer for degradation. Fig. 3.20 shows TGA comparison plot for F-PIM-1 (GP-20), MeOPEG1100 and copolymer GP-23.

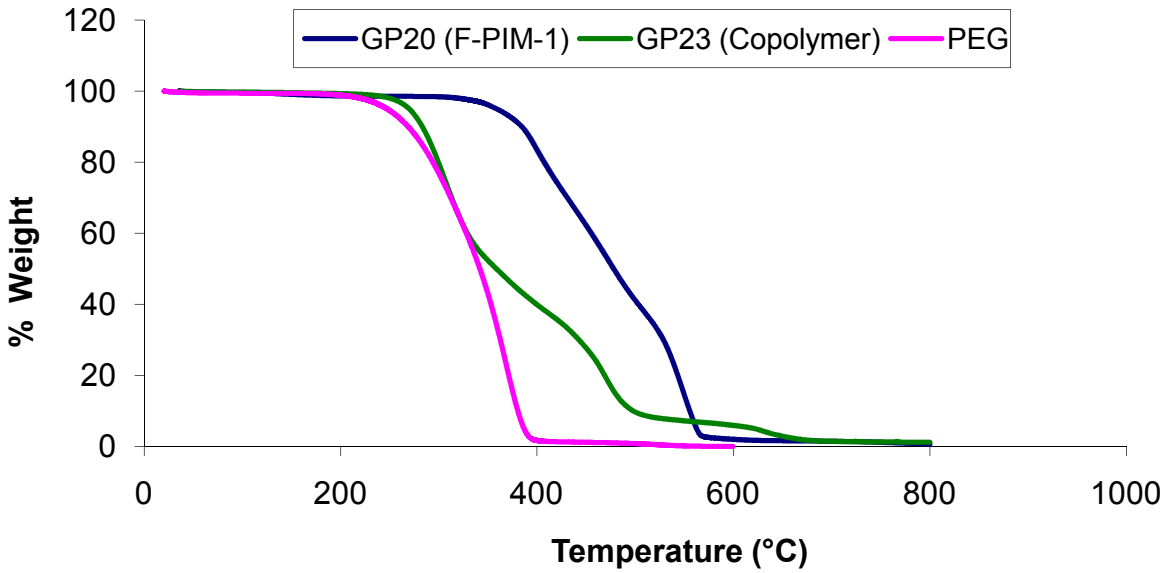

Fig. 3.20 TGA Plot for TFTPN terminated PIM-1 (GP20), MeOPEG and copolymer with MEOPEG using High shear method (GP-23)

It can be seen in the plot (Fig 3.20) that F-PIM-1, MeOPEG1100 and copolymer have very small amount of moisture. The degradation of F-PIM-1 starts around 300 °C and continues smoothly until about 570 °C. In case of copolymer it can be observed that the degradation starts in same region, however, there are two humps, one between 300-380 °C and the other between 400-650 °C. This gives an idea about presence of hard block as well as labile blocks in the backbone. Other important aspect is that all the compounds exhibit complete degradation. It can be estimated that roughly the copolymer contains 40% by mass of MeOPEG content. The plot is also an indication of successful coupling of MeOPEG1100 to F-PIM-1. The results for coupling were also supported by FT-IR and NMR analysis, which showed peaks relevant to hard as well as labile blocks in the product.

Based on TGA analysis, percent amount of MeOPEG1100 or TEGME incorporated in copolymer products was calculated. The results are given in Table 3.4.

Table 3.4 Percentage of MeOPEG1100 or TEGME incorporated in copolymers by TGA

Coupling Product	Labile block	% weight of labile block in product
GP-21	TEGME	06
GP-22	TEGME	12
GP-7	MeOPEG1100	08
GP-23	MeOPEG1100	40
GP-26	MeOPEG1100	15

It can be observed that maximum amount of MeOPEG1100 labile block was incorporated in copolymer GP-23 and minimum in GP-7. For TEGME copolymers, conventional step polymerization resulted in better product incorporating 12% TEGME by weight. The copolymer GP-23 in this context was found interesting for further investigations by fluorescence and adsorption.

The success of high shear method for synthesis of copolymers was encouraging. It is assumed that the enhanced efficiency of this approach may be due to shorter time of reaction. The reaction completes within minutes giving no time for factors like temperature fluctuations, volume change, evaporation, humidity and impurities to affect the reaction. Shorter time period also minimizes occurrence of side reaction.

It appears that change of base from BuLi to K_2CO_3 resulted in coupling of F-PIM block to MeOPEG block. The indication of successful coupling was formation of a yellow product for the first time in coupling attempts. However, colour of product cannot be a surely of coupling. Analysis of products using GPC, MALDI, NMR, FTIR and TGA supported the indication of coupling. GPC peaks showed change of molar mass to higher side, MALDI peaks showed coupling of one or more MeOPEG blocks, NMR and FTIR showed relevant peaks and TGA showed 2 distinct shoulders. It can hence be summarized that coupling of F-PIM to MeOPEG was successful.

3.3.4 Coupling reactions using larger F-PIM-1and Polyethylene Glycol Monomethyl Ether (MEOPEG) blocks

Encouraged by the success of coupling of MeOPEG1100 to F-PIM-1 (GP-23), attempts were made to repeat the synthesis using a larger F-PIM-1 and larger MeOPEG block. Two experiments were designed in this regard. In first experiment a larger F-PIM-1block (GP-24 with M_n = 6308 Daltons) was used to couple with same MeOPEG block of average M_n = 1100 Daltons. In second experiment, it was attempted to couple moderate sized F-PIM-1 oligomer (GP-27 with M_n = 3190 Daltons) with larger MeOPEG block (Average M_n = 2000 Daltons). Both the experiments were performed by the high shear method as described earlier for synthesis of copolymer GP-23. The result for first experiment was a yellow copolymer product (GP27); however the final product for second experiment (GP30) appeared to be brownish yellow.

The multidetector GPC analysis showed a significant increase in molar mass after coupling and the M_n for copolymer (GP-27) increased to 6005 compared to starting material (F-PIM-1 GP-27). The success of the synthesis for copolymer GP-27 was also confirmed by MALDI, NMR, FTIR and TGA.

The product for larger MeOPEG block had content of MeOPEG inside the final product. This was verified by MALDI spectrum which largely showed the mass distribution varying by a mass unit of 44, hence representing MeOPEG units. It appears that either only limited coupling had taken place or the sample has not run properly during MALDI analysis.

^{13}NMR spectrum of product GP-30 was not very well resolved due to its limited solubility; however, it showed strong peaks between 70-71 ppm and one weak peak between 71-72 ppm. This suggests that most of the MeOPEG remained unutilized yet a small amount was used in coupling. Rest of the spectrum has few peaks for F-PIM-1. This indicated a limited coupling taking place in product.

3.3.5 Synthesis of endcapped F-PIM-1 and its coupling to Polyethylene Glycol Monomethyl Ether (MeOPEG750)

It has been shown in sections 3.3.3 and 3.3.4 of this chapter that after using K_2CO_3 as base and adopting high shear method for reaction, copolymers of various F-PIM-1 blocks with MeOPEG1100 were synthesized. It was decided at that stage to prepare F-PIM-1 block endcapped on one side to limit the number of fluorine ends available to labile block (MeOPEG1100) for coupling and study the effect on reaction. First step in this regard would be preparation of endcapped F-PIM-1 hard block for coupling to MeOPEG. This was done as stated in experimental section. F-PIM-1 (GP-32) with M_n = 2708 Daltons was used to couple with 1,2-dihydroxy benzene (Mol. Wt = 110) in conventional way using K_2CO_3 as base. The reaction time was 6 hours and done at 65 °C under inert atmosphere and constant stirring. The final product after recrystallization from chloroform was yellow as expected. The reaction scheme is given below (Fig. 3.21).

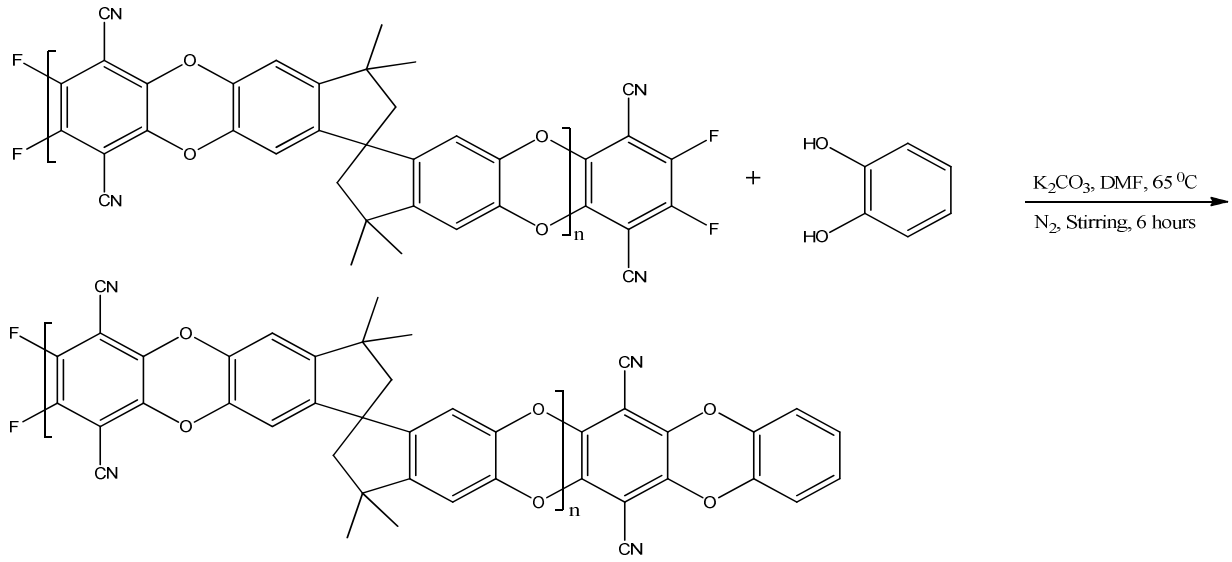

Fig. 3.21 Scheme for reaction of F-PIM1 (GP-32) with 1,2-dihydroxy benzene to form endcapped F-PIM1 (GP-37)

GPC analysis of product showed slight increase in molecular weight (M_n) of the F-PIM-1 from 2708 to 2894 after endcapping. MALDI result also showed peaks referring to endcapped product.

The endcapped F-PIM-1 product was then used for coupling to MeOPEG750. The reaction was done by high shear method as earlier adopted for coupling of other F-PIM-1 units. Again K_2CO_3 was used as base and reaction was carried out at 155 °C for 8 minutes. The scheme for coupling of endcapped F-PIM-1 with MeOPEG750 is given below (Fig. 3.22).

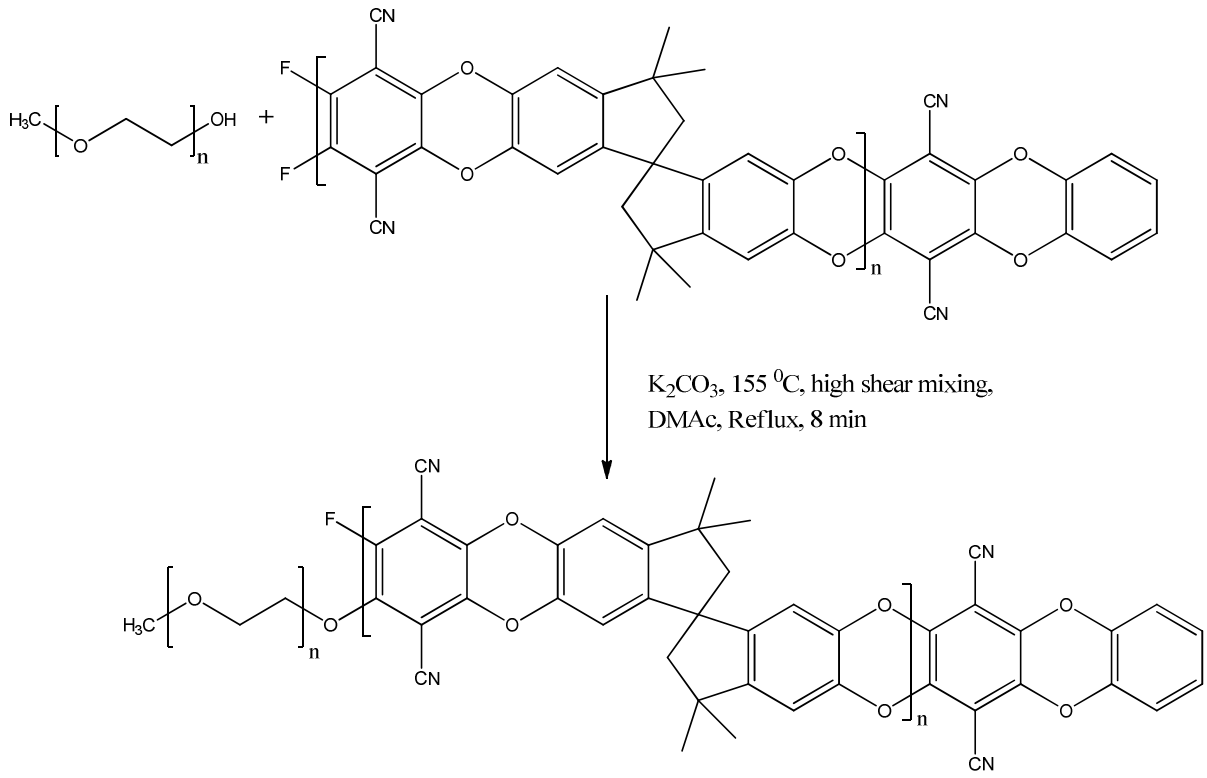

Fig. 3.22 Scheme for coupling of endcapped F-PIM1 (GP-37) with polyethylene glycol (MEOPEG750) to form copolymer (GP-38)

The reaction was monitored by NMR, GPC and MALDI analysis. It can be seen that four fluorine atoms (2 on either side) of F-PIM-1 would require twice the number of moles or 1,2-dihydroxy benzene for complete removal of fluorine atoms. Hence for endcapping on one side of the F-PIM1 polymer, equimolar amount of both reactants should be used. However, even in that case there is always a possibility that some of the F-PIM-1 chains would be fully endcapped during the course of reaction. MALDI spectrum also indicated the presence of these fully endcapped F-PIM1 chains.

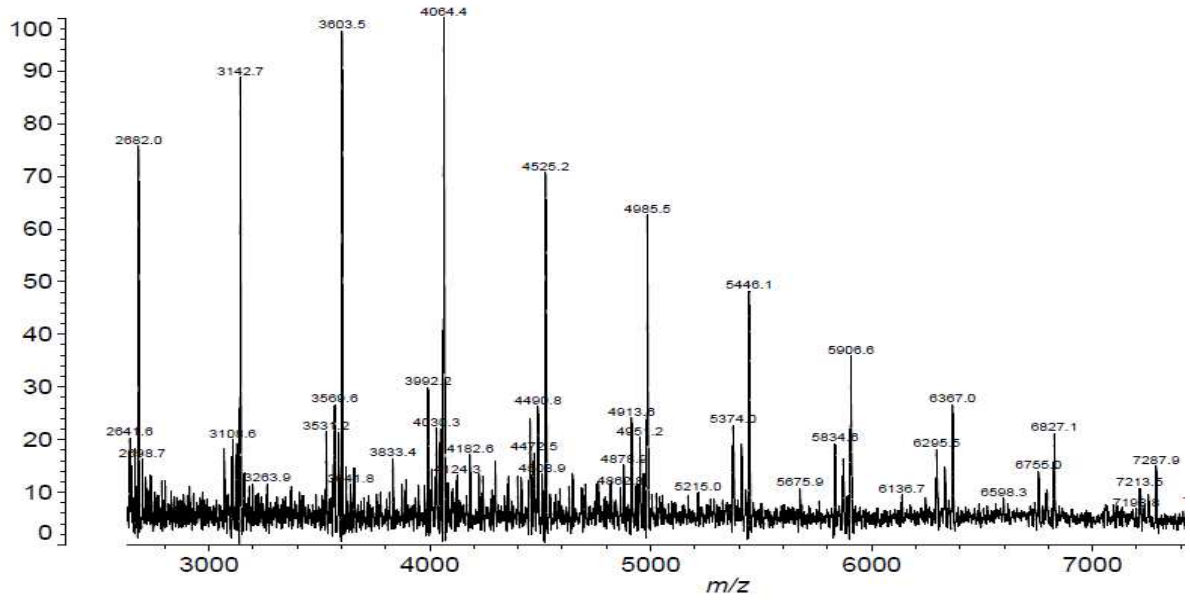

Fig. 3.23 MALDI spectrum for copolymer of endcapped PIM (GP-38)

MALDI spectrum of GP-38 (copolymer of endcappped PIM is given at Fig. 23. MALDI of copolymer indicated presence of 13 peaks referring to the formation of coupling product (at 1027, 1335, 1423, 1467, 1511, 1555, 1599, 1643, 1687, 4051, 4491, 4511, 4971 and 5475) and only 2 peaks (at 820 and 1280) referred to Fluro-PIM endcapped on both sides. The successful coupling of partially endcapped PIM-1 was satisfying in the sense that it could be used to control molecular weight of copolymer formed.

3.4 Conclusions

The main objective of this work was to synthesize the coupling products of TFTPN endcapped oligomers of PIM-1 (or F-PIM-1) with MeOPEG1100 for modification of PIM porosity and surface area. A model study was done using a model compound (GP-15) having no fluorine atoms on benzene ring to check interference or competition from nitrile groups. No coupling could be confirmed in this case. This was followed by coupling of MeOPEG with F-PIM-1 by an already specified method.[17] The product obtained by conventional step polymerization using butyl lithium as base was a brown glassy mass and analysis showed that it could be a mixture of coupling product and some side products.

It was thought appropriate to change from strong BuLi to mild K_2CO_3. However the study was started with a smaller labile block, triethylene glycol monomethyl ether (TEGME). The reaction was carried out by high shear mixing method which has been elaborated for synthesis of PIM-1 and F-PIM-1 in chapter-2. The product appeared to be a yellow solid and coupling was verified by different techniques. Same reaction was successfully repeated by conventional step polymerization. This result encouraged to undertake the reaction using MeOPEG1100. The reaction was performed by high shear mixing and coupling appeared to be successful. The techniques used for analysis of starting materials like FTIR, NMR, Polystyrene based and multidetector GPC and MALDI ToF complimented each other for successful coupling.

In a step forward, the coupling reaction was done for larger F-PIM-1 block. There was limited success while using a larger labile block (MeOPEG 2000) for coupling. In another study an endcapped F-PIM-1 was prepared by reacting F-PIM-1 (GP-32) with 1,2-dihydroxy benzene) and subsequently coupled with MeOPEG750. The coupling was again successful on the basis of results obtained for analysis of starting materials and products by FTIR, NMR, MALDI and GPC. Hence adequate numbers of coupling products were synthesized for further investigation of interest like fluorescence, interfacial activity, thermal removal of labile block, surface tension measurement and N_2 adsorption experiments for BET surface area.

References

(1) Jenkins, A.D.; Kratochvil, P.; Stepto, R. F. T.; Suter, U. W. *Glossary of Basic Terms in Polymer Science – IUPAC Recommendations 1996, Pure Appl. Chem.;* IUPAC: Vol. 68(8), 1996; pp. 1591-1595.

(2) Hamley, I. W. *Development in Block Copolymer Science and Technology;* John Wiley & Sons, England: 2004; pp. 1-2.

(3) Liu, Y. C.; Xu, W.; Xiong, Y. Q.; Xu, W. J. *J. Appl. Pol. Sci.,* **2008,** *108(5),* 3177-3184.

(4) Hadjichristidin, N.; Pispas, S.; Floudas, G. *Block Coploymers: Synthetic Strategies, Physical Properties and Applications*; John Wiley & Sons, USA: 2003; pp. 1-5.

(5) Durmaz, Y. Y.; Karagoz, B.; Bicak, N.; Yagci, Y. *Polym. Int.* **2008,** *57,* 1182-1187.

(6) Maki, Y.; Mori, H.; Endo, T. *Macromolecules*, **2008,** *41* (22), 8397–8404.

(7) Krupers, M. J.; Cabelo, F. M. E.; Moller, M. *Macromolecular Symposia,* **1996,** *102*(1), 99-106.

(8) de Espinosa, L. M.; Meier, M. A. R. *Chem. Commun.*, **2011,** *47,* 1908-1910.

(9) Myers, S. B.; Register, R. A. *Macromolecules*, **2008,** *41*(14), 5283–5288.

(10) Piirma, I. *Polymeric Surfactants;* Marcel Dekker Inc.: 1992.

(11) Grant, L. E. PhD Thesis, University of Manchester*,* 2006.

(12) Dolbier, W. R. *Guide to Fluorine NMR for organic chemists;* John Wiley & sons Inc. New Jersey, USA: 2009; pp. 9-23.

CHAPTER-4: INTERFACIAL ACTIVITY AND ADSORPTION

4.1 Introduction

4.1.1 Surface Tension and Interfacial Activity

Surface tension (γ) is defined as the force along a line of unit length, where the force is parallel to the surface but perpendicular to the line. In thermodynamic terms it is also referred as work done per unit area. SI unit for surface tension is Newton per meter (or N m^{-1}), however sometimes cgs unit of dyne cm^{-1} is also used. The phenomenon of surface tension is based on the cohesive forces among the liquid molecules. Molecules of a liquid are attracted by the neighbouring molecules in the bulk of a liquid; however, the molecules at the surface are pulled inwards. The absence of any force on the surface results in its contraction to acquire minimal area.[1]

Surfactants or surface active agents have the ability to absorb on surface of a liquid and hence alter the surface energy. They normally are composed of a polar and non polar part in their structure and orient on surface in the form of a monolayer. As a result they can expand the interface, but this may be balanced by tendency of interface to contract under normal surface tension. The net result is lowering of interfacial tension. It is governed by following equation.

$$\sigma = \sigma_0 - \pi \qquad (1)$$

Where σ_0 is the initial interfacial tension, σ is the final interfacial tension and π is the interfacial pressure (the expanding pressure for adsorbed layer of surfactant). An interfacial measurement at interface over time should be dynamic in nature. The interface between two immiscible liquids would dissolve to each other to some extent until saturation, resulting in lowering of interfacial tension.[2]

Gibbs defined the interfacial region between two liquids or solutions on the basis of a mathematical plane *Z*. Using Gibbs-Duhem equation, surface or interfacial tension can be defined as under:

$$dG^{\partial} = -S^{\partial} dT + Ad\gamma + \sum n_i \mu_i \tag{2}$$

Where G^{σ} is the surface free energy, S^{ρ} is the entropy, A is the interface area, n_i is the number of moles of component i with chemical potential μ_i at the interface. Equation (2) can take following shape in absence of any adsorption (at constant temperature and composition of the interface). [3]

$$\gamma = \left[\frac{\partial G^{\sigma}}{\partial A} \right]_{T,ni} \tag{3}$$

Equation (3) is general equation for Gibbs adsorption isotherm. According to equation (3), Surface or interfacial tension should be positive in case an interface is stable. In other words, change in free energy would be directly proportional to change in interfacial area. An increase in interfacial area would give rise to increase in free energy, while decrease in interfacial area would cause evaporation at liquid air interface and mixing of two phases for two liquid phases.

When the temperature is constant but adsorption is taking place, equation (2) will change to the following relation

$$d\gamma = -\sum \frac{ni^{\sigma}}{A} d\mu i = -\sum \Gamma i \mu i \tag{4}$$

Where Γi represents number of moles of component i adsorbed per unit area. Generally Γ is also known as surface excees. The simplest case would be a two component system in which one is surface active and can adsorb on surface or solvent. [4]

Block copolymers due to their similar structure can behave like surfactants and spontaneously self organize themselves to form various nanoscopic spherical, rodlike or lamellar structures.[5] An interesting example in this case is self aggregation of amphiphilic phthalocyanine block copolymers.[6] Block copolymers often are composed of incompatible blocks of different types of monomers and can lead to

micellization and adsorption characteristics in suitable solvents. A common example is that of ethylene oxide–propylene oxide block copolymers in solution.[7]

There are many methods available to measure surface tension of a liquid or solution. Some of them are Wilhelmy plate method, Spinning drop method, Du Nouy Ring method, Pendant Drop method, Capillary rise method and Bubble pressure method.[8]

The method chosen to determine the surface tension was pendant drop method, due to the fact that it requires relatively very small amount of material and solvent and simple to use. Another factor was availability of an instrument at university. Pendant drop is a drop suspended from a fixed solid. The forces experienced by the drop are gravitational force and surface tension. Hence the shape of the drop is function of surface tension. The important assumptions in this method are that the drop is symmetric about a central vertical axis and is not in motion. The gravitational force and surface tension are related to each other by a quantity known as Bond Number (B_o), which is defined as under:

$$B_o = \frac{\Delta\rho g R^2}{\gamma} \tag{5}$$

Where $\Delta\rho$ is change in density of liquid and fluid around it, g is the gravitational constant, γ is the surface tension and R is the maximum horizontal radius of the pendant drop. The shape of the drop as sphere changes with increasing *Bo* and R until it hangs vertically and finally detached from solid. The surface tension is determined by the software by fitting the drop shape by a video image into Young Laplace equation.

$$\Delta P = \gamma\left(\frac{1}{R} + \frac{1}{R'}\right) \tag{6}$$

Here ΔP is the change in drop pressure across the interface, while R and R' are principle radii of curvature and γ is surface tension. It is important to mention that Young Laplace equation requires drop to be distorted by gravity in order to measure surface tension. In other words surface tension for a spherical drop cannot be

determined. The liquid or solution is put in a syringe of appropriate size (normally 25 or 50 µL) and adjusted in the holder. The parameters are set in the easy to run software and drop of appropriate length is formed. This may be done with care and practice. The image needs to be adjusted on screen at horizontal axis and captured when a bright spot in the middle of drop is large enough. The instrument automatically tells the surface tension value. [9]

4.1.2 Polymer Blends

When two or more polymers are mixed together in a specific ratio, a blend with optimized material properties is formed. This concept is analogous to the alloy formation for metals. However, the concept is not as simple as it sounds. Two polymers may be miscible, partially miscible or immiscible. If two polymers are miscible in a solvent, single phase system would be obtained and if they are partially miscible, finely dispersed two phase system could be obtained employing very low interfacial energy and without need of a compatibilizer. Although theoretically correct, even simple systems need some sort of compatibilization to prevent macro-phase separation. [10] An example of Lower Critical Solution Temperature with two component polymer blend is shown in Fig. 4.1. There are three regions including miscible phase, metastable phase (only stable within small concentration fluctuations and a two phase region with spinodal decomposition.

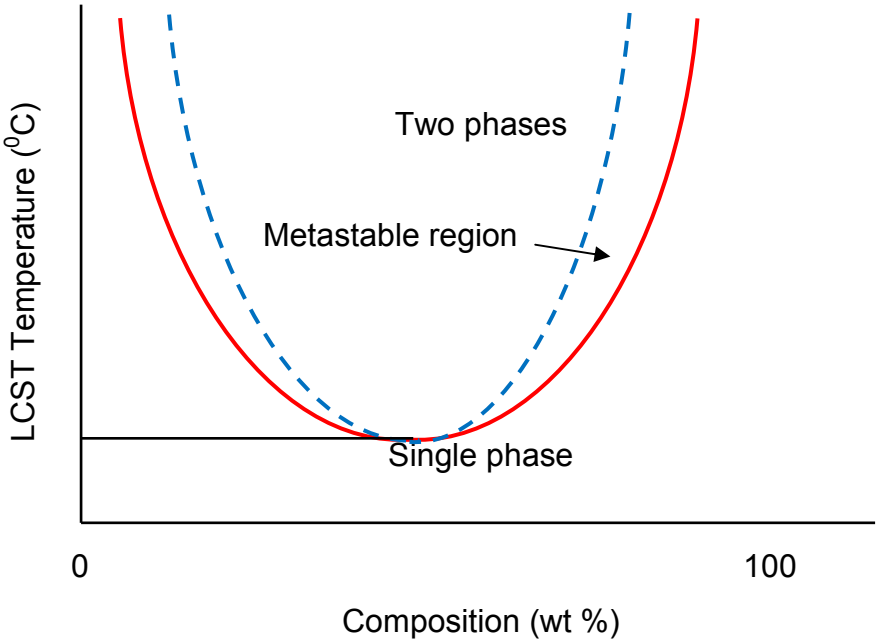

Fig. 4.1 A schematic phase diagram for a polymer – polymer blend with a lower critical solution temperature (LCST)[7]

Preparation of polymer blend of two or more polymers depends on phase behaviour. Low molecular weight polymers may show miscibility, however high molecular weight polymers usually do not mix. The reason for mixing of low molecular weight material is large value of combinatorial entropy, which in case of high molecular weight materials does not contribute significantly. For a two component system, we can start with the equation for free energy of mixing. [11]

$$\Delta G_m = \Delta H_m - T\Delta S_m \qquad (7)$$

Where ΔG_m is the free energy of mixing, ΔH_m is the enthalpy of mixing (heat of mixing) and ΔS_m is the entropy of mixing. The negative value for free energy of mixing ΔG_m, although is important but not the only factor for miscibility. If □ represents the overall composition of a component

$$\left[\frac{\partial^2 \Delta G_m}{\partial \phi_i}\right]_{T,P} > 0 \qquad (8)$$

The relation in Eq. 8 signifies that (even though $\Delta G_m < 0$), the mixing would yield a phase diagram showing one phase rich in component 1 and other rich in component

2. Mixing can be achieved by increasing temperature (hence increase in entropy and free energy of mixing) for low molecular weight materials, however, for high molecular weight materials small value of entropy is not driving force and other factors like non-combinatorial entropy and temperature dependant ΔH_m may even result in decrease in miscibility. Due to this reason polymer-polymer mixtures generally show lower critical solution temperatures (lcst). The spinodal curve is related to the position where

$$\left[\frac{\partial^2 \Delta G_m}{\partial \phi_i}\right]_{T,P} = 0 \qquad (9)$$

While binodal curve for binary system is related to the equilibrium phase boundary between the single phase and the phase separated region and dependent on the chemical potentials of an individual component being equal in both phases. [12]

$$\Delta\mu_1^{\,a} = \Delta\mu_1^{\,b} \qquad \Delta\mu_2^{\,a} = \Delta\mu_2^{\,b} \qquad (10)$$

Where 1, 2 represent the two polymers and a, b represent the phases. The chemical potential is defined as the rate of change of the Gibbs function of the system with respect to the change in the number of moles of a specific component. The region where binodal and spinodal curves intersect is defined by the equation.

$$\left[\frac{\partial^3 \Delta G_m}{\partial \phi^3}\right]_{T,P} = 0 \qquad (11)$$

The experimental phase diagrams may be non-symmetric for components with large difference of molecular weight. The volume fraction of component 1 rich phase ϕ_{1r} and component 2 rich phase, ϕ_{2r}, can be determined from the expression.

$$\left[\frac{\phi_{1r}}{\phi_{2r}}\right] = \frac{\phi_b - \phi}{\phi - \phi_a} \qquad (12)$$

Low molecular weight polymers and miscible polymers exist in single phase, however, if ucst or lcst behaviour exists, it cannot be determined. Due to glassy state at lower temperatures, ucst cannot be determined. At higher temperatures, there is a danger of polymer degradation before phase separation. Hence for highly immiscible polymer blends, the phase diagram exists in the two phase region with the binodal curves virtually overlapping the y axis at 0 and 1.0 volume fraction.

The entropy of mixing for two dissimilar components can be calculated starting with the Boltzmann relationship:

$$\Delta S_m = k \ln \Omega \tag{13}$$

Where Ω represent the summation of combinations of arranging N_1 and N_2 molecules into a regular lattice of N ($N = N_1 + N_2$) cells. Ω can be determined as

$$\Omega = \frac{N!}{N_1! N_2!} \tag{14}$$

Applying Sterling's approximation yields:

$$\ln N! = N \ln N - N \tag{15}$$

Substitution of Eq. 14 into Eq. 15 and then Eq. 13 yields:

$$\Delta S_m = k(N \ln N - N_1 \ln N_1 - N_2 \ln N_2) = -k(N_1 \ln x_1 + N_2 \ln x_2) \tag{16}$$

Where $x_1 = N_1/N$ and $x_2 = N_2/N$. This equation holds good for low molecular weight molecules of approximately equal size. However, for a polymer-solvent mixture, the term $N_1 \ln x_1 >> N_2 \ln x_2$, resulting in negligible change in the free energy of mixing. The use of mole fraction term here becomes tricky as x_1 controls both the enthalpy and entropy. It has been showed that if the value of mole fraction was replaced with volume fraction ϕ_i, to get realistic approximation of entropy. The molecular volume V_i

is equal to the product of V_{mer} and the number of mer units in a lattice of N cells with volume of V. For solvents, the number of mer units is 1. The volume fractions ϕ_1 and ϕ_2 are then can be written as:

$$\phi_1 = \frac{V_1 N_1}{V_1 N_1 + V_2 N_2} \qquad \phi_2 = \frac{V_2 N_2}{V_1 N_1 + V_2 N_2} \tag{17}$$

Substituting these values in Eq. 16 we get:

$$\Delta S_m = k(N_1 \ln \phi_1 + N_2 \ln \phi_2) = -RV(\frac{\phi_1}{\upsilon_1} \ln \phi_1 + \frac{\phi_2}{\upsilon_2} \ln \phi_2) \tag{18}$$

This equation represents combinatorial entropy of mixing for the Flory-Huggins theory. As the $\ln \phi_i$ value is negative, ΔS_m is positive and the expression $(-T\Delta S_m)$ in Eq. 7 leads to a negative contribution to ΔG_m, thus improving the potential for miscibility. As noted with high molecular weight polymers, this contribution becomes negligible. [13]

.

We can now use Flory-Huggins theory for modelling the free energy of binary polymer mixtures. The key equation is:

$$\Delta G_m = RTV(\frac{\phi_1}{\upsilon_1} \ln \phi_1 + \frac{\phi_2}{\upsilon_2} \ln \phi_2) + \phi_1 \phi_2 \chi_{12} RT\upsilon / \upsilon_r \quad \text{(Molar basis)} \tag{19}$$

Where V = total volume, R = gas constant, ϕ_i = volume fraction of component i, V_i= molecular volume, v_i = molar volume of polymer chain i, v_r = molecular or molar volume of a specific segment and χ_{12} = Flory-Huggins interaction parameter.

It can be seen that combinatorial entropy of mixing is incorporated in first part of equation. If the molecular weight of any component becomes larger than other, the negative value of this expression becomes very small. The combinatorial entropy hence contributes significantly for solvent-solvent and polymer-solvent mixtures. [12,13]

A common approach to achieve mixing of polymer blends is using a compatibilizer. A compatibilizer increases the interaction energy between two phases and temperature applied determines morphology and phase separation behavior.[8] Typical compatibilizers like AB type block copolymers reduce interfacial tension, promote finer dispersion and controls morphology. In commercial blends, 5 – 15wt% of compatibilizer decreases the interfacial tension by dissolution of the copolymer block segments within their respective homopolymer phases, leading to covalent bonds being positioned across the interface.[14]

Styrene-butadiene (SB) block copolymers show this behaviour when added in low-density polyethylene/polystyrene (LDPE/PS) blends. It has been shown that addition of some SB copolymers, resulted in decrease in the blend impact strength in spite of the fact that these SB improve the toughness of both the blend components.[15] Copolymers are also known for compatibilization effect when added to polymer-polymer interface.[16] Compatibilization effect of block copolymers has been reported for polystyrene/poly(methyl methacrylate) (PS/PMMA) with observation of a sharp decrease in dispersed phase dimension for addition of a few per cent of block copolymers. This was followed by a levelling off as the copolymer content is increased above the critical micelle concentration.[17]

4.1.3 PIMs as Adsorbents

PIM materials have shown great promise for potential use as adsorbents and catalytic supports. Phthalocyanine based network PIM (CoPc20) demonstrated high surface area and ability to adsorb small organic probe molecules. This material showed appreciable selectivity in comparison to activated carbon counterparts of almost the same surface area. The adsorption / desorption studies of the powdered phthalocyanine-containing network PIM (CoPc20) have shown that it rejects larger dye molecules while allowing smaller organic probe molecules. High concentration of active pores of sub nanometer dimensions makes it suitable for catalytic applications. The nitrogen sorption isotherms show high uptake at low pressures in both cases. The hysteresis loop for PIM extends to the low pressure region while that of active carbon closes at moderate pressure, showing that the PIM is

predominantly ultramicroporous in comparison to its counterpart which has a much broader pore size distribution in mesoporous region (Fig. 4.2). Introduction of effective mesoporous region can only enhance their efficacy for catalytic usage.[18,19] Studies have also been carried out on other network phthalocyanine, porphyrin and Hatn PIMs, reflecting the real potential of PIM materials for their use in catalysis and adsorption processes.[18, 20]

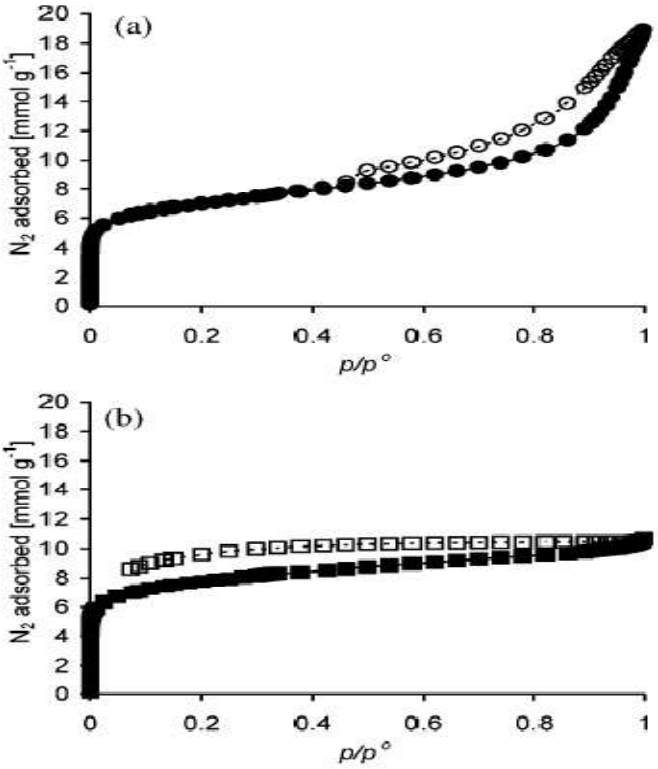

Fig. 4.2 Nitrogen adsorption (filled symbols) and desorption (open symbols) isotherms at 77 K for (a) Darco 20-40 mesh carbon and (b) CoPc20 network-PIM.[21]

Although N_2 adsorption studies for PIM-1 have already been undertaken and reported,[18, 19, 21] it would be interesting to see how these studies compare to the copolymer products of PIM materials. Another important aspect would be to undertake adsorption by PIMs from solution of another polymer. Chapter 2 and 3 discuss the synthesis of fluoro endcapped PIM oligomers and their subsequent coupling to MeOPEG. A part of this chapter would deal with N_2 as well as solution adsorption by PIM-1 from MeOPEG solutions. At a later stage, MeOPEG block will be thermally removed in order to generate new pore structure and alter surface area. Similar approach would be used to remove MeOPEG block from block copolymers

synthesized and compare the pore structure as well as surface area with parent PIM-1 material and PIM-1 with MeOPEG adsorbed from solution.

4.2 Experimental

4.2.1 Membranes of PIM-1 and its blends

PIM-1 (GP-3) (high molecular weight formed by reaction of 1:1 reaction of TFTPN and BCA) with average molecular mass 98,500 Daltons was mixed with MeOPEG1100 (average molecular mass 1100 Daltons) in various ratios. The membranes were cast by dissolving PIM-1 and blends in anhydrous $CHCl_3$ and solutions were covered and put for slow evaporation of the solvent. In the case of membrane of pure PIM-1, the requisite mass of PIM-1 was dissolved in anhydrous $CHCl_3$ following the same process.

The total mass in grams required to form a 40 micron film was calculated using the formula $m = d^2 \pi / 800$, where m is the mass, d is the diameter of the dish and π is 3.142. The amount of solvent used for each membrane was calculated by the formula $V = 50m$, where V represents volume and m is the mass.

4.2.2 Compatibilization of PIM-1 blends using coupled products of PIM-1

The membranes were formed following the same procedure as described in section 4.2.1. Total mass for 40 micron film remained the same as used before; however, in addition to PIM-1 (GP-3) and MeOPEG1100, certain percentage of compatibilizer (copolymer of PIM-1 GP-23) was also added.

4.2.3 Nitrogen Sorption Measurement

The sorption experiments were carried out on a Coulter SA 3100 Surface Area and Pore Size Analyzer. The samples were initially degassed for 960 minutes at 110 °C under high vacuum. Nitrogen adsorption / desorption isotherms were recorded at 77 K and the BET Surface Areas were accordingly calculated.

4.2.4 Thermogravimetric Analysis (TGA)

Thermal analysis was carried out using TA Q5000 V3.1 build 246 equipment. About 10-15 mg of sample were loaded in aluminum or platinum pans and weight loss as a function of temperature was measured with heating rates of 10 °C, 5 °C or 3 °C per minute. The analysis was carried out for different samples of PIM-1, TFTPN endcapped PIM-1 and MeOPEG. The TGA results for coupled products would be discussed in next chapter. The measurements were made in N_2 and air environments. The flow rate of N_2 and air was 10 mL/min and 25 mL/min for balance and sample respectively.

4.2.5 Surface Tension Measurement

Surface tension was determined on a Kruss Drop Shape Analysis System DSA 100 machine by pendant drop method. 2 mg / mL solution of polymer was prepared in tetrahydrofuran (THF) for the measurement of surface tension.

4.2.6 Solution Adsorption

200 gm of poly(ethylene glycol) monomethyl ether (MeOPEG1100) was added to 100 mL of distilled water and stirred till clear solution formed. To this solution, 125 mg of PIM-1 (GP-3) or F-PIM-1 (GP-32) were added and stirred well. The mixture was then put in fumehood to attain equilibrium. The samples were kept in fumehood for 10 days for complete adsorption. After that PIM material was filtered from mixture

through vacuum filtration and dried in dessicator (with silica bead desiccant) for 72 hours before using for N_2 adsorption analysis.

4.2.7 Heat Treatment of PIM-1 and F-PIM-1

Samples of PIM-1 and F-PIM-1 powder were heat treated for thermal removal of MeOPEG block at 300 °C in a Carbolite 1200 °C Three Zone tube furnace. The heating time was 6-8 hours under flow of nitrogen.

4.3 Results and Discussion

4.3.1. Blending of PIM-1

The compositions used in blending study are given in Table 4.1 below:

Table 4.1 Blend compositions by %mass of PIM1 (GP3), MeOPEG1100 and Compatibilizer (Copolymer GP23)

Blend Name	Composition (% mass)			Remarks
	PIM-1	MeoPEG1100	Compatibilizer (GP23) (Copolymer of Fluoro-PIM and PEG)	
GPB-1	80	20	-	Macro-phase
GPB-2	70	30	-	Macro-phase
GPB-3	60	40	-	Macro-phase
GPB-5	60	30	10	Macro-phase
GPB-6	70	20	10	Macro-phase
GPB-7	80	10	10	Macro-phase
GPB-8	70	10	20	Macro-phase
GPB-9	60	10	30	Macro-phase
GPB-12	90	5	5	Clear Film
GPB-13	95	5	-	Macro-phase
GPB-17	84	6	10	Macro-phase
GPB-18	79	7	14	Macro-phase

It was mentioned during the discussion section of previous chapter (Chapter-3, Section 3.3) that various copolymers were synthesized by coupling of fluoro ended oligomers of F-PIM-1 with polyethylene glycol monomethyl ether (MeOPEG1100). Thermogravimetric analysis (TGA) studies of those copolymers revealed that a considerable quantity (% mass) of MeOPEG1100 was incorporated to F-PIM1

oligomers. In fact different copolymers had incorporated 10-40% of MeOPEG1100 content by mass. This observation developed interest to study physical mixing of MeOPEG1100 component in high molecular mass PIM-1. If successful, this could lead to development of MeOPEG1100 containing blends and films, which could be later, thermally treated and possibly result in modification of pore structure of the matrix. Hence it could lead to develop materials for various applications.

Polymer blending is considered entropy driven process. Keeping this in mind, it is again a question of interest whether we are dealing with miscible or immiscible blends. The strategy for blend formation is different in both cases. In order to assess the viable route to successful blending of PIM-1 and MeOPEG1100, the starting point would be to examine mixing of both polymers in various ratios and assess how much MeOPEG1100 could be incorporated without use of any additive. If some amount of MEOPEG1100 could be incorporated in PIM-1 without any macrophase separation, it can lead the way to try for blending higher mass percentage of MeOPEG1100.

It is already established that pure PIM-1 can form stable and transparent yellow coloured membranes.[21] In order to check the PIM-1 (GP-3) to be used for blending process; it was dissolved in chloroform and for slow solvent evaporation to form a 40 micron thick membrane. It resulted in formation of transparent yellow film. Fig. 4.3 shows the film formed by PIM-1 (GP-3) slow evaporation of solvent.

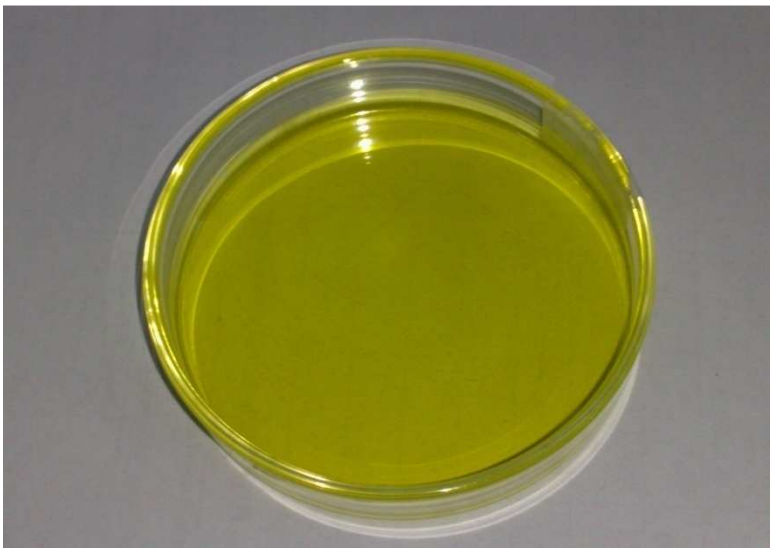

Fig. 4.3 40 micron film of PIM1 (GP3) formed by slow evaporation of chloroform.

It has already been mentioned that copolymer synthesis indicated a maximum of 40% incorporation of MeOPEG1100 into F-PIM1 oligomers. Hence to start with, three blend compositions were selected. PIM-1 (GP-3) and MeOPEG1100 were dissolved in chloroform with mass percent ratios of 80:20 (GPB-1), 70:30 (GPB-1) and 60:40 (GPB-3) (refer to Table 4.1 for compositions) are shown in Fig. 4.4.

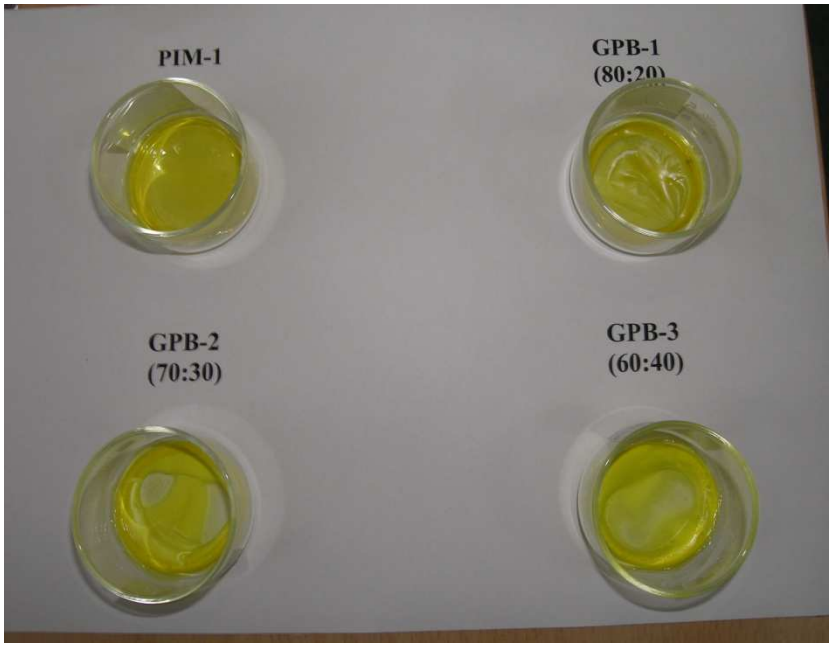

Fig. 4.4 PIM-1(GP3) and blends GPB-1(80:20), GPB-2(70:30) and GPB-3(60:40) after slow evaporation of solvent (mixed by mass percent, higher percent referring amount of PIM-1 and lower for MeOPEG1100)

Fig 4.3 reveals that the PIM-1 membrane is transparent and homogenous. The membrane was kept for more than a year and found mechanically stable. However, rest of the three blends membranes shown in Fig. 4.4 had a clear macro-phase separation. This indicated immiscibility of both phases. As expected, the macrophase separation depends on the amount of MeOPEG1100, showing a gradual increase with larger amount of MeOPEG1100 added.

As a principle we have to move from a state of low entropy to higher entropy for a change of state like blending to occur. However, amorphous polymers are already in a state of high entropy, due to random tangling up long and short polymer chains. Hence an amorphous polymer doesn't get considerable increase of entropy on

mixing up with another polymer, which makes mixing up less favourable. This is what has been observed during blending of PIM-1 with MeOPEG1100, resulting in macrophase separation.

In case of immiscible or phase separated blends a usual solution to this problem is to mix polymers in fluid state by heating. However, this practice is more useful and adopted on industrial level. Another technique used for this purpose is use of compatibilizers. In order to understand the phase separation of two immiscible polymers and use of compatibilizers to facilitate their mixing we will consider example of PIM-1 and MeOPEG1100 in a model.

In Table 4.1, GPB-5, GPB-6 and GPB-7 show blends of PIM-1 (GP-3) and MeOPEG1100 were formed with use of copolymer GP-23 as compatibilizer. In all these cases, percentage by mass of compatibilizer was kept at 10% and ratio of PIM and MeOPEG components was varied. However, all these attempts again resulted in macro phase separation. The blends prepared are shown in Fig. 4.5.

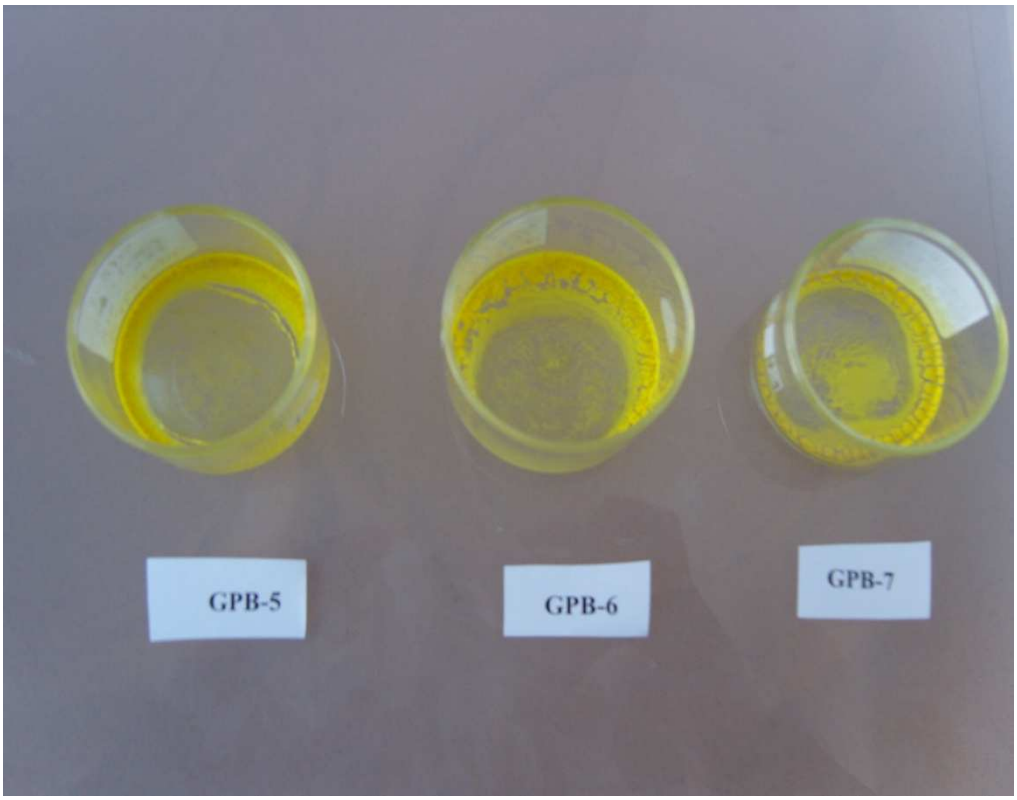

Fig. 4.5 Blends with %mass ratios of PIM1:MeOPEG1100, 80:10 (GPB-5), 70:20 (GPB-6) and 60:30 (GPB-7) with 10% of compatibilizer in all blends.

It was expected that the addition of the compatibilizer would result in increasing miscibility of two components (PIM-1 and MeOPEG1100) and maybe lead to microphase separation. However, the results were not as encouraging as expected. It can be observed that macrophase separation still existed in the blends; however, the blends were considerably more transparent than previous blends. The addition of compatibilizer helped to a small extent but could not result in complete miscibility. It was hence considered to add more compatibilizer and play with the ratios of blend membranes.

In yet another attempt, two more blends with increased amount of compatibilizer and constant MeOPEG mass were formed. GPB-8 and GPB-9 had PIM- :MeOPEG1100: compatibilizer by percent mass ratio of 70:10:20 and 60:10:30 respectively.

The resultant blends again didn't show any sign of betterment in miscibility or generation of microphase. It was now imperative to start looking at the possibility of solubilizing a minimum amount of MeOPEG1100 into a blend and explore by small increments how much more of it can be incorporated by addition of compatibilizer. Once this could be achieved, there exists a good chance for thermal or solvent treatment of the membranes to alter the pore structure of the blends.

Keeping in view the above observations, a new set of blends was tried. The first sample named GPB-12 contained PIM-1 (GP-3), MeOPEG1100 and copolymer compatibilizer (GP-23) in percent mass ratio of 95:5:5 respectively. While in the blend GPB-13 PIM-1 and MeOPEG1100 were mixed in percent mass ratio of 95:5 without any compatibilizer for comparison to GPB-12.

Although, the blend GPB-13 (PIM-1 and MeOPEG1100 in 95:5 mass percent) showed macrophase separation to some extent, however, the blend was better than previous attempts. It appeared in form of a film but opaque instead of transparent. A small macrophase could be seen around corners of the blend. The effect of compatibilizer on solubilisation of MeOPEG1100 into PIM-1 was also quite distinct in GPB-13 (blend containing PIM-1, MeOPEG1100 and compatibilizer in mass percent

ratios 90:5:5 respectively). For the first time it was a transparent film without any macrophase. This was evidence that the compatibilizer enhanced the solubility of the MeOPEG1100 component in the PIM-1. Although solubilization of just 5% MeOPEG1100 by mass was not as much as expected but at least now a narrow range was identified to work with the composition. The cutting of polymer membrane with a scissor is considered as a known test to verify the quality of a film formed. The blend membrane cast from blend GPB-12 appeared to be stable and easily cut by a scissor.

We have observed in chapter 3, section 3.3 that copolymerization of PIM-1 oligomers and MeOPEG100 could result in formation of copolymers having MeOPEG component up to 40% by mass. However blending experiments only showed 5% solubilisation of MEOPEG component.

When we mix PIM-1 and MeOPEG1100 in a blend, MeOPEG should probably stay in solvent phase and PIM in organic phase with an interface separating both polymers. The obvious compatibilizer in this case would be a copolymer of PIM and MeOPEG1100 which should sits on phase boundary. Obviously it would be directed in a way that PIM block of copolymer would interact PIM-1 phase and MeOPEG block to interact MeOPEG1100 in solvent phase. This should theoretically result in transfer of energy and decrease in interfacial tension and consequently generating microphase structure. The expected orientation of compatibilizer in blend is shown in Fig. 4.6.

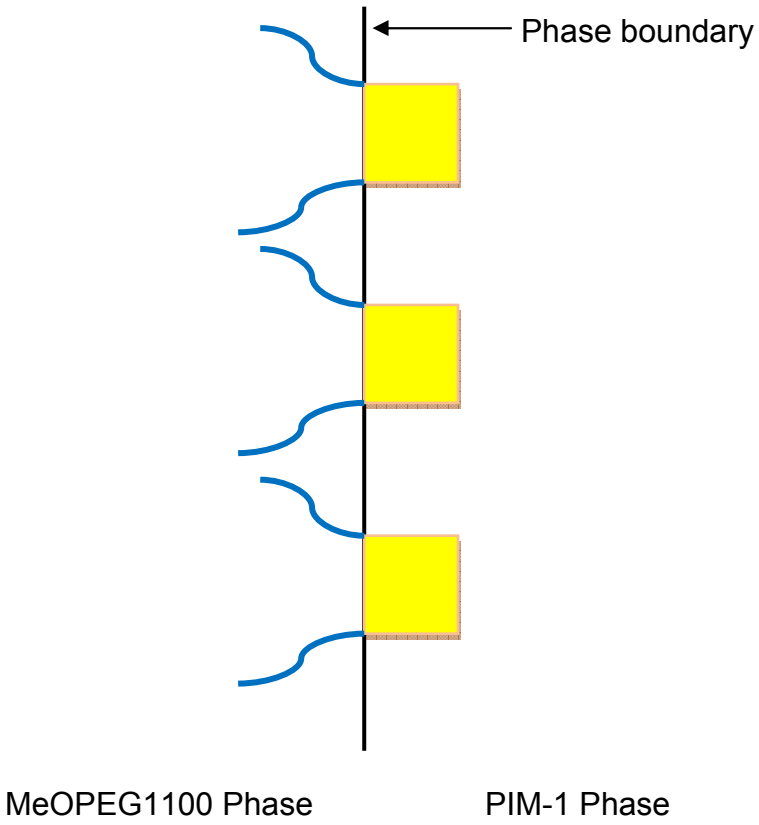

Fig. 4.6 Compatibilizer GP-23 (copolymer of F- PIM-1 and MeOPEG1100) and its orientation in blend solution. Yellow squares represent PIM-1 block in copolymer and curves blue lines represent MeOPEG1100 block of copolymer.

The reason why it's not happening (or happening to a small extent) needs to be explored. One of the possible reasons that can be referred is nature of PIM-1. PIM-1 has a micropore structure and interacts very well with anything that comes to its contact. It is believed to be dominantly hydrophobic but overall PIM-1 unlike many other organic polymers which are almost non polar, behaves more like a polymer having both hydrophobic and hydrophilic interactions. This is evident by the observation that it can absorb many solvents or their vapours coming into its contact. It is suggested that the PIM-1 component in the compatibilizer has strong interactions with its MeOPEG1100 component due to which the MeOPEG1100 block is more aligned towards the inside the PIM rather than interacting with MeOPEG1100 in aqueous phase. If that happens as assumed then the efficiency of the compatibilizer would be considerably reduced and won't generate desired impact

to solubilize the blend by sitting on the phase boundary. Considering this argument, Fig. 4.6 should modify like shown in Fig. 4.7.

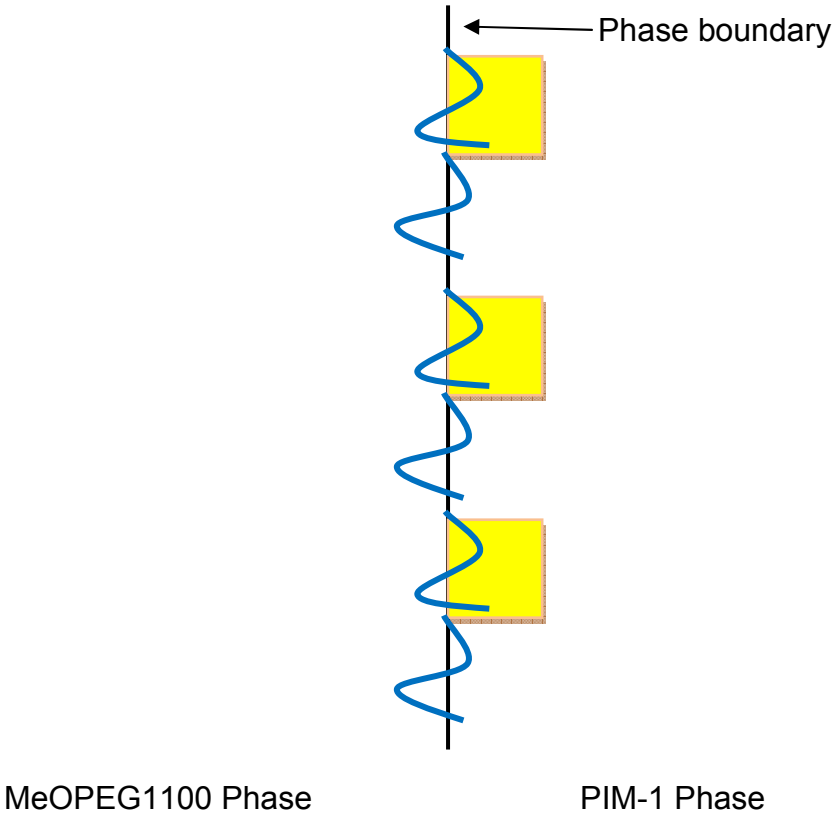

Fig. 4.7 Suggested Compatibilizer orientation in blend solution. Yellow squares represent PIM-1 block in copolymer and blue curves represents MeOPEG1100 block of copolymer

Another explanation for inefficiency of compatibilizer can be that the MeOPEG chains attached to PIM block of compatibilizer are not long enough to penetrate into solvent phase and affect the phase separation. It has been reported in literature that in order to have efficient polymer-polymer compatibilization, the block lengths in the block copolymer are of the same magnitude, or in other words the blocks are very symmetric.[22] As the MeOPEG1100 chain attached to PIM1 in the block copolymers were of shorter lengths, it might also have minimized the effectiveness of the compatibilizer. Copolymers with longer MeOPEG1100 chains may perform better as compatibilizers as they might have chains extended to the aqueous phase of the blend solution.

So far only 5% MeOPEG1100 could be solubilized into PIM-1 with the help of compatibilizer (for blend GPB-13). It was now important to determine whether we can incorporate a little bit more of MeOPEG1100 into PIM1 using some more compatibilizer or not. It was obvious to use a ternary diagram and determine what percentages of all components should be used if we have to increase MeOPEG1100 content by a small increment. The ternary diagram for the blends is given at Fig. 4.8.

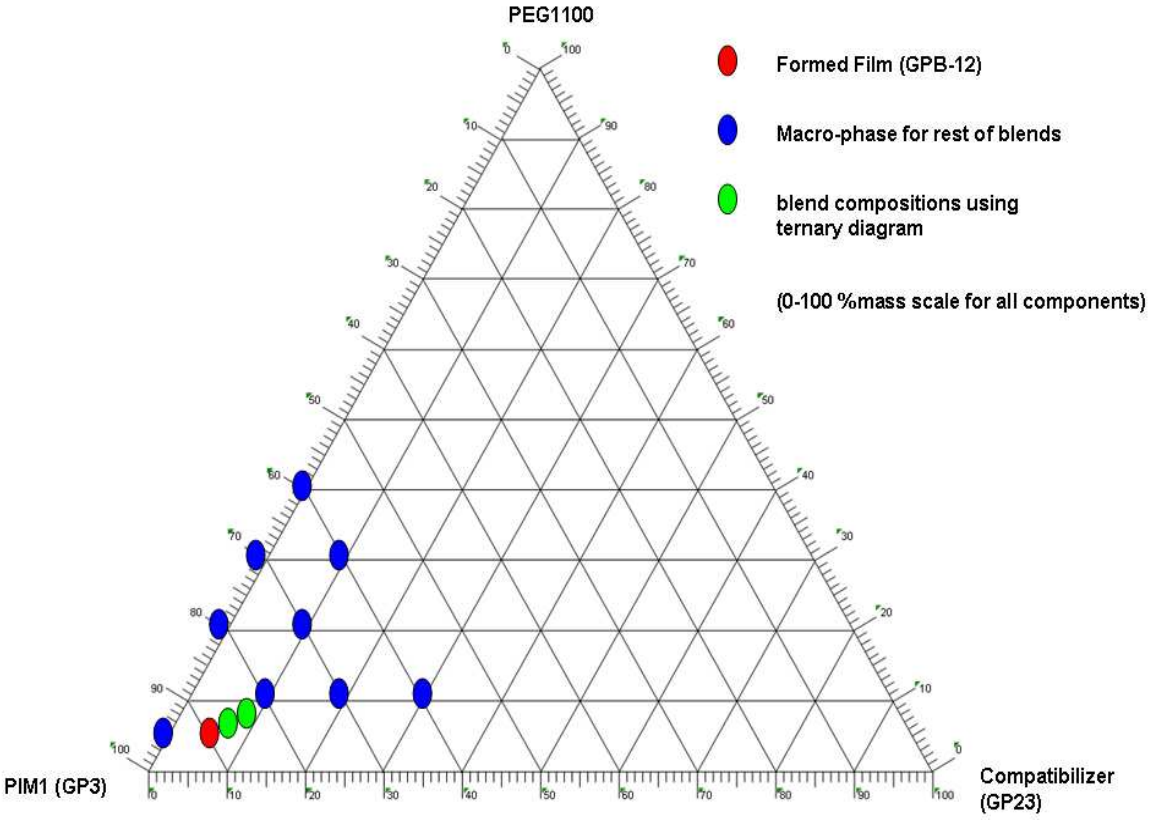

Fig. 4.8 Ternary diagram representing blend compositions. Blue ovals represent blends that resulted in macrophase separation. Red ovals representing clear film after evaporation from solvent. Green ovals show blends prepared by estimating % mass derived from ternary diagram.

Ternary diagram was used to calculate appropriate blend composition. With a small increment of 1% additional MeOPEG1100, two new blends GPB-17 and GPB-18 were prepared. GPB-17 contained 84% PIM-1 (GP-3), 6% MeOPEG1100 and 10% compatibilizer (GP-23) by mass. Similarly the blend GPB-18 had 79% PIM1 (GP-3), 7% MeOPEG1100 and 14% compatibilizer (GP-23) by mass.

Unfortunately, these two new blends also resulted in macrophase separation. Although they formed a film, it was opaque and could not completely soulbilize the

MeOPEG100 component. This indicated that a maximum of only 5% MeOPEG1100 could be solubilized.

The above observation also suggested that the compatibilizer could not act effectively as expected. The possible reasons for the ineffectiveness have already been discussed.

4.3.2. Surface Tension measurements of PIM-1, F-PIM-1 and compatibilizer

In section 4.3.1, we observed that the use of compatibilizer GP-23 (copolymer of F-PIM-1 and MeOPEG1100) could not make a large impact on solubilization of MeOPEG1100 into PIM-1. If a compatibilizer is less effective or ineffective in generating homogeneity within a blend, it is believed that it can't decrease the interfacial tension. In order to check whether the MeOPEG1100 component of compatibilizer has acted as surface active agent and decreased the surface tension of resultant copolymer, it was imperative to measure surface tension values of solvent, PIM1, F-PIM1 and copolymer to compare any change in surface tension of copolymer and PIM-1. Table 4.2 shows surface tension values measured for solvent THF, PIM-1 (GP-3), F-PIM1 (GP-20) and compatibilizer copolymer (GP-23).

Table 4.2 Measured surface tension values for solvent THF, PIM-1(GP3), F-PIM-1 (GP20) and Compatibilizer (Copolymer GP23) by Pendant Drop Method

No.	Surface Tension (mN^{-1}) at Room Temperature							
	PIM-1 (GP3)		F-PIM-1 (GP20)		Copolymer (GP23)		Solvent THF	
	Measured	mean	measured	mean	Measured	mean	measured	mean
1	29.32	26.96	28.84	26.60	24.47	26.36	25.37	26.33
2	28.28		28.03		28.32		26.34	
3	28.71		28.29		27.88		26.36	
4	24.18		23.85		28.29		26.71	
5	24.33		23.97		22.84		26.85	

The literature value for surface tension of tetrahydrofuran (THF) is 26.40 nM m^{-1} at 25 °C. [23] It can be easily seen in the table that there is no visible change in surface tension from solvent to PIM-1 or copolymer (GP-23). It might be due to the reason that the balance of hydrophobic and hydrophilic forces within PIM material is such that it does not contribute significantly towards change in surface tension. It was

earlier explained in section 4.3.1 that PIM has shows strong interaction with labile block of copolymer; hence MeOPEG chain within copolymer might orient itself inside PIM block. This would restrict the effectiveness of MeOPEG block of copolymer to act as surface active agent for change in surface tension. Hence copolymer might not show significant alteration of surface tension.

4.3.3. Nitrogen Adsorption, Solution Adsorption and thermal treatment of PIM-1and F-PIM-1

Before discussing adsorption behaviour of PIM-1 and F-PIM-1 in MeOPEG solution, it is appropriate to have a look at the N_2 adsorption – desorption isotherms for them. Fig. 4.9 shows the isotherm.

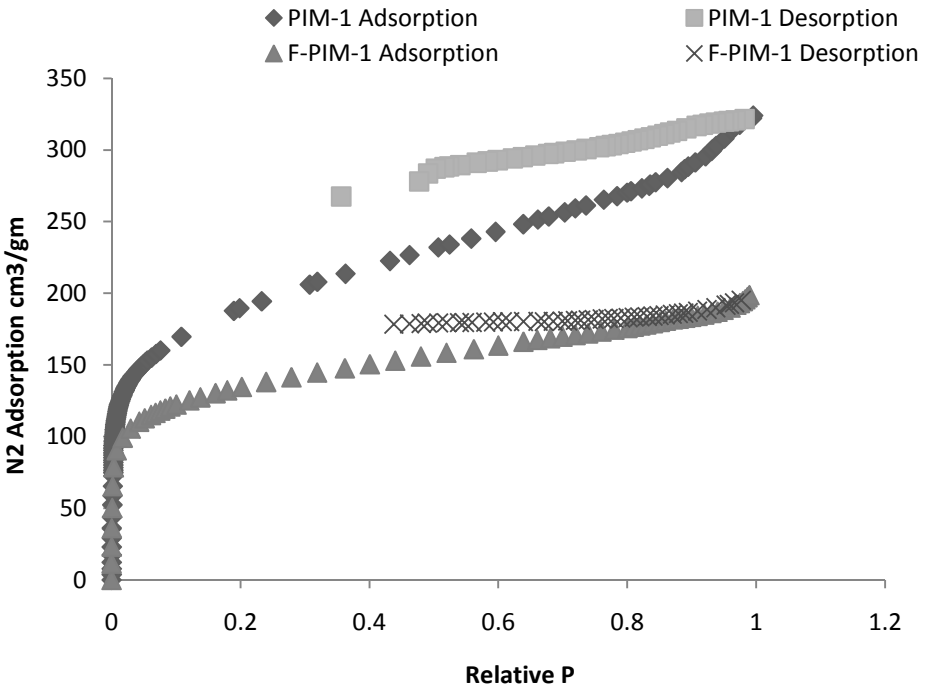

Fig. 4.9 N_2 Adsorption desorption isotherm for PIM-1 (GP-3) and F-PIM-1 (GP-32)

It can be seen in Fig. 4.9 that both PIM-1 and F-PIM-1 show characteristic isotherms for PIM-1. The adsorption rises sharply in lower pressure region and steadily moves until reaching a maximum. Desorption curves for both polymers are also smooth; however PIM-1 shows hysteresis which may be due to swelling of polymer. The hysteresis for PIM-1 might be an indication of small region of mesoporosity;

however, the isotherm is not conclusive in this regard. BET surface areas for PIM-1 and F-PIM-1 were 670 m^2/g and 470 m^2/g respectively.

Another interesting comparison of N_2 adsorption desorption isotherms for F-PIM-1, its copolymer and copolymer after heat treatment to remove MeOPEG block is given below. Fig. 4.10 shows N_2 adsorption desorption isotherms for F-PIM-1 (GP-32), copolymer (GP-26) and copolymer GP-26 after thermal treatment.

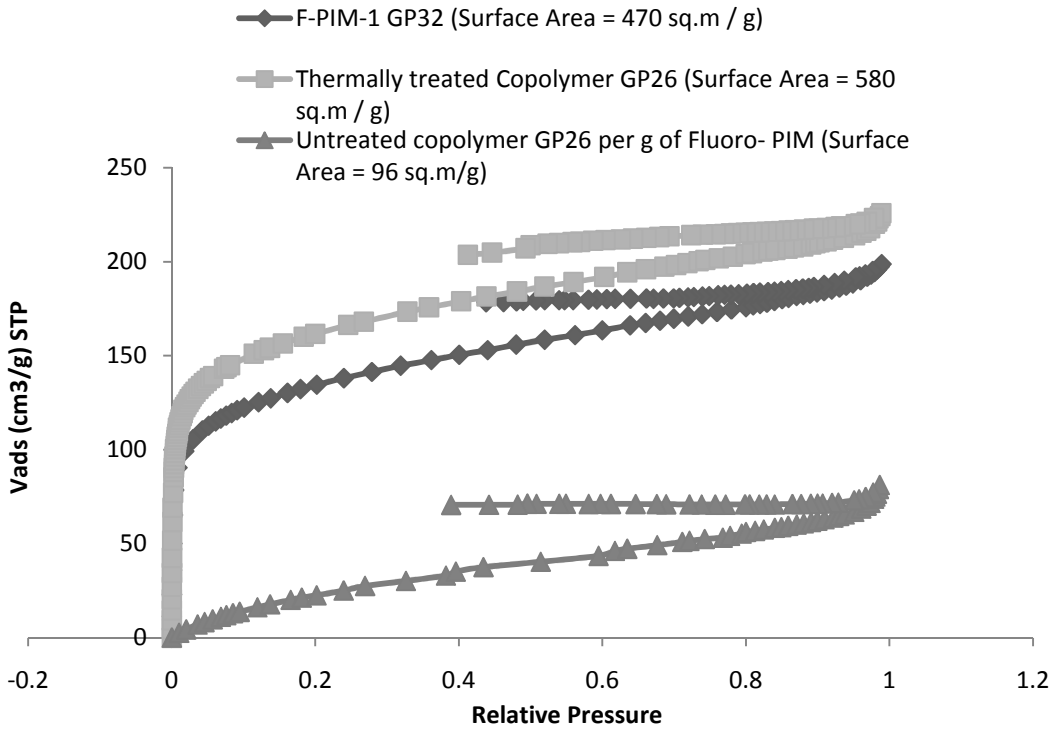

Fig. 4.10 N_2 Adsorption desorption isotherm for F-PIM-1 (GP-32), Copolymer (GP-26) and thermally treated copolymer GP-26

The behaviour of F-PIM1 (GP-32) N_2 sorption isotherm has already been discussed in Fig. 4.9. It can be seen in Fig. 4.10 that the isotherm for copolymer (GP-26) shows low surface area of (96 m^2/g). It is obvious that MeOPEG component after attaching to PIM-1 matrix in copolymer fills or blocks the pores resulting in low surface area. In this context, it was interesting to do heat treatment of the copolymer to remove MeOPEG block. This was done in a furnace at 300 °C and the material was again subjected to N_2 adsorption desorption experiment. Amazingly the surface area

attained by copolymer after thermal treatment was higher (580 m^2/g) than F-PIM-1 used in copolymer synthesis. This may indicate that thermal treatment has altered the pore structure of material during removal of MeOPEG block. However, when similar experiment was repeated for another batch of F-PIM-1 (GP-20), its copolymer (GP-23) and copolymer after heat treatment, the result was otherwise. Fig. 4.11 shows, the isotherms for F-PIM-1 (GP-20), copolymer (GP-23) and copolymer after thermal treatment.

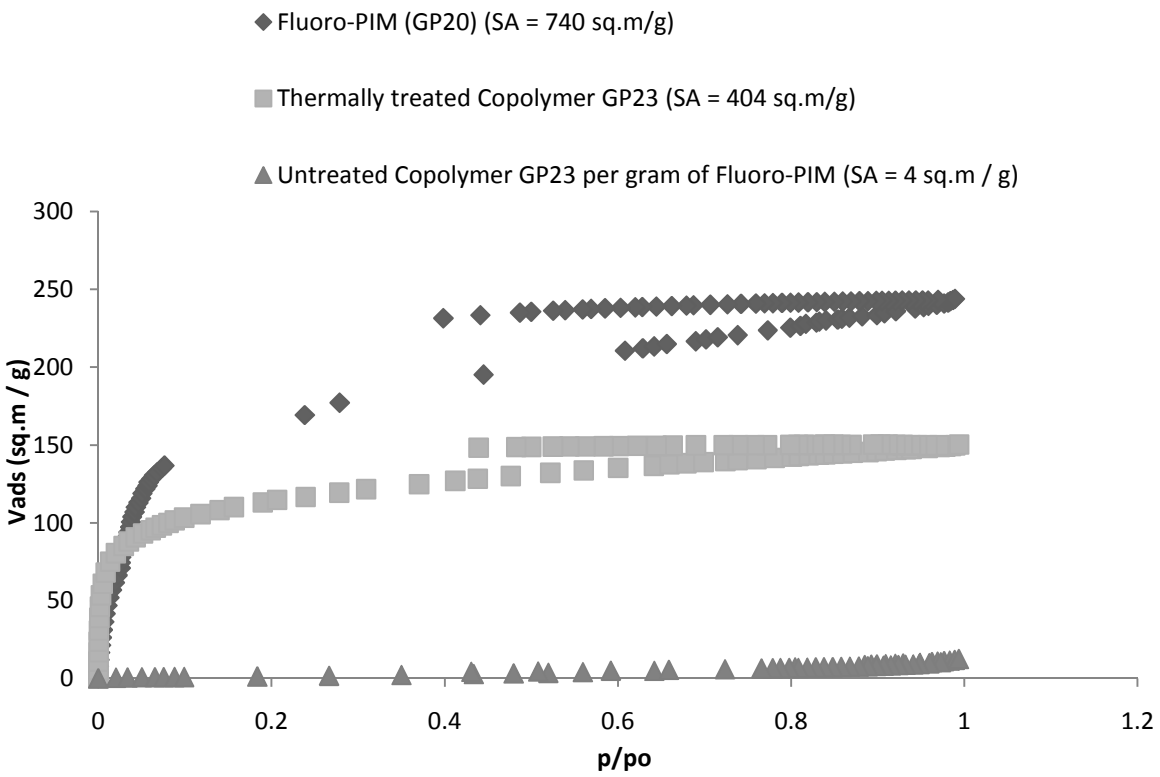

Fig. 4.11 N_2 Adsorption desorption isotherm for F-PIM-1 (GP-20), Copolymer (GP-23) and thermally treated copolymer GP-23

Looking at Fig. 4.11 it seems that F-PIM-1 has a large surface area (740 m^2/g), which is reduced to almost nothing ($4m^2/g$) when it forms copolymer GP-23). After thermal removal of MeOPEG block, the regenerated surface area is 404 m^2/g. It looks like copolymer has not altered the pore structure. However, we have to refer to section 2.3.3 of chapter 2 for the discussion of this unusual F-PIM-1 isotherm. It can be seen in Fig. 4.11 that adsorption for F-PIM-1 (GP-20) is not as sharp in low pressure region as for other materials. The reason for this as explained in section

2.3.3 may be slow adsorption kinetics. If this is true, the sample should be given more time to attain the equilibrium, however, as most of the parameters for equipment used (Coulter) are default, there was little one can do in this regard. In this context, it seems that surface area comparison shown in Fig. 4.10 is more realistic than one in Fig 4.11. However, in both cases it can be seen that heat treatment of copolymer helps regenerating stable pore structure and gain surface area.

At this point it was thought appropriate to form aqueous solution of MeOPEG, then mix PIM-1 or F-PIM-1 into it and observe adsorption behaviour. The PIM-1 (GP-3) or F-PIM-1(GP-32) after adsorption were filtered and dried. The process was done as described in Section 4.2.6. The N_2 adsorption and desorption isotherms are shown in Fig. 4.12.

(a)

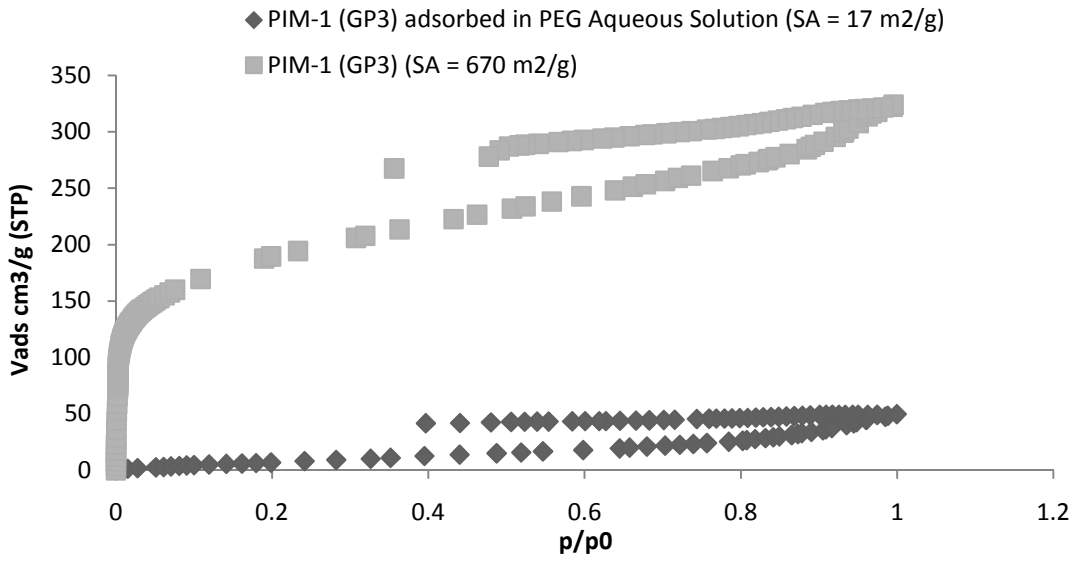

(b)

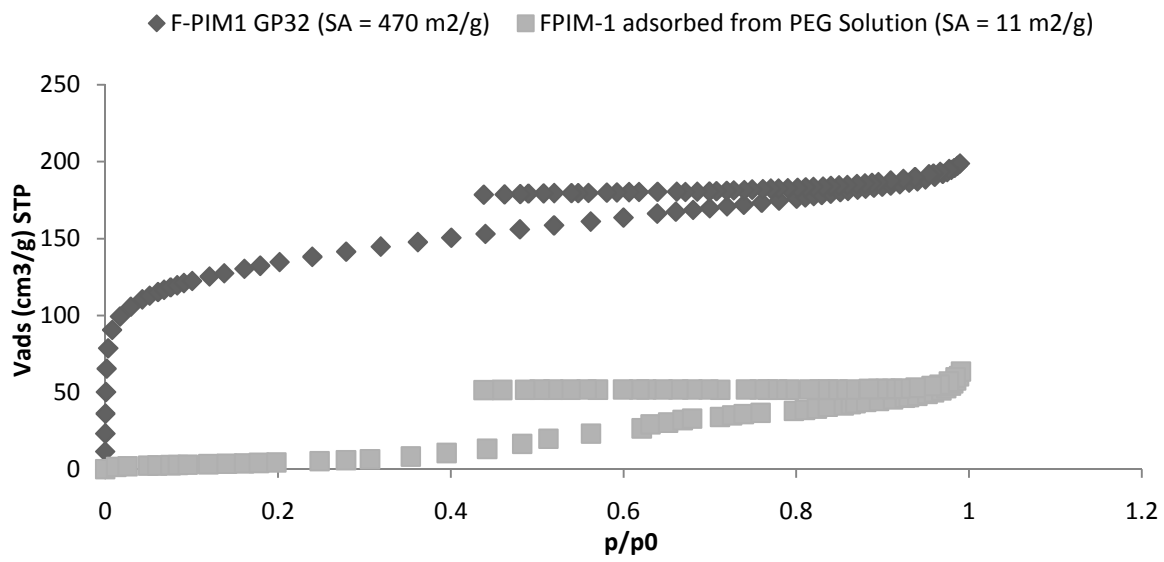

Fig. 4.12 N_2 Adsorption desorption isotherm for PIM-1 (GP-3) and F-PIM-1 (GP-32), (a) Before adsorption (b) After adsorption from aqueous MeOPEG solution

Fig. 4.12 shows that before adsorption, both PIM-1 and F-PIM-1 show sharp adsorption of N_2 in low pressure region, reach a maximum and then desorb in normal fashion. The reason for hysteresis in desorption has already been discussed. When both polymers are subjected to adsorption from aqueous MEOPEG solution and analyzed by N_2 adsorption desorption again, the surface area decreases and the plot is almost along X-axis. This shows that MeOPEG has been incorporated in PIM matrix and filled the pore structure. This consequently affects the adsorption of N_2 into the polymer. The BET surface area after adsorption for both PIM-1 and F-PIM-1 is almost identical. This behaviour of polymer MeOPEG adsorption into PIM-1 structure was an indication that MeOPEG can be physically solubilised into PIM-1 structure. However, same could not be achieved to a large extent during blending experiments. A quantitative measure of this would have been doing more adsorption experiments and determine amount of MeOPEG solubilised in PIM matrix and consequently work out adsorption isotherms. However, the same could not be done due to time constraint.

4.4 Conclusions

This chapter deals with attempts to modify PIM-1 porosity and surface area through blending and adsorption of PIM-1 with MeOPEG. In order to observe interfacial activity of PIM-1, F-PIM-1 and copolymers, blending experiments were performed using PIM-1 and MEOPEG. Several attempts were made with various blend compositions. In order to achieve microphase separation, copolymers of F-PIM-1 and MeOPEG (GP-23) was used as a compatibilizer. It was observed that only a small amount of MeOPEG (5% by mass) could be incorporated into PIM-1. It appeared that due to its strong interactive nature, PIM-1 attracted MeOPEG component of copolymer to organic phase and reduced its effectiveness as compatibilizer. Hence compatibilizer could not orient normally at phase boundary. Another explanation could be shorter length of MeOPEG component in compatibilizer not letting it to function in normal manner.

Surface tension experiments for solvent THF, PIM-1, F-PIM-1 and copolymer were performed to check the effect of MeOPEG component to alter interfacial tension. It was observed that there was almost no change in surface tension after copolymer formation from F-PIM-1. This supported the argument that MEOPEG was interacting and being incorporated in PIM structure. Thus it was unable to play its role to alter interfacial tension.

PIM-1, F-PIM-1 and copolymer were subjected to N_2 adsorption analysis. Copolymer was heat treated and changes in surface area and pore structure was monitored by N_2 adsorption experiments. It was seen in case of copolymer that surface area reduced to be almost negligible and heat treatment could alter and regenerate the pore structure.

PIM-1 and F-PIM-1 were mixed with aqueous MeOPEG solution for adsorption and subsequently filtered and dried. Later on N_2 adsorption desorption experiments indicated incorporation of MeOPEG into PIM-1 and F-PIM-1.

References

(1) Erbil, H. Y. *Surface Chemistry of Solid and Liquid Interfaces;* Blackwell Publishing Ltd. Oxford, UK: 2006; pp. 3-7.

(2) Beckett, S. T. *Physicochemical Aspects of Food Processing;* Blackie Academic Professional: Glasgow, UK, 1995; pp. 168-170.

(3) Tadros, T. F. *Colloids in agrochemicals:* Wiley-VCH Verlog USA: 2009; pp.42-44.

(4) Erbil, H. Y. *Surface Chemistry of Solid and Liquid Interfaces;* Blackwell Publishing Ltd. Oxford, UK: 2006; pp. 99-100.

(5) (a) Tew, G. N.; Pralle, M. U.; Stupp, S. I. *Angew. Chem., Int. Ed.* **2000**, *39*, 517. (b) Stalmach, U.; de Boer, B.; Post, A. D.; van Hutten, P. F.; Hadziioannou, G. *Angew. Chem., Int. Ed.* **2001**, *40*, 428. (c) Harada, A.; Kataoka, K. *Science* **1999**, *283*, 65.

(6) Kimura, M.; Ueki, H.; Ohta, K. Hanabusa, K.; Shirai, H.; Kobayashi, N. *Langmuir ,* **2002,** *18,* 7683-7687.

(7) Bahadur, P. *Current Science,* **2001,** *80(8),* 1002-1007.

(8) Hartland, S. *Surface and interfacial tension: measurement, theory, and applications;* Marcel Dekker, New York, USA: 2004.

(9) Berthier, J. *Microdrops and digital microfluids*; William Andrew Inc. New York: 2008; pp. 55-58.

(10) Wen, G.; Li, X.; Liao, Y.; An, L. *Polymer,* **2003,** *44,* 4035–4045.

(11) Vasile, C.; Kulshreshtha, A. K. Handbook of Polymer Blends and Composites Volume 3B Rapra Technology Limited Shropshire, UK pp.392-394.

(12) Robeson, L. M.; polymer blends A comprehensive Review Carl Hanser Verlah Munich Germany 2007 pp. 11-18.

(13) Baus, M.; Rull, L. F.; Ryckaert, J. P. Observation, prediction and simulation of phase transitions in complex fluids Volume 129 Kluwer Academic USA pp.517-519 1995.

(14) Bussink, J.; Grampel, H. T. V. *Polymer Blends,* Wiley-VCH Verlag GmbH & Co., 2005

(15) Fortelny, I.; Slouf, M.; Hlavata, D.; Sikora, A. *Composite Interfaces,* **2006,** *13(8-9),* 783-799.

(16) Anastasiadis, S. H.; Gancarz, I.; Koberstein, J. T. *Macromolecules*, **1989,** *22 (3),* 1449–1453.

(17) Thomas, S.; Prud′homme, R. E. *Polymer,* **1992,** *33(20),* 4260-4268.

(18) Budd, P. M.; Ghanem, B.; Msayib, K.; McKeown, N. B.; Tattershall, C. *J. Mater. Chem.*, **2003,** *13,* 2721–2726.

(19) Maffei, A. V.; Budd, P. M.; McKeown, N. B. *Langmuir* **2006,** *22,* 4225-4229 (42)

(20) Mackintosh, H. J.; Budd, P. M.; McKeown, N. B ***J. Mater. Chem.*** **2008,** *18,* 573–578.

(21) Reynolds, K. J. PhD Thesis, University of Manchester*,* 2007.

(22) Landry, C. J. T.; Coltrain, B. K.; Teegarden, D. M.; Long, T,. E.; Long, V. K. *Macromolecules* **1996,** *29,* 4712-4721.

(23) Coetzee, J. F.; Chang, T. *Pure & App. Chem.*, **1985,** *57(4),* 633-638.

CHAPTER 5

FLUORESCENCE STUDIES

5.1 Introduction

PIMs are thermally stable amorphous polymers with spiro center as site of contortion in their structure. They are soluble in many organic solvents and show high BET surface area by N_2 adsorption analysis. In solid state they behave as molecular sieves and can be transformed into membranes for both pervaporation and gas separation. They show selectivity for organic solvents over water when used for pervaporation as well as being useful for separating gas pairs.[1]

The affinity of PIM-1 for many organic solvents makes it a candidate for use in sensing devices. PIM-1 is a yellow fluorescent polymer: hence spectroscopic analysis of this material may be useful for observing change in colour as well as red or blue shifts when interacting with solvent or its vapours. A few studies in this regard show the potential of PIM-1 for use in sensing devices. [2.3]

In this context, it was appropriate to undertake fluorescence studies for PIM-1 as well as copolymers of PIM-1 to check their viability for sensing applications. Another objective for this study was to develop a solvent profile showing change of wavelength and fluorescence intensities when organic solvent vapours are adsorbed on its surface. As fluorescence would be used for this study, it is relevant to discuss basic concepts about fluorescence.

5.1.1 Basics of Fluorescence spectroscopy

Fluorescence has been widely used over the years for analysis of simple molecules and macromolecules, especially for protein and polymer analysis. Fluorescence has been used for developing analytical assays for organic molecules,[4] structural information about amino acids,[5] binding of ligands to proteins or macromolecules[6] and polymer-based sensors.[7] Fluorescence is more sensitive to the fluorophore environment than UV-Visible spectroscopy because the molecule stays for more time in the excited state.

Substances displaying fluorescence should have a rigid structure, delocalized electrons (alternate single and double bonds or aromatic rings), short excited state lifetimes (>10^{-9} sec), intense UV absorption bands and good overlap between orbitals of ground and first excited state. There are two ways of measuring fluorescence spectra. In the emission spectrum, the excitation wavelength is kept constant and the fluorescence intensity of emission is measured against wavelength. In the excitation spectrum, fluorescence intensity is measured at different excitation wavelengths, similar to an absorption spectrum. [8]

Fluorescence is enhanced due to the presence of electron donating groups such as -NH_2 or –OH, while electron withdrawing groups such as -Cl, -NO_2 –and COOH result in decrease of fluorescence. Chelation with metal ions results in rigidity so chelates are often fluorescent. However, paramagnetic ions such as Ni^{2+} or Cu^{2+} increase the possibility of intersystem crossing and hence increase the possibility of phosphorescence and quenching fluorescence. Another factor affecting fluorescence is temperature. At low temperature, substances fluoresce strongly in a viscous liquid or solid medium. Fluorescence intensity and wavelength also depends on polarity of solvents. Solvents with heavy atoms such as -Br or -I, or groups such as -NO_2, act as fluorescence quenchers. Finally, pH may also play an important role as the protonated form of weak bases and the unprotonated form of weak acids may be non-fluorescent.[9]

5.1.2 Fluorescence spectroscopy for polymer analysis

Fluorescence spectroscopy has been used as an effective tool to study polymers. It has been used to study non-aqueous dispersions of poly(methyl methacrylate) (PMMA) containing naphthalene and anthracene groups of fluorescence probes for the core shell structure.[10] Effect of surfactants on water soluble poly(2-methoxy-5-[2′-ethylhexyoxy]-1,4-phenylenevinylene) (MEHPPV) derivatives with polyacrylic acid (PAA) chains grafted onto their backbone was studied by fluorescence and exhibited a dramatic increase in their fluorescence intensity accompanied by a blue-shift in the emission maximum.[11] Fluorescence has also been used to study dyes showing both red and blue shift of wavelength. For example a laser dye Coumarin460 dissolved in

ethanol, methanol, acetone or acetonitrile showed red shift, while it showed blue shift when the solution was exposed to fumes of Heena (*Lawsonia alba*), Khus (*Vitis zizgnoides*) and Rose water.[12] Fluorescence correlation spectroscopy (FCS) has been used for diffusion of small solvent molecules (octane) and larger hydrophobic dye probes in octane-swollen poly(dimethyl siloxane) linear-chain solutions and end-linked model networks.[13]

One of the most important applications of fluorescence has been for polymers used in various types of sensors. Conjugated polymers have evolved as one of the most important class of chemical sensors. Fluorescence has widely been used in this respect for molecular recognition.[14, 15, 16] Fluorescence has also been used for devising rational design of optical chemo-sensing acridinic dye.[17] Fast Transient Fluorescence Technique (FTRF) has been employed for studying swelling of disc shaped poly(methyl methacrylate) (PMMA) gels, prepared by free radical copolymerization while Pyrene (P) was introduced as a fluorescence probe during polymerization.[18] Fluorescence characteristics of solution/film of sulphonic acid-doped polyaniline polymers upon exposure to O_2 gas showed a good potential to be exploited as sensing material for O_2 gas detection.[19] Fluorescence studies have also been used for development of optical fibre sensors for detection of volatile organic compounds (VOCs).[20] It was observed that for Acrylodan the intensity ratio of long emission (LE) and short emission (SE) bands, LE/SE, depends on the excitation wavelength through fluorescence studies.[21]

5.1.3 Fluorescence work done on PIM-1 and proposed Solvent Vapour Studies

PIM-1 in both solution and film form has already been investigated by Fluorescence spectroscopy.[19] UV-Visible studies of 0.09 mmol/L PIM-1 solutions and 40 μm thick films showed broad absorbance peaks at 283 nm and 420 nm for film. Reducing thickness to 3 μm shifted these peaks to 287 nm and 422 nm respectively. For PIM-1 solutions, the peaks were observed at 253, 294 and 433 nm. It was also observed that PIM-1 solution in THF gave a quantum yield of 88% when excited at 425 nm. The emission spectra for 2.5 mmol/L PIM-1 solution in THF resulted in a wavelength shift by 18 nm from 490 to 508 nm. The intensity in this case reduced by more than

half. Similarly fluorescence experiments for dry PIM-1 films and after their treatment with phenol or butanol were also undertaken.[22]

The proposed fluorescence study is unique in the sense that it involves using fluorescence to observe powdered PIM-1 or PIM-1 coated on a substrate in the presence of different solvent vapours. This would help to understand the effect of various solvents on the fluorescence ability of PIM-1. On this basis a profile of solvents can be developed which can shift either the wavelength or the intensity to lower or higher side. Later on the same can be applied to copolymers synthesized and a comparison made of the PIM-1 solvent profile with copolymers.

The main problem in this proposed study was how to make sure that the powdered PIM-1 can stay inside the cuvette at a particular angle so that consistency in fluorescence spectra can be achieved. The next problem was to ensure that a particular volume of solvent could be incorporated inside the cuvette without wetting the substrate containing PIM-1. In order to do this, two tiny holes were made in the lid of the quartz cuvette. One hole was required for insertion of a microsyringe to put in the solvent and the other served as an arrangement to hang the substrate. Fig. 5.1 shows the quartz cuvette containing PIM-1 coated substrate along with lid (with holes) and syringe inserted in hole.

Fig. 5.1 Quartz cuvette used for fluorescence experiments

The fluorescence experiments were initially performed by dipping a filter paper in powdered PIM-1 and placing it inside the cuvette. This was not very successful as the results were inconsistent due to the fact the powder kept falling to the bottom of the cuvette and mixed with the solvent. Some of the powder used to stick to the walls of cuvette. In order to overcome this difficulty, PIM-1 solution was prepared and filter paper was wetted and then dried. This dried filter paper was then used for the study. Fig 5.2 shows filter paper before and after being dried from PIM-1 solution.

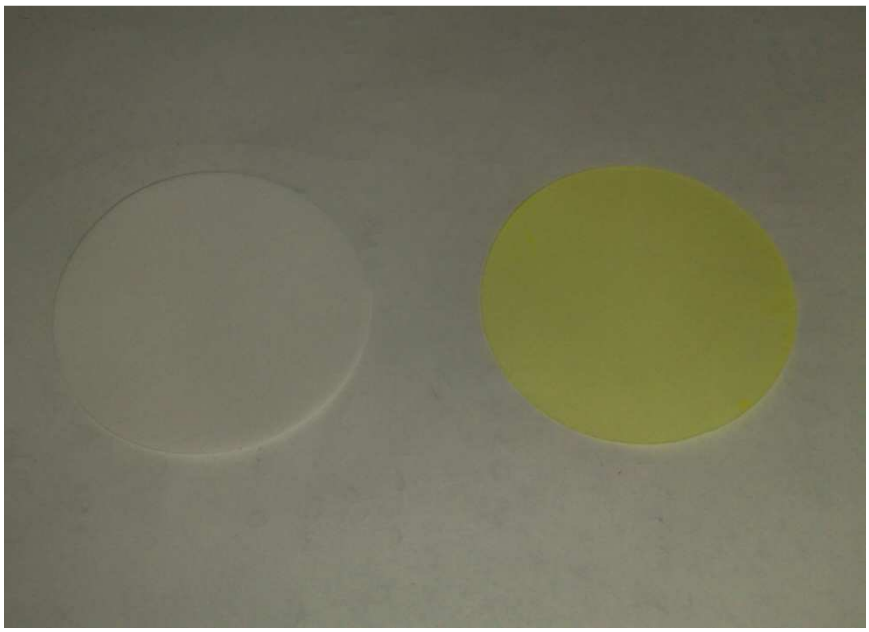

Fig. 5.2 Filter paper before and after being dried from PIM-1 Solution

This arrangement removed the danger of powder falling on bottom. However, it was felt that the consistency of readings may be improved if PIM-1 could be spin coated on a suitable substrate. In this regard, Melinex (polyester substrate) was selected as it is smooth, flexible and white in colour. PIM-1 was spin coated on this substrate and used for fluorescence studies. The fluorescence results of PIM-1 spin coated on melinex studies showed good consistency. Subsequently, these substrates were used for spin coating of copolymer for fluorescence experiments.

5.2 Experimental

0.1 mmol L^{-1} PIM-1 and copolymer solutions in THF were prepared and used for wetting and subsequent drying of Whatmann filter papers (Grade 50) to be used for fluorescence experiments. The filter papers were cut in same size to fit in the cuvette.

0.1 mmol L^{-1} PIM-1 and copolymer solution in chloroform were prepared and used for spin coating of on polyester based white Melinex substrate.

Solvents used in fluorescence studies were of analytical grade and included methanol, ethanol, 2-propnanol, tetrahydrofuran (THF), chloroform, Benzene, Toluene, Xylene, Dimethylsulfoxide (DMSO) and Dichloromethane (DCM). All the solvents were provided by Sigma-Aldrich and were used without further purification except THF and chloroform. Anhydrous THF was obtained from a THF still while Chloroform was purified by Grade 3A° zeolite molecular sieve.

Spin coating of PIM-1 dissolved in chloroform on Melinex (Polyester substrate) was done using a Laurel WS-400B-6NPP LITE manual dispense spin processor. The spin rate was kept at 1000 rpm under vacuum.

UV-Vis spectroscopy was performed using a Cary Varian 5000 UV-Vis-NIR spectrophotometer.

Fluorescence spectroscopy was carried out using a Cary Eclipse Fluorescence Spectrophotometer.

For UV-Visible spectroscopy, 0.09 mmol L^{-1} PIM-1 solution was prepared in THF or chloroform and absorbance spectrum was run on spectrometer. The experiment was repeated three times for consistency.

Fluorescence spectra were run both for solution or using substrates (filter paper, filter paper dried from PIM-1 or copolymer solution or spin coated substrates) in presence of solvent vapours. The excitation wavelength was set as 435 nm. The

wavelength scan was done for the range 445 – 700 nm. The Excitation slit and Emission slit both were kept as 2.5. All the experiments were run in “slow” mode to get smooth spectra. Every experiment was repeated at least three times for consistency.

5.3 Results and Discussion

5.3.1 UV-Visible Spectra of PIM-1 (GP-3) for λ_{max}

The UV-Visible absorption spectra for 0.09 mmol L^{-1} PIM-1 (GP-3) solution in THF were recorded on a Varian Cary 5000 UV-Vis-NIR Spectrophotometer. The spectra were almost identical after repeating three times. Fig 5.3 shows a representative PIM-1 (GP-3) UV-Visible spectrum.

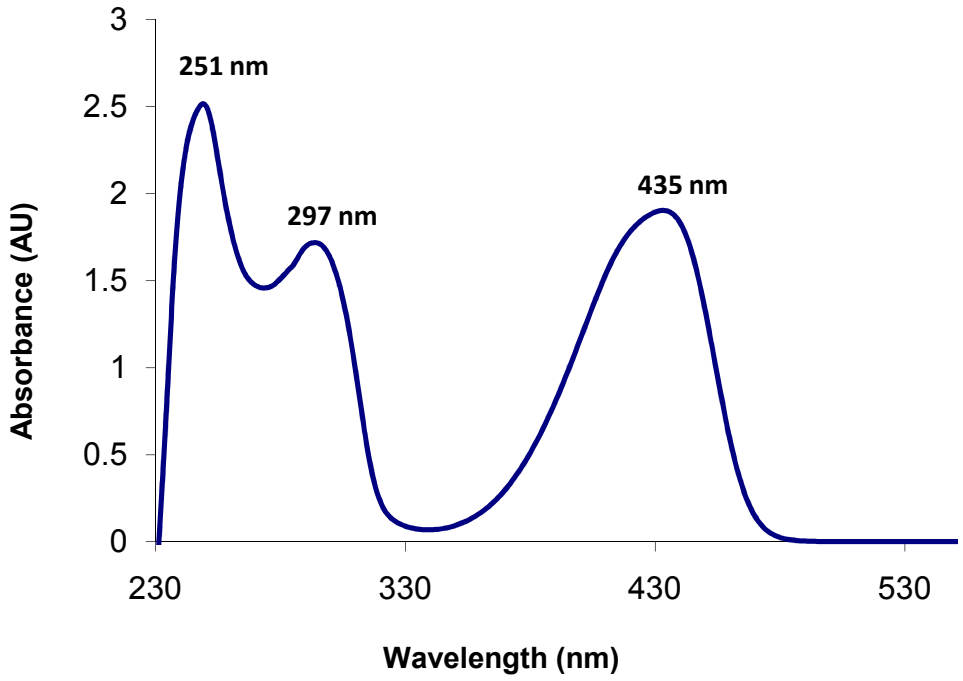

Fig. 5.3 UV-Visible Absorbance Spectrum for 0.09 mmol L^{-1} PIM-1 (GP-3) solution in THF

Fig 5.3 shows intense peaks for PIM-1 (GP-3) solution in THF at 251 nm, 297 nm and 435 nm. This is in good agreement to the previous work done for PIM-1 in THF solution with the same concentration, where the peaks were found to be 253 nm,

294 nm and 433 nm respectively. [22] The peak at 435 nm (λ_{max} in visible region) would be used as excitation wavelength for recording of fluorescence spectra.

5.3.2 Fluorescence Spectra of PIM-1 solution in various Solvents.

PIM-1 (GP-3) was dissolved in various solvents to get 2.5 mmol L^{-1} solutions. Every result was repeated three times to ensure reproducibility. Standard deviation for each result was calculated using 3 repeat measurements. The results for wavelengths and intensities are given in Table 5.1.

Table 5.1 Fluorescence wavelengths and intensities for 2.5 mmol L^{-1} PIM-1 (GP-3) solution in various solvents

Solvent in which PIM-1 (GP3) was dissolved	λ_{max} (nm)	Intensity (AU)	Polarity index (P') for solvents[20]
THF	494±1	180±1	4.0
$CHCl_3$	498±1	296±0	4.1
Benzene	492±2	377±5	2.7
Toluene	487±2	632±12	2.4
Xylene	485±4	194±8	2.5
Methanol	505±3	235±27	5.1
Ethanol	503±5	632±55	5.2
2-Propanol	503±3	745±45	3.9
DMSO	507±5	277±20	7.2

Table 5.1 shows some interesting fluorescence results for PIM-1. The solution of PIM-1 (GP3) with THF shows λ_{max} in the same range as described in earlier work on PIM-1 fluorescence, with slightly lower intensity (earlier reported λ_{max} = 490 nm with Intensity = 244 AU).[22] If we consider a solution of PIM-1 in THF as a benchmark and try to develop a trend, the obvious starting point should be the expected change for the observed λ_{max} and intensities based on polarity of solvents.

THF and chloroform fall almost in the same category based on polarity index.[23] However; there is a small red shift for chloroform with almost 50% increase in intensity. Setting THF as a benchmark, if we look at the Table 5.1, all the alcohols and DMSO show almost 10 nm or more red shift for λ_{max} which follows the trend, however the change in intensity for solution of PIM-1 in these solvents is surprisingly towards the higher side. In fact ethanol and 2-propanol show a very large change in intensity, coupled with a red shift of about 10 nm. Benzene, toluene and xylene, being less polar than THF, chloroform and alcohols, showed a blue shift. While there was a significant increase in intensity for benzene and toluene, xylene showed almost negligible change in intensity.

Polarity index is a relative measure of the degree of interaction of the solvent with various polar test solutes.[23] The values for polarity index for various solvents are given in Table 5.1. Alcoholic solvents are more polar compared to benzene and its derivatives. Generally, the interaction of polar solvents with a polar fluorophore results in red shift of λ_{max} with a decrease in intensity. Usually a fluorophore is excited to the first singlet state S_1 where excess vibrational energy is lost to the solvent. Polar solvents stabilize the fluorophore in the excited state. The fluorophore has a larger dipole moment in the excited state (μ_E) than in the ground state (μ_G). The stabilization occurs as the solvent dipoles of polar solvent in the excited state reorient or relax around the fluorophore, resulting in even lower energy of the excited state. Due to this lower energy, the emission occurs at longer wavelengths. This effect is greater for more polar solvents and vice versa.[24] In this context, the alcoholic solvents should cause red shift with reduction in the intensity and less polar solvents like benzene and derivatives should behave otherwise.

In order to explain this behaviour we need to consider the PIM-1 repeat unit. It contains a spirocycle that is responsible for fragmenting conjugation. It has already been established in earlier work on PIM-1[22] that the PIM-1 fluorophore is isolated 6,13-dicyanobenzo-1,2,4',5'-bis-1,4-benzodioxane fluorophores insulated at each end by spirocyclic carbons (Fig. 5.4). It consists of an electronically independent ensemble of fluorophores capable of absorbing or emitting light. This can be referred to as a "broken-rod" type of electronic structure.[22]

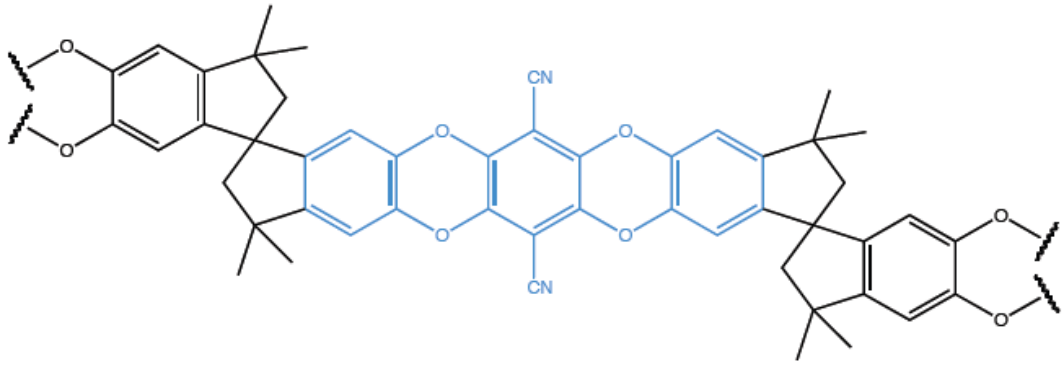

Fig. 5.4 PIM-1 structure showing its fluorophore in middle

Interaction of this complex flurophore with various solvents is not easy to predict, but it is envisaged that alcohols should interact effectively with dibenzodioxane part of fluorophore and may establish hydrogen bonding resulting in lowering of energy for excited states and subsequent red shift. The extent of hydrogen bonding type forces may be comparatively less for chloroform and THF, which should show less increase of wavelength maxima. Although the wayward change in intensity for most of solvents was unexpected and not fully explained at the moment, but it may be due to the fragmented fluorophore, branched and linear PIM-1 chains and their various possible physical interactions with solvent molecules. It can also be explained on the basis of swelling of polymers chains in the solvent environment. This may affect the quenching ability of polymer. It might also indicate that a solvent showing larger changes in intensity is able to displace traces of other residual solvents.

5.3.3 Model experiments for appropriate method to record fluorescence Spectra of PIM-1 (GP3) in presence of solvent vapours

The fluorescence work on PIM-1 was required to determine the ability of PIM-1 to alter the λ_{max} to both red or blue shift and the extent of fluorescence (change in intensity) in presence of solvent vapours. The theoretical section 5.1.3 elaborates the three strategies adopted for this purpose. As per procedure defined in section 5.1.3, a filter paper was rubbed with PIM-1 (GP3) in the first case, filter paper wetted and dried from PIM-1 solution in the second case and PIM-1 spin coated on a polyester substrate (Melinex) in the third case. The fluorescence spectra for all these methods

were recorded and repeated 3 to 5 times to check reproducibility and consistency of analytical methods. The results obtained by this analysis are given in Table 5.2.

Table 5.2 Comparison of mean fluorescence wavelengths and intensities with errors (standard deviation) (a) PIM-1 powder rubbed on filter paper, (b) Filter paper wetted and dried from PIM-1 solution and (c) PIM-1 spin coated on Melinex substrate

Substrate	Solvent vapours	Mean λ_{max} (nm)	Error (nm)	Mean Intensity (AU)	Error (AU)
(a)	-	499	±4	152	±27
(a)	MeOH	501	±4	442	±273
(a)	EtOH	503	±2	473	±236
(a)	Benzene	495	±4	697	±214
(b)	-	492	±3	205	±11
(b)	MeOH	491	±2	215	±34
(b)	EtOH	495	±2	227	±106
(b)	Benzene	490	±1	386	±10
(c)		493	±1	232	±6
(c)	MeOH	503	±2	369	±8
(c)	EtOH	499	±2	287	±12
(c)	Benzene	495	±1	791	±21

A quick look at Table 5.2 reveals that the errors in the case of wavelength maxima in all cases are within acceptable limits; however, the same is not true about errors for intensities. When PIM-1 (GP-3) powder was rubbed on filter paper and placed in a cuvette, there was a marked inconsistency to reproduce the results. There were many reasons for variation in fluorescence intensity. First of all, it wasn't possible to produce the same layer of solid powder on the filter paper, which would obviously result in inconsistent results. Once the filter paper was placed inside the cuvette, despite much care, it kept falling at the bottom and some part of it sticking to the walls of cuvette, which again made it difficult to achieve reproducibility. The filter paper needed to be placed diagonally inside the cuvette for recording fluorescence spectra and a small change in angle in placement resulted in change of fluorescence wavelength maxima and intensity. If the filter paper gets moist with solvent at the

bottom of the cuvette or the injection touched the filter paper, a single drop of solvent on the surface of filter paper changed the result of fluorescence spectra. All these problems collectively suggested that it wasn't a good idea to use powdered PIM-1 rubbed on filter paper for recording fluorescence spectra. This is also supported by the error for intensities which is as large as the reading itself in many cases.

The second approach, in which filter paper was soaked in a solution of PIM-1, then dried and cut to appropriate size, was much better as it removed the danger of polymer falling to the bottom of the cuvette or sticking to the walls. The reproducibility was markedly improved as evident from the errors. Although the error for EtOH intensity was large, later on better results were obtained by care in placement of filter paper at the correct angle and distance from the bottom of the cuvette.

In the third approach, PIM-1 was spin coated on polyester based white substrate (Melinex) for fluorescence studies. Table 5.2 shows an improvement in the errors for both wavelength maxima and intensities. Later on the experiments proved this as the best substrate with good reproducibility. The second and third methods were both used; however, most of the work was done using polymers spin coated on Melinex substrate.

5.3.4 Fluorescence Studies for PIM-1 in presence of solvent vapours

Fluorescence emission spectra were recorded for PIM-1 coated from its solution on filter paper or spin coated on polyester based Melinex substrate. The data obtained were used to monitor the reproducibility and to identify solvents that produce a shift in wavelength maxima as well as a change in fluorescence intensity. The fluorescence results presented and the discussion below is aimed at developing a solvent profile for PIM-1 and next section will be used for its comparison with its copolymers.

The fluorescence experiments were first started for alcohol solvents. The plots in Fig. 5.5 (a) and (b) shows fluorescence intensity and change in λ_{max} for both PIM-1 solution dried filter paper and PIM-1 spin coated on Melinex substrate.

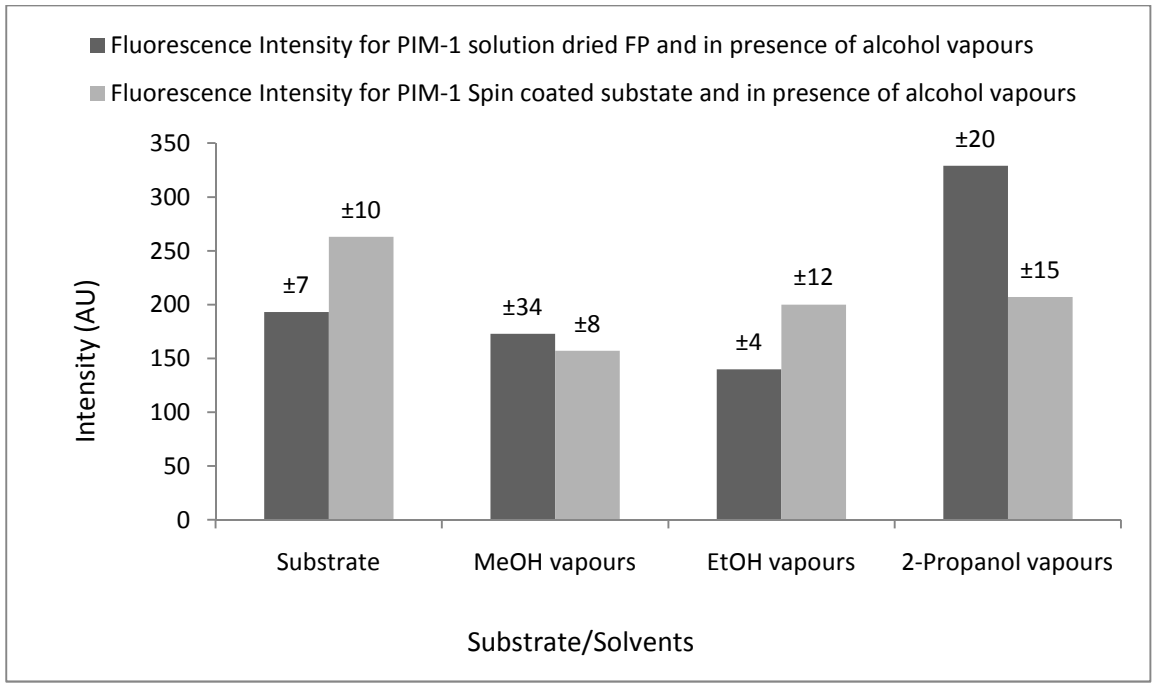

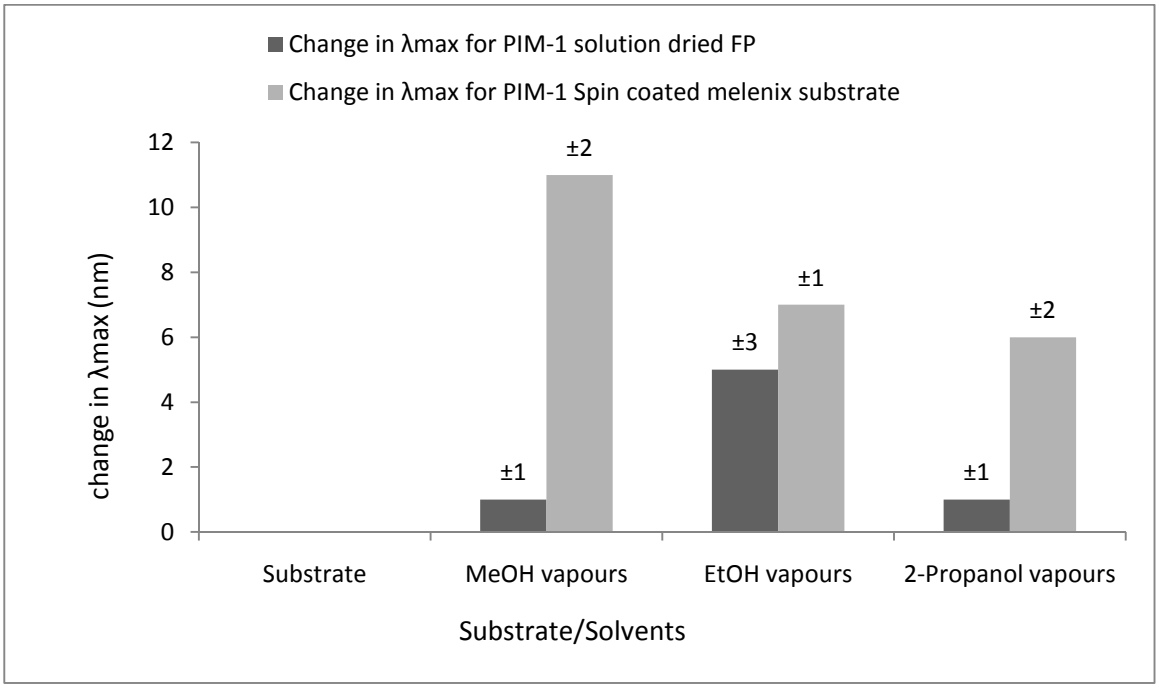

Fig. 5.5 Comparison of PIM-1 (GP-3) solution dried on filter paper and PIM-1 (GP-3) spin coated on Melinex substrates in presence of alcohol vapours for (a) Fluorescence intensity (b) λ_{max} shift (nm)

Fig. 5.5 (a) shows a comparison of intensity for PIM-1 (GP-3) solution dried on filter paper and PIM-1 (GP-3) spin coated on Melinex substrate. For PIM-1 (GP-3) solution dried filter paper there is a reduction in intensity for MeOH and EtOH solvent

vapours, relative to the dry polymer. However, 2-propanol shows an increase in intensity. In comparison, all three alcoholic solvents show a reduction in intensity while Melinex substrate was used. If we look at the error bars for both filter paper type and Melinex type substrates in Figure 5.5 (a), it can be observed that errors for 2-propanol are almost same, hence the difference of intensity may be real. In case of methanol there is a large difference of errors for both substrates, hence plot for filter paper substrate may be a bit unreliable. The errors for ethanol are in acceptable range of experimental errors. In Fig. 5.5 (b) the use of both substrates show red shift as λ_{max} is shifted to higher wavelengths. In case of wavelengths, the changes appear to be real in all cases as there is no big difference in errors for both methods.

There is a good agreement between the two methods in the case of EtOH, where almost similar intensity and λ_{max} shift is observed. However, the spin coated substrate showed a large red shift for MeOH which was almost negligible while using filter paper based substrate. The spin coated Melinex substrate was consistent in the sense that it showed a reduction in intensity and red shift for all alcohol solvents. This was also consistent in later experiments with the spin coated substrate, where a red shift always occurred for alcohols.

It appears from data for alcohols in Fig. 5.5 (a) and (b) that vapours of alcoholic solvents act as quenchers when they interact with PIM-1 based substrates. The reason for this quenching may be possible hydrogen bonding and physical forces of attraction between the PIM-1 fluorophore and alcohol molecules in excited state. These interactions of alcohol molecules with the ether part of fluorophore may cause lowering of the energy of excited state and the excited electron would remain for longer time in excited state. The lower energy of excited state corresponds to emission at longer wavelengths explaining quenching and red shift.

Another interesting comparison was to do these experiments for two different batches of PIM-1. For this purpose PIM-1 (GP-3) and PIM-1 (GP-39) were used. This comparison was also interesting in the sense that PIM-1 (GP-3) was synthesized by the conventional step polymerization technique while PIM-1 (GP-39) was synthesized by the high shear method. Fig 5.6 shows the comparison for red shift that occurred for alcohols using both batches.

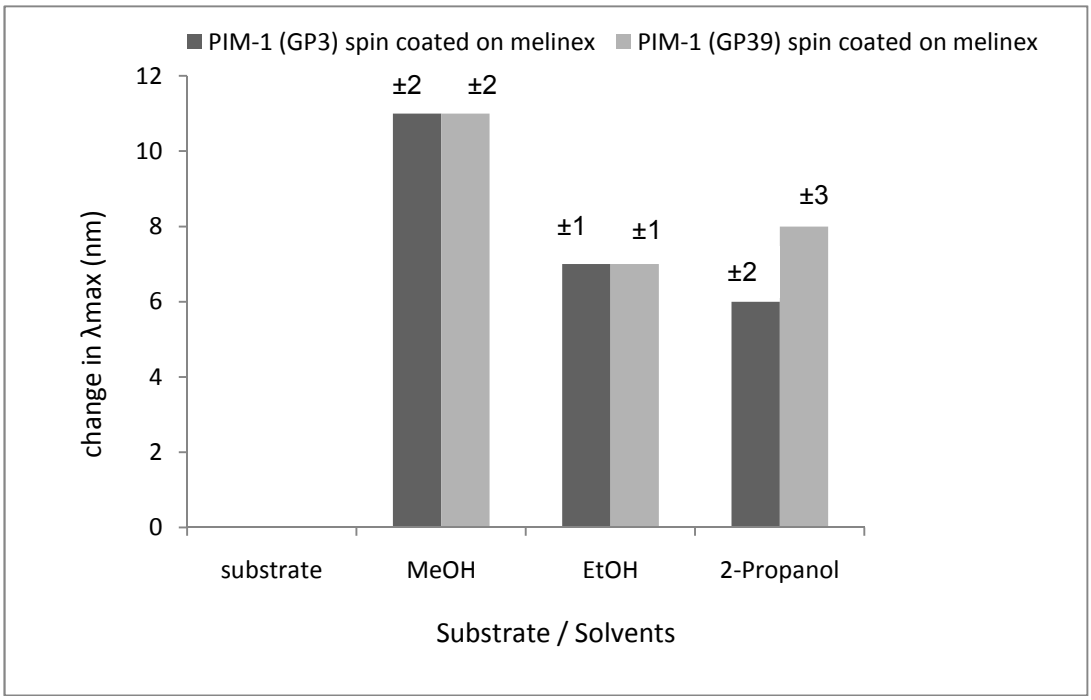

Fig. 5.6 Comparison of λ_{max} shift for two batches of PIM-1 GP3 and GP39 spin coated on melinex substrates in presence of solvent vapours

The experiments for alcohols for two different batches of PIM-1 (GP-3 and GP-39) spin coated on Melinex substrate showed very good agreement. Fig 5.6 shows that there was identical red shift for both MeOH and EtOH solvent vapours (11 nm and 7 nm respectively) while PIM-1 (GP-39) showed a slightly higher red shift in presence of 2-propanol vapours. There is almost same error sequence in wavelength shifts for both batches, which complements the results.

These results were encouraging to perform similar experiments for a set of diverse solvents in order to make a solvent profile for PIM-1 based substrates. PIM-1 is easily soluble in THF and chloroform, while its structure has aromatic rings. Hence it was appropriate to add THF, chloroform, benzene, toluene and xylene in the list of solvents. Other solvents used were DCM and DMSO. For these experiments PIM-1 spin coated Melinex substrate was used as it performed best in all the options tried. Fluorescence experiments were performed in the presence and absence of these solvents and a profile of solvents was developed on the basis of values observed for intensity and wavelength maxima. Table 5.3 shows the data for these experiments.

Table 5.3 Solvent Profile for PIM-1 (GP3) spin coated on Melinex substrate, based on change in intensity and λ_{max} shift.

Solvent vapour	Change in Intensity (AU)	λ_{max} shift (nm)
Benzene	408	-1
Toluene	479	-4
Xylene	499	-5
THF	441	-9
Chloroform	756	4
DCM	554	-2
MeOH	-106	11
EtOH	-63	7
2-Propanol	-56	6
DMSO	25	7

Table 5.3 shows that alcohols show a quenching effect on spin coated PIM-1, as the λ_{max} shows red shift and reduction in intensity. However, aromatic solvents show blue shift with substantial increase in the intensity. THF shows behaviour similar to aromatic solvent vapours. Chloroform and DCM also show a large change in intensity; however chloroform shows a small red shift while DCM shows a very small blue shift. Interestingly DMSO shows a moderate red shift with a small change in intensity. We can arrange the effect of solvent vapours on PIM-1 substrate in descending order of $\Delta\lambda_{max}$ change in intensity.

Solvents in descending order of Δ (λ_{max}): MeOH > EtOH = DMSO > 2-Propanol > Chloroform > Benzene > DCM > Toluene > Xylene > THF

Solvents in descending order of Δ Intensity : Chloroform > DCM > Xylene > Toluene > THF > Benzene > DMSO > 2-propanol > EtOH > MeOH

As discussed before, alcohols are more polar solvents than any other solvent in the list, hence can produce red shift by lower energy excited state. If the solvent accepts electrons from the fluorophore, a charge-transfer-to-solvent complex may be formed. This may be the case for PIM-1 fluorophore-alcohol vapour interactions in the excited state.

THF, DCM and aromatic solvents show blue shifts. However, this blue shift is more prominent for THF, toluene and xylene. Blue shift is usually observed when a reduction in conjugation of the fluorophore is occurring. It can also be explained on the basis of charge dipole interactions in ground and excited states. If the dipole moment in the excited state is more than in the ground state, the solvent-fluorophore interactions in the excited state may be destabilized and result in higher energy; hence a blue shift may be observed.[25]

If there are low lying unfilled orbitals in solvent/fluorophore molecules, they may have an affinity for electrons. This may be the reason for large blue shift of THF, where there is a possibility of interaction by oxygen atom on THF with the fluorophore. It is also important to mention that donor capacity of fluorophore in ground and excited state may be different and, depending upon the case, reason for red or blue shifts. If the solvent-fluorophore interactions can occur in the ground state, this would result in decrease of ground state energy, hence emission would occur at higher energy (or shorter wavelength) hence resulting in blue shift.[26] DCM has two chloro atoms on either side of the molecule, which would make the carbon of the methylene group partially positive. This could result in interaction of the solvent with the fluorophore in the ground state, lowering ground state energy and causing a blue shift. The same can be inferred in the case of toluene and xylene, where the methyl group acts as electron donor, hence becoming partially positive, and the electron rich fluorophore can interact with it in the ground state to increase the energy gap between ground and first state as well as cause higher dipole difference. This may also correspond to the blue shift observed.

An attempt was made to see how much volume of vapours of solvent are absorbed by PIM-1 spin coated on Melinex substrate before saturation and the effect on intensity. To perform this experiment, solvent was added in increments of 10 µL and fluorescence spectra were run. Four solvents were selected for this purpose and the data obtained are shown in Fig. 5.7.

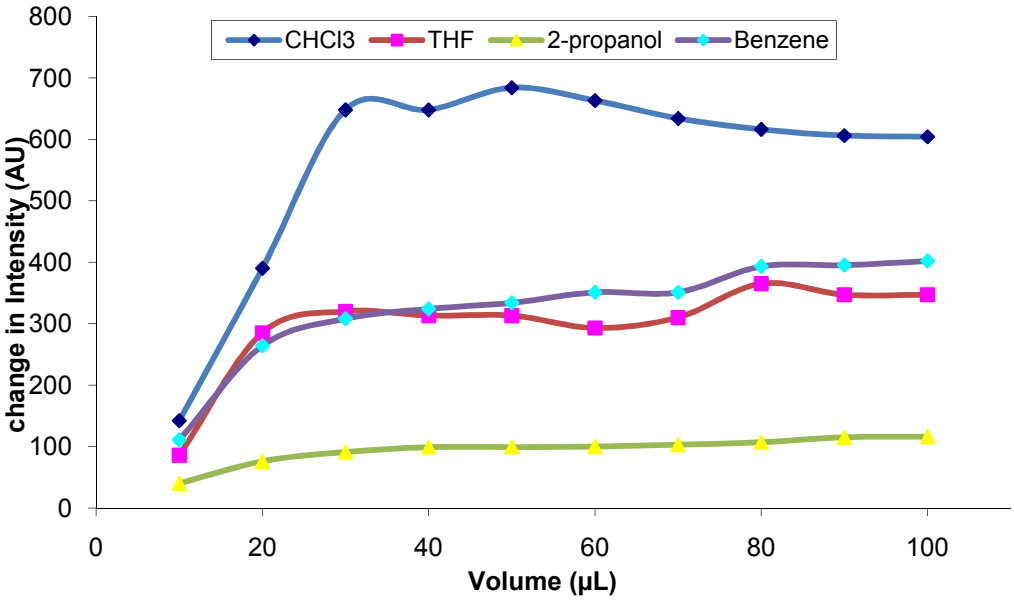

Fig. 5.7 Change in fluorescence intensity with volume for solvent vapours on PIM-1 (GP39) spin coated substrate

Fig. 5.7 shows that 2-propanol shows lowest intensity and the intensity only increases till the addition of 40 µL, after which the addition of solvent has no further effect. In the case of THF, there is a sharp increase in intensity till addition of 30 µL, after which it also becomes somewhat constant. The fluctuation between 40-60 µL increments may be due to handling and error. Similar behaviour is shown by benzene. However, chloroform shows a very high change in intensity until the addition of 40 µL after which the plot becomes flat. It was observed during the experiment that the solvent added in 10 µL increments was totally absorbed by the spin coated substrate, however, when the volume was more than 50 µL, some of the solvent could be seen in liquid state in the bottom of the cuvette.

Fig. 5.8 shows the % change in intensity with volume of chloroform for two different batches of PIM-1.

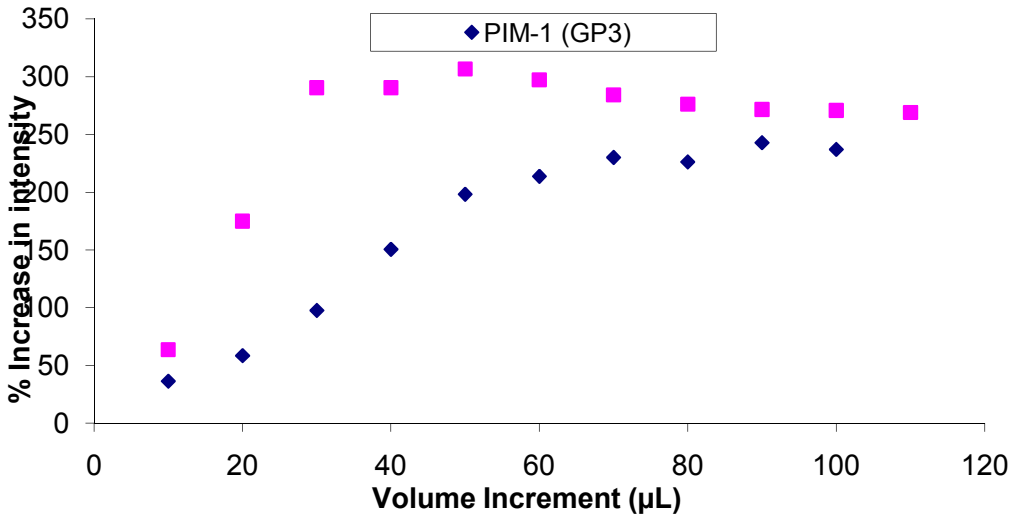

Fig. 5.8 % Change in fluorescence intensity with volume of chloroform for spin coated substrate of two batches of PIM-1.

The % change in intensity for PIM-1 (GP3) substrate appears to be smoothly increasing until 60 µL in Fig 5.8, after which it becomes constant. In comparison the % change in intensity is very sharp for PIM-1 (GP39) until 40 µL of solvent. However, after that the effect of addition of volume has nominal effect. The intensity of fluorescence and change in wavelength maxima are also related to the surface area and pore structure of a polymer. The cavities generated in a spin cast film are a mixture of different sizes and shapes. The larger cavities also facilitate effective diffusion of solvent vapours.[27] The surface area for PIM-1 (GP3) is 673 $m^2 g^{-1}$ and 772 $m^2 g^{-1}$ for PIM-1 (GP39). The different behaviour in initial absorption of solvent vapours by two PIM-1 batches may be attributed to the pore structure and surface area. It looks like GP39 has a higher number of larger cavities hence delivers effective absorption of solvent and subsequent % increase in intensity. The rate of diffusion for solvent molecules in PIM-1 (GP3) appears to be relatively slower than PIM-1 (GP39), causing a smooth increase over a small volume range unlike GP39.

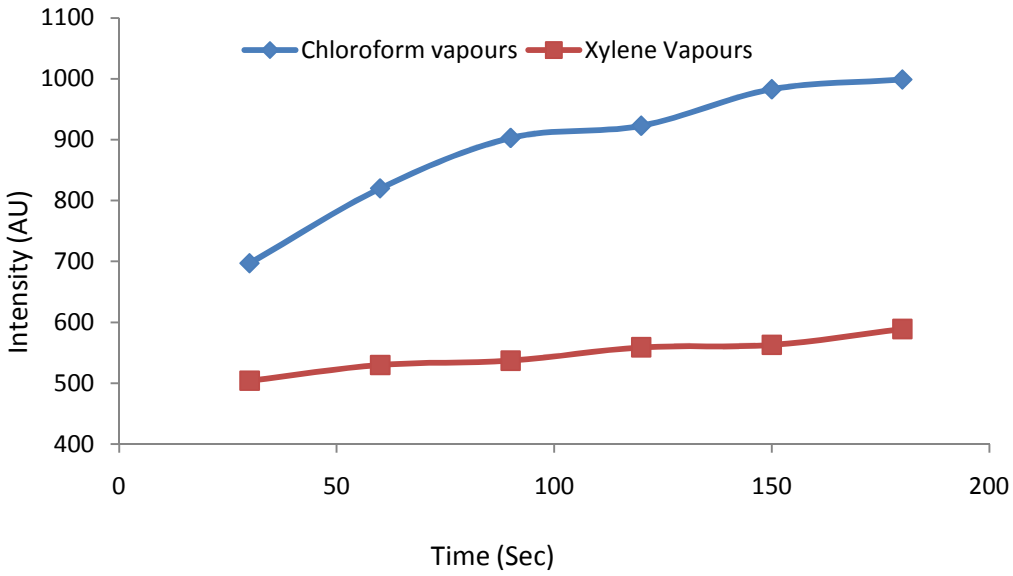

Fig. 5.9 Fluorescence intensity with 30 second time intervals in presence of solvent vapours on PIM-1 (GP39) spin coated substrate when 50 µL volume of solvent was injected

Fig. 5.9 shows the effect of time on increase of fluorescence intensity for vapours of chloroform and xylene on PIM-1 (GP3) spin coated substrate. In this experiment 50 µL volume of the solvent was injected and then fluorescence spectra were recorded with 30 second time intervals. It appears that effect of time is not significant in case of xylene vapours as it shows only small change in intensity with time. However, the intensity kept rising for chloroform until 150 seconds, showing better absorption of vapours by chloroform. The comparison of data in Fig. 5.7 and Fig. 5.9 implies that small volume increments were more effective to change in intensity as compared to a single larger volume injection over longer time periods.

Polymer films either cast from their solution or spin coated may have traces of the solvent in them and the treatment of such substrates with methanol should remove the solvent, although the film may swell to some extent. Hence the PIM-1 (GP3) spin coated substrate was treated with methanol for 72 hours and dried before using it again for fluorescence experiments. The comparison of fluorescence λ_{max} (nm) for PIM-1 (GP3) spin coated substrate and MeOH treated substrate is given in Fig. 5.10.

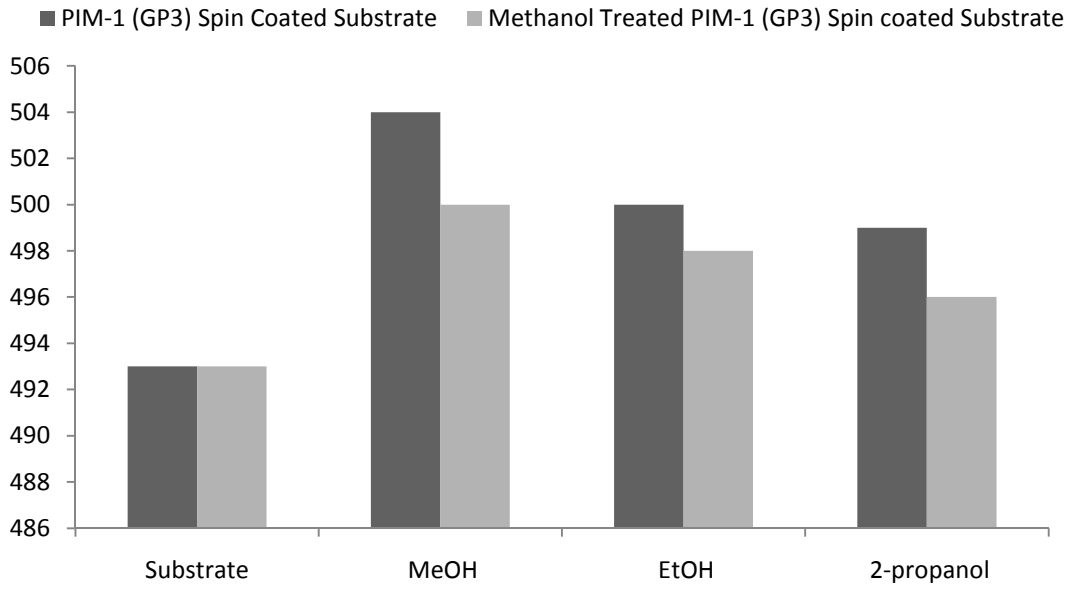

Fig. 5.10 Comparison of Fluorescence λ_{max} (nm) for PIM-1 (GP3) spin coated and MeOH treated substrates in presence of solvent vapours

Table 5.4 shows % change in fluorescence intensity in presence of solvent vapours before and after methanol treatment of the PIM-1 (GP3) spin coated film.

Table 5.4 % change in fluorescence intensity in presence of solvent vapours for PIM-1 (GP3) spin coated substrate and the same substrate after MeOH treatment.

Substrate	% change in intensity in presence of solvent vapours		
	MeOH	EtOH	2-Propanol
PIM-1 (GP3) Spin coated Melinex Substrate	-41	-25	-22
MeOH treated PIM-1 (GP3) Spin coated Melinex Substrate	-3	4	6

It is interesting to note in Fig. 5.10 that there is no change in λ_{max} for substrates before and after methanol treatment. However, in presence of solvent vapours, both the substrates show red shift. Spin coated PIM-1 shows larger red shift as compared

to methanol treated substrate, although the trend remains the same as the order of red shift is methanol > ethanol > 2-propanol. In the case of % change in intensity, Table 5.4 reveals that untreated substrate causes a larger reduction in intensity as compared to methanol treated substrate. However, it is important to mention here that in the absence of vapours, the reduction of intensity occurs in different regions. For example, untreated substrate starts reduction from 265 AU and methanol treated substrate does so starting from 180 AU remarkably in the same wavelength region of 493±2 nm.

Although there is a small difference in red shift with and without methanol treatment of the substrate (Fig. 5.10), however, as seen in Table 5.4, it is the % change in emission intensity which seems more significant. It is believed that swelling of spin coated substrate would result in separation between the 5 membered ring fluorophore of PIM-1's electronic structure. This would result in increased isolation of individual fluorophores, resulting in an increase in fluorescence intensity. It can also be described on the basis that treatment of spin coated PIM-1 substrate decreases the possibility of self quenching of the fluorescence by interchain π stacking, as the distance between the polymer chains would increase. This phenomenon of increase in fluorescence intensity is consistent with earlier work done on methanol, ethanol and butanol treated PIM-1 substrates.[22]

5.3.5 Fluorescence Studies for PIM-1 Copolymers in presence of solvent vapours

The diversity of PIM-1 substrates to alter both wavelength maxima and fluorescence intensity in presence of solvent vapours developed an interest to continue same experiments for PIM-1 based copolymers and compare the results with PIM-1. In this context, a copolymer product (GP23) was used in the same manner for fluorescence experiments. Based on the results, a solvent profile was also developed for copolymers. Fig. 5.11 shows the comparison of wavelength shift caused by PIM-1 (GP3) spin coated substrate and copolymer (GP23) spin coated substrate in presence of selected solvent vapours.

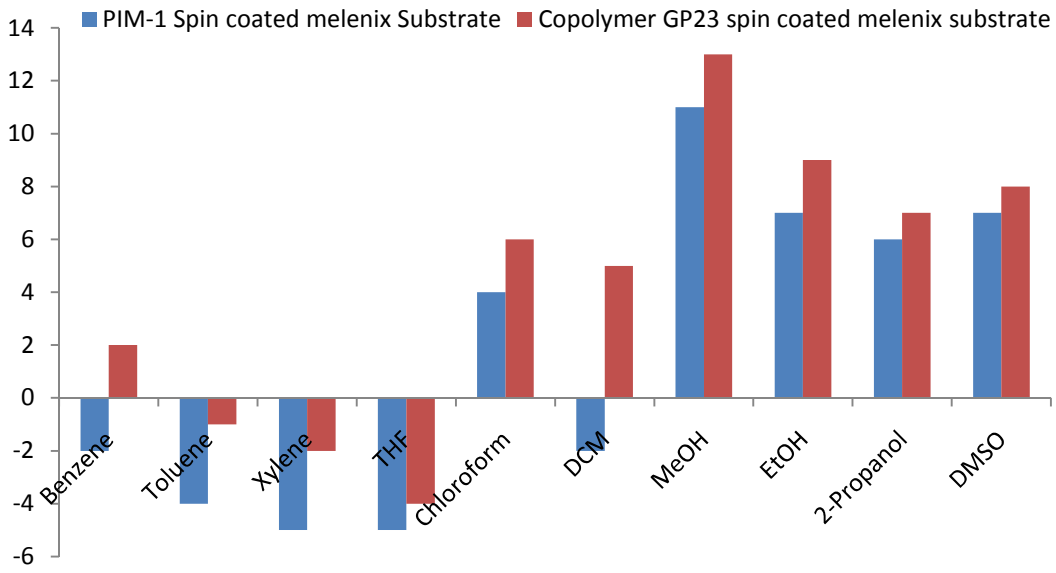

Fig. 5.11 Comparison of Fluorescence λ_{max} (nm) for PIM-1 (GP3) spin coated and Copolymer (GP23) Substrates in presence of solvent vapours

Fig. 5.11 shows an interesting comparison for wavelength maxima shift caused when solvent vapours were subjected to PIM-1 and copolymer spin coated substrates. PIM-1 spin coated substrates show an increasing blue shift in the presence of aromatic solvents until THF. A continuous blue shift is also observed for toluene, xylene and THF vapours when subjected to copolymer substrate but to a lesser extent. Interestingly benzene and DCM show a small red shift for copolymer substrate while small blue shift for PIM-1 substrate. For the rest of the solvents a red shift of wavelength maxima is observed, which is marginally higher for copolymer GP23 spin coated substrate.

The fluorophore in the case of PIM-1 and copolymer repeat unit remains the same; hence the fluorescence behaviour should in principle be comparable for both compounds. The plot in Fig. 5.11 is consistent with earlier observed behaviour of PIM-1, where it showed red shift for alcoholic solvents vapours and blue shift for vapours of benzene and its derivatives. The only reason that can be thought of marginally different behaviour of copolymer than PIM-1 is presence of polyethylene glycol monomethyl ether (MeOPEG) units attached on either side of the copolymer. These units may reduce the rate of diffusion of solvent vapours inside copolymer

spin coated substrate and cause a small variation in wavelength maxima. This is supported by the blending experiments discussed in chapter 4 revealing that the copolymer could not perform as a good compatibilizer for PIM-1. It was suggested at that time that MeOPEG units attached to PIM-1 block in copolymer may not be big enough to generate microphase and sit within PIM block. Here it can be argued that MeOPEG chains may adsorb into PIM structure and compete with other species for interaction.

Table 5.5 below shows the comparison of % change in intensity for PIM-1 (GP-3) spin coated and copolymer (GP-23) spin coated substrates.

Table 5.5 % change in Fluorescence intensity in presence of solvent vapours for PIM-1 (GP-3) spin coated substrate and copolymer (GP-23) spin coated substrate.

Solvent Vapours	% change in intensity	
	PIM-1 (GP-3) Spin coated Melinex Substrate	Copolymer (GP-23) Spin coated Melinex Substrate
Benzene	216	61
Toluene	244	193
Xylene	275	201
THF	170	93
Chloroform	134	192
DCM	454	120
MeOH	-87	-19
EtOH	-52	21
2-Propanol	-46	13
DMSO	20	-44

From Table 5.5 it is evident that PIM-1 spin coated substrate shows three times more increase in intensity compared to copolymer spin coated substrate for benzene vapours. Similarly PIM-1 substrate shows greater increase or decrease in intensity for all other solvents except for chloroform and DMSO. In the case of chloroform, the copolymer spin coat substrate performs better than PIM-1 spin coated substrate.

It is believed that the tetrahedral carbons shared by cyclopentyls in PIM-1 spirocycle fragment the conjugation and this better separation of individual fluorophores could lead to higher intensity change and blue shift. It is observed in Fig. 5.11 and Table 5.5 for vapours of alcohols, THF and DCM increase as shown for most of the solvents. On the contrary, copolymer chains may have comparatively restricted mobility and lead to lower emission.

Fig. 5.12 shows % change in intensity for vapours of selected solvents with 10 µL volume increments for copolymer GP26 spin coated Melinex substrate.

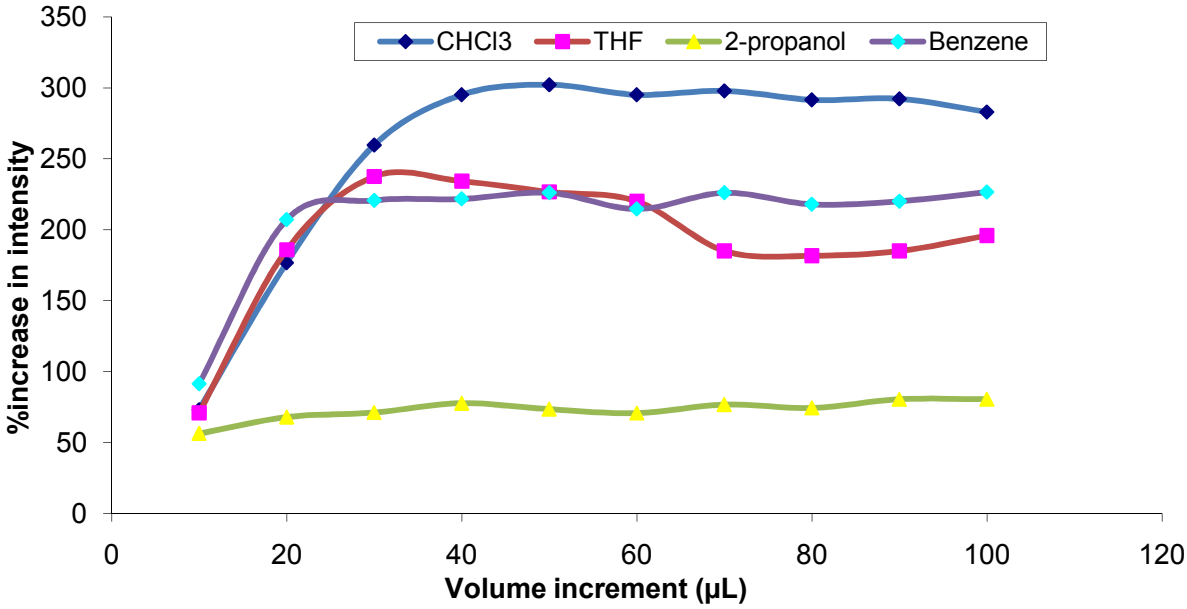

Fig. 5.12 % change in Fluorescence intensity with volume (µL) for copolymer GP26) spin coated Melinex substrate

It can be observed in Fig. 5.12 that there is very small change by percentage in fluorescence intensity up to 40 µL volume uptake of the solvent. The intensity increases rapidly for benzene and chloroform and then becomes constant. THF shows irregular behaviour as the intensity increases until 30 µL uptake and then keeps on decreasing before a small increase in the end. The plot is consistent with the behaviour shown by PIM-1 spin coated Melinex substrate, which also shows

higher intensity for aromatic solvents, chloroform and THF and relatively small increase (or decrease) in intensity for alcoholic solvents.

Table 5.6 shows intensity and wavelength with time for copolymer (GP26) spin coated Melinex substrate for chloroform vapours.

Table 5.6 Fluorescence $\lambda_{max\ (nm)}$ and intensity (AU) in presence of solvent vapours for copolymer (GP26) Spin coated melinex substrate)

Time (Sec)	Chloroform vapours		Toluene vapours	
	λ_{max} (nm)	Intensity (AU)	λ_{max} (nm)	Intensity (AU)
30	497	427	495	293
60	499	525	490	338
90	498	599	493	361
120	493	644	490	395
150	497	673	490	395
180	493	699	488	416
210	494	720	490	427
240	497	730	488	427
270	495	745	490	437
300	494	753	488	444
330	494	770	490	453
360	494	775	487	460

It can be seen in Table 5.6 that fluorescence intensity keeps on increasing for chloroform vapours with time increment of 30 seconds and becomes almost constant after 300 seconds. This behaviour is different from PIM-1 spin coated substrates where the intensity change was almost constant after 120 seconds. For toluene the intensity change in smaller compared to chloroform. However, the intensity here also keeps increasing until 240 seconds after which it becomes almost constant. It looks like that the diffusion of solvent vapours is slower in copolymer as compared to PIM-1 spin coated substrate. As stated before, the MeOPEG chains in copolymer may hinder the diffusion of solvent vapours as they might adsorb within the PIM-1 structure and fill some pores. This would slow down and limit the diffusion of solvent

vapours within the film and hence may affect the intensity. For both the solvents, the change in wavelength maxima is either within experimental (±2) or negligible.

5.4 Conclusions

Fluorescence studies were aimed at checking the suitability of PIM-1 and copolymers for sensing applications and to develop a solvent profile for PIM materials. In this respect, fluorescence experiments both for PIM-1 in solution and for both PIM-1 and copolymer on substrates in presence of solvent vapours were performed. It was observed that PIM-1 solutions showed significant red shift for alcoholic solvent and DMSO coupled with a decrease in intensity when PIM-1 in THF was taken as benchmark. In contrast, aromatic solvents caused a blue shift with increase in intensity. Chloroform showed a smaller red shift but higher change in intensity. The overall behaviour of solvents was related to the polarity of the solvents, as more polar solvents caused red shift.

The main aim of the fluorescence experiments was to observe the ability of PIM-1 to alter wavelength maxima and intensity while on a substrate in the presence of solvent vapours. Model experiments were run to determine the most appropriate method. In the first approach, PIM-1 was rubbed on Whatman filter paper and placed in a cuvette before injecting solvents to create vapours and subsequent recording of spectra. In another approach, filter paper was wet in PIM-1 solution and then dried and cut to appropriate size for use in experiments. PIM-1 was also spin coated onto polyester based Melinex substrate. It was found that spin coated substrate performed better than other two methods, as the error margin was low with good reproducibility of results.

Fluorescence experiments showed that in most cases PIM-1 spin coated substrate performed better than copolymer substrate. Generally red shift was observed for alcohols and DMSO vapours with reduction of intensity and blue shift for aromatic solvents vapours with higher intensity. The change in intensity and wavelength were related to the broken rod like electronic structure of PIM-1 fluorophores, chain mobility, polarity of solvents, stabilization of excited state, conjugation of fluorophore and other factors. Effect of volume and time on solvent vapours was also observed. It was noted that small increments of solvent result in better results instead of one large dose of volume with longer time periods.

PIM-1 spin coated substrates were also treated with methanol and the results were compared with untreated PIM-1 spin coated substrates to check the effect of swelling as well as solvent residual in film. It was observed that methanol treatment of spin coated substrates does not affect wavelength shift to a larger extent, however, reduce intensity to lesser extent. Based on all these experiments, solvent profiles for both PIM-1 and copolymers have been developed on the basis of shift in wavelength maxima as well as fluorescence intensity.

References

(1) Budd, P. M.; McKeown, N. B.; Detlev, F. *Macromol. Symp.* **2006,** *245–246,* 403–405.

(2) Rakow, N. A.; Wendland, M. S.; Trend, J. E.; Poirier, R. J.; Paolucci, D. M.; Maki, S. P.; Lyons, C. S.; Swierczek, M. J. *Langmuir,* **2010,** *26*(6), 3767–3770.

(3) Malcovati, P.; Baschirotto, A,; D'Amico, A.; Natale, C. D.; *Sensors and Microsystems – AISEM 2009 Proceedings*; Springer Science + Business Media B. V. New York: 2010; pp. 55-58.

(4) Beggs, J. D.; Tollervey, D. *Nature Reviews Mol. Cell Biology* **2005,** *6,* 423–429

(5) Taskent-Sezgin, H.; Marek, P.; Thomas, R.; Goldber, D.; Chung, J.; Carrico, I.; Raleigh, D. P. *Biochemistry*, **2010**, *49 (29)*, 6290–6295

(6) Islam, M.; Khanin, M.; Sadik, O. A. *Biomacromolecules*, **2003**, *4 (1),* 114–121

(7) Kim, T. H.; Kim, I.; Yoo, M.; Swager, T. M. *J. Of the Korean Chem. Soc.* **2007**, *51(3),* 258-264.

(8) Cantor, C. R.; Schimmel, P. R. *Biophysical Chemistry Part-II Techniques for the Study of Biological Structure and Function;* W. H. Freeman and Co. Ltd. New York: 1980.

(9) Clark, B. J.; Frost, T.; Russell, M. A. *Techniques in Visible and Ultraviolet Spectroscopy;* Chapman and Hall, London: 1993; pp. 26-30.

(10) Winnik, M. A. *Pure & Appl. Chem.,* **1984,** *56(9),* 1281—1288.

(11) Kolishetti, N.; Ramakrishnan, S. *J. Chem. Sci.,* **2007,** *119(2),* 185–193.

(12) Dadge, J. W.; Krishnamurthy, V.N.; Aiyer, R.C. *Sensors and Actuators B,* **2006,** *113,* 805–808.

(13) Modesti, G.; Zimmermann, B.; Borsch, M.; Herrmann, A.; Saalwachter, K. *Macromolecules,* **2009,** *42,* 4681–4689.

(14) McQuade, D. T.; Pullen, A. E.; Swager, T. M. *Chem. Rev.* **2000,** *100,* 2537-2574.

(15) Qin Zhou, Q.; Swager, T. M. *J. Am. Chem. Soc.* **1995,***117,* 12593-12602.

(16) Swager, T. M. *Acc. Chem. Res.* **1998,** *31,* 201-207.

(17) Sazhnikov, V.A.; Khlebunov, A. A.; Alfimov, M.V. *High Eneg. Chem.* **2007,** *41(1),* 25-28.

(18) Erdogan, M.; Pekcan, O. *Int. J. of Photoenergy,***2005,** *7,* 37-43.

(19) Draman, S.F.S.; Daik, R.; Musa, A. *World Acad. of Sci., Engg. and Tech.,* **2008,** *43,* 464-471.

(20) Elosua, C.; Matias, I. R.; Bariain, C.; Arregui, F. J. *Int. J. on Smart Sensing and Intelligent Systems,* **2008,** *1(1),* 123-136.

(21) Kawski, A.; Bojarski, P.; Kuklinski, B. *Z. Naturforsch* **2002,** *57a,* 94–97.

(22) Reynolds, K. J. PhD Thesis, University of Manchester*,* 2007.

(23) Byers, J. A. Byers *Phenomenex catalogue;* 2003.

(24) Lacowics, J. R. *Principles of Fluorescence Spectroscopy;* Springer Verlag New York, USA: 2006; pp. 205-206.

(25) Valeur, B.; Bronchon J. C. *New Trends in Fluorescence Spectroscopy;* Springer Verlag Berlin, Germany: 2001; pp. 187-194.

(26) Sukul, N. C.; Sukul, A. *High Dilution Effects: Physical and Biochemical Basis;* Kluwer Academic Publishers, Dordrecht, The Netherlands: 2004; pp. 65-66

(27) Yang, J. S; Swager, T. M. *J. Am. Chem. Soc.* **1998,** *120,* 11864-11873.

CHAPTER 6

CONCLUSIONS AND RECOMENDED FUTURE WORK

6.1 Conclusions

It was aimed at the start of this research to synthesize PIM-1 and fluoro endcapped PIM-1 oligomers of various sizes and use F-PIM-1 as hard matrix for synthesis of copolymers with poly(ethylene glycol) monomethyl ether (MeOPEG1100) in order to alter the pore structure of PIM-1 and modify BET surface area. The synthesis procedure for PIM-1 oligomers and copolymers has already been reported.[1, 2]

PIM-1 was synthesized by methods reported earlier as well as with a recently reported new high shear mixing method.[3, 4] Fluoro-endcapped PIM-1 (F-PIM-1) oligomers were first synthesized by earlier reported methods,[1, 2] and then the high shear method was successfully used for synthesis.

The products were analyzed by NMR, IR, polystyrene and multidetector GPC, TGA and MALDI ToF MS techniques. NMR and IR spectrums indicated presence of relevant peaks for PIM-1. It was shown that both polystyrene based and multidetector GPC techniques worked in good agreement for PIM-1 and F-PIM-1 in most of the cases. MALDI ToF MS analysis showed that F-PIM-1 oligomers were fluoro-endcapped. PIM-1 as expected contained cyclic peaks in low molar mass region which can be detected by MALDI. TGA analysis resulted in complete decomposition of polymer around 570 °C indicating its thermal stability. N_2 adsorption experiments for PIM-1 showed its BET surface area as 670 m^2/g. For two different batches of F-PIM-1 interesting results for N_2 adsorption were obtained. One of F-PIM-1 batch (GP-20) showed unusually lower uptake of N_2 in lower pressure region. This was thought to be due to slow adsorption kinetics. Hysteresis in PIM-1 and F-PIM-1 desorption indicated that polymer matrix might get swelled.

Synthesis of F-PIM-1 was undertaken by two different bases, K_2CO_3 and Cs_2CO_3. It was demonstrated that Cs_2CO_3 could form larger sized F-PIM-1 blocks. However, later, K_2CO_3 was used for synthesis as only medium sized F-PIM-1 blocks were required for coupling. The high shear method for synthesis was found better in some cases than the conventional PIM-1 synthesis technique.

Keeping in view results of this synthesis, the coupling experiment was started at model level. A model compound (3,13-dicyanobenzo-1,2,4',5'-bis-1,4-benzodioxane) (GP-15) (Fig. 2.7) with no fluorine atoms attached to it was synthesized. The purpose to synthesize model compound was to check if the nitrile group in PIM structure or any impurities / solvent will compete with fluoro atoms for reaction or otherwise. An attempt was made to couple model compound with MeOPEG1100, however the subsequent analysis showed no signs of coupling.

Coupling of F-PIM-1 blocks to poly(ethylene glycol) monomethyl ether (MeOPEG1100) was initially undertaken by previously reported method.[2] As both PIM-1 and copolymer have same fluorophore, the product was expected to be same like PIM-1 (yellow fluorescent) in appearance. However, the product obtained in this synthesis was brown glassy mass. This indicated that either some side reaction may be occurring or base (n-BuLi) may be interfering with the reactants.

In further investigation, the base was changed from n-BuLi to K_2CO_3 and coupling reaction was repeated for smaller ethylene glycol molecule Triethylene glycol monomethyl ether (TEGME). The coupling reaction was performed by conventional step growth polymerization as well as high shear method (used earlier for PIM-1 and F-PIM-1 synthesis). For the first time, yellow fluorescent products were obtained by both synthetic methods. The coupling of TEGME to F-PIM-1 was verified by NMR, IR, GPC and MALDI techniques. Encouraged by this result, coupling of MeOPEG was again undertaken with change of base and product was again a yellow fluorescent copolymer. Synthesis was repeated using larger F-PIM-1 and MeOPEG blocks. Coupling of larger F-PIM-1 block to same MeOPEG block was successful; however, coupling of larger MEOPEG block (MeOPEG2000) was not successful. In yet another attempt, F-PIM-1 was reacted with 1,2-dihydroxy benzene) for endcapping on one side. The endcapped product was again coupled with a shorter MeOPEG block (MEOPEG750). The analysis of endcapped F-PIM-1 and coupling product was undertaken and success of coupling was verified.

It was thought appropriate at this stage to investigate physical mixing of MeOPEG with PIM-1 and observe incorporation of MeOPEG in PIM through formation of blends. If successful, this could later be used to thermally remove MeOPEG and get new pore structure and surface area. In this respect, various compositions of PIM and MEOPEG were tried using copolymer of F-PIM-1 and MeOPEG (GP-23) as compatibilizer. Despite repeated attempts, only 5% MeOPEG by mass could be solubilised in PIM matrix. The inefficiency of compatibilizer to incorporate MEOPEG into PIM-1 was explained. It is thought that PIM-1 due to its strong interactive nature, pulls MEOPEG component of compatibilizer to itself and compatibilizer could not penetrate into MeOPEG phase hence solubilise it. This unusual orientation of compatibilizer at phase boundary would reduce its efficiency and result in macrophase formation in blends. Surface tension experiments for the solvent, PIM-1, F-PIM-1 and copolymer were performed to check ability of MeOPEG part in copolymer to lower interfacial energy. There was no visible change in surface tension. This supported earlier observation that MeOPEG component had limited efficiency to alter phase boundary.

N_2 adsorption desorption analysis for PIM-1, F-PIM-1and copolymer was carried out before and after heat treatment to remove MeOPEG block. It was shown that even after heat treatment, PIM-1 regained BET surface area and pore structure remained stable. In another attempt, PIM-1 was adsorbed from aqueous MeOPEG solution and dried. The N_2 adsorption desorption analysis showed incorporation of MeOPEG into PIM-1 matrix as BET surface area reduced to almost negligible.

Fluorescence studies were basically aimed for sensing applications of for PIM-1 and copolymers. The solutions of these compounds used for fluorescence study to check the effect of solvent vapours on wavelength shift and intensity. It was observed that PIM-1 solutions showed significant red shift for alcoholic solvent (methanol, ethanol and 2-propanol) and DMSO coupled with a decrease in intensity when PIM-1 in THF was taken as benchmark. In comparison, aromatic solvents (benzene, toluene and xylene) blue shift was observed with increase in intensity. It seemed that more polar solvents caused red shift and the behaviour of solvents was related to their polarity.

Another aim of the fluorescence experiments was to observe the ability of PIM-1 to alter wavelength maxima and intensity while on a substrate in the presence of solvent vapours. In this regard, two approaches were adopted. Initially PIM-1 was rubbed on a filter paper and placed in fluorescence cuvette. Solvent was then injected in the cuvette and after saturation, spectra was recorded. In another approach, filter paper was wet in PIM-1 solution, dried and cut in appropriate size for same experiment. Later on a polyester based substrate (Melinex) was used for spin coating of PIM-1 and subsequent use in fluorescence experiments. It was observed that spin coated substrate outperformed other two methods with better reproducibility of results. Same experiments were also performed for copolymers.

It was observed that PIM-1 performed better than copolymers with larger wavelength shifts and significant change of intensity. Normally red shift was observed for alcoholic solvents and DMSO coupled with decrease in intensity. For aromatic solvents, there was blue shift with increasing intensity. The change in intensity and wavelength were related to the broken rod like electronic structure of PIM-1 fluorophores, chain mobility, polarity of solvents, stabilization of excited state, conjugation of fluorophore and other factors. Fluorescence experiments were performed to investigate effect of time and single or multiple volume increments. It was noted that small multiple volume increments of solvents caused more wavelength or intensity change than a single large dose.

In yet another attempt, polymer spin coated substrates were treated with methanol to remove solvent traces and again fluorescence experiments were repeated. A comparison was made for results of methanol treated and untreated substrates. It was observed that methanol treatment of spin coated substrates does not affect wavelength shift to a larger extent, however, reduce intensity to lesser extent. On the basis of fluorescence experiments, solvent profiles for PIM-1 and copolymers have been developed in order of shift in wavelength or change in intensity.

6.2 Future Work

The research done in this project reflects the synthesis of fluoro-endcapped PIM-1 (F-PIM-1) oligomers and their subsequent coupling to poly(ethylene glycol) monomethyl ether (MeOPEG). This has been successfully done by using conventional as well as new high shear methods. In future, the knowledge attained by this work can be utilized for further synthesis of copolymers using MeOPEG blocks of various sizes or other labile blocks like poly(propylene glycol) (PPG).

PIM-1 synthesis has been reported using tetrachloroterephthalonitrile (TCTPN) instead of tetrafluoroterephthalocyanine.[1, 5] it would be interesting to synthesize chloro endcapped PIM-1 oligomers and their subsequent coupling to MeOPEG or PPG. In the same way, it might be worth to synthesize catechol endcapped PIM-1 oligomers and couple them to appropriate fluoro or chloro endcapped monomers/polymers.

Work is going on to make a new class of PIM materials known as PIM-polyimides. (PIM-PIs).[6] Although the blending of PIM-1 with MeOPEG was not much successful even with the use of compatibilizer, it would be worth trying to use newly reported PIM-PIs for blending with PIM-1. Another approach can be using copolymers of large size MeOPEG blocks or PPG as compatibilizers for blending.

Adsorption from MeOPEG solution was encouraging in present work and N_2 adsorption experiments showed that MeOPEG could be absorbed into PIM structure. The next step in this regard could be determining amount of MEOPEG adsorbed and develop adsorption isotherms.

Fluorescence work in this project showed potential of PIM-1 and copolymers to interact with solvent vapours and cause wavelength shift and change in intensity. A solvent profile has already been developed for PIM-1 and copolymers. Further work on fluorescence could be based on doing FT-IR, NMR, GPC and quantum mechanical calculations[7] to determine type of interactions and physical forces between PIM materials and solvent vapours. An interesting investigation in fluorescence work would be checking effect of mixed solvent system vapours in

presence on PIM-1. In this work only polyester based substrate was used and found suitable. However, it would be interesting to use a range of substrates for spin coating of PIM-1 on them and then subject to fluorescence experiments for comparison. The range of solvents for fluorescence studies also needs to be broadened.

References

(1) Reynolds, K. J. PhD Thesis, University of Manchester, 2007.

(2) Grant, L. E. PhD Thesis, University of Manchester, 2006.

(3) Du, Naiying Du; Song, Jingshe; Robertson, Gilles P.; Pinnau, Ingo; Guiver, Michael D. *Macromol. Rapid Commun.* **2008,** *29,* 783-788.

(4) Song, J.; Du, N.; Dai, Y.; Robertson, G. P.; Guiver, M. D.; Thomas, S.; Pinnau, I. *Macromolecules* **2008,** *41,* 7411-7417.

(5) Selbie, J. D. PhD Thesis, University of Manchester, 2009.

(6) Shamsipour, H. *Unpublished work,* The University of Manchester, 2010.